# Evidencing land cover dynamics and tropical forest seasonality: the benefit of 13 years of daily global observation (SPOT-VEGETATION)

INÈS MOREAU

FÉVRIER 2016

Thèse présentée en vue de l'obtention
du grade de docteur en sciences agronomiques
et ingénierie biologique

Faculté des Bioingénieurs

Université catholique de Louvain

**Jury members**

| | |
|---|---|
| President: | Pr. Bruno Delvaux (UCL, Belgium) |
| Supervisor: | Pr. Pierre Defourny (UCL, Belgium) |
| Readers: | Pr. Patrick Bogaert (UCL, Belgium) |
| | Dr. Hans Verbeeck (UGent, Belgium) |
| | Dr. Valéry Gond (CIRAD, France) |
| | Dr. Philippe Mayaux (EC, Belgium) |

# Remerciements

Ca y est, voici ce moment tant attendu de remercier toutes les personnes qui m'ont aidée ou soutenue durant ces années de thèse. Moment tant attendu, car pour moi synonyme de la fin d'un long périple dans les méandres de la vie de thésarde. La vie de thésarde, tout un programme. Si elle a parfois été source d'inquiétude ou découragement, souvent de solitude en « tête-à-écran » avec mon ordinateur, elle n'en reste pas moins une expérience unique tant au niveau professionnel que personnel. A vous tous que j'évoque dans ces quelques lignes, un énorme et chaleureux merci de m'avoir apporté chacun à votre façon tous les ingrédients indispensables à l'aboutissement de cette thèse.

Je commencerai par remercier mon promoteur, Pierre Defourny, qui m'a accueillie parmi les Enges alors que j'étais tout juste diplômée. Je suis reconnaissante de la confiance qu'il m'a accordée pour rejoindre l'équipe du projet VEGECLIM. Au fil du projet, j'ai pu développer mes connaissances et recherches dans le monde passionnant de la télédétection, mais aussi poser un regard plus réaliste sur la communication de milieux scientifiques différents et apprendre la gestion de projet. Je remercie Pierre pour sa passion transmise avec succès, son enthousiasme lors des réunions, sa qualité de cultiver une bonne ambiance de travail.

Mes remerciements vont ensuite naturellement à l'ensemble des membres de mon jury de thèse. Les précieux commentaires et conseils d'Hans Verbeeck tout au long du projet VEGECLIM m'ont permis de ne pas cantonner ma vision à la télédétection mais d'établir des ponts avec le monde de la modélisation et la réalité de terrain. Les encouragements de Valéry Gond m'ont donnés une grande confiance en mon travail, surtout compte tenu des débats actuels dans le domaine de la phénologie en forêt tropicale qui m'ont donnés bien du fil à retorde. Je remercie également Patrick Bogaert pour la qualité et la précision de ses remarques, ainsi que pour son intérêt porté à l'amélioration future de certains aspects de mon travail. Enfin, merci à Philippe Mayaux d'avoir accepté de venir compléter ce jury et d'avoir apporté des critiques constructives quant à certains points de mon travail. Je remercie également Mr Bruno Delvaux d'avoir accepté de présider ce jury.

Quant à la faisabilité d'avoir pu travailler sur un tel jeu de données qu'est la série temporelle SPOT-VEGETATION, c'est vers Eric Van Bogaert que se tourne mon entière reconnaissance. Sa patience, sa gentillesse et ses compétences techniques pour gérer et traiter ces volumes de données ont été indispensable pour ma thèse.

Lors de ces années de thèse, j'ai eu la chance de participer au projet VEGECLIM. Mes pensées vont premièrement à Marjolein avec qui j'ai passé de très bons moments lors de conférences et comités d'accompagnement. Merci également à Hans, Fabienne et Philippe pour leurs échanges scientifiques très instructifs. Enfin, je remercie particulièrement tous les membres du comité d'accompagnement : Laurent Kergoat, Philip Lewis, Xiangming Xiao, Chris Jones et Yosio Shimabukuro. Leur attention et regard critique portés à l'avancement du projet m'ont permis chaque année de mieux orienter mes recherches.

Je tiens ensuite à remercier tous mes collègues, anciens ou nouveaux, grâce à qui j'ai pu passer ces années dans une ambiance particulièrement amicale et joyeuse. A l'heure d'écrire ces lignes, une foule de souvenirs me traverse l'esprit avec un brin de nostalgie : la guerre des post-it, les (post-)soupers de Noël, la pendaison inoubliable des Globcroper's, les verres à la quinzaine de la bière, … Plus particulièrement, je pense à Aline qui, au-delà d'une collègue, est devenue une amie sur qui je peux compter en toute circonstance. Merci à elle et Manu pour leur soutien, leur écoute dans les moments difficiles mais aussi les grosses tranches de rigolade qui font tellement du bien. J'aimerais remercier énormément Astrid qui m'a expliqué dans les détails tous les tuyaux de début, milieu et fin de thèse, et avec qui j'ai passé des moments inoubliables à la Summer School de l'ESA. Merci à Jean-Paul (aka Président) pour son amitié et pour l'organisation de ses « réunions » autour d'une TK, car « le café c'est pas bon pour le cœur, allons plutôt boire une bière » ;). Merci à Nicolas et Quentin pour leur gentillesse et leur calme dans le bureau qui a été très bénéfique à ma rédaction, à Pascale pour son écoute et son soutien, à François S. et Doriane pour nos supports mutuels et discussions de "fin de thèse", à Raph pour son énergie permanente et communicative, à François W. et Damien pour leur camaraderie (je sais que ça va les faire rire) qui tombe toujours à point nommé, à Julien pour sa disponibilité pour résoudre les bugs incompréhensibles et pour nos nombreuses discussions-débats à la cafèt, à Cindy pour son agréable compagnie et pour m'avoir initié au yoga, à

Aurélie pour ses encouragements, à Catherine pour nos nombreuses discussions sur le monde et ses travers, à Thomas pour son aide technique ultra précieuse et toujours super efficace, à Sophie et Céline pour nos échanges sur le land cover et m'avoir accueillie dans le CCI, enfin à tous les nouveaux pour perdurer cette ambiance Enge si particulière !

Un grand merci à mes amis qui ont assurés les moments de détente indispensables avec brio, et qui auront si souvent entendu parler de cette fameuse thèse ! Je pense évidemment à Fanny toujours là pour moi depuis si longtemps, à Christelle, Barbara et Julie pour nos lundis musicaux si ressourçant, à Dgé pour sa présence attentionnée malgré la distance, à mes petites biogonz' pour tous ces merveilleux soupers devenus tradition incontournable et pour leurs encouragements, et à Lucie et Lara pour nos soirées « Chez Félix » avec toujours milles histoires à se raconter. Merci également à Tiphaine Rivière et son excellente bande dessinée « Carnet de thèse » que je conseille à tout thésard en questionnement.

Enfin, pilier essentiel à mon bien-être, ma famille et belle-famille a été très présente et je les remercie tous de tous cœur. Merci en particulier à mes parents pour avoir toujours cru en moi tout au long de ce parcours, pour leur écoute toujours suivie de conseils avisés, et pour leur relecture très précieuse. Dans les moments ultra fun ou plus difficiles, ma sœur Ingrid est toujours là pour moi, un grand merci pour tout. Nos nombreuses, que dis-je, infinies heures passées au téléphone nous auront certes coûté quelques deniers, mais qu'est-ce qu'elles ont été comiques et bénéfiques ! Pour passer un bon moment et quelques tranches de rire « à la Friends » ou réparer en urgence mon pc, je sais que je peux compter sur mes « cracs » de frères, Jean-Sébastien et Ludovic. Merci aussi à mes grands-parents pour leurs nombreuses attentions, toujours un petit sms ou mail au bon moment pour remonter le moral des troupes.

Enfin, last but not least, Thomas mon amour, je te remercie infiniment. Sans toi, je ne sais pas si j'aurais été jusqu'au bout… Pour m'avoir continuellement encouragée, pour ta patience face à mes nombreuses heures de travail, pour m'avoir préparé ces bons petits plats quand je rentrais tard, pour m'avoir poussée à lever le pied quand il fallait, pour partager ma vie depuis presque 5 ans maintenant contre vents et marées… de tout cœur merci !

Inès

# Framework and Fundings

This research was funded by the Belgian Science Policy (Belspo) through a STEREO II grant SR/00/135, i.e. the VEGECLIM project entitled “Integrating SPOT-VEGETATION 10-year time series and land surface modelling to forecast the terrestrial carbon dynamics in a changing climate”.

# Table of contents

**LIST OF FIGURES** ..... **V**
**LIST OF TABLES** ..... **XV**
**ACRONYMS** ..... **XVII**
**INTRODUCTION** ..... **1**
1. A GLOBAL CHANGE CONTEXT ..... 1
2. OPTICAL SATELLITE LONG TIME SERIES ..... 6
3. GLOBAL LAND COVER MAPPING ..... 8
*3.1. Current global land cover maps* ..... *8*
*3.2. A problematic "single-year" approach* ..... *10*
4. GLOBAL LAND COVER CHANGE DETECTION ..... 11
*4.1. Current land cover change detection methods* ..... *11*
*4.2. Challenges in observing land cover change* ..... *14*
5. VEGETATION PHENOLOGY ..... 15
*5.1. Remote sensing phenology* ..... *16*
*5.2. Tropical rainforest phenology under debate* ..... *18*
6. SCOPE AND OBJECTIVES ..... 21
7. OUTLINE OF THE THESIS ..... 24
**CHAPTER 1 – A MULTI-YEAR GLOBAL LAND COVER MAP AND LAND COVER CHANGE DETECTION AT GLOBAL SCALE THANKS TO 13-Y SPOT-VEGETATION TIME SERIES** ..... **27**
ABSTRACT ..... 27
1. INTRODUCTION ..... 28
2. METHODS AND DATA ..... 34
*2.1. Input time series and features* ..... *34*
*2.2. The GlobCover classification chain* ..... *35*
*2.3. Two methods for a global multi-year land cover map* ..... *38*
*2.4. Validation and quality indicators* ..... *42*
*2.5. A trajectory-based change detection method* ..... *43*
3. RESULTS ..... 46

*3.1. A large inter-annual variability among annual classifications ..... 46*
*3.2. Two multi-year global land cover maps ..... 50*
*3.3. Seven types of land cover change ..... 68*
*3.4. Quantification and distribution of global land cover change at 1km² ..... 92*
4. DISCUSSION ..... 95
*4.1. Global multi-year land cover mapping ..... 95*
*4.2. Global land cover change detection ..... 99*
5. CONCLUSION ..... 103
**CHAPTER 2 – VEGETATION PHENOLOGY OF AMAZONIAN TROPICAL RAINFORESTS FROM 11-Y SPOT-VEGETATION TIME SERIES ..... 105**
ABSTRACT ..... 105
1. INTRODUCTION ..... 106
2. DATA DESCRIPTION ..... 112
3. METHODOLOGY ..... 114
*3.1. Sites description ..... 114*
*3.2. Spectral bands analysis ..... 115*
*3.3. Vegetation indices analysis ..... 118*
*3.4. In situ measurements analysis ..... 119*
4. RESULTS AND DISCUSSION ..... 120
*4.1. Reflectance time series analysis ..... 120*
*4.2. EVI and NDVI seasonal dynamics ..... 130*
*4.3. In situ data ..... 135*
*4.4. Spatial extent of EVI dynamics of Amazonian vegetation ..... 143*
5. CONCLUSION ..... 148
**CHAPTER 3 – VEGETATION PHENOLOGY OF TROPICAL RAINFORESTS IN THE CONGO BASIN FROM 11-Y SPOT-VEGETATION TIME SERIES ..... 151**
ABSTRACT ..... 151
1. INTRODUCTION ..... 152
2. DATA DESCRIPTION ..... 155
3. METHODOLOGY ..... 156
*3.1. Climate patterns of the Congo basin ..... 157*

*3.2. Sites description* ..... *157*
*3.3. Spectral bands analysis* ..... *160*
*3.4. Vegetation indices analysis* ..... *161*
*3.5. In situ measurements analysis* ..... *162*
4. RESULTS ..... 162
*4.1. Reflectance time series analysis* ..... *162*
*4.2. EVI and NDVI seasonal dynamics* ..... *166*
*4.3. In situ data* ..... *172*
*4.4. Scaling up to 6 sites* ..... *178*
*4.5. Scaling up to basin scale* ..... *179*
5. DISCUSSION ..... 186
6. CONCLUSION ..... 189
**CONCLUSIONS AND PERSPECTIVES ..... 191**
1. FINDINGS ..... 191
2. PERSPECTIVES ..... 199
*2.1. Potential improvements to the approaches developed and future research directions* ..... *199*
*2.2. Applications of the methods developed* ..... *203*
**PUBLICATIONS ..... 207**
**BIBLIOGRAPHY ..... 211**

# List of figures

Figure 1 : Overall approach of the thesis. ..... 25

Figure 2: GlobCover 22 equal-reasoning strata. Green strata rely on annual composites and yellow strata rely on annual and seasonal composites for the classification. ..... 36

Figure 3: Flowchart of the two methodologies developed to produce a multi-year land cover map based on the 13-year SPOT-VEGETATION archive using the GlobCover classification chain: a) one classification based on 1 set of 13-y summarized annual and seasonal composites (Multi-Year Classification, MYC) and b) one synthesis of 13 annual classifications (Synthesis of Yearly Classifications, SYC)..... 39

Figure 4 : Examples illustrating different cases of SYC method developed to produce a multi-year land cover map based 13 annual classifications, according to majority voting strategy and decision rules. For complete names of the classes, see Table 1. ..... 40

Figure 5 : Examples illustrating different cases of the trajectory-based change detection method. For each example, the first line is the pixel trajectory of classes and the second line indicate the year of change detected. For complete names of the classes, see Table 1. ..... 45

Figure 6 : Example of the inter-annual variability (Montana, USA) between successive annual classifications with SPOT-VEGETATION data: (a) 2003, (b) 2004, (c) 2005. Maximum of occurrence of a same land cover label over 13 annual classifications (d). Multi-year land cover map with (e) the MYC method (classification based on 1 set of 13-y composites) and (f) the SYC method (synthesis of 13 classifications). See Table 1 for the GlobCover legend..... 47

Figure 7 : Example of the inter-annual variability (Austral Africa ) between successive annual classifications with SPOT-VEGETATION data:. (a) 2007, (b) 2008, (c) 2009. Maximum of occurrence of a same land cover label over 13 annual classifications (d). Multi-year land cover map with (e) the MYC method (classification based on 1 set of 13-y composites) and (f) the SYC method (synthesis of 13 classifications). See Table 1 for the GlobCover legend..... 48

Figure 8 : 13-y average percentage of pixels transitions from one year to the next year, for the 13 annual SPOT-VEGETATION classifications. See Table 1 for the GlobCover legend. .....50

Figure 9 : Multi-year land cover map derived from SPOT-VEGETATION times series (1999 -2011) thanks to the GlobCover classification chain, relying (a) on the MYC method (classification based on composites summaries over 13-y of data) and (c) on the SYC method (synthesis of 13 annual classifications) with the respective surfaces per land cover classes (b) and (d). (e) Spatial representation of the 15.95 % of pixels (black) which cannot be simply labeled by majority voting (SYC) method, meaning that they doesn't reach the 7 occurrence over the 13 years. (f) Percentage of highly stable pixels (max. occurrence ≥ 9) per classes compared to the total area of the class of the SYC method product. See Table 1 for the GlobCover legend.....54

Figure 10. Illustration over Liberia and Ivory Coast. Annual SPOT-VEGETATION composite 2005 (a). Annual classifications with SPOT-VEGETATION data 2005 (b), 2007 (c), 2010 (d). Multi-year land cover map with the MYC method (classification based on 1 set of 13-y composites (e)) and the SYC method (synthesis of 13 classifications (f)). Maximum of occurrence of a same land cover label over 13 annual classifications (g). See Table 1 for the GlobCover legend.....60

Figure 11. Illustration over Italy (a), (b), (c), (d) showing the ability to map irrigated croplands. Illustration over South of Russia (e), (f), (g), (h) showing the ability to map croplands. (a) and (e) are eSAT imagery (15 m of spatial resolution); (c) and (g) multi-year land cover map according the MYC method; (d) and (h) multi-year land cover map according the SYC method. Maximum of occurrence of a same land cover label over 13 annual classifications (b) and (f). See Table 1 for the GlobCover legend. .....61

Figure 12 : Spatial representation (a) of the maximum occurrence of a same land cover class over the 13 annual classifications. (c) Idem for aggregated classes (Cropland – Forest – Flooded Vegetation – Grassland – Sparse and Bare areas – Urban areas – Water – Snow). Histograms associated showing the total area of each maximum occurrence over the world (b), (d). .....65

Figure 13 : Spatial representation of degree of reliability of the cropland pixels (a) and of the forests pixels (b) mapped in the SYC, according to the step at which the label was delivered (labelled with a majority (occurrence >= 7) (green pixels), over a majority mosaic (blue pixels), or with specific decision rules (pink pixels)).....67

Figure 14 : Landes forest (France) damages caused by the windstorm "Klaus" in January 2009. Suite of annual classifications with SPOT-VEGETATION data (a). Multi-year land cover map (SYC) without taking into account land cover changes (b1), pixels detected as change (forest loss) labelled with the new land cover classes (b2), year of change (b3), pixels detected as forest loss in the Global Forest Change map (Hansen et al., 2013) (b4), and change superimposed on the multi-year land cover map (b5). Aerial photos from Google Earth in the Landes forest (c). See Table 1 for the GlobCover legend and Figure 5 for the year of change legend. ..... 70

Figure 15 : Fire forest damages in Quebec (Canada) in 2007. Multi-year land cover map (SYC) without taking into account of land cover changes (a1), pixels detected as change (forest loss) labelled with the new land cover classes (a2), year of change (a3), pixels detected as forest loss in the Global Forest Change map (Hansen et al., 2013) (a4), and change superimposed on the multi-year land cover map (a5). Landsat images from the Google Timelapse tool (b). See Table 1 for the GlobCover legend and Figure 5 for the year of change legend. ..... 71

Figure 16 : Insect infestations damages in Idaho (USA). Multi-year land cover map (SYC) without taking into account of land cover changes (a1), pixels detected as change (forest loss) labelled with the new land cover classes (a2), year of change (a3), pixels detected as forest loss in the Global Forest Change map (Hansen et al., 2013) (a4), and change superimposed on the multi-year land cover map (a5). High resolution images from Google Earth (b). See Table 1 for the GlobCover legend and Figure 5 for the year of change legend. ..... 73

Figure 17: Deforestation in North (a, c) and East (b) of DRC. Multi-year land cover map (SYC) without taking into account of land cover changes (a, b, c: 1), pixels detected as change (forest loss) labelled with the new land cover classes (a, b, c: 2), year of change (a, b, c: 3), and change superimposed on the multi-year land cover map (a, b, c: 5). FACET map of forest cover extent and loss analysis in Democratic Republic of Congo (a, b, c: 4 – losses 2000-2005 (red pixels) and 2005-2010 (purple pixels)). See Table 1 for the GlobCover legend and Figure 5 for the year of change legend..... 75

Figure 18 : Deforestation in North of Paraguay (boundaries : pink lines). Multi-year land cover map (SYC) without taking into account of land cover changes (a, c: 1), pixels detected as change (forest loss) labelled with the new land cover classes (a, c: 2), year of change (a, c: 3), pixels detected as forest loss in the Global Forest Change map (Hansen et al., 2013) (a, c: 4), and change superimposed on the multi-year land cover map (a, c: 5). Landsat

images from the Google Timelapse tool (b, d). See Table 1 for the GlobCover legend and Figure 5 for the year of change legend. .....77

Figure 19 : Mining in the Athabasca Oil Sands region, Alberta (Canada) (a, b) and in Brandebourg (Germany) (c, d). Multi-year land cover map (SYC) without taking into account land cover changes (a, c: 1), pixels detected as change (forest loss) labelled with the new land cover classes (a, c: 2), year of change (a, c: 3), pixels detected as forest loss in the Global Forest Change map (Hansen et al., 2013) (a, c: 4) and change superimposed on the multi-year land cover map (a, c: 5). Landsat images from the Google Timelapse tool (b, d). See Table 1 for the GlobCover legend and Figure 5 for the year of change legend. .....79

Figure 20 : Natural reforestation in Russia. Multi-year land cover map (SYC) without taking into account land cover changes (a1), pixels detected as change (forest gain) labelled with the new land cover classes (a2), year of change (a3), pixels detected as forest gain in the Global Forest Change map (Hansen et al., 2013) (a4) and change superimposed on the multi-year land cover map (a5). Landsat images from the Google Timelapse tool and Google Earth (b). See Table 1 for the GlobCover legend and Figure 5 for the year of change legend. .....81

Figure 21 : Plantations in Roraima (Brazil) (a, b) and in South Sumatra (Indonesia) (c, d). Multi-year land cover map (SYC) without taking into account land cover changes (a, c: 1), pixels detected as change (forest gain) labelled with the new land cover classes (a, c: 2), year of change (a, c: 3), pixels detected as forest gain in the Global Forest Change map (Hansen et al., 2013) (a, c: 4) and change superimposed on the multi-year land cover map (a, c: 5). Landsat images from the Google Timelapse tool and Google Earth (b, d). See Table 1 for the GlobCover legend and Figure 5 for the year of change legend. .....83

Figure 22 : Croplands change into sparse vegetation in Aktioubé (Kazakhstan). Multi-year land cover map (SYC) without taking into account land cover changes (a1), pixels detected as change (croplands loss) labelled with the new land cover classes (a2), year of change (a3), and change superimposed on the multi-year land cover map (a4). Landsat images from the Google Timelapse tool (b). See Table 1 for the GlobCover legend and Figure 5 for the year of change legend. .....83

Figure 23 : Croplands appearance in desert of Al Jawf (Saudi Arabia) (a, b) and in Xinjiang (China) (c, d). Multi-year land cover map (SYC) without taking into account land cover changes (a, c: 1), pixels detected as change (croplands gain) labelled with the new land cover classes (a, c: 2), year of change (a, c: 3), and change superimposed on the multi-year land cover map

(a, c: 4). Landsat images from the Google Timelapse tool (b, d). See Table 1 for the GlobCover legend and Figure 5 for the year of change legend. ..... 85

Figure 24 : Drying up of Razazza Lake (Iraq) (a, b) and of Toshka Lakes (Egypt) (c, d). 1999 classification (a, c: 1), pixels detected as change (water loss) labelled with the new land cover classes (a, c: 2), year of change (a, c: 3), and change superimposed on the multi-year (SYC) land cover map (a, c: 4). Landsat images from the Google Timelapse tool (b, d). See Table 1 for the GlobCover legend and Figure 5 for the year of change legend. ..... 86

Figure 25 : Filling of the Indira Sagar Dam (India) (a, b) and damages after the hurricane Katrina (New Orleans, USA) (c, d). 1999 classification (a1) and 2004 classification (c1), pixels detected as change (water appearance) labelled with the new land cover classes (a, c: 2), year of change (a, c: 3), and change superimposed on the multi-year (SYC) land cover map (a, c: 4). Landsat images from the Google Timelapse tool (b, d). See Table 1 for the GlobCover legend and Figure 5 for the year of change legend. ..... 90

Figure 26 : Expansion of Denver (Colorado, USA). Multi-year land cover map (SYC) without taking into account land cover changes (a1), pixels detected as change (urban appearance) labelled with the new land cover classes (a, c: 2), year of change (a, c: 3), and change superimposed on the multi-year (SYC) land cover map (a, c: 4). Landsat images from the Google Timelapse tool (b). See Table 1 for the GlobCover legend and Figure 5 for the year of change legend. ..... 91

Figure 27: Amount of pixels detected as change per trajectory for the 7 types of change. ..... 92

Figure 28: Land cover types in the Amazon basin (GlobCover 2009, Arino et al., 2010). ..... 115

Figure 29 : Annual mean profiles centered at K67 fluxtower of (a) 8-day period AOT for 1°x1° window, reflectances in blue (blue line), red (red line) and NIR (black line) bands for a 5x5 pixels window from (b) SPOT-VEGETATION time series 10-d composites (2000-2010) and (c) NBAR-MODIS time series (2000-2009). Bars in (b) are number of valid observation by decade averaged over the 11 years. Inter-annual variability corresponding to one standard deviation is represented by dotted lines. Half-year periods are repeated at the beginning and the end of the year (delimited by vertical lines). Shaded areas indicate the dry season. ..... 121

Figure 30: Aerosols Optical Thickness 550 nm dynamics from the L-3 MODIS Gridded Atmospheric Product (MOD08_E3) at 1°x1° spatial resolution for the Amazon basin, using data from January 2000 to December

2009. The average is computed on a monthly basis from the corresponding 8-day values. ..... 123

Figure 31 : Annual mean profiles of reflectances in blue (blue line), red (red line) and NIR (black line) bands from SPOT- VEGETATION time series 10-d composites (2000-2010), 5x5 km² window, for a pasture site near K67 fluxtower. Bars are number of valid observations per decade averaged over the 11 years. Inter-annual variability corresponding to one standard deviation is represented by dotted lines. Half-year periods are repeated at the beginning and the end of the year (delimited by vertical lines). Shaded areas indicate the dry season. ..... 125

Figure 32 : SPOT- VEGETATION (2000-2010) data extracted for a 1x1 pixel window centered at the K67 fluxtower: (a) Daily S1 data in the NIR band acquired in backward (green) and forward (black) configuration. (b) Annual mean profiles of 10-d forward (dashed dotted line) and backward (dotted line) composites, mean of backward and forward composites (dashed line) and original 10-d composite (solid line) in the NIR band. Half-year periods are repeated at the beginning and the end of the year (delimited by vertical lines). ..... 127

Figure 33 : Representation of daily NIR reflectance values at K67 fluxtower from SPOT- VEGETATION time series (2000-2010) in September and December as function of (a) φ and VZA in the polar diagrams and of (b) SZA and φ. Polar diagrams: view zenith angles are represented as circles every 20°, the principal plane is on the horizontal line with backscattering to the right. The small black circle corresponds to the mean sun angle during the period of observations. ..... 129

Figure 34 : Annual mean profiles of NDVI (red line) and EVI (green line) for a 5x5 pixels window centered at K67 fluxtower from (a) SPOT-VEGETATION time series 10-d composites (2000-2010) and (b) NBAR-MODIS time series (2000-2009). Bars in (a) are number of valid observations per decade averaged over the 11 years. Inter-annual variability corresponding to one standard deviation is represented by dotted lines. Half-year periods are repeated at the beginning and the end of the year (delimited by vertical lines). Shaded areas indicate the dry season. ..... 130

Figure 35 : Scatterplots between the NDVI/EVI and reflectances used to generate them, from SPOT- VEGETATION time series 10-d composites (2000-2010), at the location of the K67 flux tower, 5x5 km² window (spatial average values). ..... 132

Figure 36 : Annual mean profiles of EVI 10-d composites (black line) and inter-annual variability (dotted line), relative azimuth angle (blue dots) and

solar zenith angle (green dots, mean = black line) from SPOT-VEGETATION time series (2000-2010), 1x1 km² window, in (a) K67 fluxtower site, (b) Yangambi (Democratic Republic of Congo) and (c) the Ardennes (Belgium). Inter-annual variability corresponding to one standard deviation is represented by dotted lines. Half-year periods are repeated at the beginning and the end of the year (delimited by vertical lines). The EVI pattern for K67 is not exactly the same than in Figure 34 (a) because it is computed on a 1x1 pixel window basis, instead of 5x5, for the sake of SZA extraction. ..... 134

Figure 37 : Seasonal dynamics of 10-d composites of EVI for a 5x5 km² window from SPOT-VEGETATION time series (solid black line), decadal fluxtower derived GPP (gC/m²/s, dotted line), monthly precipitation (mm/month, bars) and daily running mean shortwave income radiation (SWdown, W/m², red line), at the location of the fluxtower K67 (2002-2004). GPP values are averaged by decade only for daytime (8h-16h). Years are separated by vertical lines. Shaded areas indicate the typical dry season. ..... 139

Figure 38: Relationship between EVI 10-d composites derived from SPOT-VEGETATION time series 10-d composites and decadal fluxtower derived GPP (gC/m²/s), at the location of the K67 flux tower (2002-2004) (a), with smoothed data (b) and with smoothed data shifted of one month. Smoothed seasonal dynamics of 10-d composites of EVI for a 5x5 km² window from SPOT-VEGETATION time series (2002-2004) (solid line), and decadal GPP data (g/m²/s) (dotted line), at the location of the K67 fluxtower (d). Years are separated by vertical lines. ..... 140

Figure 39 : Spatial distribution of EVI seasonal dynamics for the Amazon basin. Each months average is a mean of corresponding 30-d composites from the 11 years of data from SPOT- VEGETATION time series (2000-2010). ..... 145

Figure 40: Rainfall climatologies from the Tropical Rainfall Measuring Mission (TRMM) using 1998 to 2011 data, mm/dd, 0.25° by 0.25° spatial resolution. ..... 146

Figure 41: Basin wide distributions of soils under forest vegetation, based on the SOTERLAC–ISRIC soil database (version 2.0, 1:5 million scale) and the vegetation database of Saatchi et al. (2008) for South America (Quesada et al., 2011). ..... 147

Figure 42 : Location of the six sites superimposed on the Congo basin Vegetation Types Map (Verhegghen et al., 2012). ..... 159

Figure 43 : Annual mean profiles of AOT (1°x1° window, 8-day period) (a,c), of reflectances in blue (dark blue line), red (red line), NIR (black line) bands, and number of valid observation by decade (bars) from SPOT-VGT time series 10-d composites (2000-2010) for a 5x5 pixels window centered at Yangambi and Luki site (b,d). Inter-annual variability corresponding to one standard deviation is represented by dotted lines. Half-year periods are repeated at the beginning and the end of the year (delimited by vertical lines). Shaded areas indicate the dry season. ..... 163

Figure 44 : Aerosols Optical Thickness 550 nm dynamics from the L-3 MODIS Gridded Atmospheric Product (MOD08_E3) at 1°x1° spatial resolution for the Congo basin, using data from January 2000 to December 2009. The average is computed on a monthly basis from the corresponding 8-day values. ..... 166

Figure 45 : Annual mean profiles of NDVI (red line) and EVI (green line), and number of valid observations by decade (bars) for a 5x5 pixels window centered at Yangambi (a) and Luki (b) sites from SPOT-VGT time series 10-d composites (2000-2010). Inter-annual variability corresponding to one standard deviation is represented by dotted lines. Half-year periods are repeated at the beginning and the end of the year (delimited by vertical lines). ..... 167

Figure 46 : Scatter plots between the NDVI and reflectances, from SPOT-VGT time series 10-d composites (2000-2009), at the location of Yangambi (a) and Luki (b) sites, 5x5 km² window (spatial average values). ..... 168

Figure 47 : Scatter plots between the EVI and reflectances, from SPOT-VGT time series 10-d composites (2000-2009), at the location of Yangambi (a) and Luki (b) sites, 5x5 km² window (spatial average values)..... 169

Figure 48 : Annual mean profiles of EVI 10-d composites (black line) and inter-annual variability (dotted line), relative azimuth angle (blue dots) and solar zenith angle (green dots, mean = black line) from SPOT-VEGETATION time series (2000-2010), 1x1 km² window, for Yangambi and Luki sites. Inter-annual variability corresponding to one standard deviation is represented by dotted lines. Half-year periods are repeated at the beginning and the end of the year (delimited by vertical lines). The EVI patterns are not exactly the same than in Figure 45 because it is computed on a 1x1 pixel window basis, instead of 5x5, for the sake of SZA extraction. 171

Figure 49 : Annual mean profiles of NDVI (red line) and EVI (green line) at the six sites, from SPOT-VGT time series 10-d composites (2000-2010), 5x5 km² window (spatial average values). Bars are number of valid observation by decade averaged over the 11 years. Inter-annual variability corresponding

to one standard deviation is represented by dotted lines. Halves of the year are repeated at the beginning and the end of the year (delimited by vertical lines). ..... 178

Figure 50 : Spatial distribution of EVI seasonal dynamics for the Congo basin. Each months average is a mean of corresponding 30-d composites from the 11 years of data from SPOT- VEGETATION time series (2000-2010). ..... 182

Figure 51: Spatial distribution of the number of valid observations per decade for the Congo basin. Each months average is a mean of corresponding 30-d composites from the 11 years of data from SPOT-VEGETATION time series (2000-2010)..... 184

Figure 52: Rainfall climatologies from the Tropical Rainfall Measuring Mission (TRMM) using 1998 to 2011 data, mm/dd, 0.25° by 0.25° spatial resolution. ..... 185

# List of tables

Table 1 : The 22 global land cover classes of the GlobCover legend. .....36

Table 2 : Overall and global accuracies for the two multi-year land cover products computed with heterogeneous and homogeneous certain points. ..55

Table 3: Contingency matrix of the MYC versus the homogeneous validation dataset. Green cells are cells that show agreement between classification and validation. Yellow cells mark cells that have been deemed to represent samples that do not disagree with the classified results. The value in the red cell shows the overall accuracy. .....57

Table 4: Contingency matrix of the SYC versus the homogeneous validation dataset. Green cells are cells that show agreement between classification and validation. Yellow cells mark cells that have been deemed to represent samples that do not disagree with the classified results. The value in the red cell shows the overall accuracy. .....58

Table 5 : Amount of pixels (km²) detected as changed for the 7 types of change. Percentage of the total pixels changed on the total pixels of the concerned classes in the multi-year land cover map before considering change. .....95

Table 6 : Spectral channel characteristics of the VEGETATION sensor. ... 113

Table 7: Field measurements of leaves dynamics in the Amazon basin. .... 137

Table 8 : Spectral channel characteristics of the VEGETATION sensor. ... 156

Table 9 : Coordinates of sites selected to study the seasonality of tropical rainforests in Congo basin. .....159

Table 10: Field measurements of leaves dynamics in the Congo basin. The bimodal rainfall regimes of areas close to the equator is not represented in this table but the characteristics of the two wet and two dry seasons are similar. .....177

# Acronyms

| | |
|---|---|
| AMO | Atlantic Multidecadal Oscillation |
| AOT | Aerosol Optical Thickness |
| AVHRR | Advanced Very High Resolution Radiometer |
| B | Blue band |
| BRDF | Bidirectional Reflectance Distribution Function |
| C | Carbon |
| CAR | Central African Republic |
| CCI | Climate Change Initiative |
| CNES | National Centre for Space Studies |
| $CO_2$ | Carbon dioxide |
| CVA | Change Vector Analysis |
| DGVM | Dynamic Global Vegetation Model |
| DRC | Democratic Republic of Congo |
| ECV | Essential Climate Variable |
| ENSO | El Niño/Southern Oscillation |
| EO | Earth Observation |
| ESA | European Space Agency |
| EVI | Enhanced Vegetation Index |
| FACET | Forêts d'Afrique Centrale Évaluées par Télédétection |
| FAO | Food and Agriculture Organization |
| GCOS | Global Climate Observing System |
| GHG | GreenHouse Gases |
| GLC 2000 | Global Land Cover 2000 |
| GPP | Gross Primary Production |
| HRV | High Resolution Visible |
| IGBP | International Geosphere-Biosphere Programme |
| IIASA | International Institute for Applied Systems Analysis |
| IOC | Inter-Oceanic Confluence |
| IPCC | Intergovernmental Panel on Climate Change |
| ISG | Integerized Sinusoidal Grid |
| ISODATA | Iterative Self-Organizing Data Analysis Technique |
| ITCZ | Intertropical Convergence Zone |

| | |
|---|---|
| JRC | Joint Research Center |
| LAI | Leaf Area Index |
| LBA | Large Scale Biosphere-Atmosphere Experiment in Amazonia |
| LC | Land Cover |
| LCC | Land Cover Change |
| LCCS | Land Cover Classification System |
| LUE | Light Use Efficiency |
| MAIAC | Multiangle implementation of atmospheric correction |
| MC | Mean Compositing |
| MERIS | MEdium Resolution Imaging Spectrometer |
| MODIS | MOderate Resolution Imaging Spectroradiometer |
| MYC | Multi-Year Classification |
| NASA | National Aeronautics and Space Administration |
| NBAR | Nadir BRDF-Adjusted Reflectance |
| NDVI | Normalized Difference Vegetation Index |
| NDWI | Normalized Difference Water Index |
| NEE | Net Ecosystem Exchange |
| NIR | Near-infrared |
| NOAA | National Oceanic and Atmospheric Administration |
| NPP | Net Primary Production |
| OSFAC | Observatoire Satellital des Forêts d'Afrique Centrale |
| PA | Producer’s accuracy |
| PAR | Photosynthetically Active Radiation |
| PCA | Principal Component Analysis |
| POES | Polar Orbiting Environmental Satellites |
| PROBA-V | Project for On-Board Autonomy – Vegetation |
| R | Red band |
| SAA | Solar Zenith Angle |
| SPOT | Satellite Pour l’Observation de la Terre |
| SWIR | Shortwave Infrared |
| SYC | Synthesis of Yearly Classifications |
| SZA | Solar Zenith Angle |
| TRMM | Tropical Rainfall Measuring Mission |
| UA | User’s accuracy |

| | |
|---|---|
| UCL | Université catholique de Louvain |
| UMD | University of Maryland |
| UNCCD | United Nations Convention to Combat Desertification |
| UNFPA | United Nations Fund for Population Activities |
| USA | United States of America |
| VAA | View Azimuth Angle |
| VHR | Very High Resolution |
| VZA | View Zenith Angle |
| WGS84 | World Geodesic System 1984 |
| WIST | Warehouse Inventor Search Tool |

# Introduction

## 1. A global change context

***A recent global warming***

Since few last decades, the Earth is undergoing a period of considerable environmental changes. The Earth's surface and oceans have warmed at a speed with no historical precedent. The Intergovernmental Panel on Climate Change (IPCC, 2014) observes indeed a warming for combined land and ocean surface temperature of 0.85 [0.65 to 1.06]°C from 1880 to 2012, with the last three decades being successively warmer than any preceding decade over this period. Human influence on this climate change is clear. The dominant cause is the anthropogenic greenhouse gases (GHG) emissions that increase since the pre-industrial era, largely driven by economic and population growth, and that are now higher than ever despite a growing number of climate change mitigation policies (IPCC, 2014). In recent decades, these changes in climate have caused widespread impacts on natural systems, such as changing precipitation affecting water resources, and on human systems such as negative impacts on crop yields (IPCC, 2014).

***Land cover change affects biodiversity, atmosphere composition and climate***

The Earth's surface is also experiencing strong landscape changes that impact our global environment. A main cause of land cover change is the extreme weather and climate events locally devastating the vegetation, such as windstorms, droughts, wildfires or insect infestations. An increase in the frequency and intensity of these extreme events has been observed since about 1950 (IPCC, 2014). For instance, the past decade saw 410 million $m^3$ of wood felled in four major storms in Europe, a decade's worth of Amazonian carbon sequestration lost in severe droughts in 2005 and 2010, a record heat wave with forest fires affecting 23000 $km^2$ in Russia in 2010,

and the bark beetle pandemic since 2004 that has caused widespread tree mortality and significant forest loss over 130000 km² in British Columbia (Bellassen and Luyssaert, 2014) leading to a carbon source exceeding that of fire in Canada (Bright et al., 2012; Pouliot et al., 2014).

The major driver of land cover change is the human activities, e.g. deforestation for agriculture and mining, dam construction or urbanization. In addition, the extension of global croplands, pastures, plantations, and urban areas is combined with large increases in energy, water, and fertilizer consumption, along with considerable loss of biodiversity (Foley et al., 2005). Land use has generally been considered a local environmental issue, but it is becoming a force of global importance in recent decades. Even if land cover change due to human land use practices has occurred from millennia, the pace and intensity of change since the mid-20$^{th}$ century is unprecedented, driven by rapid and pervasive globalization and by world population growth (Ramankutty et al., 2006). The persistent land-use change is already thought to be causing the sixth mass extinction event in Earth's history (Pimm and Raven, 2000).

Besides a continuing wide-scale destruction, fragmentation and modification of natural habitats and ecosystems (Nunes et al., 2012), both natural and anthropogenic land cover change has substantial impact on atmospheric composition (e.g. $CO_2$ concentration) and climate. A forest conversion into cultivated lands or a windstorm damaging a forest both lead to large direct release of $CO_2$ to the atmosphere affecting the carbon cycle (e.g. by reducing vegetation productivity or destroying carbon stocks) but also to lagged ecosystems responses (e.g. increased tree mortality after severe droughts, dead wood decaying over decades) (Sitch et al., 2005; Houghton, 2010; Baccini et al., 2012; Reichstein et al., 2013). Globally, carbon stocks in forest biomass decreased by an estimated 0.5 Gt annually during the period 2005–2010, mainly because of a reduction in the global forest area (FAO, 2010). Thus, even a small shift in the frequency or severity of climate extremes could substantially reduce carbon sinks and may result in sizeable positive feedbacks to climate warming (Reichstein et al., 2013). The land use forcing of climate change may in some regions be of similar magnitude to those related to human emissions of GHGs (Bonan et al., 2008).

In addition to the effects on atmospheric level of $CO_2$ via biogeochemical mechanisms, land cover changes have biogeophysical

impacts on climate such as change in evapotranspiration, surface roughness and albedo (Sitch et al., 2005). They affect surface energy balance by changing the amount of solar energy reflected, the magnitude and duration over which absorbed energy is released as heat, and the amount of energy that is diverted to non-heating fluxes through evaporation (Turner et al., 2007; Vargo et al., 2013). Considering land cover change impacts on both biogeophysics and biogeochemistry, Sitch et al. (2005) calculated the relative role of land cover change in atmospheric $CO_2$ growth to represent 9-22%, the remainder attributable to fossil fuel emissions.

### *Vegetation is a key component of the global change*

In this context of global change, there is considerable concern at how these changes may affect the Earth's ecosystems, but also in turn how these system responses may feed back to accelerate or decelerate global change (Malhi and Wright, 2004). As a major carbon sink, vegetation is a key component of the global carbon cycle to mitigate climate change arising from the build-up of GHG in the atmosphere and provides a negative feedback in the climate/carbon-cycle system (Lewis, 2006; Reichstein et al., 2013; Richardson et al., 2013; IPCC, 2014). Indeed, while local events strongly impact forest carbon stocks, the world's terrestrial vegetation have absorbed as much as 30% (2 Pg C $y^{-1}$) of annual global anthropogenic $CO_2$ emissions in the past few decades (Pan et al., 2011). Gross primary productivity (GPP) is the largest global carbon flux and is estimated to be 123 Pg C $y^{-1}$ (Beer et al., 2010). Also, in addition to the carbon cycle, the world's forests influence climate through albedo, evapotranspiration, and other processes that affect the energy budget, the hydrological cycle, and atmospheric composition (Bonan, 2008).

But in turn, a changing climate (increase in temperature, changes in precipitations) may adversely affects vegetation and ecosystem functions, with consequences on vegetation distribution, composition, biodiversity, productivity, and phenology. These complex forest-atmosphere interactions can dampen down or amplify anthropogenic climate change.

### *Vegetation phenology under global warming*

Phenology is both a response to and a driver of global changes (Richardson et al., 2013). Indeed, influencing the seasonal and inter-annual variability of

albedo, canopy conductance, and fluxes of water, energy and carbon between the biosphere and atmosphere through biogeochemical cycles, vegetation phenology controls numerous land surface feedbacks to the climate system and has the potential to influence both regional-scale weather patterns and, in the longer term, global climate system (Menzel, 2002; Migliavacca et al., 2012; Richardson et al., 2013).

Inversely, changes in local temperature and precipitation have the potential to affect phenology, as the timing of phenological phases is driven by the weather and the climate (Morisette et al., 2009). A change in phenology, e.g. a shorter growing season and lower annual photosynthetic activity, could alter the biosphere-atmosphere exchange of $CO_2$, water vapour and energy and the annual carbon uptake. Altered forests functionality could, in turn, affect a range of biogeochemical processes with dangerous cascading effects on the climate system that could dramatically accelerate and intensify climate change (Lewis, 2006; Koltunov et al., 2009).

The phenological cycle is a key process that determines surface biophysical parameters (e.g. albedo, $CO_2$ flux, latent and sensible heat flux) required by environmental models (Menzel, 2002). Despite being a critical component in the carbon cycle, current Earth system models do not place sufficient emphasis on the simulation of accurate vegetation phenology or on the seasonality of ecosystem processes, with consequence that many of the important feedbacks to the climate system that are affected by vegetation phenology are likely misrepresented in such models (Richardson et al., 2013).

### *The fate of tropical rainforests is uncertain*

Among the tropical, temperate and boreal forest biomes, tropical rainforests are particularly under-studied concerning vegetation phenology and its drivers (Richardson et al., 2013). However, the highest exchange of $CO_2$ between the land and the atmosphere occurs in tropical forests, storing 55% of the current carbon stock in the world's forests (Pan et al., 2011) and accounting for about one-third of global terrestrial photosynthesis (Bonan et al., 2008; Beer et al., 2010). The Amazon and Congo basin are respectively the first and second largest continuous area of tropical rainforest in the world. These vast forests are thus a significant component of the Earth's carbon budget with strong influence on regional and global climate, as small

variations in their net carbon balance from climate or human driven perturbations could result in significant storage or release of carbon to the atmosphere (Rice et al., 2004; Lewis, 2006; Malhi et al., 2008; Aragão et al., 2014).

Even if there is evidence that undisturbed tropical forests are currently global carbon sink both in the Amazon (Phillips et al., 2008; Aragão et al., 2014) and Congo (Lewis et al., 2009; Fisher et al., 2013; Valentini et al., 2014) basins, the fate of these forests is uncertain as their resilience to drought, interactions of fires, warmer temperature, atmospheric rise of $CO_2$, or effects of small-scale deforestation on clouds and precipitation, are not well understood (Lewis, 2006; Samanta et al., 2010; Bonan et al., 2008; James et al., 2013; Fisher et al., 2013). For instance, since the mid-1970s, a substantial and rapid warming of 0.26°C per decade is evident in all tropical rainforest regions, with decreasing precipitation especially in Central Africa (Malhi and Wright, 2004; Fisher et al., 2013), but the vulnerability of rainforests to higher temperature is debated (James et al., 2013). Zhou et al. (2014) observed a widespread decline in forest greenness over the past decade in the Congo basin that may be attributable to this long-term drying trend. Warming may have a direct effect on rainforest trees by inhibiting photosynthesis, but the thermal tolerance of most species is poorly understood (James et al., 2013). While Nemani et al. (2003) show an increase in net primary production of Amazon rainforest in response to climate change owing mainly to decreased cloud cover and the resulting increase in solar radiation, Malhi et al. (2008) argue that the Amazonian tropical forests are vulnerable to a warmer and drier climate, which may exacerbate global warming through a positive feedback that decreases evaporative cooling, releases $CO_2$ and initiates forest dieback (Bonan et al., 2008). Drought sensitivity of the Amazon forest has already been observed during strong drought events in 2005 and 2010 causing high tree mortality and associated biomass loss (Phillips et al., 2009; Lewis et al., 2011). On the contrary, atmospheric $CO_2$ fertilization may stimulate the GPP across the tropical forest biomes (Friedlingstein et al., 2010; Ciais et al., 2011; Valentini et al., 2014), potentially causing a change in the trees phenology, but that additional growth may be limited by the availability of other nutrients, such as nitrogen (Tollefson, 2015).

# 2. Optical satellite long time series

To face environmental challenges in this period of rapid human-driven changes and to assist policy makers for the protection of our environment, it is critical to improve our knowledge about the land surface and its dynamics at global scale. Since the early 1970s, satellite remote sensing offers the opportunity to better understand and monitor the Earth's surface over large areas.

Among the numerous Earth observation satellites that have been launched, with varying spatial, temporal and spectral resolutions, coarse to moderate resolution sensors have the advantage of a highly consistent spatial and temporal coverage, compared to high spatial resolution sensors limited in observations frequency. In addition to their global coverage, their high temporal resolution enables to accumulate near-daily multi-spectral images over years and to overcome atmospheric perturbations. This accumulation of successive images leads to long time series that are ideal to provide consistent information on land surface dynamics, whether for observing long-term regional and global environmental changes or for determining vegetation seasonality in inaccessible areas. The three following sensors are the most commonly used in long-term vegetation monitoring applications at regional to global scales. They are all passive sensors as they measure electromagnetic radiation naturally reflected or emitted from constituents of the Earth's surface, atmosphere and clouds.

The first coarse resolution space-borne sensor is the Advanced Very High Resolution Radiometer (AVHRR). Onboard the National Oceanic and Atmospheric Administration's (NOAA's) Polar Orbiting Environmental Satellites (POES) since 1981, and recently on the MetOp series of satellites, the scanner provides images compiled in time series at 1°, then 8 km and 1 km spatial resolution. With data accumulated over more than 30 years, it is the longest time series available on a global scale which makes it particularly relevant to study climate change and environmental issues. However, the primary purpose of these instruments was to determine cloud cover and the surface temperature. Thus, the sensors measure the reflectance and emission of the Earth in relatively broad spectral bands much affected by atmospheric effects.

Launched in 1999 and 2002 aboard the Terra and the Aqua satellites by National Aeronautics and Space Administration (NASA), the Moderate Resolution Imaging Spectroradiometer (MODIS) offers improvements in spectral and spatial performances, capturing data in 36 finer spectral bands ranging from 0.4 μm to 14.4 μm at 250 m to 1 km resolution. It was designed to provide measurements for monitoring large-scale dynamics such as the Earth's cloud cover, the land surface radiation budget, and the processes occurring on the oceans and the land. The measurement consistency is affected at the pixel level by the instrument spatial response variability due to the whiskbroom scanner effects.

The geometric quality of images has been improved with the VEGETATION instrument, launched in 1998 and 2002 aboard Satellite Pour l'Observation de la Terre (SPOT) 4 and 5 satellites. This push-broom sensor has a data acquisition system equipped with a linear charge-coupled device array technology which produces high-quality images with a reduced distortion, making more comparable, at the pixel level, the reflectance measurements from one date to another over many years. The VEGETATION programme was the fruit of collaboration between Belgium, France, Italy, Sweden and the European Commission and was conducted under the supervision of the CNES (National Centre for Space Studies, France). It was conceived to allow daily monitoring of terrestrial vegetation cover. Thanks to the instrument swath of 2250 km, almost a global coverage is acquired every day in four spectral bands in the visible (blue, red), near-infrared, and middle-infrared, specifically selected to characterize the main features of plant canopy. The VEGETATION 1 and 2 on board SPOT satellites have been operational until May 2014 but the continuity of the programme is ensured by the small Belgian satellite PROBA-V launched on May 2013, observing daily the land surface and vegetation at similar spectral wavelengths to those of SPOT-VEGETATION with an improved spatial resolution (300 m and 100 m for the central camera), and by the Sentinel-3 satellites to be launched in the framework of the European Copernicus programme.

# 3. Global land cover mapping

Monitoring the state of the Earth surface is essential for assessing many environmental issues such as biodiversity loss and natural resource depletion for driving sustainable development policies. As explained above, through many biophysical characteristics, such as albedo, emissivity, roughness, photosynthetic capacity or transpiration, the land surface has considerable control on the biogeochemistry of the Earth system which in turn significantly influences the climate system. Indeed, the sensitivity of the cycling and exchange of carbon and water fluxes to climate variability is directly coupled, both in space and time, to land cover, land use and the distribution of vegetation (Poulter et al., 2011).

In this context, land cover information, that describes the land surface through discrete land cover classes, is particularly needed at global scale as baseline for the land surface parameterization of climate and Earth system models. Land cover is identified as one of the 50 Essential Climate Variables (ECVs) defined by the Global Climate Observing System (GCOS, 2010) and is defined as "the physical and biological cover over the surface of land, including water, vegetation, bare soil, and /or artificial structures" (Di Gregorio, 2005).

## *3.1. Current global land cover maps*

Remotely-sensed data allowed a considerable improvement in global land cover mapping. Indeed, 30 years ago, global land cover maps were still based on preexisting maps and atlases derived from field investigations, national mapping programmes or compilations of published sources (Matthews, 1983; Olson and Watts, 1982; Wilson and Henderson-Sellers, 1985). They presented strong limitations and considerable disagreement compared with each other in the relative percentages and spatial distribution of land cover types (Townshend et al., 1991).

Thanks to moderate spatial resolution satellite data, and their synoptic and repetitive view, global land cover data sets showed a rapid development in the past decades. These products recognize a limited set of vegetated and non-vegetated land cover types, based on both multispectral signals and the change in those signals through an annual cycle (Strahler et

al., 2006). The most significant global land cover mapping initiatives are briefly presented hereafter.

With the objective to produce coarse-resolution global land cover maps usable in climate models, the three first global land cover maps based on remotely-sensed data were created since the mid-1990s by researchers of University of Maryland (UMD) using 1 year of AVHRR images at 1°, 8-km and 1-km spatial resolution respectively (DeFries and Townshend, 1994; DeFries et al., 1998; Hansen et al., 2000). Again with 1-y AVHRR data, the International Geosphere-Biosphere Programme (IGBP) Discover map was generated at 1-km spatial resolution but with a legend of 17 classes against 13 for the previous ones (Loveland et al., 2000).

Then, the data improvement thanks to spectral, spatial, geometric and radiometric performances of MODIS was exploited by Boston University to build global land cover maps at 1-km and 500-m spatial resolution, the MODIS Collection 4 land cover type product and the Collection 5 product with revised algorithms and datasets (Friedl et al., 2002; Friedl et al., 2010). Among other improvements, the near infrared (NIR) spectral band of MODIS is finer than AVHRR sensor, allowing a better discrimination of vegetation types.

Using one year of daily 1-km SPOT-VEGETATION data, the Global Land Cover 2000 (GLC2000) map was created by combining and harmonizing 19 regional products realized by international experts, coordinated by the Joint Research Center (JRC) of the European Commission (Fritz et al., 2003; Bartholomé and Belward, 2005; Mayaux et al., 2006). The consistency and harmonization of the regional classifications has been allowed by the use of a hierarchical legend, the UN-FAO Land Cover Classification System (LCCS) (Di Gregorio, 2005). The regional legends has been translated to a global legend of 22 land cover classes thanks to the hierarchical set of LCCS classifiers and attributes to describe the land cover. However, this bottom up approach induces inconsistencies due to separated regional mapping and is not reproducible.

This shortcoming was fulfilled with the GlobCover 2005 and 2009 maps supported by the European Space Agency (ESA) that are produced on an automated way as an operational service, allowing regular updating. With a spatial resolution three times sharper than any previous satellite map, using 300-m data from the Envisat's Medium Resolution Imaging Spectrometer (MERIS) instrument, they give the most detailed portraits ever of the Earth's

land surface (Arino et al., 2008; Defourny et al., 2009a; Arino et al., 2010; Bontemps et al., 2011). The 22 classes legend was based on the LCCS in line with the GLC2000 land cover map.

## *3.2. A problematic "single-year" approach*

Various intercomparison studies of these satellite-based global land cover products was conducted (DeFries et al., 1998; Hansen et al., 2000; Hansen and Reed, 2000; Latifovic and Olthof, 2004; Giri et al., 2005; Jung et al., 2006; McCallum et al., 2006; Herold et al., 2008; Fritz et al., 2008; Friedl et al., 2010; Kaptué Tchuenté et al., 2011, Pflugmacher et al., 2011). These comparisons revealed general patterns of similarities but also considerable inconsistencies and discrepancies, raising strong uncertainties in the use of these products (Jung et al., 2006). For instance, uncertainty in area estimation of land cover classes can lead to large differences in terrestrial $CO_2$ fluxes estimates by dynamic vegetation models, particularly for forests classes (Quaife et al., 2008; Valentini et al., 2014). Despite their uncertainties, global land cover maps are used in many applications. Improving their quality is therefore of paramount importance in order to increase their usefulness (Bontemps et al., 2012a).

The large proportions of inconsistencies among the different global datasets cannot been explained by land cover change (Giri et al., 2005; Jung et al., 2006; McCallum et al., 2006; Herold et al., 2008; Friedl et al., 2010; Kaptué Tchuenté et al., 2011; Pouliot et al., 2014) as they substantially exceed the annual rate of any land cover change. Indeed, the most rapid change occurring nowadays is tropical deforestation with maximum yearly rates of around 3.5% in Brazil and Indonesia (Hansen et al., 2008). Among several factors responsible for the discrepancies between the maps, the sensitivity to the period of observation is highlighted. Indeed, all published global land cover products share one common characteristic: they consider only one single annual cycle of satellite data in their classification which is obviously not enough to cope with land surface inter-annual variability. The current land cover representation and mapping techniques are called into question in Bontemps et al., (2012a) to specifically focus on the critical need of stable products expressed by climate users. They suggest the use of multi-year data sets as a new approach to help land cover observation to evolve and to deal with the issue of sensitivity to annual remotely sensed time

series. Such an approach has been considered in the context of the ESA Land Cover component of the Climate Change Initiative (CCI). At a more regional level, time series analysis of multi-year dataset has been used by Gond et al. (2013) for the Congo basin land cover mapping.

# 4. Global land cover change detection

Land change science has emerged as a fundamental component of global environmental change and sustainability research (Turner et al., 2007). The importance of mapping, quantifying and monitoring the increasing change of the land surface, caused by natural processes and human activities, is now widely recognized. There is a considerable interest in deriving land cover change information for important societal concerns, for instance in terms of biodiversity impacts as well as for climate change studies. Indeed, land cover change can be a cause and a consequence of climate change (Turner et al., 2007). A better understanding of landscape changes due to human activities specifically is critical information to help policymakers to limit or anticipate environmental damages, such as large-scale deforestation that is now decimating rainforests, through the development of effective sustainable management practices (Zhang et al., 2014).

Land cover change information is also required to evaluate and model the influence of changes on environmental processes (Pouliot et al., 2014). At global scale, land cover change studies are particularly needed as the net flux of carbon from land use and land cover change is by far the most uncertain term in the global carbon budget (Lewis, 2006; Ramankutty, 2007; Houghton et al., 2012).

## *4.1. Current land cover change detection methods*

Singh (1989) defines change detection as "*the process of identifying differences in the state of an object or phenomenon by observing it at different times*". With their high temporal frequency, synoptic view and wide range of spatial and spectral resolution, the data from remote sensing satellites provide opportunities to acquire suitable information for change

detection studies (Hussain et al., 2013). In the last 30 years, a large number of change detection methodologies, techniques and algorithms, utilizing remotely sensed data, have been developed to identify the geographical location and type of changes. Numerous researches have been conducted to study land cover change from local to regional and global scales, relying on the alteration of the spectral behaviour to detect land surface changes.

Recent change detection reviews (Hussain et al., 2013; Tewkesbury et al., 2015) organized the many change detection approaches according to units of image analysis and comparison methods used to highlight change. The following description summaries their main conclusions. Typically, to identify change, the input images are compared and a decision is made as to the presence or degree of change (Tewkesbury et al., 2015). The analysis units that are compared over time to highlight change are principally individual image pixels and image-object created previously from segmentation of the image, but could also include groups of pixels, vector polygons or a combination of these. Comparing pixel intensities for change detection is a simple concept applying arithmetic operations to continuous band radiance or reflectance, or integer class labels. However, the pixel-based techniques are not considered appropriate for Very High Resolution (VHR) imagery because they face a challenge posed by higher spectral variability, mixed pixels and image registration issues on these VHR data, producing spurious change pixels. The object-based change detection techniques are considered more suitable for VHR image data as they reduce these effects. A segmentation process partitions an image into homogenous objects which are spectrally similar and spatially adjacent (Bontemps et al., 2008). Image objects get richer information such as texture or shape and allow the exploitation of the spatial context. Different techniques exist, such as the image-object overlay comparing objects segmented from one image, the image-object comparison where images are segmented independently then compared, or the multi-temporal image-object where image segmentation is applied to stacked multi-temporal images. However, in object-based analysis, the segmentation scale and image resolution must be carefully chosen so as to adequately define change features of interest, which is not straightforward. The size of the target change must be known prior to perform the analysis.

A variety of different methods of comparisons have been developed, based on the pixel-based and object-based approaches. These methods can

be categorized in pre-classification and post-classification techniques. The pre-classification approach is mainly based on the direct and continuous analysis of spectral signature (radiance or reflectance values), for instance in SPOT-HRV, Landsat images and MODIS time series (Desclée et al., 2006; Bontemps et al., 2008, 2012b; Duveiller et al., 2008; Ernst et al., 2013; Hansen et al., 2013; Jin et al., 2013; Mayaux et al., 2013; Brink et al., 2014; Huang and Friedl, 2014; Pouliot et al., 2014; Zhang et al., 2014). Among many techniques, the most common are simple arithmetic operations, such as subtraction or division applied to multi-temporal imagery depicting radiance or vegetation indices differences, change vector analysis (CVA) and principal component analysis (PCA). In CVA, the pixel values are treated as vectors of spectral bands. The magnitude of the change vector gives the degree to which the image radiance has changed, containing limited thematic content, while the direction indicates the types of change. If this technique allows the simultaneous analysis of multiple image bands, a limitation is that both the magnitude and direction can be ambiguous. Data transformation such as PCA is a method of data reduction by suppressing correlated information, supposed to be the areas of no change, and highlighting variance, corresponding to areas of change. When applied to a multi-temporal stack of remotely sensed images, there is the potential to highlight image change, since it should be uncorrelated between the respective datasets. Transformations are however scene dependent and may prove difficult to interpret. The application of spectral-based techniques at large scales is challenged by the variability in the spectral properties of the images in space and over time, and strongly requires the implementation of radiometric calibration and atmospheric corrections at broad spatial and temporal scales (Bontemps, 2010).

The post-classification and direct classification approaches compare independent classifications to derive change information (Chen et al. 2012; McRoberts, 2013; Sexton et al., 2013). Using classifications produced over a year avoid radiometric change related to illumination and viewing angles, phenology or atmospheric conditions that cause spurious change detection. It allows to directly looking at semantic changes. Post-classification change detection is the process of overlaying coincident thematic maps from different time periods to identify changes between them. The distinct advantage of this technique is that the baseline classification and the change transitions are explicitly known. It is a thematically rich technique able to answer specific change questions, making it suitable for a range of different

applications. However, it is limited by map production issues and compounded errors. Furthermore, input maps may be produced using differing data and algorithms. In this case, a distinction must be made between classification inconsistencies and real change. Another technique is the direct classification of a time series of images. However, deriving training datasets for such a classification can by very challenging and supervised approaches can prove unresponsive to small magnitude change pattern. Less frequent are the hybrid analysis that refers to the use of two or more methods for change detection (Griffiths et al., 2013).

Appropriate selection of unit of analysis and comparison method is related to the objective of the study, depending for instance on the level of change information needed (i.e. simple "change/no-change" information or a detailed change direction), on the size of the study and on the spatial resolution.

## *4.2. Challenges in observing land cover change*

Remote sensing researches mainly focused on detection of land cover change in order to highlight and sometimes to delineate the area of change. Detecting where a change is occurring is only a part of the answer. Another challenge in land cover change detection is first to identify the fate of the changed area, for example the fate of cleared land (Houghton et al., 2012). Indeed, for many applications, detailed information regarding the land cover class observed after change is needed (Ramankutty et al., 2006), but a simple binary change vs. no change is often described as sufficient for many studies (Hussain et al., 2013). Secondly, very few studies provide information on the year of change, although it is critical information for climate models. Thirdly, most of land cover change studies focus solely on forest change, because of the current focus of environmental monitoring concerning the global carbon cycle and biodiversity loss (Hansen and Loveland, 2012). Another reason is also the fact that this is easier to observe processes of forest conversion with regards to other land cover transition. However, other types of change such as urbanization, cropland extension, dryland degradation or lake and waterways drying up are also transforming the planet's surface with critical environmental impacts (Foley et al., 2005; Lepers, et al., 2005), and deserve dedicated studies. Finally, among many change detection studies, most are completed at local, national or regional scale. Except for forest change (Hansen et al., 2013), our understanding of

the extent of land cover change is limited (Giri et al., 2013) and significant uncertainties persist about the global rate and patterns of change of agricultural lands, drylands, wetlands, built-up areas or water, among others.

Launched in 1972 by NASA, Landsat has become the data source of choice for many change detection studies, especially since the opening of the USGS Landsat archive in 2009 that has enabled exploration of methods for higher-frequency, time-serial monitoring of land cover dynamics (Sexton et al., 2013). However, while such data cover the globe, working with such high resolution (30 m) raises numerous challenges for continental to global scale studies. For instance, the low temporal frequency coupled with the frequent cloud cover and phenological effects induces problems in the resulting scene coverage, and the effort involved in classifying thousands of images is consequent (Ramankutty et al., 2006; Griffiths et al., 2013).

Unlike high resolution data, medium resolution long time series provide consistency in image acquisition to get cloud-free observations, a full phenological information during the year to distinguish land cover types, and a global coverage. In addition, it allows avoiding radiometric change related to illumination or viewing geometry that are not reflecting actual change on the ground, for instance through a bi-temporal comparison with high resolution images (Tewkesbury et al., 2015). They are under-used to derive change delineation and quantification at global scale. Although their spatial resolution clearly limits their ability for detecting small changes, they could serve as a convenient and suitable alternative to fulfill challenges such as the detection of the year of change and the fate of the changed area, for all types of land cover changes and at global scale.

# 5. Vegetation phenology

Phenology is the study of recurring life-cycle events that are initiated by environmental factors (temperature, precipitations, solar radiation), such as the onset of growth and photosynthesis in the spring and the senescence and abscission of deciduous vegetation in the fall (Morisette et al., 2009).

Observing and documenting life cycle stages of plants and animals and their timing have been necessity for human survival throughout history

as phenological observations were key to successful hunting and farming (Demarée, 2009). Today phenological observation has become prime source of indicators documenting altered life cycles due to environmental changes. Indeed, the importance of phenology to the science of global change has been increasingly acknowledged over the 15 last years when it was demonstrated that plant phenology, which was known to be sensitive to year-to-year weather variability, could also serve as an important early indicator of the long-term biological impacts of climate change on terrestrial ecosystems (Reed et al., 2009; Richardson et al., 2013), with springtime phases being particularly sensitive to temperature (Menzel, 2002). Vegetation phenology is now recognized to be essential to our understanding of biogeochemical cycle and the climate system (Caldararu et al., 2014). Given the potentially important role of phenology in climate through feedback processes, the accurate representation of phenological processes as part of the land surface–atmosphere interaction is particularly important in climate models (Morisette et al., 2009; Richardson et al., 2013).

## *5.1. Remote sensing phenology*

Plant phenology is investigated through different approaches at various scales from individual plant observation, to ground-based environmental sensor instrumentation using digital web-cam or eddy covariance flux tower for $CO_2$ measurements, and to aerial and in orbit remote sensing observations. Field monitoring devices that can provide phenological information are becoming less expensive, easier to use, and smaller in size. Nevertheless, satellite imagery available globally with a daily repeat cycle provides a key source for monitoring phenological events of the vegetated land surface over large areas and in regions with limited accessibility such as tropical forests (Reed et al., 1994; Morisette et al., 2009). The study of vegetation phenology using satellite remote sensing has experienced considerable progress over the past two decades (Reed et al., 2009).

The term “land surface phenology” refers to the seasonal pattern of variation in the properties of vegetated land surfaces observed from remote sensing, at the pixel scale (Friedl et al. 2006). The spectral properties of plant canopy are retrieved over time in the visible (0.4 to 0.7 μm) and the near infrared (0.7 to 1.3 μm) parts of the wavelength spectrum that are the most suited to follow vegetation phenology. Many changes in anatomical, biochemical and physiological properties of leaves are associated with

changes in the spectral quality of light transmitted, reflected and absorbed by leaves (Roberts et al., 1998). When the vegetation is growing, plant photosynthesis, also known at the ecosystem level as gross primary production (GPP) through the assimilation of carbon, is reactivated. During this period, electromagnetic radiation in the 0.6 - 0.7 μm wavelengths is absorbed by pigments such as carotenoids and chlorophyll for photosynthesis, and thus the reflectance of the canopy decreases in the visible, while the near infrared radiation is scattered by the internal structure of plant leaves, and thus the reflectance in the near infrared increases. When the vegetation become senescent, the reflectance decreases firstly in the near infrared, and then increases in the visible when the leaves begin to turn yellow and dry out.

In phenology remote sensing, greenness is commonly quantified through a vegetation index that combines two or more spectral bands. These spectral transformations are designed to enhance the green vegetation signal related to phenological development, to minimize the soil background, to reduce the atmospheric effects, and to provide a degree of image normalization for comparison (Reed et al., 1994; Huete et al., 2002). A number of vegetation indices have been created to study vegetation phenology. The more commonly used is the Normalized Difference Vegetation Index (NDVI) (Tucker, 1979) that measured greenness with the ratio of reflectance in red and near infrared bands. It is being used since the beginning of the AVHRR Program in 1981 and it is well recognized for the characterization of the chlorophyll activity of vegetation cover over time. However, this index presents limitations especially in tropical regions. Indeed, the dense vegetation with leaf area index (LAI) of 3-4 induces saturation problems due to high values of chlorophyll activity, and atmospheric aerosols cause artefacts in NDVI variation throughout the year (Huete et al., 2002; Xiao et al., 2003; Kobayashi et al., 2005). To overcome these limitations, the Enhanced Vegetation Index (EVI) has been developed (Huete et al., 1997, 2002). It enhances the vegetation signal with improved sensitivity in high biomass and it reduces the atmosphere influences thanks to the additional blue band onboard advanced optical sensors like VEGETATION or MODIS.

Thanks to the recording of vegetation indices time series and the analysis of their seasonal change, remote sensing is thus able to detect foliage phenology. The annual cycle of plants as observed by remote sensing might then be a key proxy to understand the rates of $CO_2$ exchanges

measured by flux towers (Menzel, 2002) and GPP, one of the major processes controlling land-atmosphere $CO_2$ exchange (Beer et al., 2010). An essential question is however to what extent the phenological growing season corresponds to the carbon uptake period and to what extent the greenness of an area is linked to forest GPP. The connection of eddy covariance measurements of $CO_2$ fluxes and long-term phenological observations would offer good possibilities for upscaling carbon fluxes, which can be measured at only few expensive experimental sites (Menzel, 2002).

Like $CO_2$ fluxes measurement, ground observation of phenology and satellite-derived measure of surface greenness provide distinct but complementary information. Ground measurements are realized on individual plants and refer to specific life-cycle events corresponding to the traditional definition of vegetation phenology stages, such as budbreak, flowering, fruiting or leaf senescence. They generally do not provide a spatially integrated response pattern that depends on the mixture of species in the landscape, but rather focus on developmental switches of individual species (Badeck et al., 2004). Space-based observations, in turn, provide species-averaged information at moderate to coarse spatial resolution emphasizing dominant vegetation elements and focusing on the timing of vegetation development (growth, senescence, dormancy) (Badeck et al., 2004; Morisette et al., 2009). Also, remote sensing captures the continuous expression of phenology patterns through the gradual changes in reflectance, while ground observations are limited to the development stages involving a qualitative change. There is a great potential for a better understanding of phenological cycles by combining the strengths of both ground observation and remote sensing. Challenges remain nevertheless in reconciling scales of observations and establishing relationships between the annual course of greenness observed by remote sensing and stages of leaf phenology (e.g. leaf flushing or leaf shedding) observed from the ground (Badeck et al., 2004), especially where the magnitude of phenology is low like in tropical rainforests.

## *5.2. Tropical rainforest phenology under debate*

In 2003, an unexpected seasonal pattern of tropical forests was discovered in the Amazon region thanks to eddy flux measurements in Tapajo´s National

Forest near Santarém, Brazil by Saleska et al. The net ecosystem exchange (NEE) of $CO_2$ measured showed that the forest acts as a carbon source in the wet season and as a carbon sink in the dry season, which was the opposite to the seasonal cycles of model predictions assuming dry season declines in canopy photosynthesis because of water limitation. Nowadays, most ecosystem models still show deficiencies in reproducing the measured seasonal pattern of $CO_2$ fluxes found in Saleska et al. (2003) and consequently they consider tropical rainforest with a highly simplified or even no seasonality (Poulter et al., 2009; Verbeeck et al., 2011; Bradley et al., 2011). However, a small seasonal effect on vegetation phenology in the vast Amazon forests can have a significant impact on carbon fluxes.

This discovery led to numerous local or basin-wide satellite-based studies in the Amazon region. They permitted to observe modest but significant phenological cycles with an increase of the EVI during the dry season, interpreted as a higher photosynthetic activity (Xiao et al., 2005; Huete et al., 2006; Xiao et al., 2006; Poulter and Cramer, 2009; Pennec et al., 2011; Samanta et al., 2012; Wagner et al., 2013; Biudes et al., 2015) and coherent with the increase of $CO_2$ uptake measured at the flux tower. This recent interest in tropical forests gave rise to promising improved models taking into account tropical wet forest phenology (De Weirdt et al., 2012; Caldararu et al., 2014).

To anticipate the response of tropical forests to climate change, there is first a need to better understand the magnitude and the timing of vegetation phenology but also the mechanisms which control these seasonal cycles in tropical rainforests. Plant production requires sufficient light, water, oxygen, mineral nutrients and suitable temperature. Significant seasonal variation in any of these factors could provide a selective force on phenological behavior (Van Schaik et al., 1993). Plants may maximize production in a seasonal climate by avoiding the production of new leaves before or during unfavorable periods (e.g. water stress or biotic factors such as the abundance of herbivores), or by producing new leaves to coincide with the onset of periods of favorable conditions (e.g. high radiation) (Van Schaik et al., 1993). In temperate zones, the reproductive cycle of forests is well understood and primarily controlled by temperature and day length (Menzel, 2002). In winter, low temperature and short photoperiod limit cambial activity, corresponding to leaf fall, and cause dormancy in most plants. Then in spring, reproductive and leaf cycles resume when temperature and photoperiod rise again. Given the clearly high dependence

of these forests on climate seasonality, the response of phenology to climate change is widely studied across temperate and boreal ecosystems in Northern Hemisphere regions (Badeck et al., 2004; Menzel et al., 2006; Rosenzweig et al., 2007; Jeong et al., 2011; Migliavacca et al., 2012). However, in tropical zones, the link between phenological phases and their environmental drivers remains poorly understood (Huete et al., 2006; Richardson et al., 2013), and is still source of controversy. The timing of phenological events is less obvious as the canopy is composed of mixed-age leaves, and the ground observations are sparse.

Based on EVI dynamics and other indices such as LAI, recent researches suggest that the availability and seasonality of solar radiation could be the most important driving factor of rainforests phenology and productivity in absence of seasonal soil moisture stress (Xiao et al., 2006; Huete et al., 2006; Myneni et al., 2007; Hutyra et al., 2007; Bradley et al., 2011; Caldararu et al., 2012; Gond, et al., 2013; Wagner et al., 2013 and Biudes et al., 2015). In the same time, the consistency of remotely-sensed observation to detect phenology in the Amazon region is however questioned. Galvão et al. (2011, 2013), Moura et al. (2012) and Morton et al. (2014) claim that seasonal changes in EVI are not caused by biophysical changes in leaf reflectance, leaf area or vegetation productivity driven by radiation, but instead by a combination of shadowing effects within the canopy and the way that sensors observed the forest during the dry season causing optical artefacts. To them, Bidirectional Reflectance Distribution Function (BRDF) effects, such as variation in sensor view angle, view direction and sun elevation, introduce significant intra-annual EVI variability while the Amazon forests actually maintain a constant greenness throughout the dry season. Moreover, some uncertainties remain on vegetation indices concerning the influence of atmospheric contamination from biomass burning and sub-pixel perturbations by little clouds, both frequent in tropical regions. These difficult atmospheric conditions amplify the challenge to detect consistent temporal patterns of greenness in moist tropical regions using optical remote sensing.

While the debate concerning EVI interpretation is very active for the Amazon forests, the question is still hardly studied in Central Africa. The African tropical forests are one of the most under-researched regions in the world. They have been relatively neglected compared to the other tropical forests, for a number of reasons including challenging and fragmented

politics, civil conflicts and logistical as well as infrastructure challenges (Malhi et al., 2013). Very few studies explored the phenological characterization of tropical forests over the Congo basin using remote sensing data, maybe because of the persistent cloud cover preventing clear images of some Congo Basin areas. Nevertheless, two recent studies bring crucial elements for the EVI interpretation in tropical rainforests. Viennois et al. (2013) showed in West-Central African forests that a large share of the variability in canopy reflectance as captured by the MODIS EVI is due to variations in the proportion of leaved trees in the upper canopy, and Gond et al. (2013) found higher MODIS EVI values in Central Africa when solar radiation is maximal.

# 6. Scope and objectives

Facing environmental challenges in a global change context requires improving our knowledge about the land surface and its dynamics that play a major role in the climate system and the global biogeochemical cycles. The overall objective of the thesis is to understand and exploit the multispectral surface reflectance variability as observed by long term daily time series in order to characterize the land surface dynamic over seasonal and multi-annual scales.

As explained above, the land cover is a key information for land surface parameterization of Earth system models as well as a key source of data to assess the natural and anthropogenic impacts through multiannual land use/ land cover change. Moderate resolution satellite time series are the global and systematic data sets to map the land cover and quantify the change, but the annual land cover maps generated until now are known to be sensitive to the period of observation. There is thus a need to improve this current land cover mapping approach, using a multi-year data set such as long time series of Earth observations. The latter offers today the best opportunity to build a consistent global land cover characterization, but also to describe the evolution of land surface over time. Global land cover change detection suffers indeed from many lacks. The interest of change studies focus generally on forest cover dynamics to the detriment of other land cover types, the year of change remain undetermined in many cases, and the fate of

the land cover after a disturbance is generally unknown. A pressing need is to develop robust, efficient and accurate automated or semi-automated method necessary for cost effectively monitoring land cover changes at the regional to global scales (Jin 2013).

At the seasonal scale, the vegetation phenology is driving the carbon, water and energy fluxes and can become a sensitive indicator of climate evolution as described previously. Earth observation is particularly appropriate to assess the phenology in remote areas like tropical rainforests where limitations such as accessibility and lack of field measurements are prevalent. In principle, long time series at medium resolution offer the advantage of a highly consistent spatial and temporal coverage of land observation over extended periods of time, ideal to describe vegetation phenology. Given the global importance of tropical forests on the climate system, and their vulnerability to climate change, it is of crucial importance to understand the carbon dynamics of these forests. As it affects strongly GPP, studying leaf phenology through remote sensing is one important way to better understand these carbon fluxes. However, as reported from the literature, the capabilities of optical remote sensing to monitor tropical rainforest foliage phenology are currently under debate.

In order to extract reliable land surface dynamics information over a multi-year period, the SPOT-VEGETATION time series spanning from 1999 to 2011 is selected for three major reasons. The first one is the consistency of the pixel footprint along the swath and over time making the time series analysis very consistent. Its very high geometric and radiometric performances are the two others key assets for long-term pixel-based monitoring. In addition, the great potential of this SPOT-VEGETATION time series is still to be exploited at the regional and global scales.

To address the overall objective, four specific objectives have been formulated.

***1. Building a multi-year global land cover map can reduce the sensitivity to the inter-annual variability and to the year of observation as reported in current annual land cover maps***

The accumulation of global long-term time series of Earth observation is an opportunity to improve global land cover mapping that currently suffers from its single year strategy. The objective is to develop a new mapping

approach to optimize the use of Earth observation time series in land cover mapping. It aims to deliver for the first time a multi-year land cover map at global scale which does not reflect temporary conditions.

***2. Detecting land cover change globally is possible from medium resolution time series by disentangling the surface change from the inter-annual variability of the signal***

Land cover change occurred in many regions of the world over 13 years. The objective is to develop a new land cover change detection strategy that allows determining at global scale the new land cover class for a change area in order to integrate it to the multi-year land cover baseline. The originality of the method is to take advantage of the whole time series to distinguish actual surface conversion from spurious change and to determine the fate of the land cover change after disturbance. In addition, the developed method not only deals with forest change, compared to many studies, but also with croplands, grasslands, bare areas, urban areas and water bodies dynamics to show up a complete portrait of the Earth's land surface transformation.

***3. Understanding the various perturbing factors of surface reflectance over tropical forests is a prerequisite to the vegetation indices use for studying vegetation phenology***

Remote sensing is often claimed to be particularly appropriate for remote areas like tropical rainforests where limitations such as accessibility and lack of field measurements are prevalent. It is also known that spaceborne optical assessment of tropical vegetation dynamics is inherently difficult due to frequent cloud cover and high aerosol concentration. The ability of optical satellite data to describe a frequently cloudy region must be questioned. In addition, the current debate concerning the BRDF effects on seasonal changes of the EVI in the Amazon basin is still open. The objective is to determine the seasonal effects of atmospheric conditions and sun-sensor geometry on the intra-annual variability of individual spectral bands and vegetation indices, in order to assess the consistency of remotely-sensed observations to detect phenology in tropical regions.

***4. In situ phenological and meteorological observations are crucial to validate the remotely-sensed vegetation seasonality and to question the mechanisms driving the tropical forest foliage phenology***

In tropical regions where phenology is still poorly understood, and where atmospheric conditions complicate the use of remote sensing, the temporal variation of satellite-based vegetation indices has to be used with caution. A deeper understanding of the meaning of satellite-based greening compared to ground reality is needed to validate the relevance of remote sensing in the characterization of tropical vegetation phenology. In addition, an improved understanding of the environmental drivers controlling phenology would be helpful to reduce the uncertainty concerning the tropical forest resilience or dieback to climate anomalies. The objective is to make the link between the satellite-based variation and ground observation of phenology, flux tower $CO_2$ seasonal patterns and climate conditions to question the phenological mechanisms for the seasonal greening of Earth observation data.

# 7. Outline of the thesis

The thesis is organized in 3 chapters described hereunder. Figure 1 illustrates the connecting thread of the thesis and the interactions between the chapters.

**Chapter 1** responds to the two first specific objectives by proposing new approaches for land cover mapping and land cover change detection at global scale using a multi-year data set of Earth observations. First, the year-to-year variability observed in successive annual maps is investigated as a prerequisite to highlight the classes and regions difficult to map. Then, two methods are developed to build a multi-year land cover map according the first objective. The resulting maps are compared through quantitative and qualitative validations, and with annual land cover mapping. Finally, the implementation of a trajectory-based change detection method using a post-classification approach responds to the second objective. Each type of change is analyzed through case studies and quantified at global scale within the period of observations.

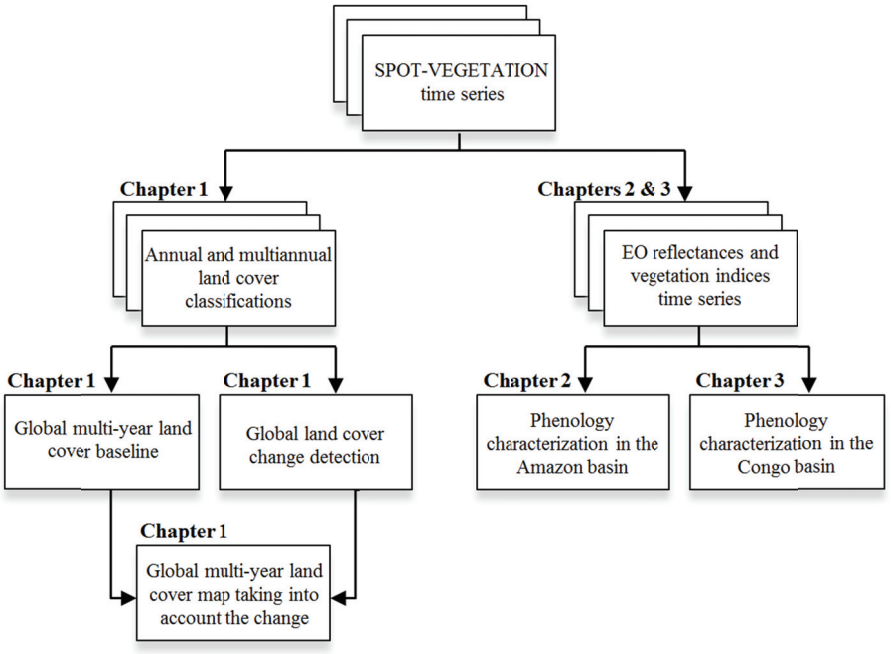


Figure 1 : Overall approach of the thesis.

**Chapter 2** and **Chapter 3** answer both to the third and fourth specific objectives of the thesis, to provide a better understanding of how optical remote sensing time series can help detecting spatial and seasonal variations of tropical rainforest phenology. **Chapter 2** focuses on the Amazon basin and **Chapter 3** on the Congo basin. Various factors potentially perturbing the reflectance and vegetation indices, like aerosols or directional effects, are investigated, responding to the third objective. Then, following the fourth objective, the seasonal variations contained in multi-year time series are interpreted with regards to ground data and climate seasonality. As the Amazon basin is much more studied than the Congo basin on this topic, the particular effort in **Chapter 2** is to bring a critical analysis with regards to the current literature, whereas **Chapter 3** presents rather a first investigation.

Finally, the main findings are summarized and discussed, the current applications of the proposed strategies are exposed, and suggestions on future works are proposed in the **Conclusions and Perspectives** part of this document.

# Chapter 1 – A multi-year global land cover map and land cover change detection at global scale thanks to 13-y SPOT-VEGETATION time series

## Abstract

Information relative to land cover is of considerable importance with regard to environmental concerns such as climate change or the study of ecosystems and global cycles. Global land cover mapping activities have evolved rapidly in the past decades along with the availability of global moderate spatial resolution satellite observations. The current global land cover maps are however sensitive to the period of observation, as they are based on a single annual cycle of satellite data, and do not provide change information. The aim of this study is to develop and demonstrate a new remote sensing approach to map the land cover consistently over time at global scale while integrating the land cover change occurring during the period of observations. The accumulation of global and long-term time series of Earth observation is an opportunity to address this innovative land cover approach. We take advantage of the automated GlobCover Processing Chain, developed by UCL-Geomatics, and of the 13-y SPOT-VEGETATION time series to produce at global scale 13 annual land cover classifications and one classification on a 13-y basis. It allows firstly to highlight the large inter-annual variability between annual land cover maps and secondly to build two multi-year land cover maps according to two methods: (i) one classification based on 1 set of annual and seasonal composites summaries over 13-y of data; (ii) one synthesis of 13 annual classifications. These two maps are validated, visually compared, and different pixel-based flags document the products quality. Using multi-year time series as source of data for

classification has proved efficient to reduce the sensitivity to the period of observation found in current annual mapping approaches. Among the two methods tested, the synthesis method is recognized to better perform and present the advantage of pixel-based quality indicators. Then, a change detection method is designed based on a post-classification strategy and pre-determined conditions concerning the time series behaviour to detect global land cover changes that may occur over the 13 years. The specific aim is to derive the new land cover class for a change area in order to integrate it to the multi-year land cover baseline. The challenge is to distinguish actual surface conversions from spurious change. The change results show a complete portrait of the Earth's land surface transformations, at 1-km spatial resolution, by providing forests, croplands, grasslands, bare areas, urban areas and water bodies losses and gains accompanied with the year of change and the new land cover after disturbance. Omission errors in detection of change occur because the moderate spatial resolution imagery hampers depicting small conversion less than a pixel size. If more accurate results are expected with higher resolution time series, the developed method already shows the power of satellite remote sensing time series for long-term monitoring of surface transformations.

# 1. Introduction

Monitoring the land surface of the Earth is essential for assessing many environmental issues such as climate change, biodiversity loss or natural resource depletion for driving sustainable development policies. Land cover is identified as one of the 50 Essential Climate Variables (ECVs) defined by the Global Climate Observing System (GCOS, 2010) and is recognized to play an important role, with land use, in the global carbon cycle (IPCC, 2014). Land cover mapping is notably crucial as baseline for the land surface parameterization of climate and Earth system models, such as dynamic global vegetation models (DGVMs) which produce carbon flux estimates and attempt to predict the future behaviour of such global cycles (Quaife et al. 2008). Indeed, the sensitivity of the cycling and exchange of carbon and water fluxes to climate variability is directly coupled, both in space and time,

to land cover, land use and the distribution of vegetation (Poulter et al., 2011).

In response to this growing need of land cover information for environmental monitoring, modelling and policy makers, global land cover mapping activities have evolved rapidly in the past decades along with the availability of global moderate spatial resolution satellite observations. Currently, a number of global land cover products derived from satellite observations exist, such as the University of Maryland (UMD) land cover product (Hansen et al., 2000) and the International Geosphere-Biosphere Programme (IGBP) DISCover (Loveland et al., 2000) using 1-km Advanced Very High Resolution Radiometer (AVHRR) images, the 1-km and 500-m Moderate Resolution Imaging Spectrometer (MODIS) land cover products (Friedl et al., 2002; Friedl et al., 2010), the Global Land Cover 2000 (GLC2000) (Bartholome and Belward, 2005) using 1-km SPOT-VEGETATION data, and the European Space Agency (ESA) GlobCover products (Defourny et al., 2009a; Bontemps et al., 2011) with the 300-m Envisat's Medium Resolution Imaging Spectrometer (MERIS) instrument.

Various intercomparison studies of these satellite-based global land cover products was conducted to assess the distribution of agreements, inconsistencies and mapping uncertainties across the maps, to compare the different methods and remotely sensed data used, to evaluate the relevance of products and to select global land cover data needed for specific applications (DeFries et al., 1998; Hansen et al., 2000; Hansen and Reed, 2000; Latifovic and Olthof, 2004; Giri et al., 2005; Jung et al., 2006; McCallum et al., 2006; Herold et al., 2008; Fritz et al., 2008; Friedl et al., 2010; Kaptué Tchuenté et al., 2011, Pflugmacher et al., 2011). These comparisons revealed general patterns of similarities but also considerable inconsistencies and discrepancies, raising strong uncertainties in the use of these products (Jung et al., 2006), and leading for example to large differences in terrestrial $CO_2$ fluxes estimates by dynamic vegetation models (Quaife et al., 2008). Even using data acquired by the same sensor, significant year-to-year variations in land cover labels appear: the proportion of pixels differently labelled from one year to another ranges from 30 % before and 10 % after applying a classification stabilization in the suite of MODIS Collection 5 products (Friedl et al., 2010) and is around 25 % between the GlobCover 2005 and 2009 maps (Bontemps et al., 2012a).

Most of the cases where land cover datasets disagree are areas with complex and heterogeneous land cover such as transition zones and edges around large areas of homogeneous cover, while homogeneous classes such as evergreen broadleaf trees, snow and ice, bare or sparsely vegetated land show high agreement. Confusion typically occurs between similar surfaces such as different forest types (Brown de Colstoun et al., 2006), and in areas characterized by mosaics of trees, shrubs and herbaceous vegetation specific to heterogeneous landscapes (Herold et al., 2008) or managed by human exposing small-patch spatial patterns often smaller than the resolution cell (Colditz et al., 2011). High uncertainty at biome borders and in areas of human activity is a major concern, because these zones are most vulnerable to climate and socio-economic changes (Pflugmacher, 2011).

These large proportions of inconsistencies among the different global datasets cannot be explained by land cover change (Giri et al., 2005; Jung et al., 2006; McCallum et al., 2006; Herold et al., 2008; Friedl et al., 2010; Kaptué Tchuenté et al., 2011; Pouliot et al., 2014) as they substantially exceed the annual rate of any land cover change. Indeed, the most rapid change occurring nowadays is tropical deforestation with maximum yearly rates of around 3.5% in Brazil and Indonesia (Hansen et al., 2008). Several factors are identified as potentially responsible for the discrepancies between the maps. First, the different approaches are obviously pointed out in terms of methodology, such as the type of algorithm applied for classifications, the input dataset used and their pre-processing steps. Second, the limited discriminating powers of medium sensors at both spatial and spectral levels are recognized to be source of confusion. On one hand, the moderate spatial resolution imagery hampers the ability to accurately classify heterogeneous areas characterized by a landscape mosaic more fragmented than the resolution cell. On the other hand, the current spectral resolution and coverage limit the capability to clearly discriminate certain land cover types, inducing inconsistency between products which exacerbates the land cover semantic discrepancies or ambiguities. Third, various thresholds applied for separating classes, such as the diverse percentages of tree cover or height defined for the forest classes, and unclear descriptions can strongly reduce the correspondence of the maps. This highlights the need to use a standardized classification system, such as the Land Cover Classification System (LCCS, Di Gregorio, 2005), to elaborate unambiguous classification schemes and to increase the reliability of intercomparisons.

Bontemps et al. (2012a) show through comparisons among a suite of annual land cover maps over Africa using the same classification method, the same classification system (LCCS) and same sensor data that disagreements remain high and typically occur in heterogeneous landscapes or areas showing contrasted seasonal cycles, as for previous comparison between the different land cover datasets. In this case, the classification scheme, the legend, or the different characteristics of sensors are obviously not causes of discrepancies. Thus, these divergences between successive annual products could be due to spatial and spectral sensor resolutions incompatibility with the landscape complexity, as already mentioned, but also to the inter-annual variability of the biome seasonality. With this regard, method-external factors can influence the surface reflectances in certain zones such as year-to-year variations in phenology, fires and associated atmospheric contaminants, droughts or insect infestations (Friedl et al., 2010), or inter-annual variability of climate conditions, which can lead to relative vegetation development. These temporary impacts on land cover may induce misinterpretation of the reflectance recorded by the sensor.

This last source of discrepancies between land cover maps raises concerns about their sensitivity to the period of observation. Indeed, all published global land cover products share one common characteristic: they consider only one single annual cycle of satellite data in their classification, being snapshots of a particular time period (Giri et al., 2013), which is obviously not enough to cope with land surface inter-annual variability. Contrarily, the use of multi-year Earth observation dataset could help (i) avoiding classification mistakes due to temporary effects, (ii) better differentiating spectrally close classes and (iii) determining the most likely land cover classes in heterogeneous areas. This new approach could answer the requirement of the climate modelling community in terms of satellite-based global land cover products, highlighted by Bontemps et al. (2012a), namely a stable land cover information. The stable component of the land cover definition refers to the set of land elements that remain stable over time and thus define the land cover independently of any sources of temporary variability (Bontemps et al., 2012a).

Mapping land cover from multi-year Earth observation dataset requires however dealing with the natural and anthropogenic land cover changes that may occur during this period. There is a considerable interest in deriving land cover change information in terms of biodiversity impacts or for climate change issues. For instance, land cover changes substantially

impact atmospheric composition (e.g. $CO_2$ concentration) and climate via biogeochemical mechanisms, such as the forest conversion leading to large direct emissions of carbon, and through biogeophysical mechanisms including the effects of changes in evapotranspiration, surface roughness and albedo (Sitch et al., 2005). A better understanding of landscape changes due to human activities is also critical information for the development of effective sustainable management practices (Zhang et al., 2014). However, our understanding of the extent, rates, patterns, causes and consequences of land cover change is limited (Giri et al., 2013) and the net flux of carbon from land use and land cover change is the most uncertain term in the global carbon budget (Lewis, 2006; Ramankutty, 2007; Houghton et al., 2012).

In the last 30 years, a large number of methodologies, techniques and algorithms have been developed to identify the geographical location and type of changes with remotely sensed data, relying on the alteration of the spectral behaviour to detect land surface changes. The analysis units that are compared over time to highlight change are principally individual image pixels and image-object created previously from segmentation of the image (Hussain et al., 2013; Tewkesbury et al., 2015). A variety of different methods of comparisons have been developed, based on the pixel-based and object-based approaches. These methods can be categorized in pre-classification and post-classification techniques. The pre-classification approach is mainly based on the direct and continuous analysis of spectral signature (radiance or reflectance values), for instance in SPOT-HRV, Landsat images and MODIS time series (Desclée et al., 2006; Bontemps et al., 2008, 2012b; Duveiller et al., 2008; Ernst et al., 2013; Hansen et al., 2013; Jin et al., 2013; Mayaux et al., 2013; Brink et al., 2014; Huang and Friedl, 2014; Pouliot et al., 2014; Zhang et al., 2014). The post-classification and direct classification approaches compare independent classifications to derive change information (Chen et al. 2012; McRoberts, 2013; Sexton et al., 2013). The distinct advantage of this technique is that the baseline classification and the change transitions are explicitly known. Less frequent are the hybrid analysis (Griffiths et al., 2013).

Among these studies, very few are giving information on the year of change (Bontemps et al., 2008; Hansen et al., 2013; Hang and Friedl, 2014), and none have the ability to identify the fate of the land cover over changed areas. Indeed, a simple binary change vs. no change is described as sufficient for many studies (Hussain et al., 2013). A remaining challenge in land cover

change studies is to provide detailed information regarding the land cover class observed after change, for instance the fate of cleared land, which is needed for many applications (Ramankutty et al., 2006; Houghton et al., 2012). In addition, a large number of land cover change studies focus solely on forest change, because of the current focus of environmental monitoring concerning the global carbon cycle and biodiversity loss (Hansen and Loveland, 2012), or because it is easier to observe processes of forest conversion with regards to other land cover transition. However, other types of change such as urbanization, cropland extension, dryland degradation or lake and waterways drying up are also transforming the planet's surface with critical environmental impacts (Foley et al., 2005; Lepers, et al., 2005). Finally, except for forest change (Hansen et al., 2013), all of these studies are realized at local, national and regional scale. Significant uncertainties persist about the global rate and patterns of change of agricultural lands, drylands, wetlands, built-up areas or water, among others.

Many change detection studies use a bi-temporal change analysis, either by direct comparison of two-date images which have tend to be performance limited (Lunetta et al., 2006), or between only two land cover maps leading to cumulative error. Although until now, to our knowledge, there is common agreement within the land cover mapping community that the discrete global land cover classifications at moderate spatial resolution are unable to detect reliably land cover changes (Strahler et al., 2006; Jung et al., 2006; Colditz et al., 2011; Giri et al., 2013), the availability of moderate resolution long time series makes possible to face this challenge today. An analysis based on a yearly classification time series instead of a comparison of two distinct land cover maps will allow avoiding errors of classification to propagate. In addition, this technique is advantageous as identified changes are thematically labelled. Furthermore, the date of the change can be determined on a yearly basis, compared to bi-temporal change detection method that cannot provide this information.

In this study, the research goal is to design and demonstrate an innovative land cover mapping approach based for the first time on a multi-year Earth observation dataset. It proposes to map the land cover consistently over time at global scale while integrating the land cover change. It aims specifically to (i) reduce the sensitivity to the period of observation found in current annual land cover mapping approach, (ii) determine the most likely land cover in areas difficult to classify, (iii) deliver quality layers giving spatial information on the relevance of the multi-year

product, (iv) identify the land cover change occurring during the period of observations and the year of change, (v) determine the new land cover class for a change area, (vi) integrate it to the multi-year map and (vii) make the complete process automatic and capable of yearly updates. First, two methods to derive a global multi-year land cover map are explained, and the generated maps are validated and compared. Second, seven types of change are treated through a multi-annual post-classification approach to detect global land cover changes that may occur over the 13 years and to identify new land cover classes.

# 2. Methods and data

In order to reduce significantly the sensitivity of land cover classification to specific year, a multi-year classification strategy has to be selected. Two major alternatives have been tested: (i) a classification based on 13-y summarised composites (hereafter Multi-Year Classification, MYC) and (ii) a synthesis of 13 annual classifications (hereafter Synthesis of Yearly Classifications, SYC). At this stage, no land cover change is considered. Once the multi-year land cover map is established, a land cover change mapping strategy is proposed in order (i) to detect changes occurring during the period of observations and (ii) to integrate it to the multi-year map.

## *2.1. Input time series and features*

The 13-year global SPOT-VEGETATION images (Jan. 1999 – Dec. 2011) provides a consistent 1-km time series spatially and temporally, although not as long as the AVHRR time series. Indeed, the VEGETATION sensor presents the advantage of a better data acquisition, being equipped with a linear charge-coupled device array which scans the Earth's surface by the so called "push-broom" method. It permits an acquisition with almost no distortion on image edges, unlike the MODIS sensor. In addition, the length of exposition is higher for the same satellite velocity, giving an improved ratio signal/noise.

The high temporal frequency of data acquisition of moderate spatial resolution data permits to follow accurately continuous processes like phenology or to generate a reliable and cloud-free synthesis of a time period through compositing. Thanks to its 2250-km swath, SPOT-VEGETATION covers almost the entire Earth's surface each day. Daily synthesis of land surface reflectance atmospherically corrected (S1 composites) have been selected for this research. Multispectral annual and/or seasonal composites were produced using the Mean Compositing (MC) method (Vancustem et al., 2007). This method averages valid cloud-free reflectance values of the concerned time period through mean computation over each pixel and for each band to generate composites. The MC process aims at minimizing the cloud contamination but also at reducing the directional effects due to variations of view geometry in the successive measurements of surface reflectances. It has proved to significantly reduce the BRDF and atmospheric artefacts while resulting in spatially homogeneous cloud-free composites with good radiometric consistency even in humid tropical regions (Vancutsem et al., 2007; Langner et al., 2007; Bontemps et al., 2012). In addition, MC algorithm does not require any model adjustment or additional parameterizations, hence contributing to the generalization and automation of the process.

## *2.2. The GlobCover classification chain*

Based on GLC2000 and then GlobCover experiences, the legend (Table 1) contains 22 classes and is strictly based on the LCCS of the UN-FAO (Di Gregorio, 2005). LCCS describes land cover according to a hierarchical series of classifiers in a dichotomous phase (vegetated or non-vegetated, terrestrial or aquatic/flooded, cultivated or natural) and by attributes (life-form, fractional cover, leaf type, phenology, etc.). Each class obtained by the classification process is explicitly described by a thematic label, which is directly associated to a land cover class name and a LCCS code. The use of LCCS reduces the ambiguity in land cover class definition thanks to the standardization of the combination of independent classifiers. These classifiers allow defining a highly flexible and systematic land cover typology, with the capacity to describe the land cover features at a variety of scales and to derive enough classes to cope with the real world diversity (Di Gregorio, 2005).

Table 1 : The 22 global land cover classes of the GlobCover legend.

| ID Value | Global Globcover legend (level 1) | Color | LCCS major descriptor |
|---|---|---|---|
| 11 | Post-flooding or irrigated croplands (or aquatic) | | Cultivated terrestrial areas and managed lands |
| 14 | Cultivated and managed areas / Rainfed croplands | | |
| 20 | Mosaic Cropland (50-70 %) / Vegetation (grassland, shrubland, forest) (20-50 %) | | |
| 30 | Mosaic Vegetation (grassland, shrubland, forest) (50-70 %) / Cropland (20-50 %) | | |
| 40 | Closed to open (> 15 %) broadleaved evergreen and/or semi-deciduous forest (> 5 m) | | Natural and semi-natural terrestrial vegetation |
| 50 | Closed (> 40 %) broadleaved deciduous forest (> 5 m) | | |
| 60 | Open (15-40 %) broadleaved deciduous forest/woodland (> 5 m) | | |
| 70 | Closed (> 40 %) needle-leaved evergreen forest (> 5 m) | | |
| 80 | Closed (> 40%) needle-leaved deciduous forest (> 5 m) | | |
| 90 | Open (15-40 %) needle-leaved deciduous or evergreen forest (> 5 m) | | |
| 100 | Closed to open (> 15 %) mixed broadleaved and needle-leaved forest (> 5 m) | | |
| 110 | Mosaic forest or shrubland (50-70 %) / grassland (20-50 %) | | |
| 120 | Mosaic grassland (50-70 %) / forest or shrubland (20-50 %) | | |
| 130 | Closed to open (> 15 %) shrubland (< 5 m) | | |
| 140 | Closed to open (> 15 %) grassland | | |
| 150 | Sparse (< 15 %) vegetation | | |
| 160 | Closed (> 40 %) broadleaved forest regularly flooded - Fresh water | | Natural and semi-natural aquatic vegetation |
| 170 | Closed (> 40 %) broadleaved semi-deciduous and/or evergreen forest regularly flooded - Saline water | | |
| 180 | Closed to open (> 15 %) vegetation (grassland, shrubland, woody vegetation) on regularly flooded or waterlogged soil - Fresh, brackish or saline water | | |
| 190 | Artificial surfaces and associated areas (Urban areas > 50 %) | | Artificial surfaces and bare areas |
| 200 | Bare areas | | |
| 210 | Water bodies | | Inland waterbodies, snow and ice |
| 220 | Permanent snow and ice | | |

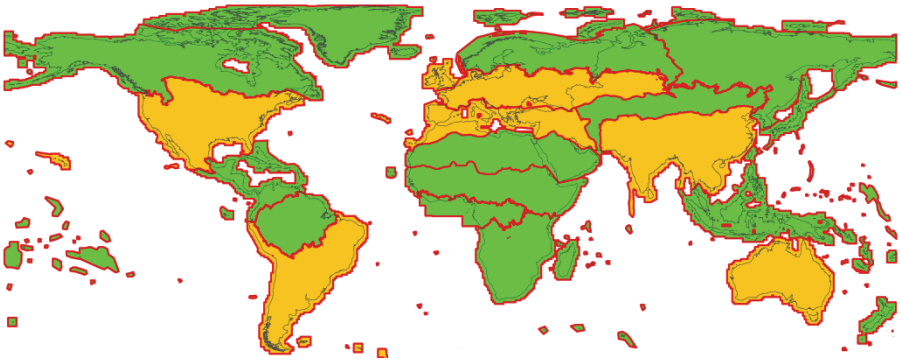

Figure 2: GlobCover 22 equal-reasoning strata. Green strata rely on annual composites and yellow strata rely on annual and seasonal composites for the classification.

Being the first automated mapping approach of land cover on a global scale, GlobCover provides a basis for the detailed description of the land surface states needed for climate modelling (Arino et al., 2008). The GlobCover classification chain, developed with the support of ESA, is a fully automated chain that delivers classification using multispectral

seasonal, annual or multi-annual composites (Bicheron et al., 2008; Bontemps et al., 2011).

Before the classification process, the world is stratified in 22 equal-reasoning regions (strata) which have been delineated taking into account bio-climatic and remote sensing criteria (Figure 2). The purpose is (i) to reduce the land surface reflectance variability in the dataset in order to increase the spectral differentiation among classes and (ii) to allow a regional tuning of the classification parameters to take into account the regional characteristics (vegetation seasonality, cloud coverage, etc.). The great but much controlled flexibility of this strategy allows defining a classification process valid at global scale while tackling both the regional heterogeneity of the land cover characteristics.

The classification module of the GlobCover processing chain consists in transforming the SPOT-VEGETATION cloud-free reflectance composites produced by the pre-processing step into meaningful global land cover maps at 1-km spatial resolution. The algorithms are designed to run independently for each of the 22 strata with specific parameters.

First, a supervised classification is applied to identify the low represented classes, i.e. urban areas and wetland areas. Second, the pixels classified through the supervised classification are masked and an unsupervised classification algorithm, which relies on the Iterative Self-Organizing Data Analysis Technique (ISODATA) clustering technique, is applied to create a large number of clusters of spectrally similar pixels from the selected composites. Using an unsupervised classification algorithm allows reaching a rather high degree of automation while reducing the processing time. It is a classification process based solely on the image statistics, without availability of training data or other a priori knowledge of the area. The ISODATA is an iterative optimization clustering procedure. It is based upon estimating some reasonable assignment of the pixel vectors into candidate clusters and then moving them from one cluster to another in such a way that the sum of squared error is progressively reduced. It assigns a set of pixels into clusters so that the pixels in the same cluster are more similar to each other than to those in other clusters. The assignation is based on natural groupings present in the reflectance values. The basic premise is that reflectance values within a given land cover class should be close together in the measurement space, whereas pixels belonging to different land cover classes should be comparatively well-separated.

This unsupervised classification step relies on the annual composite when the stratum presents a low seasonality and/or high cloud cover frequency (Figure 2, green strata). For the other strata, a supplementary seasonal or bi-monthly composite is selected, according to the season showing the best contrasts for land cover classes, to be part of the unsupervised classification with the annual composite (Figure 2, yellow strata). The spectral clusters produced by the unsupervised classification in the strata which present a high seasonality are then temporally characterized by the computation of phenological metrics (minimum and maximum of vegetation), derived from the SPOT-VEGETATION time series and spatially averaged for each cluster. The key idea is to combine the spatial consistency of the clusters delineation obtained from well selected multispectral composites with the discrimination power of the temporal profiles analysis to group clusters with similar characteristics in a manageable number of spectro-temporal classes.

Then, the supervised and unsupervised classification results are merged. The unsupervised algorithm generates however separable clusters for which the land cover label is not known and needs to be determined by comparing them to some auxiliary reference dataset. The reference dataset was compiled from 16 global, continental, national or regional land cover maps merged and superimposed on the GLC2000 land cover map, and translated in the GlobCover legend thanks to the LCCS classifiers information. The referenced-based labelling function automatically assigns previously defined LCCS land cover classes (GlobCover classes) to the spectro-temporal clusters according to their correspondence with the reference land cover classes. For each cluster, a histogram of class frequency is computed based on the reference dataset. The most represented classes inside the cluster are identified and ranked using the number of pixels they cover and their label. Several decision rules have been defined with the help of international land cover experts to interpret the class frequency and to derive unique label for each spectro-temporal class.

## *2.3. Two methods for a global multi-year land cover map*

Figure 3 (a) illustrates the MYC methodology developed to produce a multi-year land cover map. In this scenario, the daily SPOT-VEGETATION data

from 1999 to 2011 are summarized into one set of averaged 13-y annual and seasonal composites. These 13-y composites are expected to give more stable spectral profiles and thus to be of higher quality. Then, they are processed by the GlobCover classification chain to provide a single land cover map on a 13-y basis according to the methodology described in 2.2.

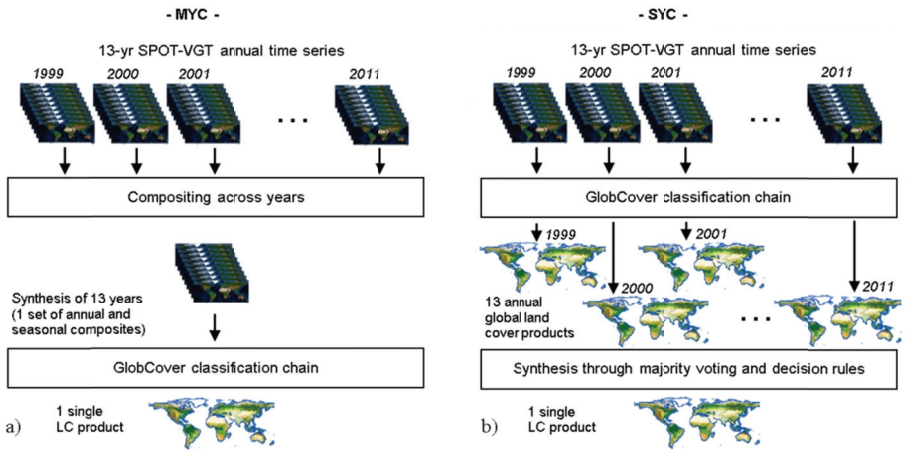


Figure 3: Flowchart of the two methodologies developed to produce a multi-year land cover map based on the 13-year SPOT-VEGETATION archive using the GlobCover classification chain: a) one classification based on 1 set of 13-y summarized annual and seasonal composites (Multi-Year Classification, MYC) and b) one synthesis of 13 annual classifications (Synthesis of Yearly Classifications, SYC).

Alternatively, the SYC method (Figure 3 (b)) consists of first producing 13 consecutive global classifications on an annual basis for the years 1999 to 2011 thanks to the GlobCover chain, according to the methodology described in 2.2 for each year. Then, a pixel-based synthesis of these 13 classifications is built through a majority voting and specific decision rules to decide a unique class per pixel. The logic behind these decision rules is the way clusters are labelled during the reference-labelling step of the GlobCover classification chain, explained in 2.2. The thresholds are established through careful analysis of known land cover, inter-annual variabilities between the annual classifications detailed in the result 3.1 section, and semantic distance between classes. In a general manner, they are common for the entire world and specific to groups of classes, but some differ slightly for peculiar regions. They are illustrated in Figure 4 and explained hereafter.

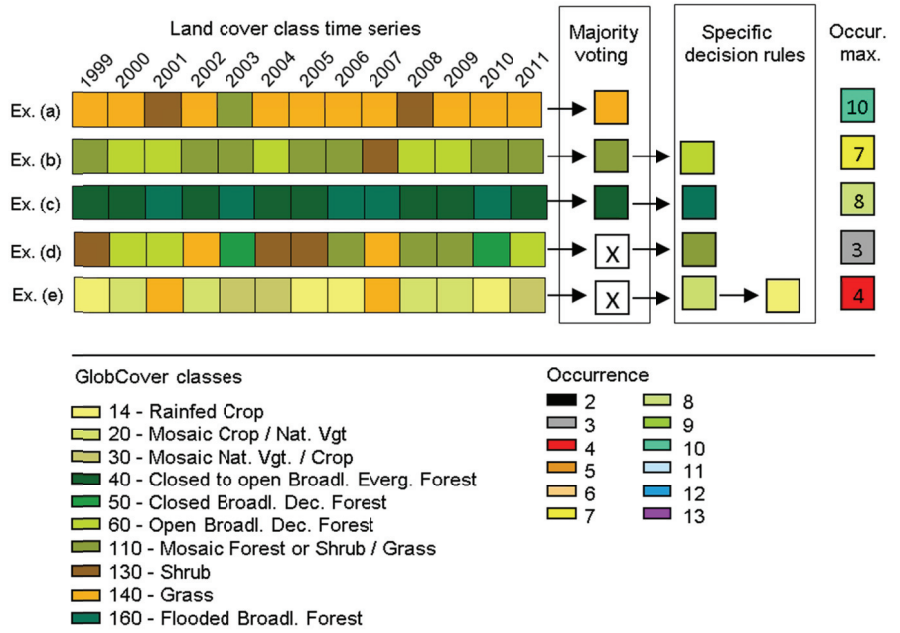


Figure 4 : Examples illustrating different cases of SYC method developed to produce a multi-year land cover map based 13 annual classifications, according to majority voting strategy and decision rules. For complete names of the classes, see Table 1.

For each pixel, the 13 successive labels of land cover classes are extracted over the 13 classifications. Then, the occurrence of each land cover class present in the pixel time series is computed. The most represented classes inside the pixel time series are identified and ranked using the number of occurrence. From the maximum number of occurrence, stable and unstable pixels are distinguished and the following rules are applied to derive a unique label for each pixel:

- The maximum occurrence reaches 7 or more over the 13-y time series. In this case, the pixel is considered as stable. The majority class corresponding to this maximum occurrence is considered as the most likely land cover class and is the label chosen for the synthesis (i.e. Figure 4 ex. (a), maximum occurrence = 10, label chosen = class 140).

  - The majority class is a mosaic. In this case, a pure class can be chosen instead of the mosaic if it is semantically close to the mosaic class and if it has an occurrence of 4 or more in the pixel time series. For instance, in Figure 4 ex. (b), the pixel has a majority voting of 7 with

the mosaic class 'forest or shrubland / grassland' (class 110). As a pure forest class (class 60) semantically closed of the 110 mosaic class has an occurrence of 5 over the 13 years, the pixel is labelled with this pure forest class. The purpose is to limit the proportion of the mosaic classes in the multi-year map because of their ambiguity for users. If the pure class threshold is not met, the label stays the mosaic class.

- Specific decision rules are applied for several classes with small extent, known to be difficult to classify and often confounded with other classes. The example (c) is a well-known case of closed broadleaved flooded forest (class 160) confused with closed broadleaved evergreen forest (class 40) in tropical regions. In a case where these two classes only are present in the time series, flooded forest is chosen even if it is minority. Same kind of rules are applied for irrigated croplands, urban areas, others types of flooded vegetation or for classes often confused with others but not semantically close (e.g. grassland and bare soil).

- The maximum occurrence of classes does not reach 7. In this case, the pixel is considered as unstable. For these pixels, no majority label is chosen initially (i.e. Figure 4, ex. (d), max. occ. = 3). Instead, a mosaic class semantically the closest to all classes of the time series is attributed, given the proportion of the classes. For instance, in the time series of ex. (d), only natural vegetation classes are present but with occurrence per class no more than 3. Given the majority of shrub and forest classes (8) and the minority of grasslands (2), the mosaic 110 is chosen instead of the mosaic 120.

  - A pure class is present with an occurrence of 4 or more and is semantically closed to the determined mosaic class. In this case, it is selected to classify the pixel (i.e. Figure 4 ex. (e)). If the pure class threshold is not met, the temporary mosaic class remains the best option to label the pixel.

- Previous specific rules are not enough because of occurrence equalities in the time series. In this very rare case, spatio-temporal information on a 3x3 pixels window over the 13 years is taken into account and a majority voting is applied to determine the most likely label.

These decision rules are designed to have a control on the land cover results based on a priori knowledge on classification mistakes. It aims to (i)

take advantage of the long time series to determine the most likely land cover class, (ii) limit the proportion of the mosaic classes because of their ambiguity for users, (iii) favor classes with small extent, known to be difficult to classify and (iv) deal with areas presenting large inter-annual variabilities and showing an ambiguous time series.

## 2.4. Validation and quality indicators

A quantitative thematic accuracy assessment based on international standards is performed for the two maps, using 3134 ground reference points globally distributed around the world which include homogeneous and heterogeneous landscapes. This dataset has been built in the framework of the GlobCover project (Defourny et al., 2013; Bontemps et al., 2011) thanks to the support of 16 independent international experts. They have described the ground truth according to the LCCS classifiers and attributes. Homogeneous points are validation points for which the experts reported only one land cover type. Heterogeneous points are those for which the experts needed to use two or three land cover types to describe the area covered by a sample. For 2428 cases, constituting the first dataset, the experts were certain that the information they provided was correct. A second dataset was constituted with the 1141 homogeneous and certain samples. For all validation points, the set of classifiers was translated to classes of the GlobCover legend in order to build the confusion matrices. For heterogeneous points, this translation process becomes less obvious and mosaic classes are considered when deriving classifiers to a land cover class (Bicheron et al., 2008). Overall accuracy results indicate the percentage of correctly classified samples, derived with equal weighting for each of the sampled reference points. The global accuracy is obtained by weighting the user's accuracy value of each class by its area proportion, calculated after reprojected in an equal area projection as proposed by Strahler et al. (2006).

Although global accuracy is the most common metric for accuracy assessment, it varies according to the thematic class and the region of interest and it does not completely reflect the product's quality and usefulness, especially at global scale. Accuracy indices derived from the error matrix provide information on the quality of the map as a whole but cannot be used to characterize distinct areas of the map (Mayaux et al., 2006). Indeed, two maps can have the same overall accuracy, but a different spatial distribution of error (Pflugmacher et al., 2011). To give spatially

transparency on the strength and weaknesses of the product, the SYC map is accompanied by several per-pixel confidence layers. The first one documents the stability of the multi-year map. A spatial representation of the maximum occurrence of a same land cover class over the 13 years gives for each pixel the consistency over time of the successive classifications. It allows the user to locate quickly unstable regions and to measure the degree of certainty of the land cover he is looking at. Moreover, additional map layers indicate by groups of classes the step at which the label was delivered (majority voting or specific decision rules). It reveals the level of reliability of the final label chosen for the synthesis.

## *2.5. A trajectory-based change detection method*

Once the multi-year land cover map is established from the 13-y SPOT-VEGETATION time series, a new change detection method is proposed to deal with the land cover change occurring during this period. This study focuses on conversion from one land cover class to another in a permanent way.

The change detection is based on a multi-year post-classification approach. The use of the GlobCover chain is a major advantage for monitoring land surface transformations and estimating their spatio-temporal dynamics at global scale as it allows delivering automatically 13 annual global classifications from the 13-y SPOT-VEGETATION time series (1999-2011). The purpose is to capture gradual change at global scale during this 13-y period and identifying the land cover class after a change. To do so, the use of post-classification as comparison method is advantageous to determine the fate of the land cover as identified changes are thematically labelled.

With moderate spatial resolution data such as SPOT-VEGETATION, using pixels as analysis unit is faster and more suitable than objects (Tewkesbury et al., 2015). For each pixel, the 13 successive labels of land cover classes are extracted over the 13 classifications.

The change detection method relies on pre-determined conditions of supposed land cover trajectories over the 13-y in cases of land cover change. Then, the algorithm searches for pixels that fulfill these conditions over the 13-y and flag them as change. For instance, an important constrain is that a change occurring in the time series has to be confirmed over several

successive classifications. These conditions help to sort out actual change from inter-annual variabilities due to temporary events such as year-to-year variations in phenology and climate conditions.

In the pre-defined conditions, two periods of eight and five years of the 13-y pixel time series are opposed. The first one take into account the classes of the considered pixel extracted from the 1999 to 2006 classifications to certify capturing the original thematic group and its stability over time. The second one looks at the labels from 2007 to 2011 to potentially identify a change with regards to the first period. Specific decision rules with strict thresholds are applied according to the sensitivity of classes and to the stratum considered. For example (Figure 5, ex. (a)), for the detection of deforestation leading to a cropland, the sum of the forests labels of all types must be higher or equal to 6 or 7 (according to the strata) over the 8 first years and then inferior or equal to 2 between 2007 and 2011. The pixel is flagged as change if the total of crop classes in this second period is superior or equal to 3, with the constraint that the labels of the years 2010 and 2011 are croplands to ensure the persistence of the change. As the 13 labels of the time series in ex. (a) fulfill these conditions, the pixel is flagged as change. Then, the type of the cropland is chosen depending on the occurrence of the different classes of crops and the label in 2011. In addition, the transition year is revealed by identifying the year of the first label which doesn't correspond anymore to the original thematic group.

In general, this trajectory-based change detection method allows detecting changes occurring since 2005 at the earliest (for example, forest labeled 6 times over the first period of 8 years from 1999 to 2004, and appearance of crops since 2005) until 2010 (changed pixels are required to be classified as change at least two consecutive years and until 2011 to ensure the persistence of the change). This condition is relaxed if classes semantically very different and easily discriminated, e.g. 'forest and 'bare soil' co-exist in the time series. The first period is reduced to 1999 – 2002 and the second is extended from 2003 until 2011 (Figure 5, ex. (b) and (c) respectively). The threshold values are determined through careful examination of known multi-year change.

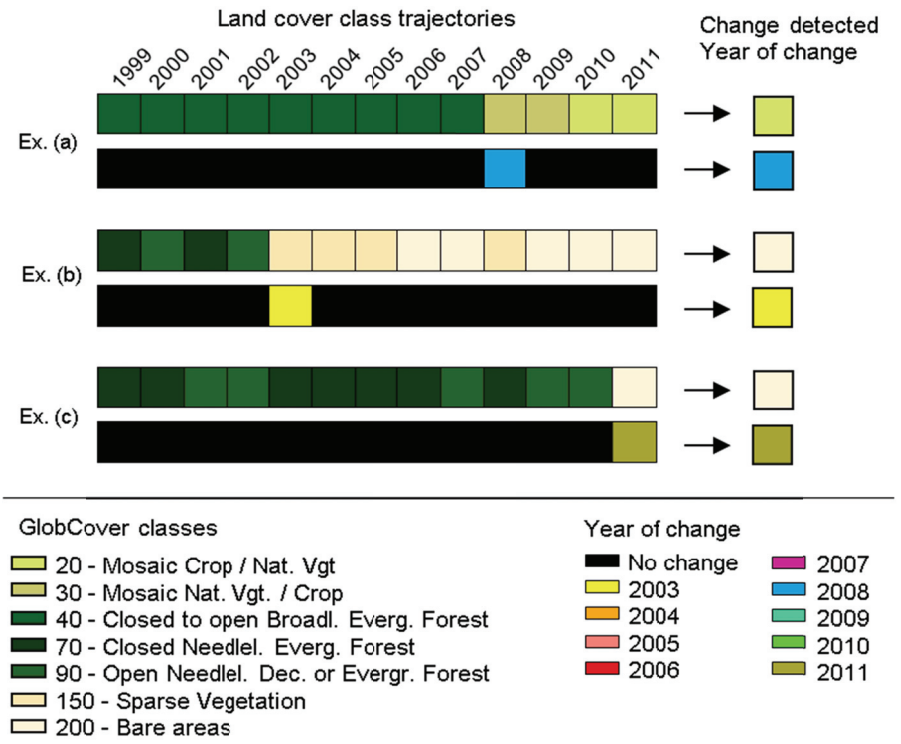


Figure 5 : Examples illustrating different cases of the trajectory-based change detection method. For each example, the first line is the pixel trajectory of classes and the second line indicate the year of change detected. For complete names of the classes, see Table 1.

In the examples (a) and (c) (Figure 5), the pixel would have been labelled 'Closed to open broadleaved evergreen forest' and 'Closed Needleleaf Evergreen Forest' respectively in the multi-year land cover map as these classes appear 9 and 7 times over the 13 years. Looking at the trajectory for detecting potential change is thus essential to correctly map actual land cover. A pixel for which the change occurs before 2005 (example (b), Figure 5) is already labeled with this change in the multi-year land cover map. However, it is interesting to follow the spatio-temporal progression of several types of forest transformation such as the deforestation due to mining, especially as forest and sparse vegetation or bare soil present very distinct spectral characteristics allowing detecting change easily and sooner.

Based on the analysis of the annual land cover variability and the high confidence for the aggregated land cover map, the trajectory-based change method is assessed on 7 types of change. The change detection

proposes the comparison between eleven groups of thematically close classes: forest, flooded forest, shrub, crop, grass, flooded grass, sparse vegetation, bare soil, urban area, water and snow. For instance, it won't be possible to detect change from semantically close classes like 'broadleaved deciduous forest' to 'mix forest', but from all types of forest to 'bare soil'. The two mosaic classes comprising crops and natural vegetation (classes 20 and 30) belong to the thematic group 'crop' and the mosaic class of forest and shrub/grass (class 110) belong to the thematic group 'forest', but are constrained with specific thresholds and decisions rules.

As there is no global reference information related to change, except for forest loss and gain (Hansen et al., 2013), visual examination of pixels flagged as change are made thanks to comparisons with historical high spatial resolution imagery from Google Earth™ as well as the abundant comments and pictures on events or land exploitation added by local populations, with the Google Timelapse tool displaying images of Earth collected by NASA's Landsat program since 1984 until 2012, with medias archives, etc.

To summarize, this original trajectory-based change detection method allows (i) giving information on the year of change, (ii) determining the land cover class appearing after the change which remains unknown in current studies, (iii) detecting seven types of change instead of looking solely at forest change, (iv) updating annually the pixels trajectory thanks to the automatic classification chain. The new land cover classes of pixels identified as changed are then integrated on the SYC multi-year land cover map to provide a coherent final product.

# 3. Results

## *3.1. A large inter-annual variability among annual classifications*

As results of the GlobCover classification chain, 14 global land cover maps were produced, one according to the MYC and 13 according to the SYC. The analysis of the 13 classifications allows notably highlighting the inter-

annual variabilities between these annual classifications and revealing their characteristics and locations.

When considering any pair of consecutive annual classifications in the 13-y suite, the inter-annual variability reaches an average proportion of 31.5 ± 0.4 % of pixels differently labelled from one year to the next land cover. These differences are clearly too large to correspond to actual change and must be considered mainly as discrepancies. As expected, they are mainly observed (i) in regions of heterogeneous cover, (ii) at transition zones around large homogeneous cover, or (iii) in areas showing contrasted seasonal cycles. This significant year-to-year variations in pixel classifications quantifies the limits of single-year mapping approaches currently used for global land cover maps.

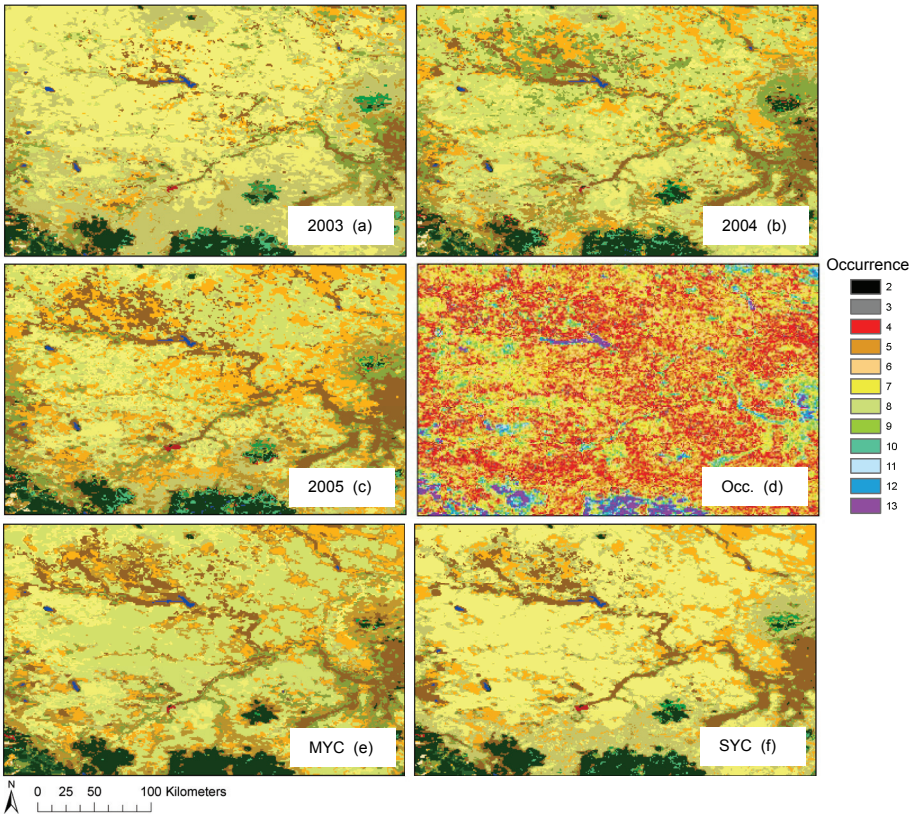


Figure 6 : Example of the inter-annual variability (Montana, USA) between successive annual classifications with SPOT-VEGETATION data: (a) 2003, (b) 2004, (c) 2005. Maximum of occurrence of a same land cover label over 13 annual classifications (d). Multi-year land cover map with (e) the MYC method (classification based on 1 set of 13-y composites) and (f) the SYC method (synthesis of 13 classifications). See Table 1 for the GlobCover legend.

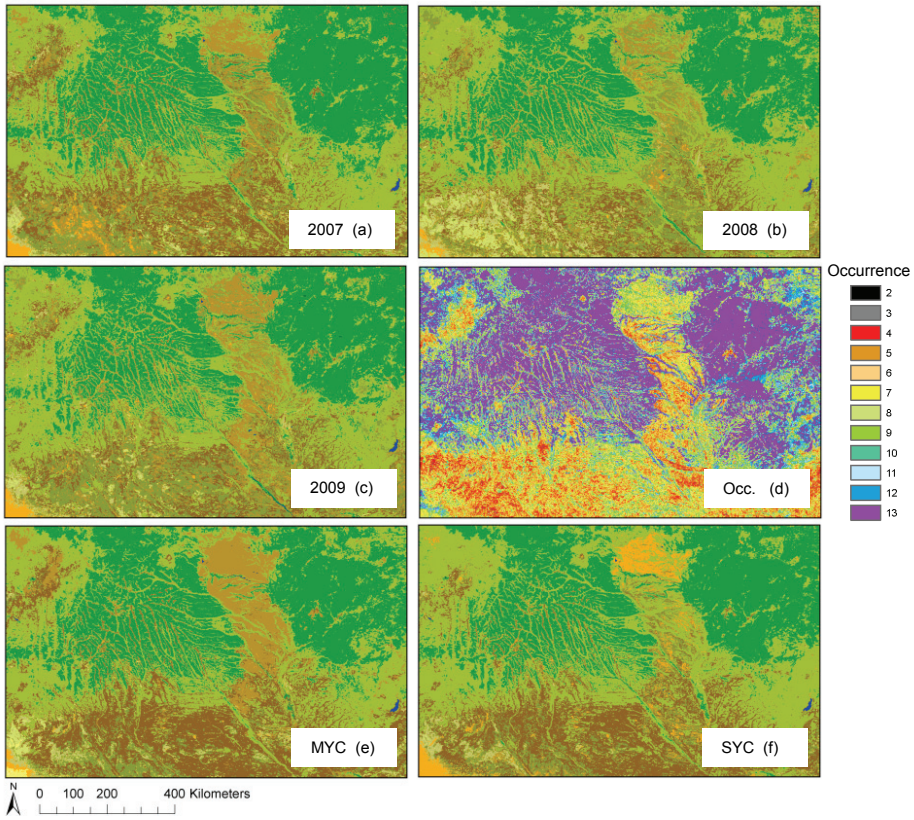


Figure 7 : Example of the inter-annual variability (Austral Africa ) between successive annual classifications with SPOT-VEGETATION data:. (a) 2007, (b) 2008, (c) 2009. Maximum of occurrence of a same land cover label over 13 annual classifications (d). Multi-year land cover map with (e) the MYC method (classification based on 1 set of 13-y composites) and (f) the SYC method (synthesis of 13 classifications). See Table 1 for the GlobCover legend.

In the example below (Figure 6 (a), (b), (c)), the instability between successive years clearly shows that an annual land cover map cannot depict a stable land cover in all regions at this spatial resolution. The confusion between croplands, grasslands and mosaics 'cropland / natural vegetation' classes is very high, as well as the confusion between shrublands and the mosaics 'forest / grassland'. The maximum occurrence of a same land cover label over the 13 years is indeed very low, indicating the instability (Figure 6 (d)). Inter-annual variability in precipitations could affect the croplands and the development of nearby vegetation, which could induce a different classification of the land cover from one year to another. The same cause

could explain the year-to-year extent variation of shrubs and grasses in Austral Africa (Figure 7 (a), (b), (c)). As observed in Figure 7 (d), the low number of occurrence matches the location of savannas (shrubs and grasses) strongly prone to annual fires, while the 'closed and open broadleaved deciduous forest' is consistently classified across almost all years. This may be also explained by grasslands being stressed during a specific year whereas it can recover a normal photosynthetic activity the year after (Kaptué Tchuenté et al., 2011). In most cases, yearly variations of climate and natural conditions can be at the origin of these inconsistent classification results, with the consequence of assigning different land cover classes from one year to another particularly if the event occurs during the period of the seasonal composites processed by the classification chain.

Figure 8 summarizes the land cover maps inter-annual variability by showing the average percentage of pixels transitions from one year to the next year over the 13 successive SPOT-VEGETATION classifications. For instance, on average over the 13 years, 92% of the pixels labelled as water (class 210) in one annual land cover map are also classified as water in the next land cover map, the remaining 8% being shared in a very small percentage between the other classes. Unsurprisingly, other very stable classes are snow/ice (class 220, 91% of stability from one year to another) and bare soil (class 200, 93% stability). Forest classes show a relatively good stability in the pixel transitions, especially for broadleaved evergreen forest (class 40, 89% stability) and needleleaved evergreen and deciduous forests (classes 70 and 90, 74% and 78% stability). By contrast, natural vegetation mosaic classes clearly show a high confusion with semantically close pure classes (classes 110 and 120), with on average only 29% and 27 % labelled as mosaic classes the next year respectively. Irrigated croplands (class 11, 64% stability) and regularly flooded broadleaved forests (class 160, 41% stability) are particular cases of classes confounded in a large proportion with one other class. Irrigated crops are confounded in 30% of cases with rainfed crops (class 14), and flooded broadleaved forests are confounded in 52% of cases with broadleaved evergreen forests (class 40). These are typical classes that will benefit of specific threshold rules in the synthesis (SYC) process even with low occurrence, as they are known to be difficult to classify but confounded with a very close class semantically.

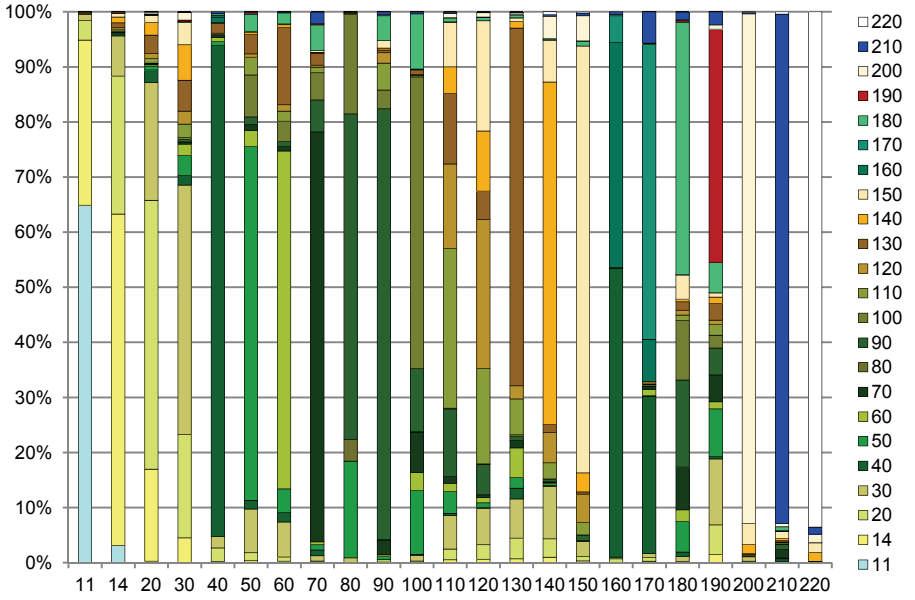


Figure 8 : 13-y average percentage of pixels transitions from one year to the next year, for the 13 annual SPOT-VEGETATION classifications. See Table 1 for the GlobCover legend.

Figure 8 mostly reflects inter-annual variabilities in pixel labelling as most of transitions occur among similar classes. But land cover changes are also glimpsed between land cover types spectrally and semantically very distant, such as the few transition percentage of broadleaved evergreen forests (class 40) into the two croplands mosaic classes (classes 20 and 30, 2,5% and 2% respectively) illustrating deforestation. Another example is the transition of water (class 210) to sparse vegetation (class 150, 1,5%) potentially representing a desiccation of water bodies.

## *3.2. Two multi-year global land cover maps*

In order to depict the stable land cover component, two global 1-km 13-y land cover maps have been produced: one classification based on 13-y composites (MYC method, Figure 9 (a)) and one synthesis of 13 annual classifications (SYC method, Figure 9 (c)). The overall distributions of land cover classes are visually very similar between the two maps. Most differences between the total surfaces of land cover classes for each product (Figure 9 (b) and (d)) concern mainly the proportion of the four mosaic

classes and, consequently, the pure classes associated to them. The surfaces of mosaic classes decrease for the synthesis (SYC), from 2.6% to 1.3% for the mosaic ‘grassland / forest’ (class 120) and from 6.6% to 2.8% for the mosaic ‘cropland / nat. vgt’ (class 20). Consequently, the surface of rainfed croplands (class 14) is almost doubled (5.8% to 9.9%) and most of the forest types are slightly more present in the SYC compared to the MYC. This difference is due to the specific decision rules designed to prioritize a pure land cover class in case of ambiguity with the related mosaic class. Irrigated croplands (class 11) are also more present in the SYC with 0.9% compared to 0.6% in the MYC. Thanks to the analysis of inter-annual variability in Figure 8, irrigated croplands are known to be often confounded with rainfed croplands. Thus, specific decision rules are applied in the synthesis to favour irrigated croplands if it is present in a sufficient number in the time series.

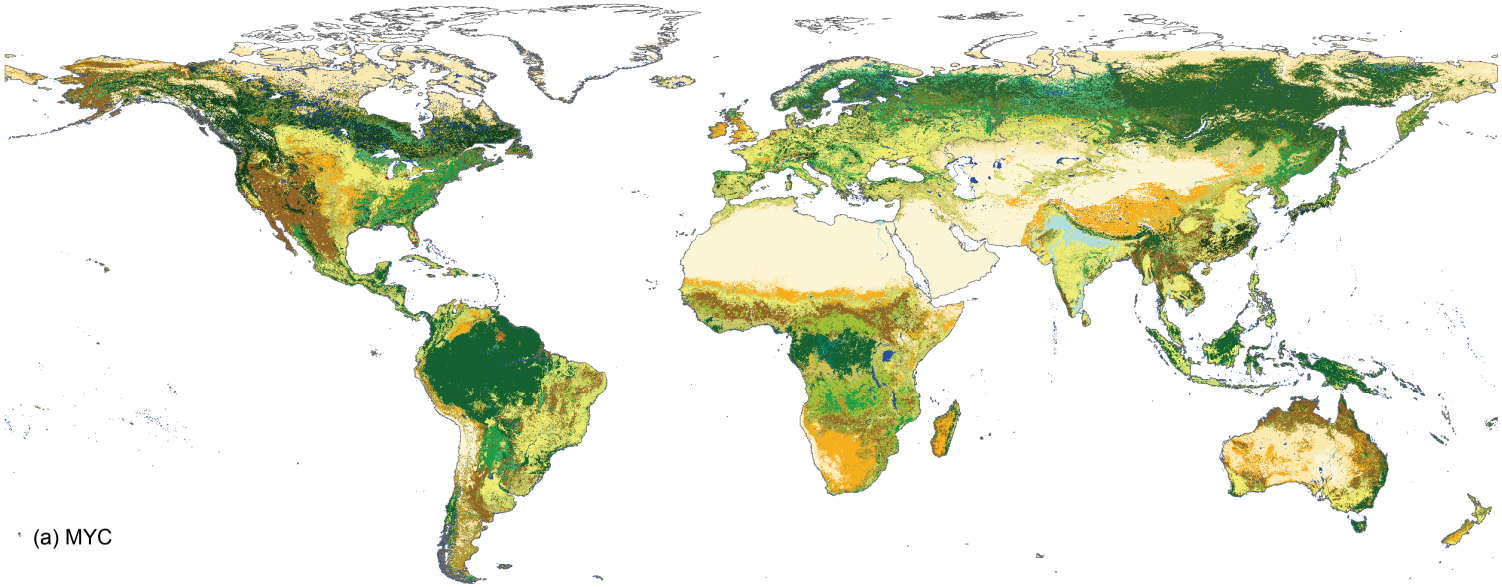

(a) MYC

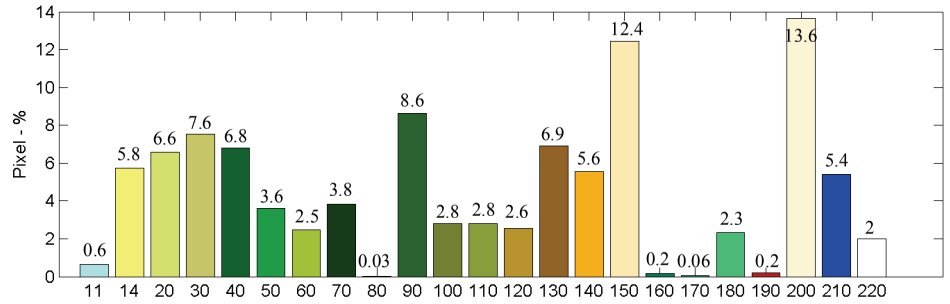
Pixel - %
0
2
4
6
8
10
12
14
0.6
5.8
6.6
7.6
6.8
3.6
2.5
3.8
0.03
8.6
2.8
2.8
2.6
6.9
5.6
12.4
0.2
0.06
2.3
0.2
13.6
5.4
2
11 14 20 30 40 50 60 70 80 90 100 110 120 130 140 150 160 170 180 190 200 210 220

(b)

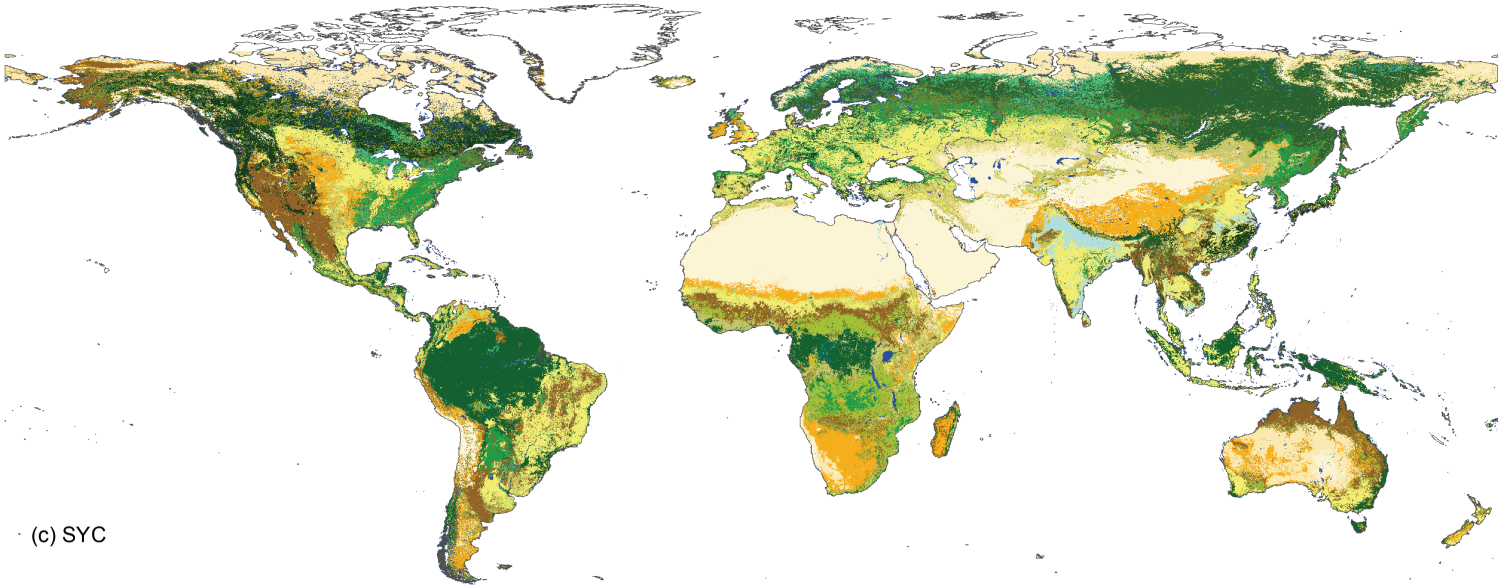

(c) SYC

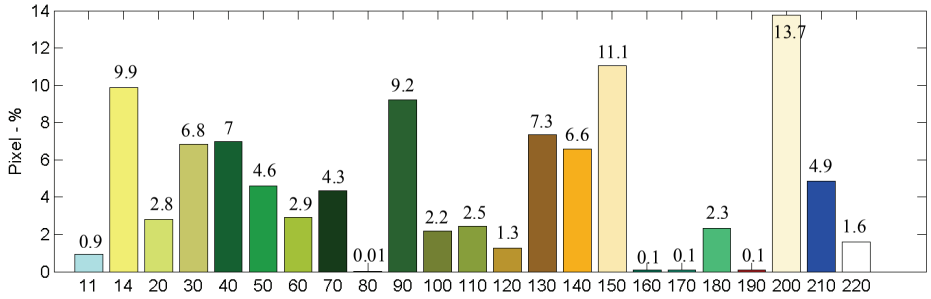
Pixel - %
14
12
10
8
6
4
2
0
0.9
9.9
2.8
6.8
7
4.6
2.9
4.3
0.01
9.2
2.2
2.5
1.3
7.3
6.6
11.1
0.1
0.1
2.3
0.1
13.7
4.9
1.6
11 14 20 30 40 50 60 70 80 90 100 110 120 130 140 150 160 170 180 190 200 210 220

(d)

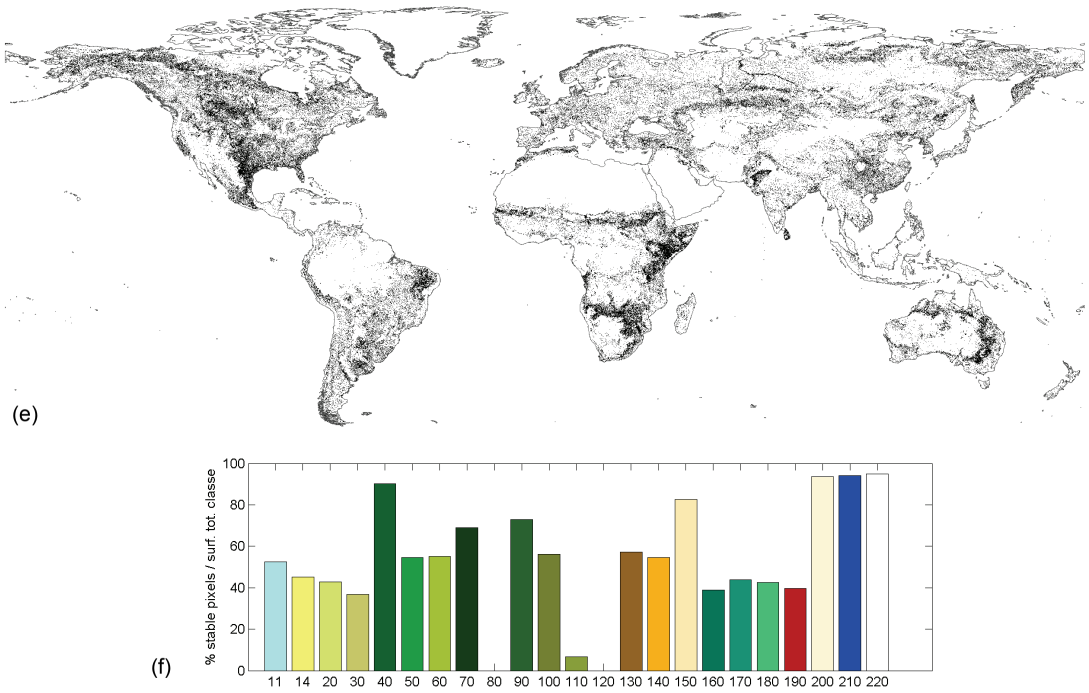


Figure 9 : Multi-year land cover map derived from SPOT-VEGETATION times series (1999 -2011) thanks to the GlobCover classification chain, relying (a) on the MYC method (classification based on composites summaries over 13-y of data) and (c) on the SYC method (synthesis of 13 annual classifications) with the respective surfaces per land cover classes (b) and (d). (e) Spatial representation of the 15.95 % of pixels (black) which cannot be simply labeled by majority voting (SYC) method, meaning that they doesn't reach the 7 occurrence over the 13 years. (f) Percentage of highly stable pixels (max. occurrence ≥ 9) per classes compared to the total area of the class of the SYC method product. See Table 1 for the GlobCover legend.

### 3.2.1. Quantitative accuracy assessment

The overall and global accuracies obtained with all the certain validation points, presented in Table 2, ranges from 70% to 75%. In a general manner, accuracy increases when considering only the homogeneous validation points as expected. Overall accuracies are slightly better for the MYC while global accuracies are higher for the SYC. These results are however very similar and cannot help to decide which product better performs.

Table 2 : Overall and global accuracies for the two multi-year land cover products computed with heterogeneous and homogeneous certain points.

| | **Overall Accuracy** | | **Global Accuracy** | |
|---|---|---|---|---|
| | **2428 heterogeneous and homogeneous certain points** | **1141 homogeneous certain points** | **2428 heterogeneous and homogeneous certain points** | **1141 homogeneous certain points** |
| **MYC method** | 71.08 % | 75.11 % | 71.46 % | 72.35 % |
| **SYC method** | 70.00 % | 74.76 % | 72.23 % | 73.27 % |

The confusion matrices with the homogeneous dataset in Table 3 and Table 4 indicate that rainfed croplands (class 14), mosaic classes 'cropland / nat. vgt.' (classes 20, 30), closed broadleaved evergreen and/or semi-deciduous forests (classes 40), bare areas (class 200), water (class 210) and snow/ice (class 220) perform very well for both maps with more than 80 % for both producer's and user's accuracies (PA and UA). Mosaic classes perform generally well concerning the UA because pure classes being components of the mosaics are considered to be in agreement for the validation (yellow cells). In a general manner, UA and PA are similar for both maps, although omission errors are a little lower for the SYC method product.

Concerning the forest classes, most of the commission errors comes from the confusion between the mixed forest class (class 100) and both the closed broadleaved deciduous class (50) and the two needle-leaved classes (classes 70, 90). However, a mixed forest class is labelled during the reference-labelling step of the GlobCover processing chain if the majority label of a cluster of pixels ranges between 40 and 60% and if the two main labels belong to broadleaved and needle-leaved forest classes. This does not

imply that individual pixels contain both broadleaved and needle-leaved trees. On the contrary, experts who label validation points define the mixed forest class as a pixel containing both types of trees, thanks to the analysis of high resolution data, although this distinction is not possible with 1-km SPOT-VEGETATION images. This ambiguity is solved by accepting mixed forest classes in the UA calculation (yellow cells). Class 80 and 90 present a very large number of omission errors for both products. It seems difficult to detect correctly needle-leaved areas. By contrast with the closed broadleaved deciduous class (class 50), the open broadleaved deciduous class (class 60) is often misclassified for both maps. Validation points indicate that this class is mostly confounded with class 50 and with shrublands (class 130) which are very close semantically to class 60. However, the confusion between deciduous and semi-deciduous in the reference dataset prevents a relevant assessment for broadleaved deciduous forests.

Concerning the flooded vegetation classes (classes 160, 170, 180), both PA and UA of classes 160 and 180 are very low for the two maps. On one hand, the very few validation points for these classes may not be representative. On the other hand, the PA of class 170 is doubled for the SYC to reach 100%. This might be a benefit from the SYC decision rules to prioritize flooded vegetation instead of the closed broadleaved evergreen forest class (class 40) if both classes compose the time series. In the same vain, it is observed that the irrigated crop class (class 11) is absent in the MYC while 2 pixels appear in the SYC, leading to a 100% UA.

Shrubland, grassland, sparse vegetation and bare area (classes 130, 140, 150 and 200 respectively) present high confusion between them, especially the grasslands that should be classified as shrubland or sparse vegetation in a large number of cases.

Finally, the urban class presents a very high UA (100% for the MYC and 75% for the SYC) but very low PA (30% for both MYC and SYC). It indicates that pixels classified as such in the maps are actual urban areas, but that many urban areas are missing. The omission errors are clearly due to the difficulty to map urban areas with SPOT-VEGETATION data. The high UA comes from large cities that are well detected. But well-known problems such as snow areas often classified as urban are not reflected in this UA.

Table 3: Contingency matrix of the MYC versus the homogeneous validation dataset. Green cells are cells that show agreement between classification and validation. Yellow cells mark cells that have been deemed to represent samples that do not disagree with the classified results. The value in the red cell shows the overall accuracy.

| Count | Reference | | | | | | | | | | | | | | | | | | | | | | | |
|---|---|---|---|---|---|---|---|---|---|---|---|---|---|---|---|---|---|---|---|---|---|---|---|---|
| Product | 11 | 14 | 20 | 30 | 40 | 50 | 60 | 70 | 80 | 90 | 100 | 110 | 120 | 130 | 140 | 150 | 160 | 170 | 180 | 190 | 200 | 210 | 220 | SUM | User's Acc. |
| 11 | | | | | | | | | | | | | | | | | | | | | | | | | |
| 14 | 8 | 84 | | | 1 | | | | | | | | | 1 | 1 | | | | | 1 | | | | 96 | 95,83% |
| 20 | 4 | 25 | | | 5 | | | | | | | | | 8 | 6 | 1 | | | | | | | | 49 | 97,96% |
| 30 | | 17 | | | 2 | 4 | 1 | | | | 1 | | | 11 | 17 | 3 | | | | 1 | 1 | | | 58 | 91,38% |
| 40 | 1 | | | | 208 | 4 | 2 | | | 1 | 1 | | | | | | 1 | 2 | | | | | | 220 | 95,00% |
| 50 | | 1 | | | 2 | 35 | 2 | 2 | | 1 | 15 | | | 1 | 1 | | | | | | | | | 60 | 83,33% |
| 60 | | 2 | | | 2 | 8 | 3 | 1 | | | 1 | | | 5 | 1 | 1 | | | 1 | | | | | 25 | 16,00% |
| 70 | | | | | 3 | | | 16 | | 5 | 15 | | | 2 | | | | | | | | 1 | | 42 | 73,81% |
| 80 | | | | | | | | | | | | | | | | | | | | | | | | | |
| 90 | | | | | | | | 3 | 4 | 1 | 14 | | | 1 | | | | | | | | | | 23 | 65,22% |
| 100 | | | | | | 11 | 1 | 3 | | 2 | 10 | | | 2 | | | | | 1 | | | | | 30 | 33,33% |
| 110 | | | | | | 1 | | | | 1 | 5 | | | 7 | 6 | 1 | | | | | 4 | | | 25 | 80,00% |
| 120 | | | | | | | | | | | | | | 8 | 3 | 2 | | | | 2 | 2 | | | 17 | 64,71% |
| 130 | | 4 | | | 5 | 3 | 1 | 1 | | 1 | 6 | | | 49 | 8 | 9 | | | | 1 | 5 | | | 93 | 52,69% |
| 140 | 4 | 7 | | | 1 | | | | | | | | | 15 | 19 | 14 | | | | 2 | 5 | 1 | | 68 | 27,94% |
| 150 | | 2 | | | | | | 2 | | 2 | 1 | | | 7 | 11 | 17 | | | | | 14 | 1 | 3 | 60 | 28,33% |
| 160 | | | | | 8 | | | | | | | | | | | | | | | | | | | 8 | 0,00% |
| 170 | | | | | | | | | | | | | | | | | | 2 | 1 | | | | | 3 | 66,67% |
| 180 | | | | | | 3 | | 2 | | | 5 | | | 1 | 1 | | 1 | | 2 | | | 1 | | 16 | 12,50% |
| 190 | | | | | | | | | | | | | | | | | | | | 3 | | | | 3 | 100,00% |
| 200 | 1 | | | | | | | | | | | | | 3 | 4 | 3 | | | | | 138 | 1 | | 150 | 92,00% |
| 210 | 1 | | | | | | | | | | | | | | | | 1 | | | | 3 | 58 | 4 | 67 | 86,57% |
| 220 | | | | | | | | | | | | | | | | | | | | | 1 | 1 | 26 | 28 | 92,86% |
| SUM | 19 | 142 | | | 237 | 69 | 10 | 30 | 4 | 14 | 74 | | | 121 | 78 | 51 | 3 | 4 | 5 | 10 | 173 | 64 | 33 | 1141 | |
| Prod. Acc. | 63,2% | 88,7% | | | 90,7% | 58,0% | 40,0% | 53,3% | 0,0% | 14,3% | 83,8% | | | 68,6% | 65,4% | 33,3% | 0,0% | 50,0% | 40,0% | 30,0% | 79,8% | 90,6% | 78,8% | | 75,11% |

Table 4: Contingency matrix of the SYC versus the homogeneous validation dataset. Green cells are cells that show agreement between classification and validation. Yellow cells mark cells that have been deemed to represent samples that do not disagree with the classified results. The value in the red cell shows the overall accuracy.

| Count | Reference | | | | | | | | | | | | | | | | | | | | | | | |
|---|---|---|---|---|---|---|---|---|---|---|---|---|---|---|---|---|---|---|---|---|---|---|---|---|
| Product | 11 | 14 | 20 | 30 | 40 | 50 | 60 | 70 | 80 | 90 | 100 | 110 | 120 | 130 | 140 | 150 | 160 | 170 | 180 | 190 | 200 | 210 | 220 | SUM | User's Acc. |
| 11 | 2 | | | | | | | | | | | | | | | | | | | | | | | 2 | 100,00% |
| 14 | 10 | 106 | | | 4 | 1 | | | | | | | | 6 | 6 | 1 | | | | 1 | | | | 135 | 85,93% |
| 20 | | 4 | | | 3 | | | | | | 1 | | | 1 | | | | | | | | | | 9 | 100,00% |
| 30 | | 11 | | | 4 | 3 | 2 | | | | | | | 12 | 16 | 2 | | | | 1 | 2 | | | 53 | 90,57% |
| 40 | 1 | 1 | | | 212 | 5 | 1 | | | | 1 | | | | | | 1 | | | | | | | 222 | 95,95% |
| 50 | | 1 | | | | 39 | 3 | 2 | | 1 | 17 | | | 3 | 3 | | | | | | | | | 69 | 81,16% |
| 60 | | 1 | | | 1 | 7 | 3 | 1 | | | | | | 5 | 1 | 2 | | | 2 | | | | | 23 | 13,04% |
| 70 | | | | | 2 | | | 16 | | 5 | 17 | | | 2 | | | | | | | | 1 | | 43 | 76,74% |
| 80 | | | | | | | | | | | | | | | | | | | | | | | | | |
| 90 | | | | | | | | 3 | 4 | 3 | 15 | | | 2 | 1 | | | | | | | | | 28 | 64,29% |
| 100 | 1 | | | | | 8 | | 2 | | 1 | 11 | | | | | | | | 1 | | | | | 24 | 45,83% |
| 110 | | 3 | | | | | | 1 | | | 2 | | | 2 | 6 | 4 | | | | | 4 | 1 | | 23 | 47,83% |
| 120 | | | | | | | | | | | | | | 4 | 3 | | | | | 2 | 5 | | | 14 | 50,00% |
| 130 | 2 | 3 | | | 6 | 4 | 1 | 1 | | 2 | 6 | | | 52 | 7 | 5 | | | | 1 | 2 | | | 92 | 56,52% |
| 140 | 1 | 11 | | | 1 | 1 | | | | 1 | | | | 22 | 24 | 18 | | | | 2 | 8 | 1 | | 90 | 26,67% |
| 150 | | 1 | | | | | | 1 | | 1 | 1 | | | 6 | 7 | 16 | | | | | 10 | 1 | 3 | 47 | 34,04% |
| 160 | | | | | 4 | | | | | | | | | | | | | | | | | | | 4 | 0,00% |
| 170 | | | | | | | | | | | | | | | | | | 4 | 1 | | | | | 5 | 80,00% |
| 180 | | | | | | 1 | | 3 | | | 3 | | | 1 | 1 | | 2 | | 1 | | | | | 12 | 8,33% |
| 190 | | | | | | | | 1 | | | | | | | | | | | | 3 | | | | 4 | 75,00% |
| 200 | 1 | | | | | | | | | | | | | 3 | 3 | 3 | | | | | 138 | 1 | | 149 | 92,62% |
| 210 | 1 | | | | | | | | | | | | | | | | | | | | 2 | 59 | 1 | 63 | 93,65% |
| 220 | | | | | | | | | | | | | | | | | | | | | 1 | | 29 | 30 | 96,67% |
| SUM | 19 | 142 | | | 237 | 69 | 10 | 31 | 4 | 14 | 74 | | | 121 | 78 | 51 | 3 | 4 | 5 | 10 | 172 | 64 | 33 | 1141 | |
| Prod. Acc. | 63,2% | 85,2% | | | 92,4% | 60,9% | 50,0% | 54,8% | 0,0% | 21,4% | 86,5% | | | 58,7% | 62,8% | 31,4% | 0,0% | 100,0% | 20,0% | 30,0% | 80,2% | 92,2% | 87,9% | | 74,76% |

### 3.2.2. Qualitative assessment of the two products

The quantitative accuracy assessment provides information on the quality of the maps as a whole but does not capture all the differences between them, especially those that are specific to certain areas. The two maps are thus visually compared systemically with available very high resolution imagery.

In a general manner, the SYC method provides better results. It was designed to (i) take advantage of the long time series to determine the most likely land cover class, (ii) limit the proportion of the mosaic classes because of their ambiguity for users, (iii) favor classes with small extent, known to be difficult to classify and (iv) deal with areas presenting large inter-annual variabilities and showing an ambiguous time series. These characteristics are illustrated with the following examples.

First, the advantage of the long time series to determine the most likely land cover class is shown with the interesting spatial consistency in Figure 10 (e, MYC) and (f, SYC) compared to annual classifications ((b), (c), (d)). Patches of broadleaved evergreen forests, corresponding to protected areas in an agricultural landscape, observed on the 2005 annual SPOT-VEGETATION composite (a), clearly appear in both multi-year products and are better delineated in the SYC (f) than in the MYC (e). It suggests that multi-year maps avoid omission errors compared to annual land cover classifications thanks to a removal of inter-annual variabilities. These inter-annual variabilities are clearly observed at the borders of the patches with the maximum of occurrence (g). It highlights that annual classifications have difficulties in mapping these areas the same way each year. Landscape structures are also visible in the USA example (Figure 6), where both MYC and SYC methods reveal more homogeneous patterns compared to the annual products.

Second, the SYC proposes a product that limits as much as possible mosaic classes. The important difference in proportion of pure classes and mosaic classes between the two products is already highlighted in histograms (b) and (d) in Figure 9. It is illustrated in Figure 6 where pure croplands much more present in the SYC (f) than in the MYC (e) which is composed principally of mosaic ‘cropland / nat. vgt’. This difference is also illustrated in Figure 11, South of Russia, where pure croplands are clearly underestimated in the MYC (g) while eSAT imagery (15 m of spatial resolution) confirms the presence of croplands (e). In this example, the cropland area presents a high inter-annual variability, as observed with the

maximum occurrence, compared to water and sparse vegetation. It confirms that this area is difficult to map and deserve particular attention.

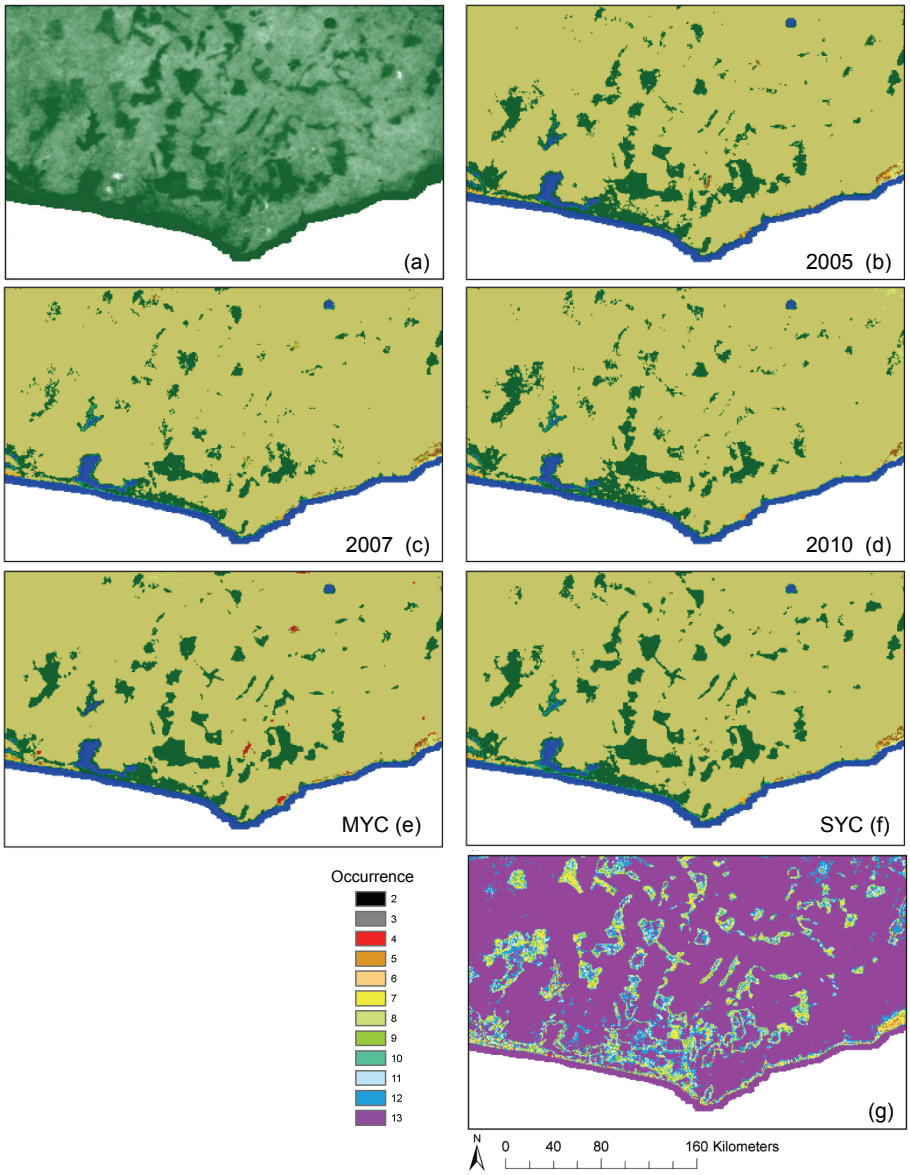


Figure 10. Illustration over Liberia and Ivory Coast. Annual SPOT-VEGETATION composite 2005 (a). Annual classifications with SPOT-VEGETATION data 2005 (b), 2007 (c), 2010 (d). Multi-year land cover map with the MYC method (classification based on 1 set of 13-y composites (e)) and the SYC method (synthesis of 13 classifications (f)). Maximum of occurrence of a same land cover label over 13 annual classifications (g). See Table 1 for the GlobCover legend.

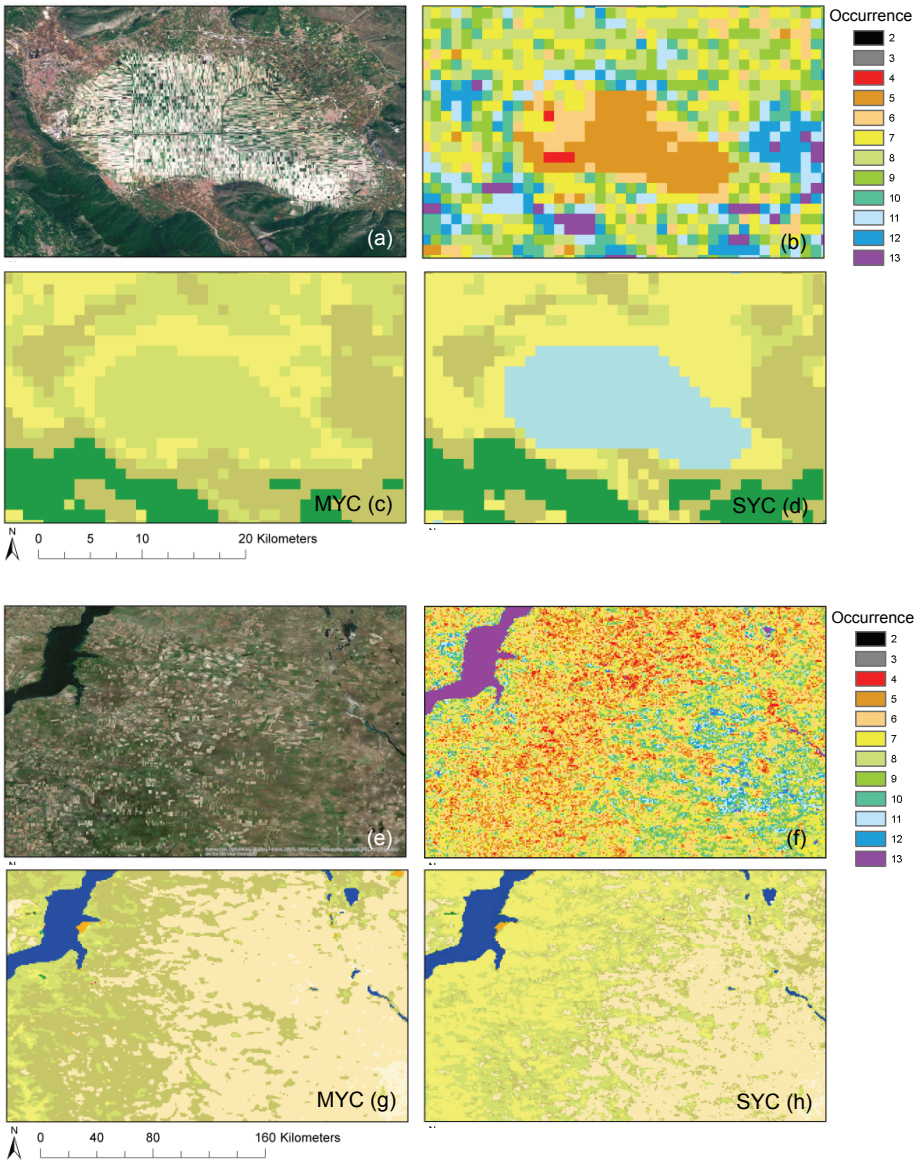


Figure 11. Illustration over Italy (a), (b), (c), (d) showing the ability to map irrigated croplands. Illustration over South of Russia (e), (f), (g), (h) showing the ability to map croplands. (a) and (e) are eSAT imagery (15 m of spatial resolution); (c) and (g) multi-year land cover map according the MYC method; (d) and (h) multi-year land cover map according the SYC method. Maximum of occurrence of a same land cover label over 13 annual classifications (b) and (f). See Table 1 for the GlobCover legend.

Also, in temperate regions often characterized by significant intra- and inter-annual variability in terms of climate conditions, land cover does not behave exactly in the same way every year. Thus, a classification on an averaged composite (MYC) has less meaning and prevents good land cover discrimination, while the SYC method allows a summary of these seasonal conditions to map the land cover.

Third, the ability of the SYC to prioritize classes with small extent, known to be difficult to classify, is illustrated in Figure 11 a, b, c, d). The maximum of occurrence clearly shows a patch with high inter-annual variability (b). This area is actually covered by irrigated croplands, confirmed by the presence of irrigated canals (a). It was observed that this class is often missing in annual classifications, because confounded with rainfed croplands (see inter-annual variabilities in Figure 8), but always confirming the ground truth when it is classified. Therefore, a specific decision rule of the SYC process, explained in Figure 4, ex. (c), admit bringing out a class difficult to map such as irrigated cropland if it is present at least 4 times in the time series and if others classes are semantically close. It is also the case for other land cover types such as flooded vegetation and urban areas. Thus, the SYC method allows depicting this irrigated croplands (light blue pixels, class 11), while the MYC classify this area in mosaic 'cropland/nat. vgt.' or rainfed croplands. For both maps, the detection of urban areas is particularly difficult. Figure 8 shows indeed that the urban class (190) is confused with a very large number of other classes. This can be due to the design of VEGETATION instruments adapted for the characterization of the main features of the plant canopy and to the fragmented form of urban areas containing simultaneously buildings, trees, parks, etc.

### 3.2.3. Quality indicators for the synthesis

The product of the SYC method – the synthesis of 13 annual classifications – presents some interesting advantages such as transparency and quality assessment of the map. The following indicators have the interest to be spatially represented for the whole world compared to very local measures of accuracy with the classical validation method.

First, the spatial representation of the maximum occurrence of a same land cover class over the 13 years (pixel-based) illustrates the degree

of inter-annual consistency and quantifies the confidence of the synthesis (Figure 12 (a)). A histogram is associated to this layer with the areas covered by each level of maximum occurrence over the world (Figure 12 (b)). The worst regions showing a very low maximum of occurrence, meaning a strong instability throughout the 13 years and uncertainty in the labels of the synthesis, are located in fragmented regions, in temperate regions presenting high inter-annual variations in climate conditions or in transition zones such as the center of U.S.A, the horn of Africa, Austral Africa at the transition between forest and grassland, the Sahel region at the transition between cropland and grassland, Australia around the edge of the desert, etc. The global land proportion of areas difficult to label (black pixels in Figure 9 (e) with maximum occurrence of a same land cover lower than 7) corresponds to 15.95 % of the terrestrial surface. These pixels can't be labeled by majority voting and need specific decision rules to determine a unique label. By contrast, 84.05 % of the land can be considered as quite confident as its maximum occurrence is higher or equal to 7 over the 13 years (white pixels inside the strata, Figure 9 (e)), and 35.1 % of the land, mostly covering deserts and equatorial forests, is always consistently mapped throughout the years (occurrence = 13, Figure 12 (b)). Pixels with a maximum occurrence superior or equal to 9 represent 65.7 % of the land.

The histogram in Figure 9 (f) represents within each class the percentage of pixels mapped in the SYC with a maximum occurrence higher or equal to 9. More than 80% of the area of the closed broadleaved evergreen forests (class 40), needleleaved forest (classes 70 and 90), sparse vegetation (class 150), bare soil (class 200), water (class 210) and snow (class 220) are classified the same at least 9 years out of 13, which indicates the label confidence and the high ability to classify these land cover classes. By contrast, the mosaic 'grassland/forest' (class 120) is never classified 9 times over the 13 years, and the percentage of the mosaic 'forest/grassland' (class 110) is very low. Less than 50 % of flooded vegetation (classes 160, 170, and 180) are classified the same at least 9 years out of 13. Indeed, these classes are known to be difficult to classify as there are often confused with non-flooded forests. Specific decision rules with a low threshold help these classes to be more labeled in the SYC. Generally, inter-annual variability is low for forest classes but high for crops, grasses, shrubs, and mosaics more present in heterogeneous landscapes and more sensitive to climate conditions.

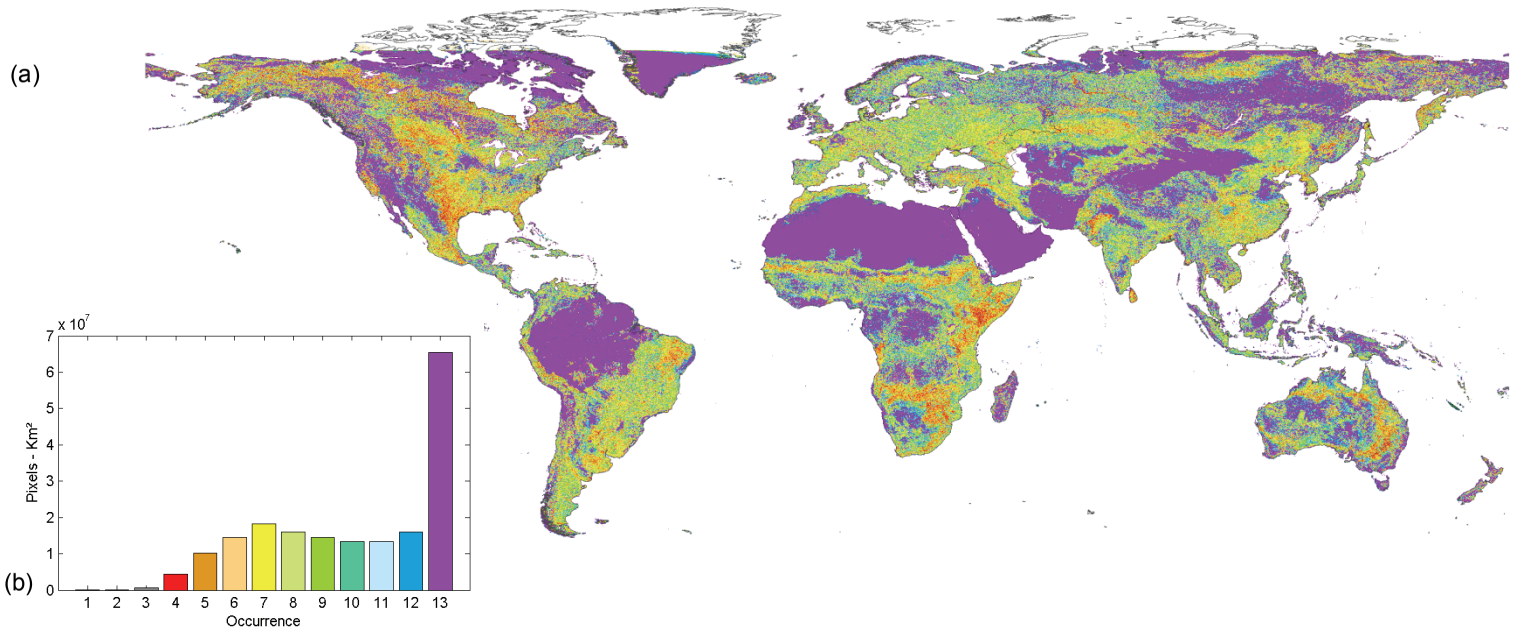
(a)
(b)
x 10^7
Pixels - Km²
0
1
2
3
4
5
6
7
1 2 3 4 5 6 7 8 9 10 11 12 13
Occurrence

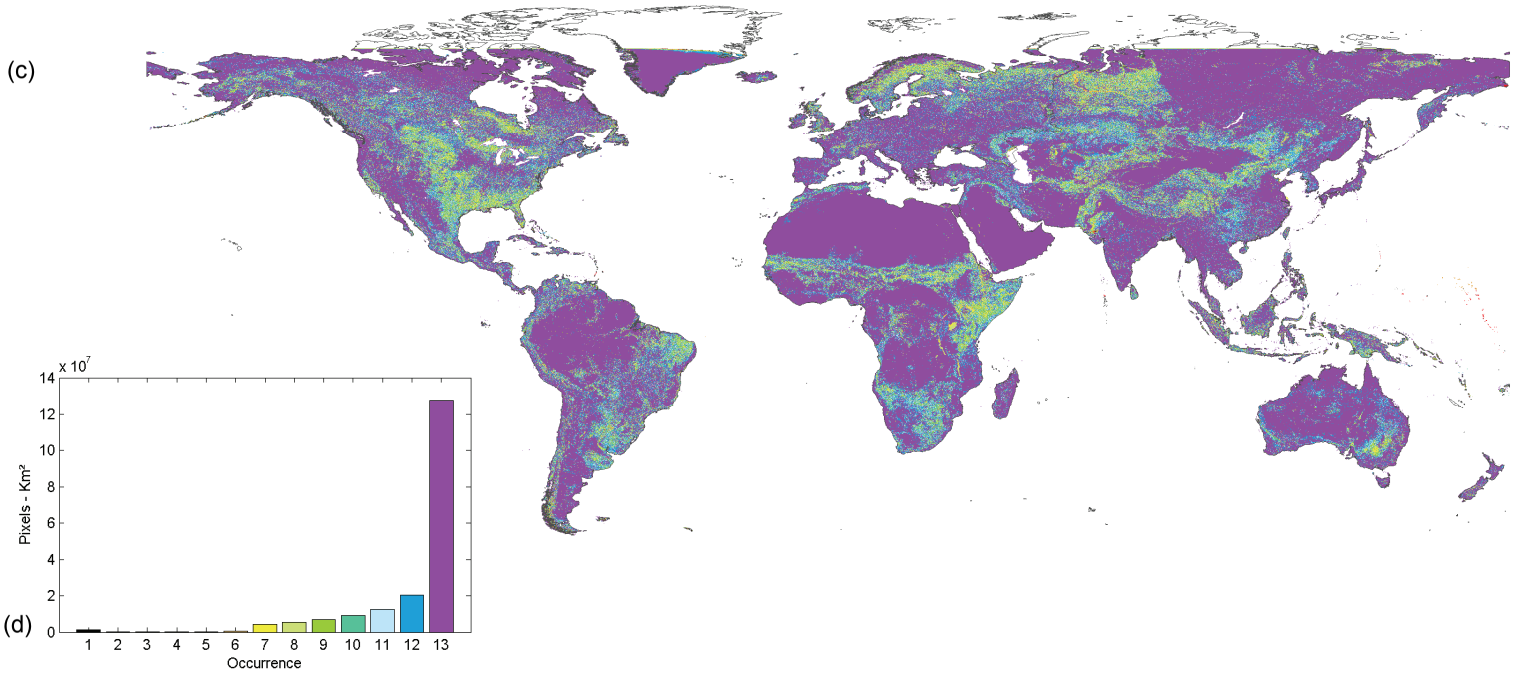


Figure 12 : Spatial representation (a) of the maximum occurrence of a same land cover class over the 13 annual classifications. (c) Idem for aggregated classes (Cropland – Forest – Flooded Vegetation – Grassland – Sparse and Bare areas – Urban areas – Water – Snow). Histograms associated showing the total area of each maximum occurrence over the world (b), (d).

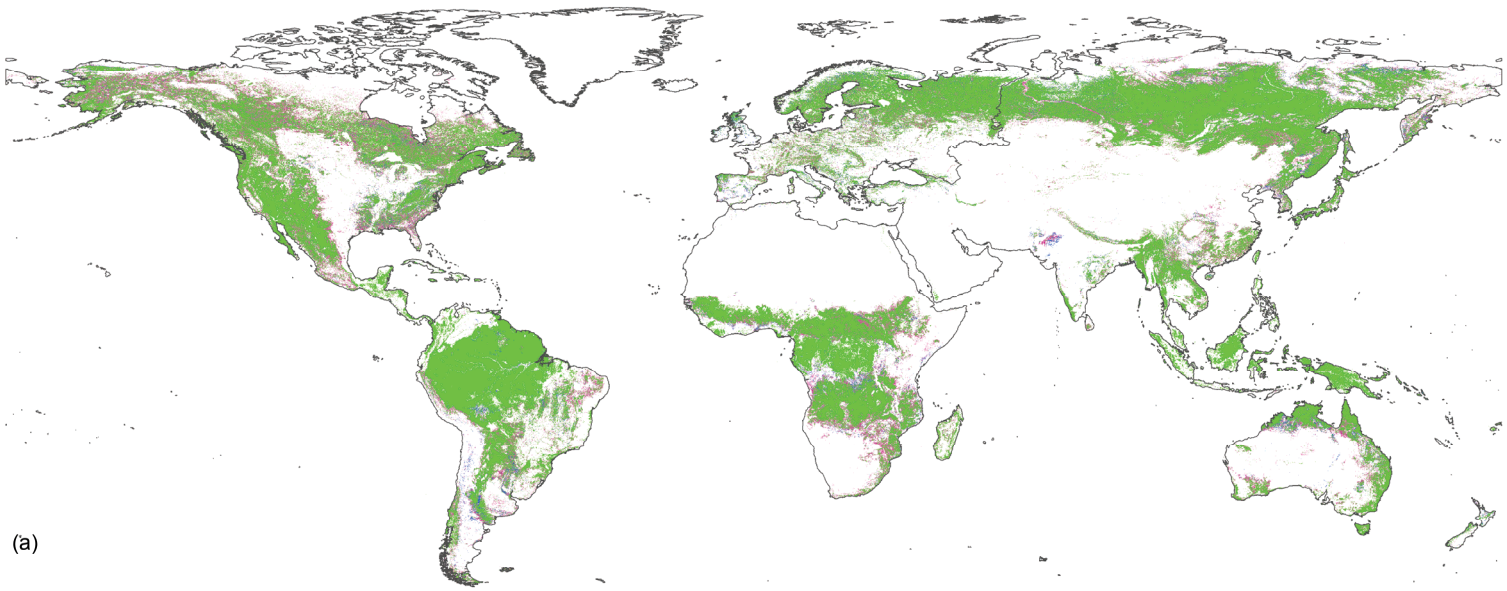

(a)

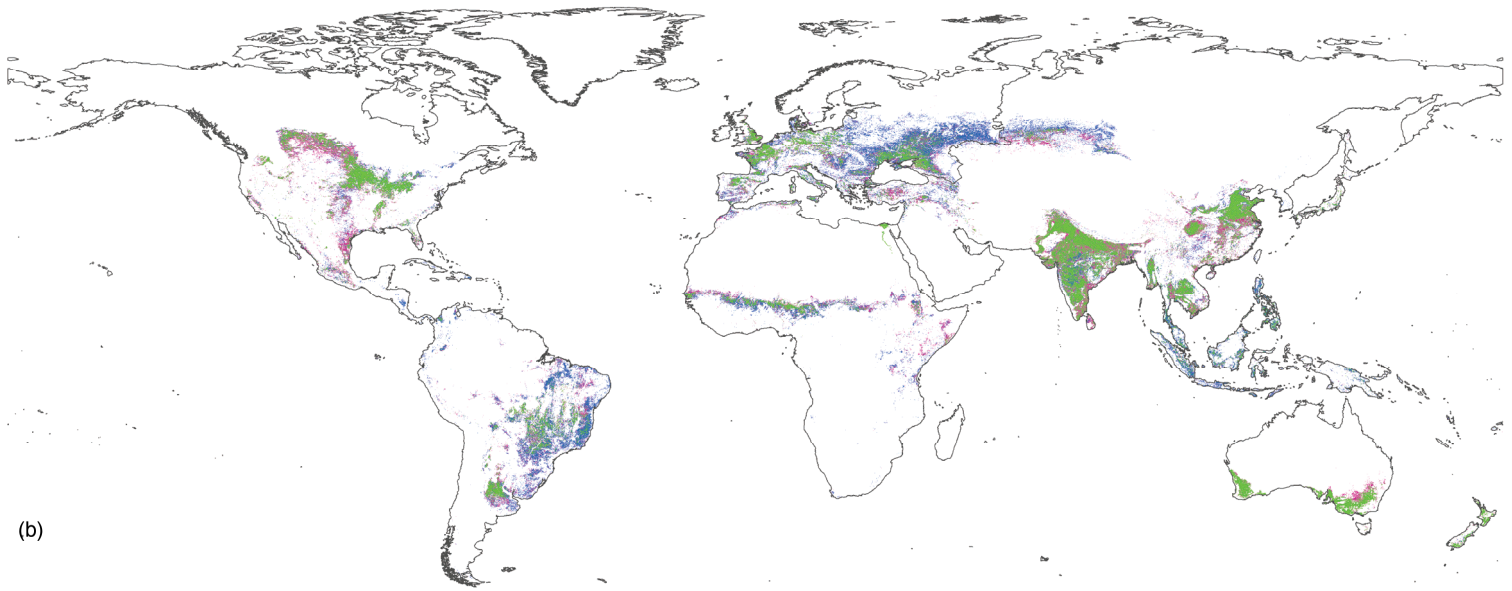


Figure 13 : Spatial representation of degree of reliability of the cropland pixels (a) and of the forests pixels (b) mapped in the SYC, according to the step at which the label was delivered (labelled with a majority (occurrence >= 7) (green pixels), over a majority mosaic (blue pixels), or with specific decision rules (pink pixels)).

It is also of interest to investigate the semantic distance between different classes in individual pixel time series. To this end, the 22 land cover classes have been aggregated into eight main classes (Cropland – Forest – Flooded Vegetation – Grassland – Sparse and Bare areas – Urban areas – Water – Snow) according LCCS criteria. Shrublands are grouped to the Forest class. The mosaic classes are comprised in several groups according to their definition. For instance, the mosaic class comprising grassland (50-70%) / forest or shrubland (20-50%) belongs both to the Grassland and the Forest main classes. A new layer of maximum occurrence is built for these aggregated land cover classes (Figure 12 (c)). At the level of 8 classes, a very large part of the world is stable with 93.7% of pixels having a maximum occurrence higher or equal to 9. It reveals that in most cases the different labels over the 13 years belong to the same aggregated class and confirms that inter-annual variability is mostly observed between classes that are semantically close.

Finally, additional map layers indicate the step at which the label was delivered in the SYC algorithm. It provides the level of confidence of the final label chosen in the synthesis. For instance, in Figure 13, pixels labelled with a majority voting (occurrence >= 7, green pixels), are mapped with more confidence than pixels labelled over a mosaic majority (blue pixels) or according to specific decision rules (pink pixels). Only 40 % of all croplands of the synthesis (Figure 13 (a)) are labelled with the majority voting, located mostly in North of America, Europe, India, China, and South of Australia, against almost 85 % for the forest classes all over the world (Figure 13 (b)). The rest of the pixels are labelled with more uncertainties.

## *3.3. Seven types of land cover change*

Land cover change is affected by its ecological and economic environment (Lambin et al., 2001). Indeed, while some of these changes have natural causes, such as storms, fires, droughts or insect infestations, others occur because of human activities, increasingly playing an important role in changing the land cover throughout the world through land use or land use change (Jin et al., 2013). Land use refers to the arrangements, activities and inputs people undertake for human use in a certain land cover type to produce, change or maintain it (Jansen and Di Gregorio, 2002; Foley et al., 2005). The relation between land cover and land use is complex and needs careful examination in each situation (Jansen and Di Gregorio, 2002), which

we try to do in the following selected examples. This global land cover change mapping not only treats forest losses and gains but also croplands, grasslands, bare areas and water losses and gains as well as urban areas gains, showing up a complete portrait of the Earth's land surface transformations.

### 3.3.1. Forest loss

The forest loss considered in this study is characterized by the disappearance of the forests and flooded forests groups giving way to crops, shrub, grass, flooded grass, sparse vegetation, bare soil or urban area. Changes in forest cover affect important ecosystem services such as biodiversity richness, climate regulation, carbon storage and water supplies (Foley et al., 2005). Among the variety of different land conversions (e.g. deforestation, urbanization, etc.), the removal of forest cover has been shown to dramatically affect hydrological processes such as evapotranspiration, canopy interception, and runoff at scales ranging from small plots to large river basins (Townsend et al., 2009). Despite the recognized importance of ecosystem services provided by forests of all types either for material or non-material human benefits (FAO, 2010; Brown, 2013), two of the five main causes of forest losses observed with this global change detection method are indubitably caused by human activity, namely deforestation for agriculture and mining. Natural disasters may also destroy forests, and when the area is incapable of regenerating naturally and no efforts are made to replant, it converts to other land (FAO, 2010). Among natural disturbances, the three main phenomena exposed firstly are windstorms, wildfires and insect infestations. Information availability and quality continues to be poor for most of these disturbances (FAO, 2010).

***The ravages of storms***

Figure 14 illustrates damages caused in the Landes forest by the windstorm "Klaus", which made landfall near Bordeaux (France) in January 2009. This storm, said to be the most damaging storm in Europe since "Lothar" in 1999, was characterised by very intense winds causing severe losses in maritime pine and oak forests, estimated to 23 % of the standing volume (McGuire, B., 2009; Gardiner et al., 2010).

The suite of annual classifications in Figure 14 (a) clearly shows the forest losses detected since 2009. The "hole" in the forest is however growing until 2011 illustrates the work of foresters who removed progressively the damaged but not fallen stands, as it is observed on high resolution images (Figure 14 (c)). Figure 14 (b) displays the multi-year land cover map without taking into account the land cover changes (b1), the pixels detected as forest loss by the algorithm and labelled with the new classes appearing after the change (b2) as well as the year of change (b3), the pixels detected as forest loss in the Global Forest Change map (Hansen et al., 2013) (b4), and finally the change superimposed on the multi-year land cover map (b5). The pixels trajectories identify the storm damages as a transition from high density mixed forest to mosaics of cropland and natural vegetation, confirmed by aerial photos from Google Earth (Figure 14 (c)), for almost 2000 km².

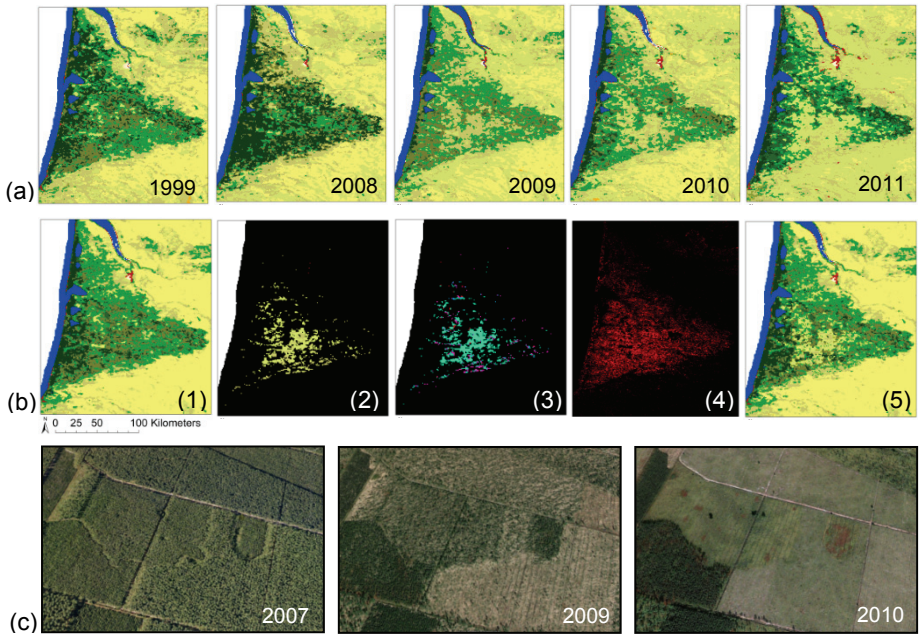


Figure 14 : Landes forest (France) damages caused by the windstorm "Klaus" in January 2009. Suite of annual classifications with SPOT-VEGETATION data (a). Multi-year land cover map (SYC) without taking into account land cover changes (b1), pixels detected as change (forest loss) labelled with the new land cover classes (b2), year of change (b3), pixels detected as forest loss in the Global Forest Change map (Hansen et al., 2013) (b4), and change superimposed on the multi-year land cover map (b5). Aerial photos from Google Earth in the Landes forest (c). See Table 1 for the GlobCover legend and Figure 5 for the year of change legend.

### *The damages of fires*

While some forest ecosystems depend on fire for their regeneration, in others forest fires can be devastating. On average, 1 percent of all forests were reported to be significantly affected each year by forest fires (FAO, 2010).

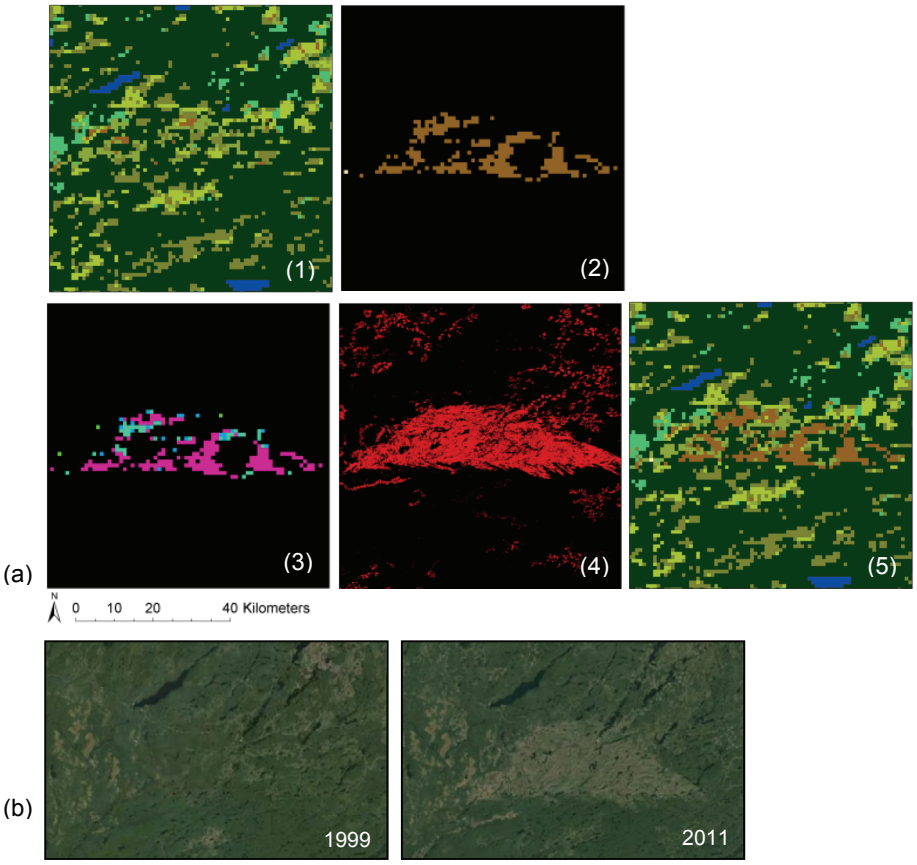


Figure 15 : Fire forest damages in Quebec (Canada) in 2007. Multi-year land cover map (SYC) without taking into account of land cover changes (a1), pixels detected as change (forest loss) labelled with the new land cover classes (a2), year of change (a3), pixels detected as forest loss in the Global Forest Change map (Hansen et al., 2013) (a4), and change superimposed on the multi-year land cover map (a5). Landsat images from the Google Timelapse tool (b). See Table 1 for the GlobCover legend and Figure 5 for the year of change legend.

The 260 km² of forest transformation into shrublands detected in Quebec in Figure 15 (a2) is a typical example of damages observed due to forest fires. These fires in dense forests cause real land cover changes for

years, compared to fires in savannas where the resilient vegetation burned recover the year after (Bucini and Lambin, 2002) inducing perturbation in the signal and inter-annual variabilities in classifications but not land cover change. In addition to forest loss and a release of carbon in the atmosphere, fires can induce relevant impacts on the air quality affecting human health and ecosystems downwind of fires because of the large amount of compounds emitted (Carvalho et al., 2011). The suite of Landsat images Figure 15 (b) indicates that the fire occurred in 2007, confirmed by photos and comments posted on Google Earth, such as year of change of most of the pixels in Figure 15 (a3), and did not yet regenerate in 2011. Omission errors are observed compared to the Global Forest Change map (a4) but the general shape of the damages is well captured. In North America, the decrease of the needleleaf class is attributed mostly to fires as the regeneration is slow (Pouliot et al., 2014) and to insect damage.

***The insect infestations***

Outbreaks of forest insect pests damage some 35 million hectares of forest annually, primarily in the temperate and boreal zone (FAO, 2010).

Since the late 1990s, mountain pine beetle outbreaks have caused widespread tree mortality and significant forest loss in North American forests and even led to a carbon source exceeding that of fire in Canada (Bright et al., 2012; Pouliot et al., 2014), an unprecedented outbreak exacerbated by higher winter temperatures (FAO, 2010). After trees are attacked and killed, tree needles begin to fade from green to red as needle desiccate and lose chlorophyll pigment. After 3-5 years, most red needles have fallen and only branches remain on the tree until it falls after a decade. Figure 16 shows the impacts of insect infestations, leading to a conversion of conifer to bare soil. The forest losses detected by the algorithm (a2) match very well with those on the Global Forest Change map (a4). The various years of change (a3) confirm the gradual nature of the disturbance, compared to a storm or a fire.

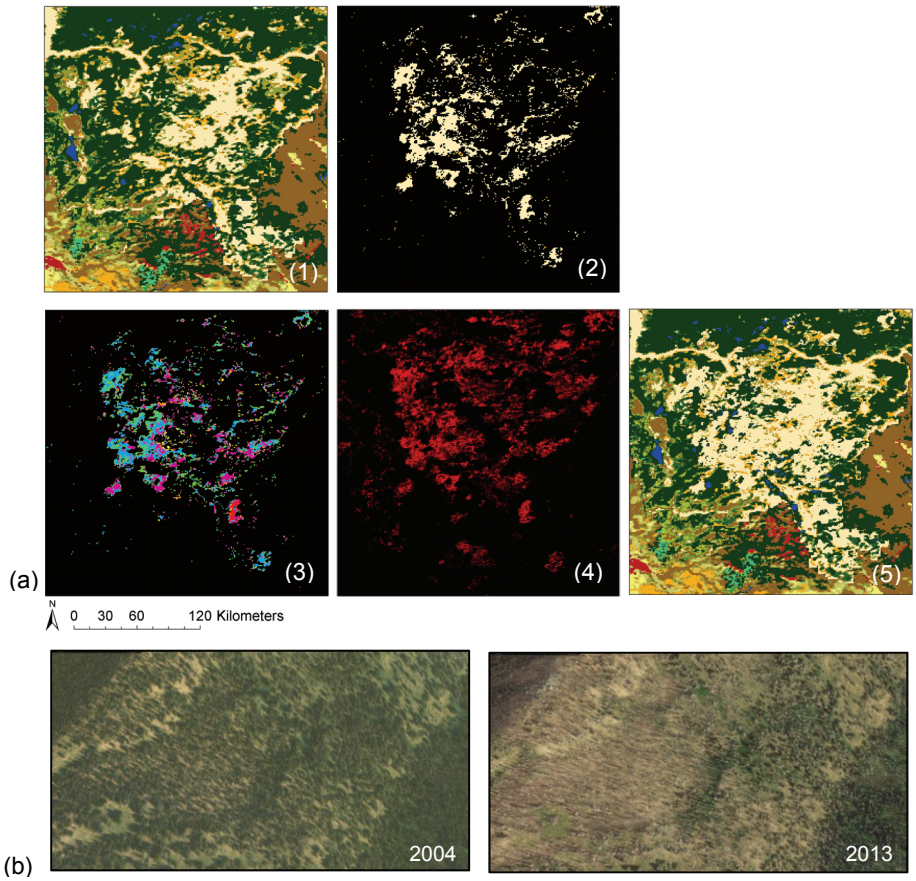


Figure 16 : Insect infestations damages in Idaho (USA). Multi-year land cover map (SYC) without taking into account of land cover changes (a1), pixels detected as change (forest loss) labelled with the new land cover classes (a2), year of change (a3), pixels detected as forest loss in the Global Forest Change map (Hansen et al., 2013) (a4), and change superimposed on the multi-year land cover map (a5). High resolution images from Google Earth (b). See Table 1 for the GlobCover legend and Figure 5 for the year of change legend.

### *The growing needs of croplands*

Globally, the conversion of land to croplands is responsible for the largest emissions of carbon from land-use change, especially when forests are converted to croplands (Houghton, 2010). When forests are cleared, carbon stored above and below ground in leaves, branches, stems and roots is released to the atmosphere. Consequently, forest clearing is a major source

of $CO_2$ in the atmosphere (Baccini et al., 2012). The two examples below refer to deforestation due to different types of agriculture.

The first one shows three regions in Democratic Republic of Congo (DRC) where the main underlying cause of deforestation is the demographic pressure leading to agricultural expansion and fuel wood extraction (Ernst et al., 2013; Mayaux et al., 2013). The deforestation around villages is clearly visible in Figure 17 (a2) and (c2) and matches the forest cover losses within primary forests identified in the FACET (Monitoring the forests of Central Africa using remotely sensed data sets) map (Mane et al., 2010) (Figure 17 (a4) and (c4) – losses 2000-2005 (red pixels) and 2005-2010 (purple pixels)). This reference product uses Landsat multi-year composites for 2000 to 2005 and 2005 to 2010 to quantitatively evaluate the spatiotemporal dynamics of forest change in DRC with a wall-to-wall interpretation method (OSFAC, 2010). The Eastern DRC characterized by a high deforestation rate is among the most populated areas of the country (Ernst et al., 2013).

The second example highlights the huge amount of deforested zones at an agro-industrial scale over North of Paraguay. Deforested areas reach more than 17000 km² (Figure 18 (a2)) between 2005 and 2011, equaling to 7.62 % of the forest cover in the multi-year land cover map (without changes integrated) showed in Figure 18 (a1). The Landsat images extracted from Google Timelapse demonstrate the fast progression of agricultural areas that is happening in these subtropical dry forests (Figure 18 (b), (d)), poorly documented compared to changes occurring in tropical rainforest although greatly affected by human activities (Ramankutty et al., 2006). They experience a very recent intensive forestry practices resulting in the highest rates of forest change globally (Hansen et al., 2013). The zooms illustrate the obvious anthropogenic structured patches of new croplands encroaching upon broadleaved evergreen and deciduous forests (Figure 18 (c2), (d). It seems that the rapid forest loss during the 1973-2000 period driven by settlers and by large private land owners devastating nearly two thirds of the forest in Paraguay's Atlantic Forest Ecoregion (Huang et al., 2007) is moving to the North. Beyond the deforestation, even if modern agriculture is successful in increasing food production, it also causes extensive environmental damages such as soil erosion, reduce fertility, degraded water quality or overgrazing (Foley et al., 2005).

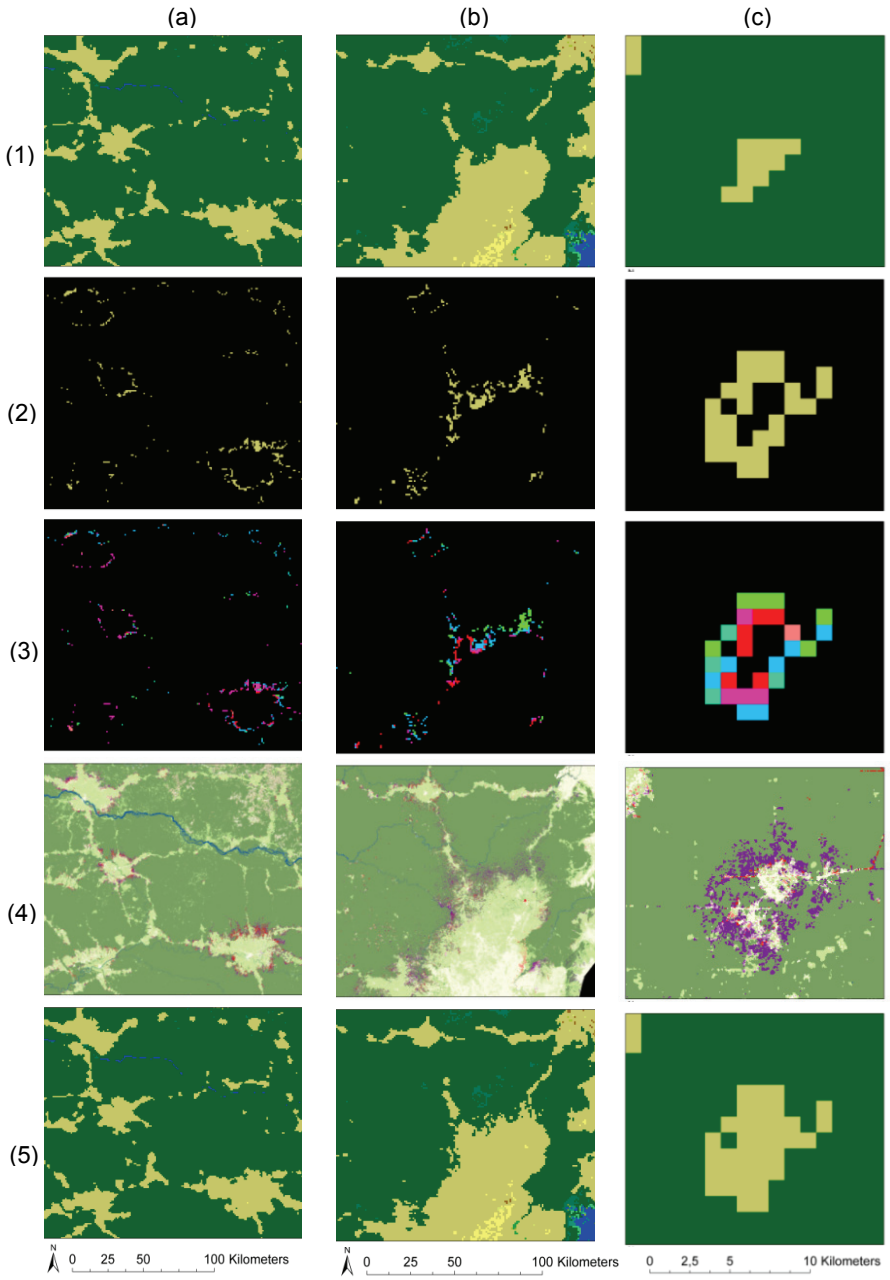


Figure 17: Deforestation in North (a, c) and East (b) of DRC. Multi-year land cover map (SYC) without taking into account of land cover changes (a, b, c: 1), pixels detected as change (forest loss) labelled with the new land cover classes (a, b, c: 2), year of change (a, b, c: 3), and change superimposed on the multi-year land cover map (a, b, c: 5). FACET map of forest cover extent and loss analysis in Democratic Republic of Congo (a, b, c: 4 – losses 2000-2005 (red pixels) and 2005-2010 (purple pixels)). See Table 1 for the GlobCover legend and Figure 5 for the year of change legend.

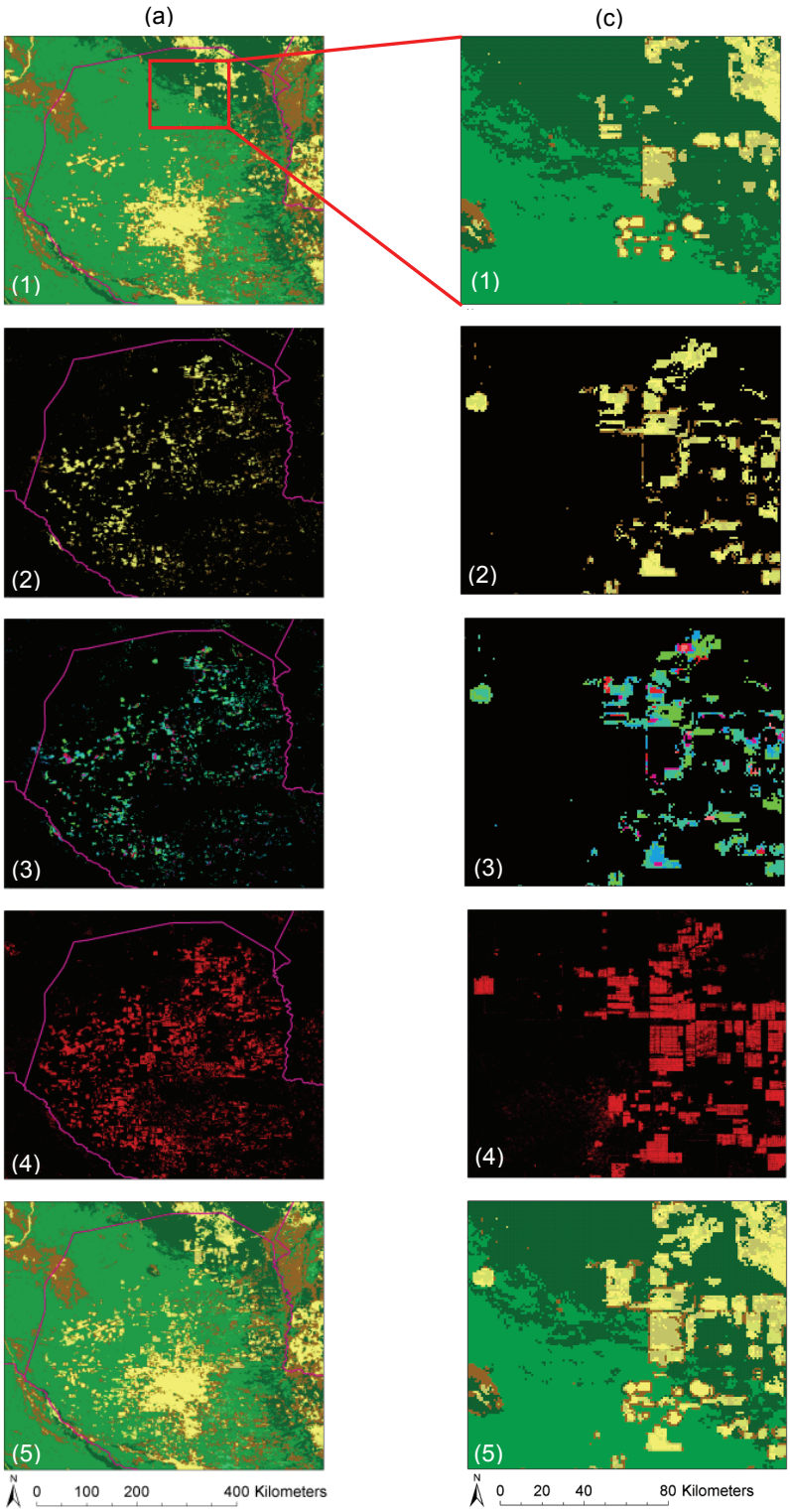
(a)
(c)
(1)
(1)
(2)
(2)
(3)
(3)
(4)
(4)
(5)
(5)
N
0 100 200 400 Kilometers
N
0 20 40 80 Kilometers




Figure 18 : Deforestation in North of Paraguay (boundaries : pink lines). Multi-year land cover map (SYC) without taking into account of land cover changes (a, c: 1), pixels detected as change (forest loss) labelled with the new land cover classes (a, c: 2), year of change (a, c: 3), pixels detected as forest loss in the Global Forest Change map (Hansen et al., 2013) (a, c: 4), and change superimposed on the multi-year land cover map (a, c: 5). Landsat images from the Google Timelapse tool (b, d). See Table 1 for the GlobCover legend and Figure 5 for the year of change legend.

While land cover changes due to natural events are abrupt and identified around 2-3 years, anthropogenic deforestation behaviors can be followed gradually year after year as observed in Figure 17 (c3) where pixels in the center correspond to deforestation in 2006 (red pixels) and 2007 (pink pixels) and pixels on the edges indicate changes in 2009 (turquoise pixels) and 2010 (green pixels).

***The destructive mining***

Mining activities can have strong impacts on the surrounding environment, either due to evident direct pressure on forest cover through logging, to local pollution from the mining operations, especially for processing oil sands, or to increased risk of flooding hazards because of changes in soil infiltration capacity (Latifovic et al., 2005; Townsend et al., 2009). The spatial changes mapping of the Athabasca bitumen (oil sands) region in Alberta (Canada) showed an increase in mining areas of 176 km² and of in forest cut-blocks of 61 km² from 1992 to 2001 (Latifovic et al., 2005). This change detection method counts 405 km² of forest losses from 2003 to 2011 (Figure 19 (a2)).

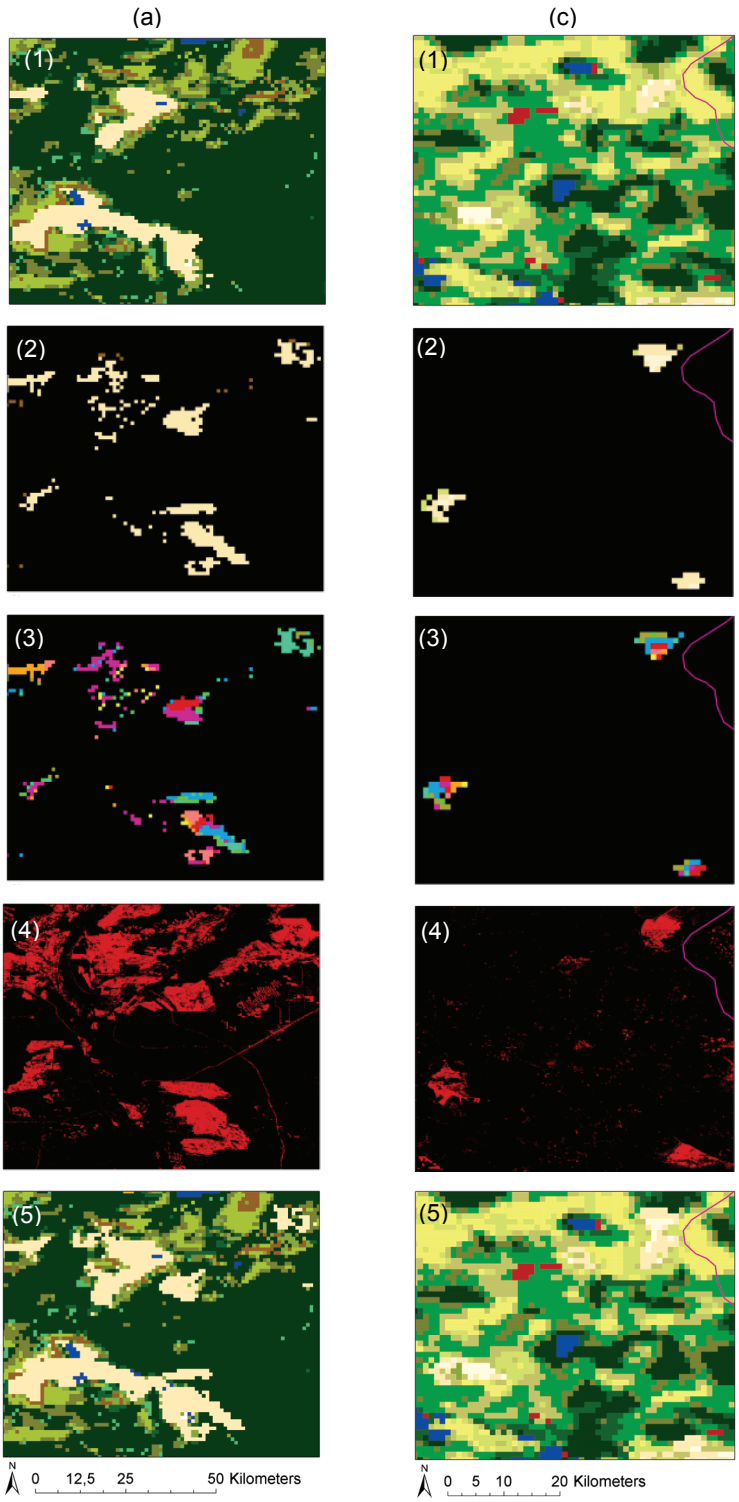
(a)
(c)
(1)
(2)
(3)
(4)
(5)
N
0 12,5 25 50 Kilometers
N
0 5 10 20 Kilometers

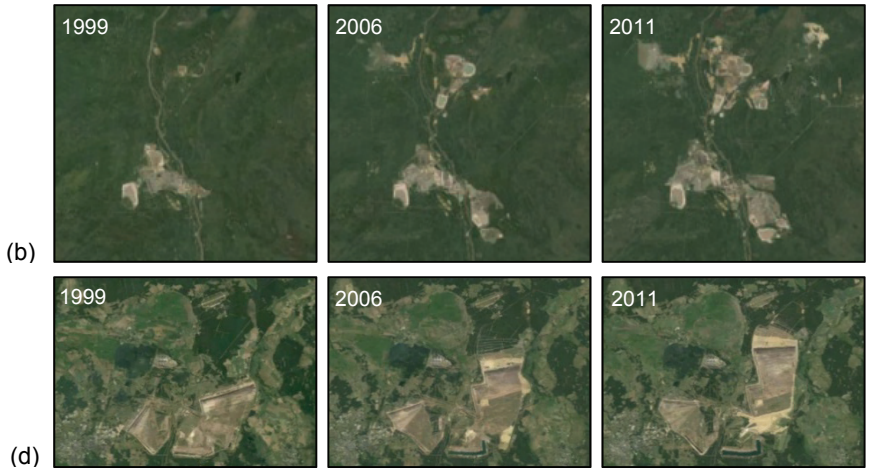


Figure 19 : Mining in the Athabasca Oil Sands region, Alberta (Canada) (a, b) and in Brandebourg (Germany) (c, d). Multi-year land cover map (SYC) without taking into account land cover changes (a, c: 1), pixels detected as change (forest loss) labelled with the new land cover classes (a, c: 2), year of change (a, c: 3), pixels detected as forest loss in the Global Forest Change map (Hansen et al., 2013) (a, c: 4) and change superimposed on the multi-year land cover map (a, c: 5). Landsat images from the Google Timelapse tool (b, d). See Table 1 for the GlobCover legend and Figure 5 for the year of change legend.

While disturbances are generally detected since 2005 to certify the stability over time for the 7 first years, the abrupt change from forest to sparse vegetation or bare soil spectrally very distinguishable offers the possibility to highlight the land conversions since 2003. Despite its different projection, Landsat images (Figure 19 (b)) clearly confirm the timing and extent of mining development detected with the trajectory-based method encroaching on the boreal forest (Figure 19 (a3)). Assuming these change assessments accurate, the deforested surface is almost doubled in two decades which is not surprising as the production from tar sands in Alberta is projected to nearly triple by 2030 (Tollefson, 2013).

The emissions from extracting and burning tar sands petroleum are 14-20 % higher than the average oil emissions. However, thinking in terms of climate change, initial focus should be on coal which would have 30 times the climate impact of oil if the world burned all proven coal reserves (Tollefson, 2013). One of the many active open-cast lignite mines of Europe used as fuel for electricity is presented on Figure 19 (c, d). The change surface trajectory in the mined zone, confirmed by Landsat imagery and the

Global Forest Change map (Figure 19 (d), (c4)), represents 62 km² from 2003 to 2011(Figure 19 (c 2-3)).

### 3.3.2. Forest gain

An increase in forest area can happen in three ways: through reforestation, through afforestation (i.e. planting of trees on land that was not previously forested in recent times) or through natural expansion of forests (e.g. on abandoned agricultural land, a process which is quite common in some European countries). The area of planted forest, mostly afforestation, is increasing and it now accounts for 7% of total forest area (FAO, 2010).

Subtle land cover dynamics, such as forest recovery, are considerably more challenging to detect with satellite data than forest loss because forest growth is a more gradual process and as a consequence there is limited change seen within most regrowing canopies over a single year (Strahler et al., 2006; Hansen and Loveland, 2012; Houghton et al., 2012; Griffiths et al., 2013). In addition, finding evidences of land cover change on high resolution imagery is much easier for rapid transformations like deforestation, either natural or anthropic, than for natural forest regeneration with slower dynamic. Figure 20 shows one of the rare examples of natural forest recovery accompanied with high resolution imagery clearly confirming the regeneration, probably after a fire (Russia). The forest gain (a2) very well matches those of the Global Forest Change map (Hansen et al., 2013) (a4). Anthropic reforestation or afforestation can be very fast and is thus more straightforward to observe, as shows Figure 21. Two plantations, confirmed by the details on Landsat images, are observed in Roraima (Brazil) (Figure 21 a, b) and in South Sumatra (Indonesia) in previously deforested areas (Figure 21 c, d). In Figure 21 (a1), the forest gain occurring since 2006 was already detected as forest in the multi-year land cover map thanks to specific decision rules. Omission errors are observed compared to the Global Forest Change map but the general shapes of the forest gains are well captured.

The admitted difficulty in capturing natural forest growth consistently through time and across space does not lessen their importance notably in term of carbon sequestration (Rudel et al., 2005; Hansen and Loveland, 2012). However, plantations are not a large net sink of carbon globally as they are often established on forest lands that have suffered

emissions from deforestation and as, being generally periodically harvested, they have an average carbon density lower than a natural forest (Houghton, 2010). In addition, such forest types often do not provide the ecological services provided by natural forests (FAO, 2010).

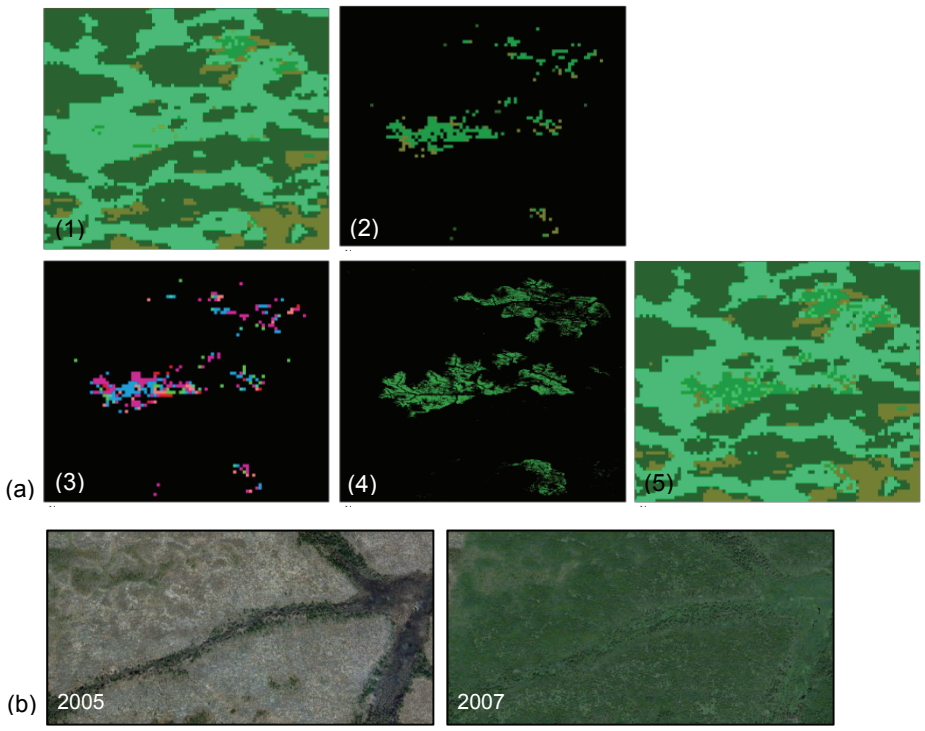


Figure 20 : Natural reforestation in Russia. Multi-year land cover map (SYC) without taking into account land cover changes (a1), pixels detected as change (forest gain) labelled with the new land cover classes (a2), year of change (a3), pixels detected as forest gain in the Global Forest Change map (Hansen et al., 2013) (a4) and change superimposed on the multi-year land cover map (a5). Landsat images from the Google Timelapse tool and Google Earth (b). See Table 1 for the GlobCover legend and Figure 5 for the year of change legend.

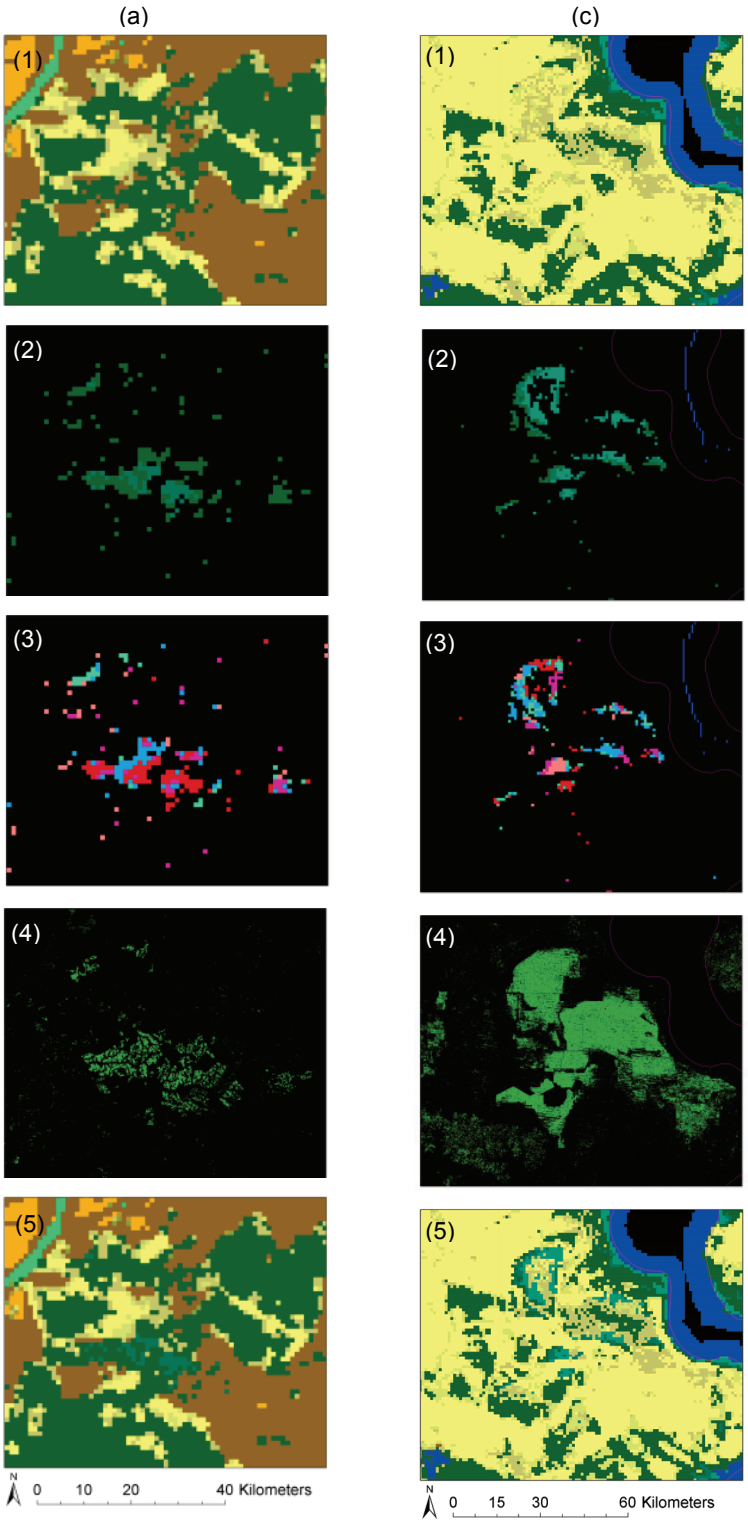
(a)
(c)
(1)
(2)
(3)
(4)
(5)
N
0 10 20 40 Kilometers
N
0 15 30 60 Kilometers

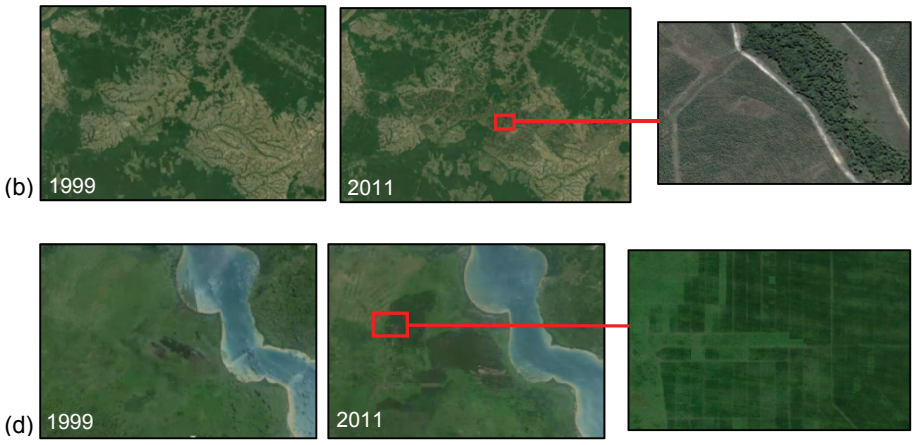


Figure 21 : Plantations in Roraima (Brazil) (a, b) and in South Sumatra (Indonesia) (c, d). Multi-year land cover map (SYC) without taking into account land cover changes (a, c: 1), pixels detected as change (forest gain) labelled with the new land cover classes (a, c: 2), year of change (a, c: 3), pixels detected as forest gain in the Global Forest Change map (Hansen et al., 2013) (a, c: 4) and change superimposed on the multi-year land cover map (a, c: 5). Landsat images from the Google Timelapse tool and Google Earth (b, d). See Table 1 for the GlobCover legend and Figure 5 for the year of change legend.

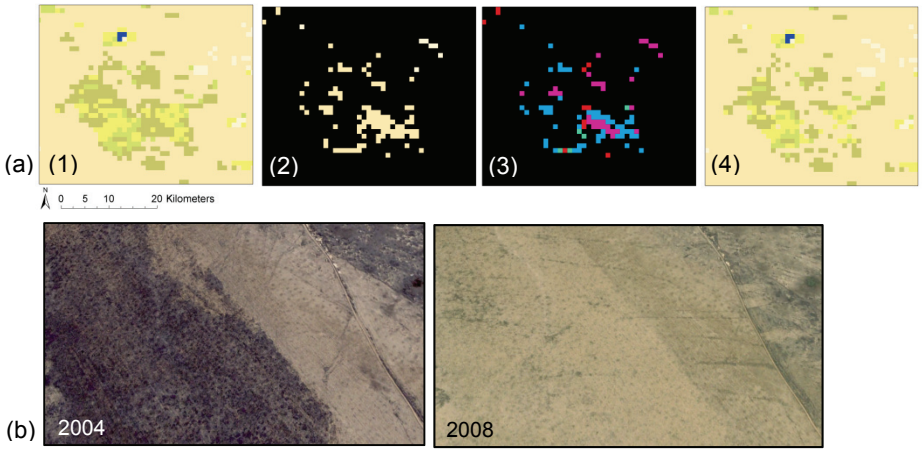


Figure 22 : Croplands change into sparse vegetation in Aktioubé (Kazakhstan). Multi-year land cover map (SYC) without taking into account land cover changes (a1), pixels detected as change (croplands loss) labelled with the new land cover classes (a2), year of change (a3), and change superimposed on the multi-year land cover map (a4). Landsat images from the Google Timelapse tool (b). See Table 1 for the GlobCover legend and Figure 5 for the year of change legend.

### 3.3.3. Crop and grassland loss

Crop and grassland loss refers here to a conversion of these land cover types into sparse vegetation or bare soil. This desertification process is defined by the United Nations Convention to Combat Desertification (UNCCD) as land degradation (decrease or destruction of the biological productivity of the land) in arid, semi-arid and dry sub-humid areas resulting from various factors, including climatic variations and human activities. Figure 22 illustrates losses of croplands or rangelands at the transition zone between the large crop area in South West Russia - North Kazakhstan and the Kazakh semi-desert, a region that has already suffered from overgrazing leading to land degradation (Karnieli et al., 2008) but also strongly dependant on the precipitation regime (de Beurs et al., 2004). The Asian continent currently has the greatest concentration of dryland degradation (Lepers et al., 2005). However, dryland change are less complete and understood than on other types of land cover change because of the difficulties of satellite interpretation in these regions and an inability to distinguish human-induced trends from climate-driven inter-annual variability in vegetation cover (Lepers et al., 2005; Ramankutty et al., 2006). Thanks to their structured landscape, confirming the detection of croplands losses with high resolution images is much easier than observing a transformation of grassland into sparse vegetation.

### 3.3.4. Crop and grassland gain

Cropland and grassland gains from deforestation were already discussed in the forest loss section. Here, it refers to a greening process through the conversion of sparse vegetation or bare soil into crops or grasses. As for the crop and grass loss, the observation of gain is more straightforward for the emergence of agricultural areas than for new grasslands. A typical anthropogenic oasis appearing suddenly in the desert is the center-pivot irrigated land in Al Jawf (Saudi Arabia) (Figure 23 (b)), an arid region with low annual rainfall and limited groundwater but producing a variety of crops. The year of change (Figure 23 (a3)) starts a little lately in 2008, probably because of too small crops patches before this date. As the contribution of rainfalls to agriculture is minimal in this region, it primarily depends on limited non-renewable groundwater sources, which may not survive for a long time at the current rate it is consumed (Chowdhury et al., 2009). Indeed, extraction of groundwater reserve for irrigation is almost

universally unsustainable and has resulted in declining water tables in many regions (Foley et al., 2005).

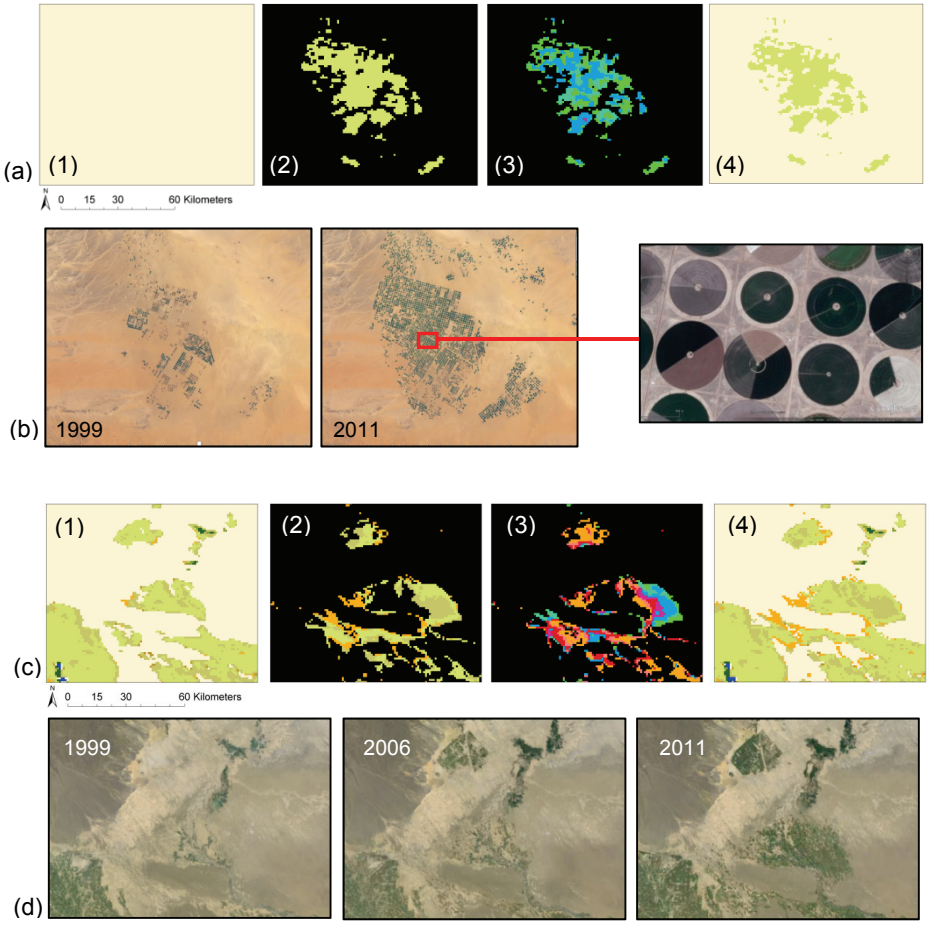


Figure 23 : Croplands appearance in desert of Al Jawf (Saudi Arabia) (a, b) and in Xinjiang (China) (c, d). Multi-year land cover map (SYC) without taking into account land cover changes (a, c: 1), pixels detected as change (croplands gain) labelled with the new land cover classes (a, c: 2), year of change (a, c: 3), and change superimposed on the multi-year land cover map (a, c: 4). Landsat images from the Google Timelapse tool (b, d). See Table 1 for the GlobCover legend and Figure 5 for the year of change legend.

Water scarcity in the Karamay Agricultural Development Area (KADA) in the Xinjiang province (Figure 23 (c, d)) is got around with the water transferred from IrtySh River approximately 300km away to the north

of Karamay (Han et al., 2011). Although being one of the most arid regions in the northwest of China, this province is one of the world's most important cotton production region (Thevs et al., 2014). This type of extensive irrigation without adequate drainage has caused rising groundwater levels since the beginning of the land development in 2000. As water levels rise, dissolved slats move by capillary action, causing degradation of the soil. Implementation of salinity management strategies is considered necessary in order to reduce the risk of further salt accumulation and damage to farming and local ecosystems (Han et al., 2011).

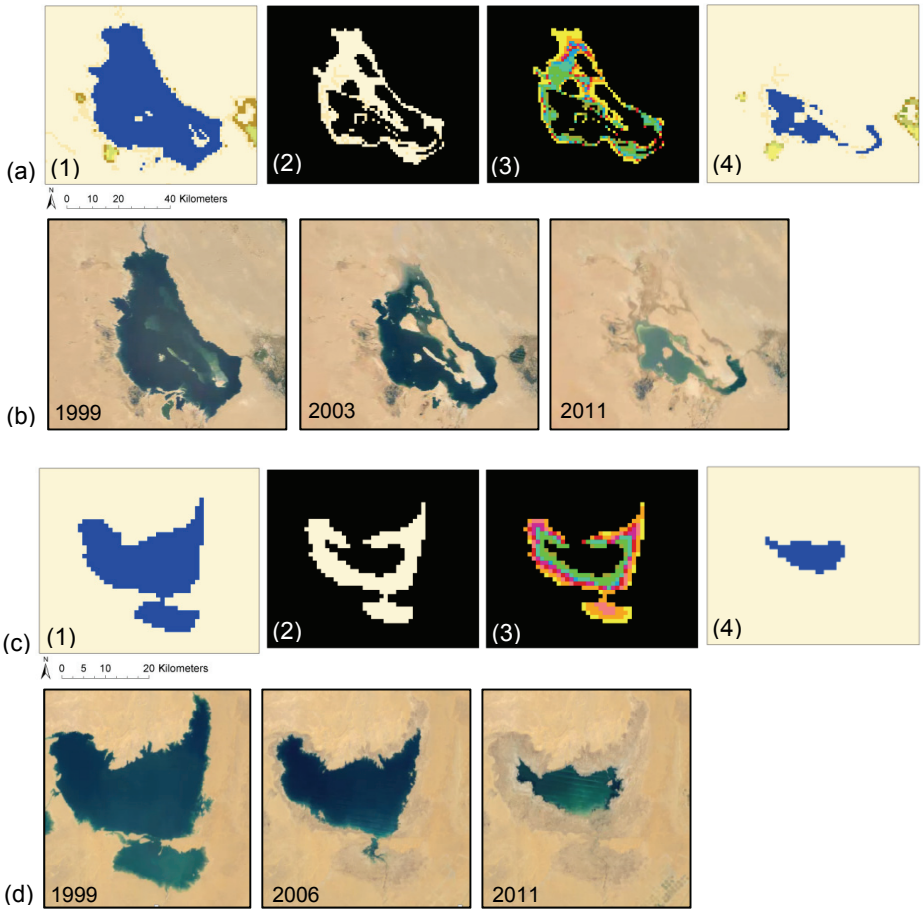


Figure 24 : Drying up of Razazza Lake (Iraq) (a, b) and of Toshka Lakes (Egypt) (c, d). 1999 classification (a, c: 1), pixels detected as change (water loss) labelled with the new land cover classes (a, c: 2), year of change (a, c: 3), and change superimposed on the multi-year (SYC) land cover map (a, c: 4). Landsat images from the Google Timelapse tool (b, d). See Table 1 for the GlobCover legend and Figure 5 for the year of change legend.

### 3.3.5. Water loss

Losses of water are principally observed in arid and semi-arid regions. Lakes in these arid landscapes are indicators of environmental change like alteration in precipitation and evaporation, but also important sources of water for human use such as irrigation or hydropower generation (Chipman and Lillesand, 2007; Klein et al., 2014). They are particularly vulnerable to the effects of human interventions, as illustrated by the case of the Razzaza Lake in Iraq (Figure 24 (a, b)). The lake, formed in the 1970s as a storage reservoir to divert the annual floodwaters of the Euphrates River and to prevent flooding across southern Iraq, reached around 1800 km² and was teeming with commercial activity, fish and avian life. It was principally fed by the Euphrates River through the Sin-Al-Thibban canal. In addition to the increase of annual evaporation and decrease of annual rainfall since 1970 (Othman et al., 2014), the lake began to shrink in 1991 because the water allocation via the Sin-Al-Thibban canal was suspended. Indeed, the closure of the waterway had been ordered to aggressively drain the southern Iraqi marshes after they became a refuge for Iraqis involved in anti-governmental rebellions. As consequence, the Razzaza Lake is dying a slow death (Figure 24 (a3)) and is now characterized by very high salinity levels which have increased during the past ten years due to the shortage in water it receives and increased evaporation during Iraq's searing summer months. The migratory birds have mostly left as well as hundreds of fishermen, the only fish remaining being the tiny Shanak resistant to salinity. The area is heading for economic, social and environmental disaster.

Figure 24 (c, d) shows the fast drying up of one of the newly large endorheic lakes formed in 1998 in the Toshka Depression (Sahara) of southern Egypt. Large quantities of Nile River water were introduced into this hyper-arid environment from Lake Nasser, a giant reservoir created by construction of the Aswan High Dam (Chipman and Lillesand, 2007) to regulate extreme events of droughts or floods (Warner, 2013). As the reservoir was too small, the rising water in Lake Nasser has being conveyed into the Toshka region which served as a spillway to protect the dam and downstream communities from flooding. From space, astronauts noticed the growing of a first lake, the easternmost one, in 1998. In subsequent years, four additional lakes were created to the west. The floodwater deviated to the Toshka Depression was then utilized to "green the desert" (Warner, 2013). Irrigation infrastructure was constructed to provide water for up to 336000 ha of new agricultural land in the region, legitimized by a discourse of

overpopulation (Warner, 2013). However, this pharaonic project only counted 21000 ha of farmland in 2012, less than 10 per cent of the goal, and none of the cities, factories, schools or hospitals promised has been built (Hope, 2012). The scheme of the project (contribution to food security, solution to overpopulation and unlimited availability of water) seemed to vanish with the water. The lakes, which increased to a maximum of 1740 km² before declining (Chipman and Lillesand, 2007), started shrinking at a very constant rate (Figure 24 (c3)) because of a reduction of water supply. The high water loss rate was mainly caused by the evaporation, the percolation of water through the ground being quite limited and the flow out toward the sea impossible in this Depression. This evaporation caused rapidly increasing salinity which led to a declined of the new established flora and fauna coming from the Nile.

As this type of change between such different land cover classes is easily detected and verified in most of cases, the period of change detection is extended to 2003 until 2011. The years of change detected (Figure 24 (a3, c3)) revealed high logical temporal change trajectories with 2003 change (yellow pixels) on the edges and 2011 change (khaki pixels) near the center of the lakes. In addition, evidences of change on high-resolution images are easily found for most of the groups of pixels flagged as water loss.

These two examples show that ecological problems such as land desertification, salinization and biodiversity losses are strongly connected to lake surface decrease. An accurate spatial detection and monitoring of water bodies is important for the assessment of driving forces and for future political activities and decisions in terms of sustainable land and water management (Klein et al., 2014).

### 3.3.6. Water gain

New water bodies principally arise due to the construction of reservoirs or ice melting caused by rising temperatures (Klein et al., 2014). Most of the conversions of vegetated land to water detected are explained by hydroelectric projects begun during the 10 last years. Compared to water loss, years of change for water gain from hydropower dam (Figure 25 (a3)) show logically the opposite trajectories with 2003 change (yellow pixels) at the center of the water body and 2009-2010 change (turquoise and green pixels) on the edges, reflecting the filling period of the reservoir. The

reservoir development in Figure 25 is the consequence of the Indira Sagar Hydroelectric Project, situated on River Narmada in central India, with a dammed water area of 913 $km^2$. Being one of the biggest dams in India, it serves to produce electricity and to irrigate 1230 km² of farmland, but cost the rehabilitation and resettlement of 249 villages and around 175000 people. As seen in the "crop and grass gain" section, increasing population leads to increasing demand for agricultural products and thus to increasing water demands, as well as to energy consumption which is likely to grow faster than the population growth (FAO, 2012; Sharma et al., 2013). After decades of comparatively modest development in India, recent years have seen a major intensification in the construction of new hydropower dams due to this growing energy demand (Erlewein, 2013). Although it is a clean source of energy, hydropower project reservoirs have a deleterious effect on downstream water quality of the rivers, principally due to the blue–green algae blooms, which develop in these slowed, warmed waters, and have environmental consequences related to encroachments upon nature with submergence area (Sharma et al., 2013; Kumar and Katoch, 2014; Erlewein, 2013).

Water appearance in Figure 25 (c, d) is the consequence of the Hurricane Katrina which made landfall on the Louisiana coast on August 2005 as a strong Category 3 storm and struck low-lying coastal plains particularly vulnerable to storm surge flooding (Fritz et al., 2007). The change, well observed in 2005-2006 (Figure 25 (c3)), does not indicate a temporary flood but new permanently submerged lands, as a flagged change means that water is still present in 2011. If Katrina was the most destructive and costliest natural disaster in the history of the United States (Link, 2010), it also had a profound impact on the environment with many effects on biological resources including wetland and timber loss, and declines in fisheries and wildlife populations (Sheikh, 2005). The storm surge caused substantial beach erosion, in some cases completely devastating coastal areas, and land loss on the barrier island resulting in an increased vulnerability of the US Gulf Coast to future hurricane storm surges (Fritz et al., 2007). Finally, the temporary submergence of 80% of New Orleans epitomizes the risk of living below sea level in a coastal city (Link, 2010).

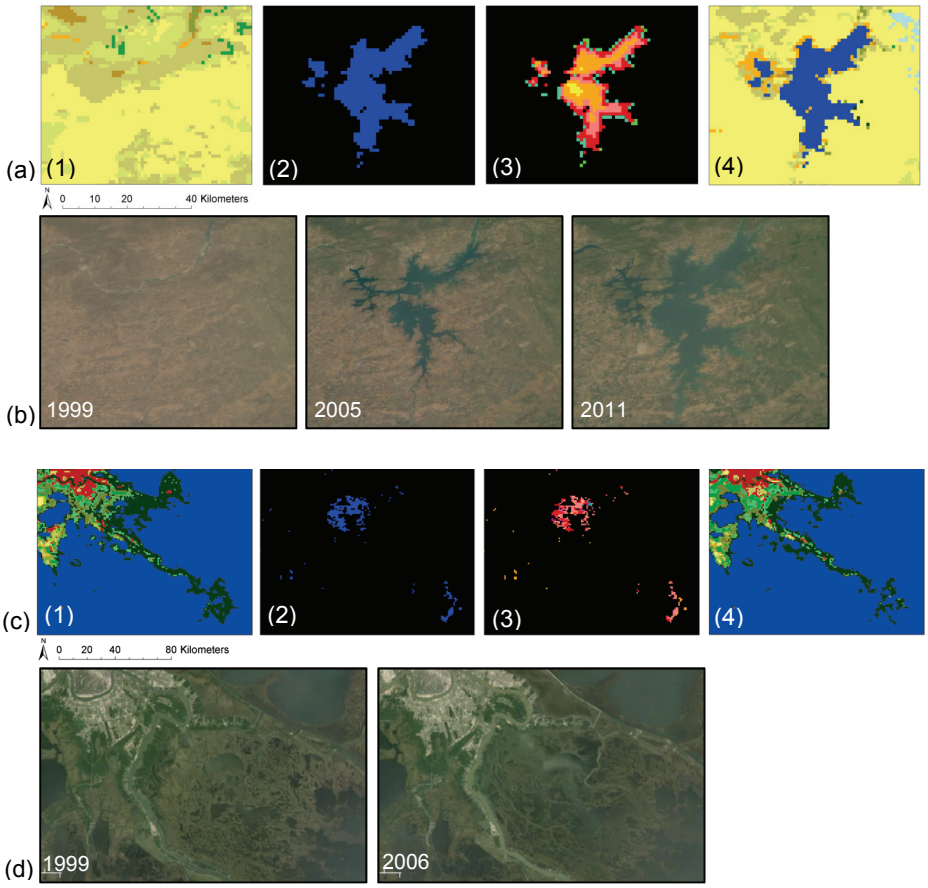


Figure 25 : Filling of the Indira Sagar Dam (India) (a, b) and damages after the hurricane Katrina (New Orleans, USA) (c, d). 1999 classification (a1) and 2004 classification (c1), pixels detected as change (water appearance) labelled with the new land cover classes (a, c: 2), year of change (a, c: 3), and change superimposed on the multi-year (SYC) land cover map (a, c: 4). Landsat images from the Google Timelapse tool (b, d). See Table 1 for the GlobCover legend and Figure 5 for the year of change legend.

### 3.3.7. Urban gain

Currently, over 50% of the population lives in urban areas, but by 2050 United Nations estimates suggest that 70% of the global population will be urbanites (UNFPA, 2007). Urban growth is illustrated here with the expansion of the city of Denver in Colorado (USA) (Figure 26). It shows a sprawl development patterns characterized by low-density housing that rely heavily on private automobile transportation (Figure 26, b). In the developed world, large-scale urban agglomerations and extended peri-urban settlements

fragment the landscapes (Lambin et al., 2001) and for fast growing cities in which new population growth is predominantly directed toward suburban zones, land cover change is many times greater than for regions in which most population growth is directed toward established urban zones (Vargo et al., 2013). Locally, urbanization substantially degrades water and air quality (Foley et al., 2005) and alters local land surface through the loss of vegetative cover, which impacts several climatic parameters including surface roughness, albedo, emissivity and shifts in the sensible-latent heat flux, leading to change in the local climate (Hutyra et al., 2011; Vargo et al., 2013) and to the increase of the flood generation potential with addition of impervious surfaces (Townsend, 2009). But urbanization also affects land change elsewhere through the ecological footprint of cities (Lambin et al., 2001; Ramankutty et al., 2006). Even if urban areas currently cover only a small fraction of the Earth surface, global consequence of the creation and expansion of cities are associated with significant carbon emissions through (i) the removal of natural vegetation for construction, industrial purpose or agriculture, (ii) the demand by the urban populations for energy, often derived outside the urban areas, (iii) increases in local fossil fuel consumption especially with car-dependant metropolitan areas and industrial activities (Houghton, 2010; Hutyra et al., 2011; Vargo et al., 2013).

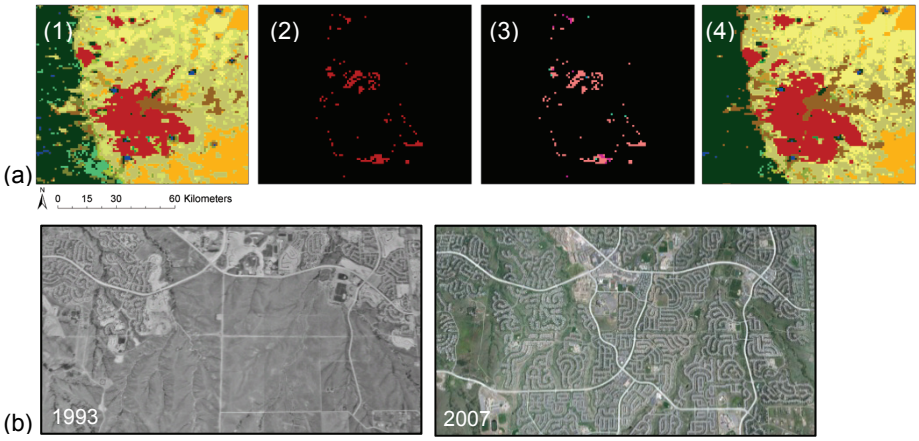


Figure 26 : Expansion of Denver (Colorado, USA). Multi-year land cover map (SYC) without taking into account land cover changes (a1), pixels detected as change (urban appearance) labelled with the new land cover classes (a, c: 2), year of change (a, c: 3), and change superimposed on the multi-year (SYC) land cover map (a, c: 4). Landsat images from the Google Timelapse tool (b). See Table 1 for the GlobCover legend and Figure 5 for the year of change legend.

## 3.4. Quantification and distribution of global land cover change at 1km²

Figure 27 shows the number of pixels of the new land cover classes after change, for each type of change. Change trajectories are listed in descending order per type of change. In Table 5, the total changed pixels per type of change is divided by the total pixels of the concerned classes (e.g. all forest classes for the forest loss and gain) present in the SYC multi-year land cover map before considering change, in order to give a proportion of change compared to the total surface of the concerned classes. These results have however to be interpreted with caution as the SYC does not represent an independent baseline. Indeed, some changes occurring at the beginning of the time series can already be included in the SYC thanks to the majority voting. The results are thus interesting to give a relative comparison of change between classes, but the absolute values cannot be used alone. The SYC was nevertheless chosen instead of the 1999 annual classification given the high rate of classification mistakes in annual land cover maps.

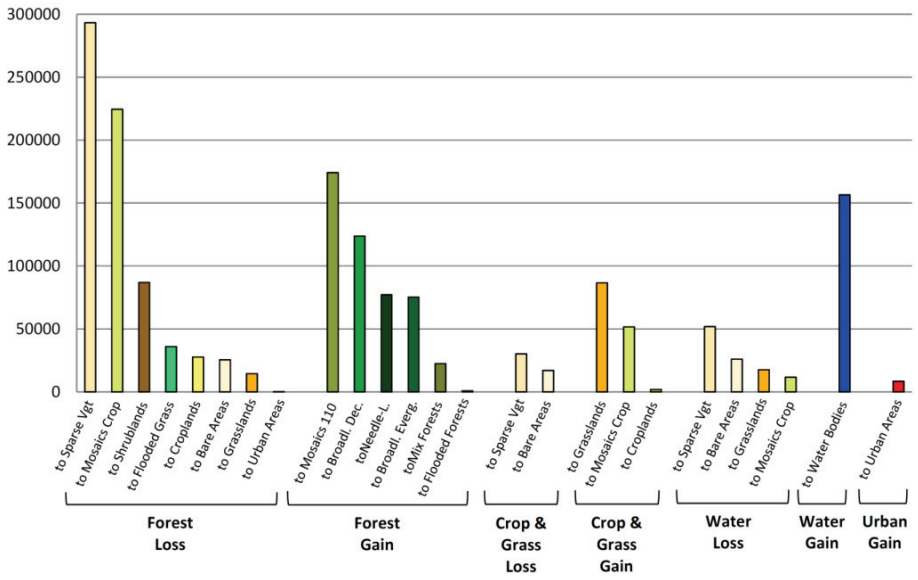


Figure 27: Amount of pixels detected as change per trajectory for the 7 types of change.

Forests are principally converted into sparse vegetation and croplands, followed by shrublands, while transition into grasslands, bare areas and urban areas are minority (Figure 27 ). The total amount of 708460 km² of change corresponds to 1.84 % of the forest surface counted up in the SYC before considering changes. Conversions of forest into sparse vegetation and bare areas are principally found in temperate and boreal forests as a consequence of fire (Russia, Canada, Alaska, Australia) or insect infestations (North America), as well as all around the world locally with the presence of mines. The transition into croplands is observed mostly in tropical humid forests (Indonesia, Papua New Guinea, Malaysia, Congo basin, Amazon basin) but also in tropical dry forests of South America (Paraguay, Bolivia, Argentina) where the deforestation rate is much higher than in Brazil. Indeed, Brazil's well-documented reduction in deforestation was offset by increasing forest loss in Indonesia, Malaysia and in tropical dry forests of South America (Hansen et al., 2013). More locally, storms damage forests giving way to mosaic 'natural vegetation/cropland' or shrublands. Most impressive scars are found in France, Canada and North Eurasia. Forest gains are less clustered than clear patches of forest losses and more dispersed in all types of forests. This difference is explained by the more gradual process of a forest growth. A major part of the new forest classes is the mosaic 'forest or shrubland (50-70%) / grassland (20-50%)' (Mosaic 110) indicating this regrowth in progress. Forest gain is either due to agricultural abandonment, forest recovery after a storm of a fire, or forestry especially in boreal forests (Hansen et al., 2013), and plantations especially in the tropical regions or to afforestation.

Croplands and grasslands loss giving way to sparse vegetation or bare areas are principally observed at the edge of deserts, and especially around the Sahara, Turkestan, Gobi, and Australian deserts. At the limit of the Sahara, the grassland gain, from a previous sparse vegetated or bare land cover, is more continuous and clustered than the grassland loss. The Horn of Africa is experiencing lot of grassland loss without any gain, while the opposite is observed for the deserts of Kalahari and Namib in Southern Africa. Grassland gains are present at the edges of the Indian, Iranian, Gobi and Australian deserts. Croplands appearance over a sparse vegetated or bare soil is easily observable as it appears in clear and large patches such as around the Nile Delta, in Saudi Arabia, in China and in Kazakhstan. Some new crops are also found in North Africa, in South of Spain and in Kenya. These two types of change are practically absent in America and Europe.

Water bodies are principally converted to sparse vegetation and bare areas when they shrink. Arid regions are the principal domains where this type of change is flagged because of the particular vulnerability of water bodies to the effects of human interventions where precipitations are very low. A dramatic example is the Aral Sea steadily disappearing since the 1960s due to the diversion of its two source rivers to produce mass of cotton. The fast and clear losses of water bodies are mostly due to human interventions, as well as for the appearance of water principally due to dams. New dam reservoirs are particularly present in Turkey, Mexico, China, India, Russia and Spain. For both cases, these anthropogenic disturbances alter natural hydrologic cycles causing extreme water level fluctuations that can surpass the physiological or behavioral adaptability of many organisms (Coops et al., 2003). Lots of small patches of both water loss and gain are observed around the millions of lakes in the boreal regions of North America and Eurasia, but also at the edges of great lakes and large rivers, such as the Amazon, the Tocantins, the Lena, the Mississippi, or the Angara. Without clear evidence on high resolution images such as for the shrinking of a lake or the creation of a reservoir, it is difficult to determine whether it is actual change, natural water level fluctuations due to climate conditions or classifications mistakes in these heterogeneous areas. Clear false change is however detected in Africa and Australia where new water bodies appearing in 2010 are only the result of high yearly fluctuations due to climate variability.

Urban gain has the highest rate of expansion of all types of change with a surface increase of 4.29 % compared to urban areas in the SYC multi-year land cover map. This urbanization is particularly observed in the USA. However, false change detection is present in mountain ranges where snow is confused with urban area. This is the reason why the decision rules for this type of change are quite strict with a period of possible detection from 2005 to 2009 only.

Table 5 : Amount of pixels (km²) detected as changed for the 7 types of change. Percentage of the total pixels changed on the total pixels of the concerned classes in the multi-year land cover map before considering change.

| Type of change | Total per type of change (km²) | Pixels changed/total pixels of classes of interest before change (%) |
|---|---|---|
| Forest loss | 708460 | Forest loss/All forest classes |
| | | 1,84 |
| Forest gain | 473512 | Forest gain/All forest classes |
| | | 0,80 |
| Crop and grass loss | 47260 | Crop & grass loss/Crop & grass classes |
| | | 0,10 |
| Crop and grass gain | 140053 | Crop & grass gain/Crop and grass classes |
| | | 0,28 |
| Water loss | 106837 | Water loss/Water bodies |
| | | 1,22 |
| Water gain | 156521 | Water gain/Water bodies |
| | | 1,78 |
| Urban gain | 8470 | Urban gain/Urban areas |
| | | 4,29 |

# 4. Discussion

The use of moderate resolution time series to characterize land cover and its changes through a multi-year approach presents both interesting innovations but also remaining challenges. The benefits and limitations of the methods developed in this research are discussed in this section, at the light of the results.

## *4.1. Global multi-year land cover mapping*

Intercomparisons between the 13 annual classifications from SPOT-VEGETATION time series confirms an expected large year-to-year variability, especially for crops, grasses, shrubs and mosaics, calling into question the current global mapping approach based on 1 year of Earth

observations. The characterization of global land cover benefits from a multi-year Earth observation dataset as source of data, compared to current single year mapping approaches, to derive a better structuration of the landscape. Indeed, both MYC and SYC maps, that summarize 13 years of land cover information, were proved efficient to reduce the sensitivity to the period of observation found in annual SPOT-VEGETATION classifications. Actually, multi-year observations are acquired under different conditions resulting in high inter-annual reflectance variability (Bontemps et al., 2012; Pouliot et al., 2014). It was however demonstrated with pixels transitions (Figure 8) and maximum occurrence of aggregated classes (Figure 12 (c)) that most of the year-to-year variations occur between semantically close classes, arising from poor spectro-temporal separability or variations in climate conditions. This finding of 'acceptable' confusions led to the idea of summarizing the 13-year time series to determine the most likely land cover on a pixel basis.

The innovative multi-year approach reveals improvements in mapping certain regions and classes compared to annual classifications, especially with the SYC method. A main advantage of this approach is that it provides a product limiting the proportion of the mosaic classes and favoring classes with small extent, known to be difficult to classify, such as irrigated croplands or flooded natural vegetation. The specific decision rules created to provide this result, after the majority voting, are based on careful analysis of inter-annual variabilities between annual classifications detailed in the result 3.1 section, to find out which classes deserve particular attention. In addition, the use of the semantic distances and the number of the classes that compose the time series allows determining the most appropriate choice between a mosaic and a pure class for a given pixel. It permits to deal with the issue of areas presenting large inter-annual variabilities or similar land cover types difficult to discriminate with such spectral and spatial resolution. This ability is not possible with the MYC method which summarizes first the 13-y spectral reflectance before classification. For an area with high inter-annual variability of reflectance, this step leads to a composite with ambiguous average reflectance values for the ISODATA algorithm of the unsupervised classification and to averaged temporal profiles with a diminished discrimination power. This limitation impacts the land cover map that contains much more mixed pixels in temperate regions and in heterogeneous areas difficult to classify.

The methods MYC and SYC both show a global accuracy around 72 %. It seems difficult to exceed the threshold of 75% of accuracy for a global land cover map, the IGBP-Discover, GLC2000, GlobCover 2005 and 2009 and MODIS Coll. 5 maps reaching around 68 – 75 % irrespective of the techniques that are implemented. It is considered as satisfactory for their main applications, as most of the misclassifications are attributable to the year-to-year variability of the seasonality and to natural disturbances related to fires or climatic conditions (Friedl et al., 2010). However, this exercise shows that the use of a multi-year dataset does not improve the accuracy. A source of error in the accuracy calculation can resides in the interpretation of the validation points by regional experts into LCCS classifiers, especially in the case of fragmented an seasonal landscapes where one image may not be sufficient to catch the correct land-cover type (Mayaux et al., 2006). For instance, choosing between the semi-deciduous and deciduous phenological attributes in tropical areas seems to be a difficult task and has serious impact. The first one leads to the evergreen broadleaved and/or semi-deciduous forest class (class 40) while the other is translated in the broadleaved deciduous forest (class 50). In this case, this error was corrected in the validation dataset, based on regional land cover maps, leading to a 1% increase of the overall accuracy in both products. The use of semantic distance calculated from the most discriminant LCCS classifiers to weight the confusion matrix, developed for GLC2000 by Mayaux et al. (2006), could be used to reduce the impact of this kind of mistakes.

Concerning quality assessment of the maps, a strong point of the SYC method is the ability to derive indicators that document spatially the relevance of the product. These quality layers are conceived to help the producer to locate areas difficult to map and classes needing special treatment. It can also help the users taking the most advantage of the map. For instance, the distribution of uncertainty on a pixel-basis could be more useful for models than a general assessment obtained through classical validation.

Despite the originality of the SYC and efforts realized to improve land cover characterization, this method has its limitations. Even if both semantic distance between classes, typical confusions from the analysis of inter-annual variabilities and visual analysis of pixel trajectories scenarios in the different strata are carefully taken into account, the majority voting and specific decision rules to generate the multi-year synthesis are to some degree empirical and rather subjective. The logic behind these decision rules

is the way clusters are labelled during the reference-labelling step of the GlobCover classification chain. However, the thresholds used are determined in an empirical and arbitrary way, for instance the majority voting of 7 occurrence of a same land cover class to derive the final label. It implies that the land cover resulting lacks rigorous analysis of the relationship between classes that compose the pixel time series. The SYC methodology could greatly benefit from results of the confusion matrix of the MYC. Instead of using current empirical thresholds, the confusion matrix could help determining the most likely land cover class based on a probability analysis considering all classes composing the time series, their number and their relation to each other in the matrix. Specific relationships between classes that are not taken into account in the confusion matrix, because of the low number of validation points, should nevertheless complete this approach. In addition, a deeper understanding of the links between inter-annual variabilities and particular meteorological events could be helpful to improve these decision rules. Potential causes such as fires, droughts, El Nino events or climatic variability in general warrant a dedicated quantitative study which should investigate it in comparison with the 13 annual land cover maps.

Even if the results already show that our method brings interesting improvements compared to 1-y based land cover maps, the use of higher spatial resolution data will probably provide significant gains in accuracy. The next generation of global land cover maps at finer spatial and thematic resolutions, if it copes with the challenges of data volume, cloud-free images acquisition, revisiting cycle or validation, will probably describe the Earth's surface at a level of detail never reached. However, high resolution data sets acquired in terms of decades, such as Landsat (30-m), have currently low temporal repeat visits and thus a limited ability to provide annual global updates of land cover because of cloud-cover and phenological variability (Houghton et al., 2012; Hansen and Loveland, 2012). Improving the temporal revisit rate of the land surface at high spatial resolution is the most pressing need regarding large area land cover and change monitoring (Hansen and Loveland, 2012). New sensors from the small Belgian satellite PROBA-V (300-m and 100 m for the central camera) launched on May 2013 and the Sentinel-3 (300-m) satellites to be launched in the framework of the European Copernicus programme, with a short revisit time of less than two days, will ensure the continuity of the SPOT-VEGETATION time series. A finer scale may be not indispensable for use in global models running

generally at a degree scale. Nevertheless, migrating to higher resolution data source could greatly reduce mixed pixels effects.

## *4.2. Global land cover change detection*

The change detection algorithm developed in this study illustrates that a suite of 13 land cover classifications allows bringing out actual surface transformations, despite the current agreement within the land cover mapping community that the discrete global land cover classifications at moderate spatial resolution are unable to detect reliably land cover changes (Strahler et al., 2006; Jung et al., 2006; Colditz et al., 2011; Giri et al., 2013). Indeed, as a general rule, the accuracy of change detection based on post-classification comparison is the product of the map accuracies. Taking the upper bound of 75% as the accuracy of two maps used to evaluate change, the theorical change accuracy based on this product rule would be 56% assuming errors are independent (Pouliot et al., 2014). These restricted classification performances constitutes an a priori limitation of the use of classification for change detection purpose.

However, the moderate resolution time series acquired now since a decade or more provide a unique dataset to monitor land change surface. In this study, the main strength of the change detection method developed is to take advantage of a long classification time series and consecutive information to reliably distinguish actual surface transformations from inter-annual variabilities. Spurious change detection due to annual classification mistakes are avoided thanks to pre-determined conditions of change that search for class transitions consistency over the 13 years on a pixel-basis. These conditions search notably for persistence of change. A pixel is identified as a changed area only if the change is confirmed over several years, which is possible thanks to the use of the long time series. These conditions based on a yearly classification time series provide a new approach in the post-classification change detection. Instead of a simple comparison between distinct maps, it takes into account the entire time series to find out which pixels fulfil a potential change trajectory over years. It allows avoiding errors of classification to propagate. In addition, the pre-determined conditions avoid interpreting the numerous possible cases of a 13-y pixel time series which is a non-negligible gain of time.

The use of post-classification approach presents some interesting advantages compared to change detection based on the direct analysis of full time series. First, using a classification of time series over a year avoid radiometric change related to illumination and viewing angles, phenology or atmospheric conditions that cause spurious change detection. It allows to directly looking at semantic changes. The application of spectral-based techniques at large scales is indeed challenged by the variability in the spectral properties of the images in space and over time, and strongly requires the implementation of radiometric calibration and atmospheric corrections at broad spatial and temporal scales (Bontemps, 2010).

Second, the use of post-classification technique is advantageous as identified changes are thematically labelled. Indeed, a key advantage of this method, in addition to provide change location, is the ability to determine the fate of the land cover. This information is missing in most of land cover change studies, either at local or global scales. It is nevertheless needed for many applications (Ramankutty et al., 2006; Houghton et al., 2012). The fate of land cover change permits to have an indication on the state of the surface after a disturbance, e.g. the new albedo or surface roughness. It also helps in determining natural from anthropogenic source of disturbance. Nevertheless, the new land cover class identified may be part of a surface transformation in progress. For instance, a deforested area for agricultural purposes may be classified the first years as shrubland before being identified clearly as a crop.

Third, the date of the change can be determined on a yearly basis, compared to bi-temporal change detection method that cannot provide this information. The year of change allows showing the sudden character of changes in certain regions compared to gradual disturbances in others. It helps determining the cause of the transformation.

Finally, to detect change at global scale, post-classification is undeniably more advantageous in terms of time, cost, computing requirements and volume of data analyzed. The product can be easily and continuously updated with adding of new annual classifications over time.

Despite its ability to detect actual land cover changes that affects the land surface, the method developed presents some limitations. First, the decision rules forming the conditions to detect a change in a pixel time series are determined empirically, although through careful examination of known multi-year land cover change. Among the seven types of land cover change

examined, some are easier to depict and to confirm than others. For instance, the water changes are much more detectable than a transformation of grassland into sparse vegetation as water is spectrally very distinct from vegetated lands. Some types of change will thus need to be classified two or three consecutive years to ensure an actual change, such as the gradual regeneration of a forest on another type of vegetation. Using information contained in the matrix confusion of the multi-year maps would allow determining reliably the probability that the time series contains an actual change.

Second, this method relies on a long time series. A shorter time series would imply fewer years to observe the persistence of change. On the contrary, a time series longer than 15 years would bring a new challenge concerning potential re-change. Further analysis should determine the optimum length of the time series as a compromise between enough information and avoiding dealing with re-change. Then, a moving window could be applied as long as the time series increases.

Third, the approach only represents land cover changes that the change detection method is able to reliably detect. Some important changes could go undetected, leading to errors. Therefore, the uncertainty concerning the capture of all relevant changes for an application implies that results are not appropriate for use in any rigorous assessment of land cover changes, but more dedicated for use in modeling. More precisely, omission errors are certainly numerous because of the moderate spatial resolution imagery that hampers catching sufficient details to depict small conversion less than a pixel size (1 km), but fine visual analysis of each groups of pixels highlighted as land cover change revealed a very limited number of commission errors. It gives confidence in the method but induces a likely underestimation in the rate of change estimated. For example, SPOT-VEGETATION classifications have difficulties in mapping urban areas. The process of urban expansion results in complex patterns of intermixed high- and low- density built-up areas and a fragmentation of the natural landscape but is an important driver of deforestation and land cover change and can result in significant carbon emissions (Hutyra et al., 2011). This phenomenon would obviously be better detected with higher spatial resolution data. Other omission errors can occur because the method is not sensitive enough to certain types of land cover changes such as reforestation, or because the pre-determined conditions do not cover all possible change trajectories. In addition, some types of change are not explored because of

the spectral resolution of the SPOT-VEGETATION data. For instance, the snow classification is not enough reliable as it is often confused with the urban classes in mountain ranges. This is notably the reason why urban gains are depicted only until 2009, because three consecutive years of urban appearance are needed in the pixel time series to confirm the change. Also, croplands change into grasslands and the opposite are not tested as these classes are difficult to distinguish on high resolution images, preventing clear evidence to validate detection method for these types of change. In addition, the method is not able to depict subtle changes such as forest degradation. These processes lead to a temporary or permanent deterioration in the density or structure of vegetation cover or diffuse deforestation affecting its species composition (Lepers et al., 2005) which need continuous land cover characterization.

In the future, cyclic changes like shifting cultivation may be depicted with longer time series. The same method applied on long time series of higher resolution images will obviously allow to fully evaluate the forest disturbance and succession cycle, and to detect and quantify the change more precisely and at the scale more compatible with most human activity (Giri et al., 2013). Nonetheless, even if it remains a broad global spatial pattern of land cover change, the use of 1-km SPOT-VEGETATION dataset showed that the developed method allowed capturing the dominants land cover transitions. It is illustrated through different examples that hot-spots of change detected strongly modify the multi-year land cover map initially created, because of natural events such as storms, wildfires, insect infestations, land degradation or because of anthropogenic activities like the alarming expansion of agriculture, irrigation, mining, diversion of rivers, dam constructions or urbanization showing how land use affects the land cover. Our results show that some disturbances differ considerably among the countries and their policies (e.g. dams, deforestation for agriculture, irrigation, …). The human-driven changes observed across the world are generally the outcome of an acquisition of natural resources for immediate human needs, often at the expense of degrading environmental conditions and ecosystem services in the long term, changing the global carbon cycle and regional climates, increasing losses of biodiversity and leading to possible declines in human welfare (Foley et al., 2005). Understanding the role human plays in modifying ecosystems through changing land cover is central to addressing environmental challenges and to implement better resource managements (Hutyra et al., 2011). However, remote sensing

observations are not always sufficient to fully understand these cause-effect relationships of land cover change (Latifovic 2005). The ability to distinguish natural and anthropogenic source of disturbance at this spatial resolution is only possible in cases where available high resolution imagery allows visual analysis. The inspection of all pixels detected as change is a huge task. Therefore, automated sorting out of causes of change and validation is a future challenge.

In addition, the change of flooded forest and the grass classes could be more investigated in the change detection process, because very few studies on carbon emissions from land cover change include emissions from the degradation of peatlands (Houghton et al., 2012).

Finally, the year of change extracted from the sequence of the time series capture interesting information concerning the gradual change. This information could be used in future research to derive annual land cover time series by updating each year a consistent baseline, in order to deliver a dynamic land cover dataset.

# 5. Conclusion

Thanks to the increasing availability of global and long-term Earth observation time series, an innovative land cover mapping approach has been proposed based on a multi-year dataset, the 1-km SPOT-VEGETATION time series. To our knowledge, this is the first attempt to create a consistent global land cover product using multi-year data set that explicitly takes into account the change occurring during the period of observations.

Using multi-year time series as source of data for classification has proved efficient to reduce the sensitivity to the period of observation found in current annual mapping approaches, and therefore to produce a more stable land cover product. Among the two methods tested, the synthesis method showed more advantages as it permits to decrease the proportion of mosaic pixels, to handle the difficulty to discriminate similar land cover types at medium spatial resolution, to show transparency in the decision

process and to document spatially the product quality through different pixel-based indicators.

The original post-classification change detection method is designed to take advantage of the long classification time series and consecutive information to reliably distinguish actual surface transformations from inter-annual variabilities, thanks to pre-determined conditions of pixel trajectories. It is able to provide for the first time at global scale detection of land cover change for seven types of change (forest loss, forest gain, crop & grass loss, crop & grass gain, water loss, water gain and urban gain) systematically described by the year of change and the land cover transition, showing up a complete portrait of the Earth's land surface transformations. At this spatial resolution, the results highlight hot spots of land cover change, but the method can be applied on higher resolution time series as far as it as a sufficient temporal coverage.

Change results are integrated to the SYC multi-year map in order to provide a coherent product. The effort to conceive a more stable component of the land cover taking into account long term data and surface transformation makes it a relevant product for use in global vegetation or climate models. This land cover map can be continuously updated thanks to the automated mapping approach, for instance with recent PROBA-V data which has the same sensor than SPOT-VEGETATION. More accurate results are expected with these higher spatial resolution images but the method developed already shows the power of satellite remote sensing for long-term monitoring of surface transformations. A future challenge remains nevertheless concerning the validation of the change.

# Chapter 2 – Vegetation phenology of Amazonian tropical rainforests from 11-y SPOT-VEGETATION time series

## Abstract

Understanding vegetation phenology of tropical rainforests and its controlling mechanisms are crucial for anticipating how rainforests will respond to climate change. In a context of debate with regards to the optical remote sensing ability to monitor vegetation in tropical regions, this study explores the potential of vegetation indices derived from the 11-y SPOT-VEGETATION time series (2000-2010), under-exploited compared to MODIS data, to characterize leaf seasonal variations in Amazonian tropical rainforests. The research investigates deeply the causes of the intra-annual dynamic of reflectance and vegetation indices, from artefacts such as atmospheric contamination and directional effects to phenological events and environmental mechanisms that could explain the seasonal greening of Earth observations during the dry season. Indeed, the underlying mechanism of the dry season increase of EVI in the Amazon is still in open debate. Some suggest a leaf flush adaptation in the dry season to an increase in solar radiation or avoidance of herbivory, while others assert artefacts related to solar illumination effects or relative position between the sun and the sensor throughout the year. First, it is demonstrated that the EVI is better suited than NDVI to study the vegetation dynamic in the Amazon region as it follows the NIR dynamic less affected by atmospheric contaminations than the red band. The latter vary indeed irrespectively of vegetation dynamic in this region. Then, it is shown that the variations of sun-sensor geometry are not the cause of the EVI seasonality. Instead, it is concluded that the EVI seasonal cycle at site level and at basin scale is driven by leaf phenological events that are organized to enhance

photosynthetic gain during the light-rich dry season. Presenting also good agreement with gross primary production pattern derived from a fluxtower, this study suggests that EVI provides useful information about tropical rainforest phenology and productivity over time in the Amazon basin.

# 1. Introduction

Vegetation is a major carbon sink and is as such a key component of the global response to climate change caused by the build-up of greenhouse gases in the atmosphere. The highest exchange of $CO_2$ between the land and the atmosphere occurs in tropical forests, storing 55% of the current carbon stock in the world's forests (Pan et al., 2011) and accounting for about one-third of global terrestrial photosynthesis (Beer et al., 2010). Particularly, the aboveground live biomass of old-growth Amazonian rainforests are estimated to 93 ± 23 Pg of carbon (Malhi et al., 2006), representing about 50% of the total stock in tropical forests (Saatchi et al., 2011; Baccini et al., 2012). Accounting for emissions from deforestation, logging, fires and uptake from recovering vegetation, the Brazilian Amazon is estimated to be a net carbon sink of 0.16 ± 0.05 Pg C $y^{-1}$ (Aragão et al., 2014). These vast Amazon forests are thus a significant component of the Earth's carbon budget with strong influence on regional and global climate, as small variations in net carbon balance from climate or human driven perturbations could result in significant storage or release of carbon to the atmosphere (Rice et al., 2004; Malhi et al., 2008). Influencing the seasonal and inter-annual variability of these carbon fluxes through biogeochemical cycles, phenology controls feedback of vegetation to the climate system (Richardson et al., 2013). However, vegetation phenology of tropical rainforests and its environmental drivers are poorly understood (Huete et al., 2006; Richardson et al., 2013), and still source of controversy.

An unexpected seasonal pattern of this ecosystem was discovered thanks to eddy flux measurements in Tapajo´s National Forest near Santarém, Brazil (Saleska et al., 2003). The net ecosystem exchange (NEE) of $CO_2$ measured showed that the forest acts as a carbon source in the wet season and as a carbon sink in the dry season indicating a dry season

increase in total canopy photosynthesis. The dry season is defined as the consecutive months with less than 100 mm of long-term mean monthly precipitation, when potential evapotranspiration exceeds precipitation (Roberts et al., 1998). The trees actually consumed several hundred Kg C $ha^{-1}$ $mo^{-1}$ during these driest months. It is the opposite to the NEE prediction by land surface model representing Amazonian ecosystems as water-limited during months with little or no rain, with declining evapotranspiration and photosynthesis. It suggested that intact Amazonian forests could be more resilient to variations in climate than these models predicted.

Even though essential knowledge is gained from carbon flux tower network with on-the-ground evidence of forest processes, it is difficult to directly upscale site information to large areas. The limited number of stations is too widely scattered to describe seasonal changes across the whole Amazon. By contrast, optical satellite time series at moderate spatial resolution offer the advantage of a highly consistent spatial and temporal coverage of land observation allowing to describe vegetation types and their phenology through reflectances in visible and infra-red spectral range. Local or basin-wide satellite-based studies in the Amazon region reported Enhanced Vegetation Index (EVI) variations along the year with gradually increasing EVI values from the beginning to the end of the dry season (Xiao et al., 2005; Huete et al., 2006; Xiao et al., 2006; Poulter and Cramer, 2009; Pennec et al., 2011; Samanta et al., 2012; Wagner et al., 2013; Biudes et al., 2015; Bi et al., 2015) coherent with the increase of $CO_2$ uptake measured at the flux tower. Satellite-based Leaf Area Index (LAI, one-sided green leaf area per unit ground area) also exhibited large seasonal cycle in most regions of the basin with a gradual increase through the dry season and a corresponding decrease through the wet season (Myneni et al., 2007; Samanta et al., 2012; Caldararu et al., 2012; Bi et al., 2015). As for eddy flux tower measurements, these results were opposite to dynamic global vegetation model (DGVM) simulation which assumed that water limitation due to relatively low precipitation should cause dry season decline in canopy photosynthesis (Huete et al., 2006).

Given the EVI increase and the unexpected NEE patterns with carbon gain during the dry season across Amazon forests, a “green-up” (increase in photosynthesis) theory was proposed to explain this seasonal dynamic. The dry season in Amazonia lasts from 0 to 5 months in a year according to the region (Xiao et al., 2006) and is characterized by a decrease in precipitation and cloud cover. The Amazon basin presents thus a large

intra-annual variation of photosynthetically active radiation (PAR) with much larger values in the dry season than in the wet season (Xiao et al., 2005). The green-up theory is based on two adaptive mechanisms that could be responsible for dry season resilience and that may have evolved in response to this large seasonal variation of light and water to maximize carbon uptake (Saleska et al., 2003; Xiao et al., 2005, Huete et al., 2006). The first one proposes that trees of tropical forests in Amazon have a deep rooting system to reach water reserves in soil moisture layers beyond 10 meters, where the rainfall water is stored, allowing maintaining high rate of canopy photosynthesis and evapotranspiration in the dry period (Nepstad et al., 1994; da Rocha et al., 2004; Ichii et al., 2007; Poulter et al., 2009; Verbeeck et al., 2011). Model-based studies demonstrated that accurate simulation of dry season gross primary production (GPP, or photosynthesis) at tropical moist forest locations requires accounting for deeper soils providing more soil water storage and for increased rooting depth especially in regions with longer dry period (Ichii et al., 2007; Poulter et al., 2009) such as much of the eastern and southern regions of the basin where the dry season lasts 4-5 months (Asner and Alencar, 2010). Deeper root distribution leads to much lower drought stress sensitivity of photosynthesis during the dry season and thus improves model representation of tropical rainforest seasonality (Verbeeck et al., 2011). This contradicts the frequent hypothesis arguing that water availability is both the proximate and ultimate factor controlling phenology of many tropical forest plants (van Schaik et al., 1993). Precisely, the second adaptive mechanism of green-up may be that these drought-tolerant species tend to produce new leaves (leaf flushing) in the dry season thanks to a specific seasonal dynamic of leaf fall and leaf emergence (phenology) (i) in response to increased solar radiation to optimize access to light (Wright and van Schaik, 1994; Xiao et al., 2005; Huete et al., 2006; Xiao et al., 2006; Myneni et al., 2007; Hutyra et al., 2007; Doughty and Goulden, 2008; Brando et al., 2010 ; Pennec et al., 2011; Caldararu et al., 2012; Wagner et al., 2013; Restrepo-Coupe et al., 2013; Bi et al., 2015) or (ii) as an effective widespread strategy to avoid insect herbivores which have low abundance during the dry season, herbivory damages being greatest on young leaves because of their high nutritional quality (van Schaik et al., 1993; Coley and Barone, 1996; Huete et al., 2006; Albert et al., 2014). Such a leaf strategy enhances photosynthetic gain during the light-rich dry season. In summary, in absence of seasonal soil moisture stress, tropical rainforest phenology and productivity in the Amazon would

be mainly driven by the availability and seasonality of solar radiation rather than seasonal rainfall variation, as concluded by Xiao et al. (2006), Huete et al. (2006), Myneni et al. (2007), Hutyra et al. (2007), Bradley et al. (2011), Caldararu et al. (2012), Wagner et al. (2013) and Biudes et al. (2015).

Despite the convergence of these studies, considerable controversies question the variation of satellite observations in the Amazon region. Uncertainties reside in the interpretation of the annual cycle of vegetation indices. A first uncertainty about the EVI interpretation concerns its inter-annual variability, especially for drought years. Even with a deep root system, it cannot be concluded that the forest is not stressed in some years (da Rocha et al., 2004), especially when strong El Niño/Southern Oscillation (ENSO) events, the most common driver of drought in Amazonia (Asner and Alencar, 2010), or Atlantic Multidecadal Oscillation (AMO) (Li et al., 2006) lead to severe and extended decline in rainfall and soil moisture exceeding the dry-season tolerance of Amazon forest canopies (Asner et al., 2004). However, Saleska et al. (2007) stated that Amazon forests experienced a higher photosynthetic activity in the severe 2005 drought when compared to other years as indicated by higher EVI values. Conversely, using an EVI product with refined atmospheric corrections, Samanta et al. (2010a) and Anderson et al. (2010) reported a less extensive area and lower intensity of the 2005 EVI increase over intact Amazon forests. They attributed this difference to inclusion of atmosphere-corrupted data in the previous product associated with higher aerosol loading from biomass burning compared to non-drought years (Samanta et al., 2010a, 2010b), as anomalous peak of fires is observed in the 2005 drought year (Aragão et al., 2007). The excessive greening depicted by satellite observation is also contradicted by higher tree mortality and reduced growth from ground observations, i.e. biomass loss of 1.2 to 1.6 Pg C in 2005 (Phillips et al., 2009) correlated with a strong water deficit (Saatchi et al., 2013). It reaches 2.2 Pg C for the 2010 event (Lewis et al., 2011). According to Anderson et al. (2010), the EVI positive anomalies could be related to the structural change of the canopy affected by droughts (decrease of shadows due to leafless tree).

This second interpretation of the EVI increase was also used for explaining EVI intra-annual variability, not only for drought years. Anderson et al. (2011) argue that the leaf shedding of emergent trees in the dry season changes the canopy structure and decreases the shade fraction, which directly leads to an augmentation of the vegetation index response. Other recent studies also claim for variations of shade as the main cause of intra-

annual dry season EVI variation over mature forest, but because of solar illumination effects (Galvão et al., 2011; Moura et al., 2012; Galvão et al., 2013). These authors suggest that the decrease of the solar zenith angle (SZA) during the dry season, resulting in a reduction in shade fraction and a predominance of sunlit canopy components visible from the sensor, would be responsible for the EVI increase. More recently, Morton et al. (2014) argues that the apparent greening observed in Amazon forests with optical remote sensing data is an artefact of variation in sun-sensor geometry. In addition to the reduction in self-shading near the equinox, they consider the decrease of the relative azimuth angle (φ, difference between the solar azimuth angle (SAA) and the view azimuth angle (VAA)) of MODIS observations during the dry season until the sensor reaches the principal plane in October (φ = 0° - 180°, sensor and sun are aligned) is the reason of an apparent green-up, as reflectance values acquired in the hot spot of the principal plane are higher. They eliminated seasonal changes in surface reflectance after correcting bidirectional reflectance effects on MODIS EVI. In summary, they all claim that EVI seasonal change is not caused by biophysical change in leaf reflectance, leaf area or vegetation productivity driven by radiation, but instead by a combination of shadowing effect within the canopy and the sun-sensor geometry observing the forest during the dry season. According to these studies, the Amazon forests maintain a constant greenness throughout the dry season. However, Maeda et al. (2014) and Bi et al. (2015) showed more recently that, even if the annual EVI seasonality is partly explained by sun-sensor geometry variation, it remains an evident MODIS EVI seasonal pattern over the Amazon after removing atmospheric contamination and accounting for sun-sensor geometry effects, unlike Morton et al. (2014) findings.

Giving these recent works, the underlying mechanism of the dry season EVI increase in the Amazon is still in open debate. To recapitulate this controversial subject, some suggest a leaf flush adaptation in the dry season to an increase in solar radiation or avoidance of herbivory, while others assert optical artefacts due to a decrease of shade because of shedding leaves, decrease in the SZA or relative position between the sun and the sensor. Moreover, some uncertainties remain concerning the influence of atmospheric contamination from biomass burning and sub-pixel perturbation by little clouds on vegetation indices, which amplifies the challenge to detect temporal patterns of greenness in moist tropical regions using optical remote sensing.

Nowadays, most DGVMs consider a highly simplified or even no seasonality for moist tropical forests and they still show deficiencies in reproducing the measured seasonal pattern of $CO_2$ fluxes found in Saleska et al. (2003) and in simulating the timing of tropical vegetation phenology (Poulter et al., 2009; Verbeeck et al., 2011; Bradley et al., 2011). However, a key issue in modelling the biosphere-atmosphere interface is to simulate the vegetation activity (Bradley et al., 2011), because a small vegetation phenology in the vast Amazon forests can have significant impacts on carbon fluxes and their global dynamics. In addition, it is important to model leaf turnover correctly, because this process not only affects GPP but also drives litterfall, litter decomposition and biogeochemical cycling of carbon and nutrients (De Weirdt et al., 2012). In a context of climate change and mitigation policies for effective forest management, understanding the seasonal and spatial functioning of tropical rainforests such as leaf phenology, photosynthetic activity and carbon fluxes is an important basis for anticipating the response of these forests to future human or climate disturbances. An improved understanding of the satellite-based greening during dry period and of the underlying processes that drive canopy scale photosynthesis would then be helpful to reduce the uncertainty in models prediction, such as the tropical forest resilience or dieback (Hutyra et al., 2005; Malhi et al., 2008; Poulter et al., 2010; Huntingford et al., 2013; Aragão et al., 2014) to more frequent and severe dry anomalies expected in the coming century due to climate change (Cox et al., 2000; Li et al., 2006, 2008).

In this study, the intra-annual dynamics of Amazonian rainforest canopy as observed by optical satellite time series is examined in detail in order to provide a better understanding of how remote sensing can help detecting spatial and seasonal variations of tropical rainforests phenology. Various factors potentially perturbing the reflectance values, like aerosols and directional effects, are first investigated. Then, the seasonal variation derived from multi-year time series are interpreted in terms of vegetation dynamics and with regard to the famous green-up phenomenon. Specifically, the objectives of this study are threefold: (i) investigating at site level the potential perturbation on the intra-annual variations of spectral reflectance and vegetation indices time series by seasonality of aerosols, clouds, number of valid observations and directional effects; (ii) linking the satellite-based EVI variation with ground observations of phenology, flux tower $CO_2$ seasonal patterns and light availability to question a phenological mechanism

for the seasonal greening of Earth observation data; and (iii) mapping and exploring the spatial extent of EVI dynamics for the whole Amazon forest.

## 2. Data description

Unlike most former studies that mainly used MODIS data, a long time series of daily multispectral SPOT-VEGETATION surface reflectance measurements (S1) is the main dataset selected here to track the tropical forest phenology. These S1 images, recorded from January 2000 to December 2010 at a spatial resolution of 1 km, are daily synthesis of land surface reflectance well calibrated and atmospherically corrected. Thanks to the instrument swath of 2250 km, almost a global coverage is acquired every day in four spectral bands (Table 6), specifically selected to characterize the main features of plant canopy. In addition, the VEGETATION instrument presents the advantage of a data acquisition system equipped with a linear charge-coupled device array technology (push-broom sensor) which greatly reduces distortion, unlike other medium resolution scanner sensors such as MODIS. The reflectance measurements from one date to another are more comparable, at the pixel level, over many years. The exposition length is higher for the same satellite velocity, implying an improved signal to noise ratio and a more consistent pixel footprint. Daily images include the blue, red, near-infrared (NIR), and shortwave infrared (SWIR) spectral bands and information about the pixel quality. They also contain the view and solar zenith angles (VZA and SZA respectively) and view and solar azimuth angles (VAA and SAA respectively), useful to investigate Bidirectional Reflectance Distribution Function (BRDF) effects on reflectance values. Last but not least, a specific VEGETATION cloud screening strategy significantly improves the cloud and cloud shadow mask, in particular in equatorial regions.

The wavelength-specific anisotropy of surface reflectivity is characterized by BRDF that quantifies the angular distribution of radiance reflected by an illuminated surface. Downloaded from the Warehouse Inventor Search Tool (WIST), the Level 3 Nadir BRDF-Adjusted Reflectance (NBAR, MCD43B4 Collection 5) product provided by the MODIS BRDF/albedo product (Schaaf et al., 2002) is used for comparison

with SPOT-VEGETATION results concerning viewing effects. Indeed, the NBAR product provides surface reflectance measurements standardized to a nadir-view geometry based on BRDF-models of surface anisotropy, at the mean solar zenith angle (local solar noon) of observations over a 16-day period, in order to minimize the influence of seasonal variations in acquisition geometry (Schaaf et al., 2002). It is acquired at a spatial resolution of 1 km, from January 2000 to December 2009. The tiles provided in the Integerized Sinusoidal Grid (ISG) projection were converted to the more common WGS84-Geographic Lat/Lon. The NBAR data are extracted in the red (0.62-0.67 μm), blue (0.46-0.48 μm) and NIR (0.84-0.88 μm) bands.

Table 6 : Spectral channel characteristics of the VEGETATION sensor.

| **Channel** | **Wavelength Interval (μm)** | **Potential Applications** |
|---|---|---|
| B0 (Blue) | 0.43-0.47 | Atmospheric state |
| B2 (Red) | 0.61-0.68 | Absorption peak of chlorophyll |
| B3 (Near-Infrared, NIR) | 0.78-0.89 | Maximum vegetation spectral reflectance |
| SWIR (Shortwave-infrared) | 1.58-1.75 | Reflectance related to the water content of canopy components |

In order to document the potential atmospheric contamination of reflectance values caused by biomass burning in the Amazon, the Aerosol Optical Thickness (AOT) at 550 nm from the Level 3 MODIS Gridded Atmospheric Product (MOD08_E3 Collection 5) is used in this study. AOT is a dimensionless measure of how aerosol particles (dust, cloud droplet, biomass smoke, desert dust etc.) distributed from the Earth's surface to the top of the atmosphere prevent the light transmission, mainly due to scattering and absorption. The data are collected from January 2000 to December 2010 at 1°x1° spatial resolution and on 8-day temporal interval.

Vegetation canopy dynamics is also characterized by in situ measurements of Gross Primary Production (GPP, $gC/m^2/s$), the gross carbon dioxide uptake by vegetation through photosynthesis per unit time and area, obtained from a 64-m-high eddy covariance flux tower located in the Tapajós National Forest near Santarém (Saleska et al., 2003). The eddy covariance technique has become a standard for measuring fluxes of $CO_2$, water and energy between the land and atmosphere and provides an excellent opportunity for validation of model estimates of carbon flux from terrestrial

ecosystems (Sjöström et al., 2011). This flux tower site, described in the next section, belongs to the Large Scale Biosphere-Atmosphere Experiment in Amazonia (LBA), an international research initiative led by Brazil promoting notably a comprehensive data set from a observational network of flux towers across Amazonia for an improved understanding of regional carbon exchange between the Amazonian primary forest and the atmosphere (de Gonçalves et al., 2013). It is well suited for eddy covariance measurements as it lies on exceptionally flat plateau with favorable wind regime (Saleska et al., 2003). Eddy covariance and meteorological half-hourly data, including precipitation (mm/month) and shortwave down radiation (W/m²), are available from 2002 to 2004. Hutyra et al. (2007) provide a complete description of the instrument functioning and calibration.

# 3. Methodology

## *3.1. Sites description*

In this study, emphasis is given on the Km67 $CO_2$ fluxtower site located in the Tapajós National Forest near Santarém (2°51'S, 54°58' W, Figure 28) in the State of Para, Brazil (hereafter referred to as the K67 site). This site is located on the eastern side of the Tapajós River in a *terra firme* primary tropical forest of evergreen species, characterized by large emergent trees up to 55 m tall and a closed canopy at approximately 40 m (Saleska et al., 2003). Abundant tree species are listed in Malhado et al. (2009). Representing the main forest type across the Amazonian forest landscape, *terra firme* forests lie above the maximum flood level of Amazonian rivers and perennial streams and therefore have heavily leached and nutrient-poor soils (Haugaasen and Peres, 2005). The forest site receives an average of 1920 mm $y^{-1}$ of precipitation (Saleska et al., 2003) with a strong inter-annual variability. The typical 5-month dry season is pronounced and extends from approximately June to November (Saleska et al., 2003; Xiao et al., 2005) (see rainfall climatologies from the Tropical Rainfall Measuring Mission (TRMM) using 1998 to 2011 data, Figure 40) with solar radiation peak in September to November (Ichii et al., 2007). The dry season is characterized by higher temperatures and an increase in downward shortwave radiation (de Gonçalves et al., 2013). The site shows signs of disturbance-recovery like

current high wood productivity, resulting possibly from a recent period of high mortality possibly triggered by the strong El Niño Southern Oscillation events of the 1990s (Rice et al., 2004). Soils are nutrient-poor clay oxisols with low organic content.

For the sake of comparison with tropical rainforests, an additional pasture land cover site is examined. This previously forested area converted to pasture is located around 25 km away from K67 fluxtower (2°42' S, 54°43' W). The proximity with the fluxtower forest site aims to minimize the impact of various sources of signal variability like sun-sensor geometry, haze, residual atmospheric effects, etc. (Huete et al., 2006).

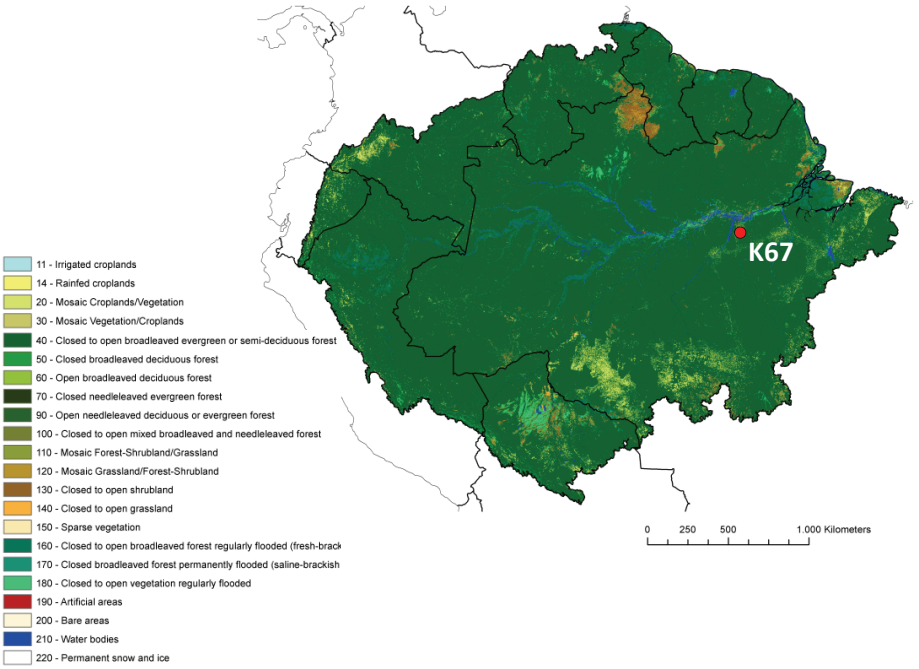


Figure 28: Land cover types in the Amazon basin (GlobCover 2009, Arino et al., 2010).

## *3.2. Spectral bands analysis*

SPOT-VEGETATION time series is compiled and multi-spectral reflectance dynamics are inspected with regards to perturbing factors such as clouds, aerosols and sensor specific artefact like sun-sensor geometry.

The frequent cloud cover in a moist tropical region and its strong variability between the wet and dry season may introduce seasonal perturbations in optical remote sensing. Compositing the VEGETATION-S1 reflectance products on a 10-day interval using the Mean Compositing (MC) method (Vancutsem et al., 2007) reduces significantly the cloud impact. This method averages valid atmospherically-corrected and cloud-free reflectance values based on an enhanced cloud screening. All the quality-controlled reflectance values are averaged over each pixel and within each band. In order to document the quality of the composite, the number of valid observation available and used in the mean estimation is associated to each pixel of a composite. In order to further reduce the noise in the time series, outliers were removed using fixed thresholds selecting observations with low red and blue reflectance (< 0.25) and NIR reflectance typical of vegetated surfaces (0.15 – 0.7).

The VEGETATION 10-day composites are compiled in temporal reflectance profiles in the blue, red and NIR bands from 2000 to 2010. The reflectance values extracted for the K67 and pasture sites are averaged within a 5x5 km² window by calculating the mean value at each time point. To characterize the average seasonal behaviour, a mean annual profile, also named a "climatological year", is compiled by averaging for each decade over the 11-year time series the reflectance value for each band. The standard deviation of each spectral reflectance is also calculated over the whole time series for each decade of the year.

These "climatological" multispectral profiles are compared with external factors which could corrupt the signal received by the sensor. Intra-annual variability is analyzed with regards to mean annual profiles of AOT distribution in order to depict the impact of dry season fire-induced aerosols on the reflectance values. Number of valid observations and seasonality of cloud cover are also taken into account. The pasture land cover type selected in the neighborhood of the flux tower also helps untangling the contribution of the land surface versus the atmosphere one to the reflectance.

Then, the BRDF that gives the reflectance of a target as a function of illumination and viewing geometry is explored to evaluate the variability of the directional reflectance measurements, especially for the NIR band more affected than the red band in dense vegetation biome (Maignan, 2011). Indeed, varying sun-sensor positions can influence recorded reflectance values of a terrestrial surface. Even if BRDF effects are difficult to separate

from temporal effects like plant phenology (de Wasseige et al., 2002), it is of crucial importance to try to assess the potential impact of geometry acquisition cycle on intra-annual variability of reflectance values in order to provide a reliable interpretation of vegetation indices temporal patterns.

The analysis investigates viewing effects (VZA variation), illumination effects (SZA variation) and the relative position of the sun and the sensor (φ variation) in three steps. First, mean annual profiles are computed over the 10 years of the MODIS NBAR product on an 8-day basis, for comparison of products exempt of viewing geometry effects with SPOT-VEGETATION profiles. Second, seasonal dynamics of daily S1 data acquired only in the forward configuration (sensor position in front of the sun) are composited and computed into mean annual profiles in the NIR band. Indeed, complete BRDF over vegetation targets in this wavelength is characterized by a strong increase toward backscattering and much smaller variations in forward directions (Bacour and Bréon, 2005). It is thus interesting to observe if seasonal variation is still observed with forward observations alone. Third, relationships between the SZA, the relative azimuth angle (φ) and NIR reflectance values are reported to investigate the impact of low SZA and φ on NIR values highlighted by Galvão et al. (2011, 2013), Moura et al. (2012) and Morton et al. (2014). Their analyses are all restricted for few months, from highest to lowest values of SZA or φ corresponding to the end of the dry season. Instead, we investigate the behavior of NIR values when SZA and φ start to increase again in December compared to the middle of the dry season in September.

In polar plots, the radial distance from the centre and the length of arc represents the VZA and the φ respectively. The principal plane resides in the 0°-180° azimuthal plane with the sun located in the 0° azimuthal direction. With this definition, the right half circle represents backward scattering and the left half circle forward scattering. The backward configuration indicates that the sensor is on the same side of the sun and it implies a relative azimuth angle (φ) inferior to 90°. The forward configuration indicates that the sun is opposite to the sensor and it implies a relative azimuth angle superior to 90°.

### 3.3. Vegetation indices analysis

Two vegetation indices are computed from individual spectral bands to characterize the vegetation phenology. These are the Normalized Difference Vegetation Index (NDVI) (Tucker, 1979) and the Enhanced Vegetation Index (EVI) (Huete et al., 1997, 2002) defined as:

$$NDVI = \frac{\rho_{NIR} - \rho_R}{\rho_{NIR} + \rho_R} \quad (1)$$

$$EVI = 2.5 \frac{\rho_{NIR} - \rho_R}{\rho_{NIR} + C_1\rho_R - C_2\rho_B + L} \quad (2)$$

where $\rho_{NIR,R,B}$ are surface reflectances in near-infrared (NIR), red (R) and blue (B) bands, respectively; $C_1$ and $C_2$ are the aerosol resistance weights designed to correct for aerosol scattering and absorption; L is the canopy background adjustment factor for correcting nonlinear, differential NIR and red radiative transfer through a canopy. The coefficients of the EVI equation are $C_1 = 6$; $C_2 = 7.5$ and $L = 1$ (Huete et al., 2002).

NDVI remains very popular and widely used in spite of its limitations especially in tropical region. Indeed, the dense vegetation with LAI of 3-4 induces saturation due to high chlorophyll content, and atmospheric aerosols cause artefacts in NDVI variation throughout the year (Huete et al., 2002; Xiao et al., 2003; Kobayashi et al., 2005). The EVI is a proven proxy for the potential photosynthetic carbon fixation by vegetation (Xiao et al., 2005; Huete et al., 2006; Brando et al., 2010). It was developed to minimize these atmospheric and saturation effects. First, it enhances the vegetation signal with improved sensitivity to high green biomass level. Second, it improves vegetation monitoring through a reduction in atmosphere influences by using the additional blue band available on advanced optical sensors (VEGETATION, MODIS). The EVI directly adjusts the reflectance in the red band as a function of the reflectance in the more atmospheric-sensitive blue band to correct the red band for aerosol influences (Huete et al., 2002). This is an important feature in the Amazon basin where seasonal burning of pasture and forest takes place throughout the dry season, either for agricultural purpose or natural fire events (Xiao et al., 2005). Precisely, Huete et al. (2002) showed that EVI performs well in the heavy aerosol, biomass burning conditions in Brazil. Both indices are

matched to individual spectral bands to track the source of their variation. Based on these analysis results, only the EVI is further used in the analysis.

Seasonal change in greenness is assessed by the EVI at two different spatial scales. First, the annual mean profile of EVI is computed in the same way than the reflectance profile for the K67 site. The intra-annual variation is compared to SZA and φ distribution over the entire year, rather than only for the dry season, in order to explore how illumination effects (SZA variations) and the relative position of the sun and the sensor (φ) influence the seasonal pattern of EVI. Two additional sites are studied in order to compare the relationships between these three variables in similar and very different conditions. The first site is located in another moist tropical forest in the UNESCO Man and Biosphere reserve at Yangambi (0°46'N, 24°27'E) near Kisangani, Democratic Republic of Congo. It presents the advantage of having a very similar view-illumination geometry. The site receives up to 1800 mm per year of rain and has one dry season from January to February (Kearsley et al., 2013). It corresponds to the future location of an eddy covariance flux tower. The second site is situated in a temperate forest in the Ardennes (50°44' N, 5°22' E), Belgium and has a well-known phenology with very different view-illumination conditions than the K67 site.

Second, the time series analysis is extended to the whole Amazon forest biome in order to map the spatial variability and consistency of EVI seasonal dynamics across the basin. As for the sites, a "climatological" year is computed on a monthly basis. First, EVI 30-day composites are computed from the individual spectral bands. Then, each month composite is averaged pixel by pixel from the 11 corresponding EVI 30-day composites (2000 to 2010). For this spatial analysis, Amazon rainforest boundaries are delineated thanks to the GlobCover 2009 map (Arino et al., 2010), instead of taking the Amazon basin limits which include shrublands, grasslands, croplands and dry forest in South and West of the basin. In addition, the Amazon basin limits do not integrate moist forests of French Guiana, Guyana, Suriname, North Venezuela and Centre of Colombia.

## *3.4. In situ measurements analysis*

Based on the time series analysis, relationships between remotely sensed EVI dynamics and *in situ* measurements are discussed, firstly concerning the GPP obtained at the K67 flux tower site from 2002 to 2004. Terrestrial GPP

is the largest global carbon flux and, along with respiration, is one of the major processes controlling land-atmosphere $CO_2$ exchange (Beer et al., 2010). The eddy flux data processing is described in detail in De Weirdt et al. (2012). The 10-day moving averages include daytime data (08:00–16:00) of measured GPP. For daily GPP means, only days with more than 80% of half-hourly data available were retained. The footprint of GPP as measured by the K67 tower-based eddy covariance systems is likely to cover areas up to 3 km² (Maeda et al., 2014). Secondly, EVI dynamics are compared with leaf and litterfall phenology observations from literature data. Finally, shortwave downward radiation seasonal variation is examined in comparison with GPP and EVI variations at the light of the green-up hypothesis which suggests a response of photosynthetic activity to increased solar radiation during the dry season.

# 4. Results and discussion

## *4.1. Reflectance time series analysis*

Annual mean profiles in the Blue, Red, and NIR bands compiled from the SPOT- VEGETATION 10-day composites for the Tapajo's site are shown along with the number of valid observation for each decade composite in Figure 29 (b). The annual profile over the 10 years of the MODIS NBAR product is also shown in Figure 29 (c). For visualizing the cycle over these yearly profiles, half-year periods are repeated at the beginning and at the end of the year (delimited by vertical lines). The typical dry season period in this region, extending from July to November, is indicated by the shaded areas. The Amazon is very cloudy especially in the rainy season. A direct consequence is higher standard deviation values in the wet season (Figure 29 (b), dotted lines), indicating the higher cloud cover frequency which is confirmed by low number of valid observations (Figure 29 (b), bars). Indeed, cloudy conditions considerably decrease the number of valid images that can be exploited and thus the reliability of the 10-day composites is reduced.

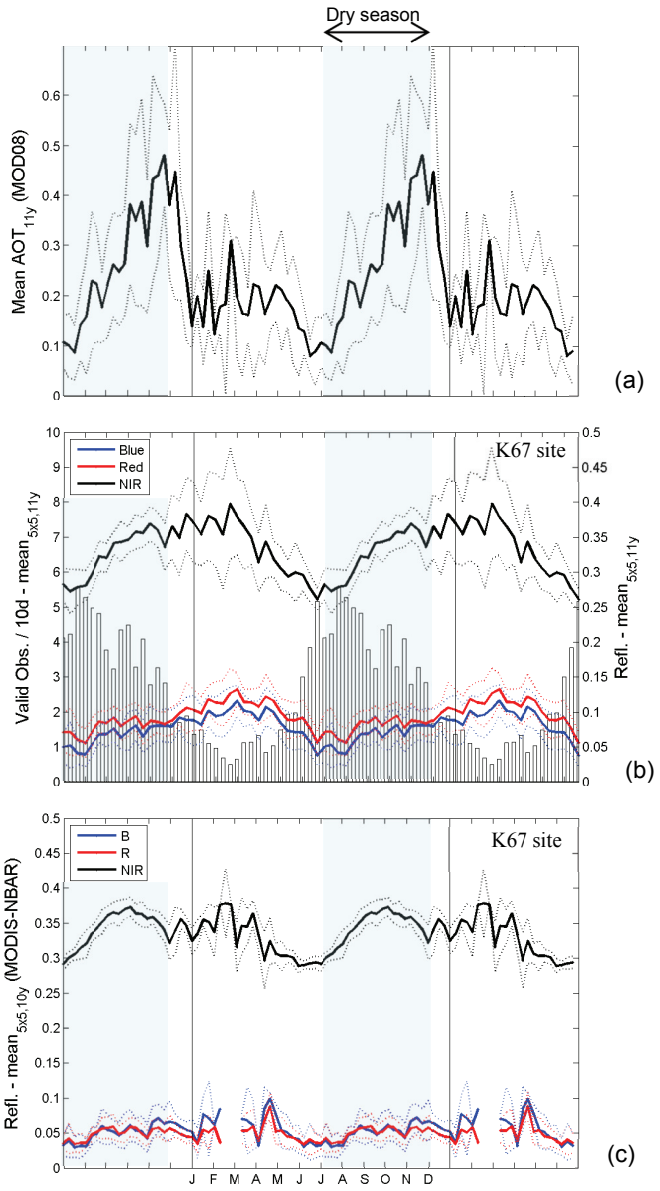


Figure 29 : Annual mean profiles centered at K67 fluxtower of (a) 8-day period AOT for 1°x1° window, reflectances in blue (blue line), red (red line) and NIR (black line) bands for a 5x5 pixels window from (b) SPOT- VEGETATION time series 10-d composites (2000-2010) and (c) NBAR-MODIS time series (2000-2009). Bars in (b) are number of valid observation by decade averaged over the 11 years. Inter-annual variability corresponding to one standard deviation is represented by dotted lines. Half-year periods are repeated at the beginning and the end of the year (delimited by vertical lines). Shaded areas indicate the dry season.

### 4.1.1. Sensitivity to atmospheric contamination

The investigation tries first to untangle the respective contribution of atmosphere and land radiance in the Amazon region, both being inherently coupled along the year throughout the different seasons. Such analysis is a prerequisite to support the interpretation of the temporal patterns to be related to tropical vegetation dynamics as the strong seasonality in clouds and aerosols between the wet and dry seasons may interfere with passive optical satellite measurements.

A seasonal pattern of the reflectances is clearly observed, from both VEGETATION (Figure 29 (b)) and MODIS (Figure 29 (c)) sensors. Increasing values in the NIR band from the mid-year (early dry season) reach a peak at the end of dry season and fluctuate then until January-February (early wet season) to finally decrease during the wet season. Similarly, Asner et al. (2004) showed with spaceborne hyperspectral measurements that visible reflectances were higher and NIR reflectances were lower in the early dry season in comparison with the late dry season in the Tapajós National forest. The major effect occurred in the infrared spectral range where the signal increased almost by 0.1 during the dry season. Taking into account the leaf-flush phenomenon, this pattern confirms the hypothesis arguing in one hand for an emergence of young leaves during the dry season, leading to an increase of NIR reflectance due to strong scattering from internal-leaf cellular structures and, in the other hand, for a NIR absorptance increasing during the wet season because of necrosis and covering of old-leaves by epiphylls – lichens, fungi, liverworts, etc. infesting leaf surfaces – found throughout the humid forests (Roberts et al., 1998; Toomey et al., 2009). This is discussed in detail in section 4.3.1.

However, according to this green-up interpretation, reflectance in the shorter red wavelength would have to decrease during the dry season because of the emergence of new leaves. Indeed, as young leaves have a higher photosynthetic capacity (Doughty and Goulden, 2008; Albert et al., 2014), due to more chlorophyll and water content, they tend to absorb more red light than older leaves. The opposite behavior, for both sensors, questions the sensitivity of the red signal to the Amazonian vegetation. For the VEGETATION values, the profiles of red and blue reflectance seems mainly driven by the number of valid observation count (Figure 29 (b), bars), suggesting that an increase of blue and red reflectance corresponds to higher atmospheric perturbations. Even if high values of reflectance in the

red and blue bands can be explained by the cloud cover residuals and vapor content in the atmosphere during the wet season, the sudden increase of the two bands starting in the middle of dry season, when the number of valid observations is still high, raises question.

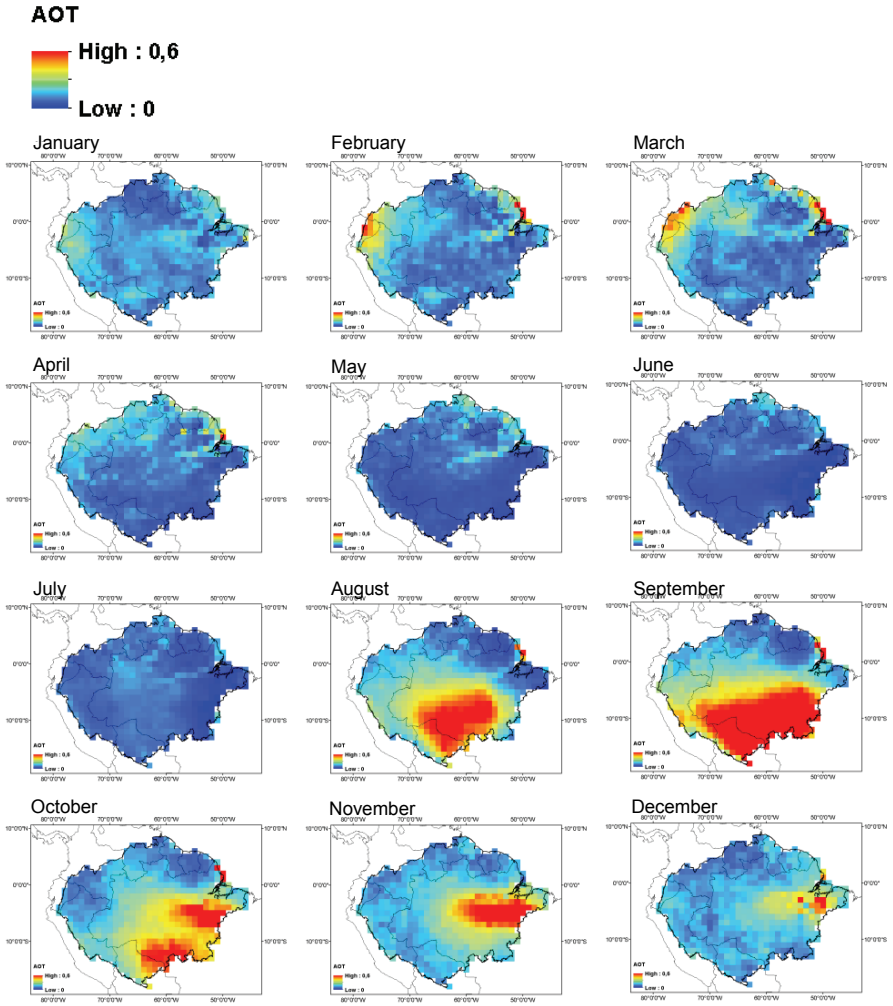


Figure 30: Aerosols Optical Thickness 550 nm dynamics from the L-3 MODIS Gridded Atmospheric Product (MOD08_E3) at 1°x1° spatial resolution for the Amazon basin, using data from January 2000 to December 2009. The average is computed on a monthly basis from the corresponding 8-day values.

A study performed by Kobayashi et al. (2005) on atmospheric conditions in the Amazon region showed that the aerosol optical thickness AOT associated with biomass burning from fires was higher in the end of the 1999 dry season and at the transition period to the wet season. Indeed, it can be observed in Figure 29 (a) that the annual profile of AOT 550 nm, averaged from 2000 to 2009, starts to increase in August, precisely when the red and blue band show unexpected reflectance rise. They are driven by biomass burning from land clearing and agricultural activities. In fact, aerosols scatter sunlight directly to the optical sensor and thus increase the apparent reflectance in the red band, and aerosols also absorb sunlight in higher wavelength and thus decrease, although to a lower level, the near infrared band (Karnieli et al., 2001; Xiao et al., 2003). These aerosols are precisely highly present in the Amazon basin, particularly in the southern and eastern region of the Amazon strongly prone to fires during the dry season notably from slash and burn deforestation and agriculture (Figure 30). The seasonal cycle of AOT appears to be the cause of the red and blue bands sudden increase. The AOT decreases rapidly at the end of the year, though the values in the red and blue bands stay high, because of the higher cloud cover residuals and water vapor in the atmosphere early in the wet season.

To further understand the underlying causes of these particular seasonal patterns, the site converted to agricultural use located near the K67 fluxtower site is analyzed in terms of spectral signature, and compared with results of the dense forest at the fluxtower site. The annual mean profiles of reflectance on a 5x5 pixels window over the pasture site is presented in Figure 31. Reflectance in the red and blue bands varies strongly similarly throughout the year over both sites. They have high values during the wet season (December to May), low values during the early dry season (June to August) and then increase during the dry season to reach high values again for the wet season. The reflectance in the red band is usually lower for the dense forest site, still suggesting more absorbance thanks to a higher rate of photosynthesis. At the opposite, the NIR reflectance profile of this herbaceous area shows a completely different pattern than for the nearby dense forest. It stays flat during the dry season in comparison with the strong increases during this period for the forest site, likely caused by water limitation. Here, in contrast with the majority of the *terra firme* forest, the grassland with superficial roots is very sensitive to the lower rate of precipitation in the dry season, creating a water stress and inhibiting grassland growth (Huete et al., 2006; Bradley et al., 2011). The NIR

wavelength appears typically quite related to the leaf internal structure and is thus less affected by atmospheric conditions. This figure also confirms the hypothesis that reflectance in the red and blue band vary irrespectively of vegetation dynamics in this area. For this reason, the following analysis is based on the NIR wavelength.

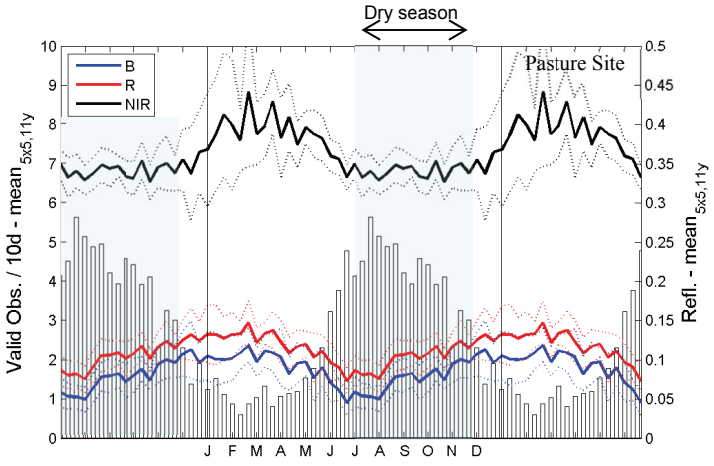


Figure 31 : Annual mean profiles of reflectances in blue (blue line), red (red line) and NIR (black line) bands from SPOT- VEGETATION time series 10-d composites (2000-2010), 5x5 km² window, for a pasture site near K67 fluxtower. Bars are number of valid observations per decade averaged over the 11 years. Inter-annual variability corresponding to one standard deviation is represented by dotted lines. Half-year periods are repeated at the beginning and the end of the year (delimited by vertical lines). Shaded areas indicate the dry season.

### 4.1.2. Sun-sensor geometry influence on intra-annual variations

The signal in the NIR wavelength seems better related to vegetation dynamics, as it is less sensitive to atmospheric scattering which tends to be larger in the visible part of the spectrum, but is however affected by larger amplitude of the bidirectional effects for a dense vegetation cover (Maignan et al., 2004). To investigate the sun-sensor geometry consequences on reflectance values, temporal profiles of NIR, VZA, SZA and φ were extracted on a daily image basis from SPOT-VEGETATION time series (2000-2010).

The viewing directional effects are clearly observed when separating daily data acquired in backward and forward configurations (Figure 32). Green dots in Figure 32 (a) are daily NIR reflectance values acquired in the backward direction, when the sun and the sensor are in the same side. There are higher throughout the years than reflectance measured in the forward direction (black dots, Figure 32 (a)) when the sensor position is opposite to the sun. This viewing effect is easily explained by the vegetation roughness that induces high reflectance anisotropy and higher values when the sun is behind the sensor. Indeed, in the backward scattering, the sensor observes minimal tree shadows and the forest looks brighter, especially in the retrodiffusion direction (or hot spot direction) when the SZA and VZA are identical and the relative azimuth angle is null (the sun and the sensor are perfectly aligned).

Beyond these well-known viewing effects, forward NIR values alone still present an intra-annual variation with an increase during the dry season following the backward NIR values. However, BRDF variations are supposed to be much smaller than those in the backscattering (Bacour and Bréon, 2005). The complete BRDFs modelled by Morton et al. (2014) even shows a forward scattering exempt of any variations. According to his model, NIR values acquired in forward direction would have to show a flat pattern from June to October, compare to backward NIR values. As it is not the case, one should expect that the NIR intra-annual variation is not exclusively due to BRDF effects.

The variation of forward values is also illustrated on the 10-d forward composite (Figure 32 (b), dashed dotted line), computed from daily reflectance data and angle information. As the cycle of the VEGETATION sensor position relative to the sun is 5 days, the day-to-day viewing directional effect are smoothed out by the temporal averaging of 10 days related to the MC (Vancutsem et al., 2007). Indeed, the mean of backward and forward composites (Figure 32 (b), dashed line), supposing to correspond to a nadir view composite, is really matching the original 10-d composite (Figure 32 (b), solid line).

In addition, the similar annual mean patterns of VEGETATION (Figure 29 (b)) and MODIS NBAR (Figure 29 (c)), providing surface reflectance that has been corrected as if they were obtained with a nadir viewing instrument, indicate that VEGETATION composites are rather independent to the viewing effects. These viewing effects have thus no

impact on the shape of NIR profile. However, directional effects are a combination of view and illumination geometries. The new MultiAngle Implementation of Atmospheric Correction (MAIAC) MODIS product (Lyapustin et al., 2012) realized with MODIS Collection 6 data could be used in the future instead of the NBAR product to account for both view and illumination geometries, as MAIAC values have been normalized for both a nadir viewing direction and sun zenith at 45°.

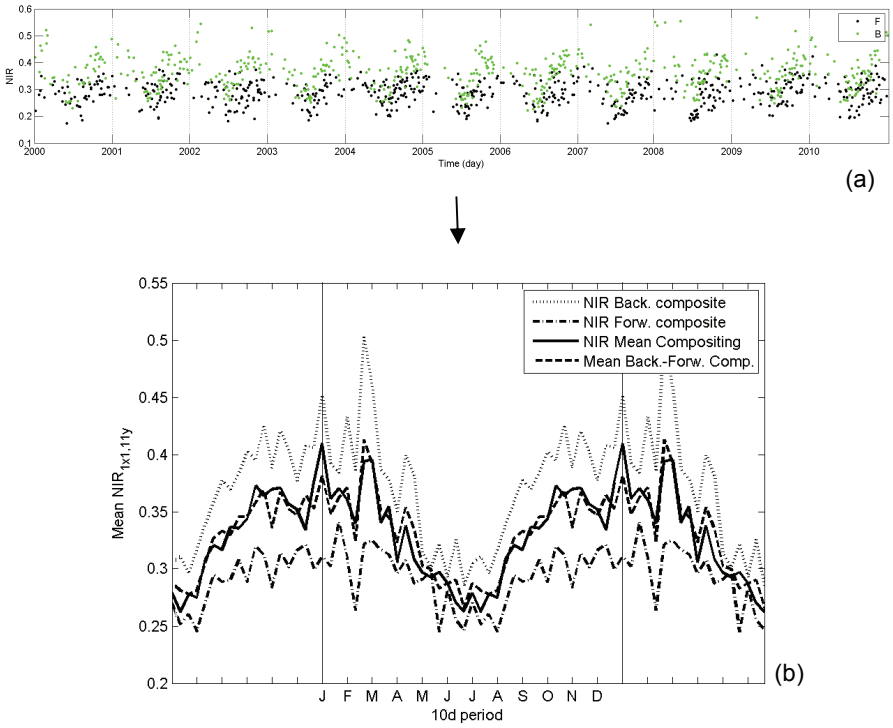


Figure 32 : SPOT- VEGETATION (2000-2010) data extracted for a 1x1 pixel window centered at the K67 fluxtower: (a) Daily S1 data in the NIR band acquired in backward (green) and forward (black) configuration. (b) Annual mean profiles of 10-d forward (dashed dotted line) and backward (dotted line) composites, mean of backward and forward composites (dashed line) and original 10-d composite (solid line) in the NIR band. Half-year periods are repeated at the beginning and the end of the year (delimited by vertical lines).

The much more enhanced BRDF in the backward relative to the forward scattering direction is also illustrated in the polar representation of daily NIR reflectance values (radial axis : VZA, azimuth axis : φ = SAA-

VAA) (Figure 33 (a)). These three polar plots show directional sampling of daily NIR reflectance measurements acquired with the VEGETATION instrument in September, October and December. According to Morton et al. (2014), the apparent increase of greenness in Amazon forests during the dry season is an optical illusion created by the relative positions of the sun and the sensor during this season. They argue that NIR values are higher in October compared to the beginning of the dry season because of the reduction in the proportion of shadow cast by canopy elements when the sensor is perfectly aligned with the sun in October. At this moment of the year, the relative azimuth angle, i.e. the relative position of the sun and the sensor φ, is close to zero as observed in Figure 33 (a), meaning that the sensor samples in the principal plane (retrodiffusion direction). The reduction of the shadow was also mentioned by Galvão et al. (2011, 2013) and Moura et al. (2012) but because of the decrease of SZA during the dry season until October.

However, these four studies stop their analysis in October when φ and SZA are at their lowest level. We looked what happens a little later for the sun-sensor geometry and NIR values in December, when SZA and φ start to increase again (see Figure 36 (a) for the yearly profiles of SZA and φ). From September to December, the φ goes through his lowest values (October) then starts increasing again. Similarly, the SZA decreases from September (mean backward = 23°) until October (mean b. = 21°) then rises again in December (mean b. = 30°) (Figure 33 b). With a similar φ configuration than in September but a higher mean SZA causing more shades, NIR values of December would have to be lower than September NIR values, following the hypothesis that sun-sensor geometry is the main driver of NIR variations. But then how to explain that NIR values continue to increase, from 0.37 in September to 0.41 in December (backward)? The NIR values still increasing while φ and SZA increase again could reveal an actual increase of vegetation photosynthesis activity. This is further discussed in section 4.3.2 with the support of GPP fluxtower measurements.

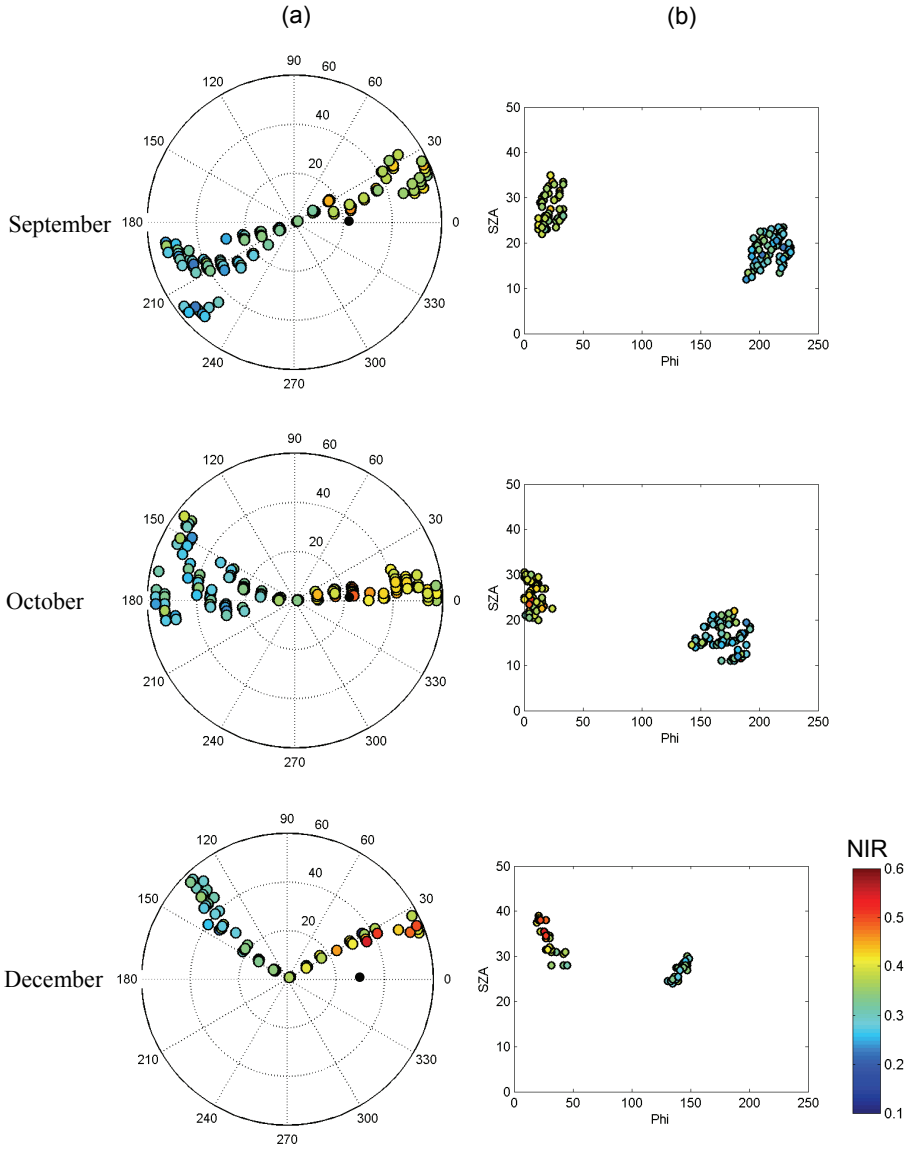


Figure 33 : Representation of daily NIR reflectance values at K67 fluxtower from SPOT-VEGETATION time series (2000-2010) in September and December as function of (a) φ and VZA in the polar diagrams and of (b) SZA and φ. Polar diagrams: view zenith angles are represented as circles every 20°, the principal plane is on the horizontal line with backscattering to the right. The small black circle corresponds to the mean sun angle during the period of observations.

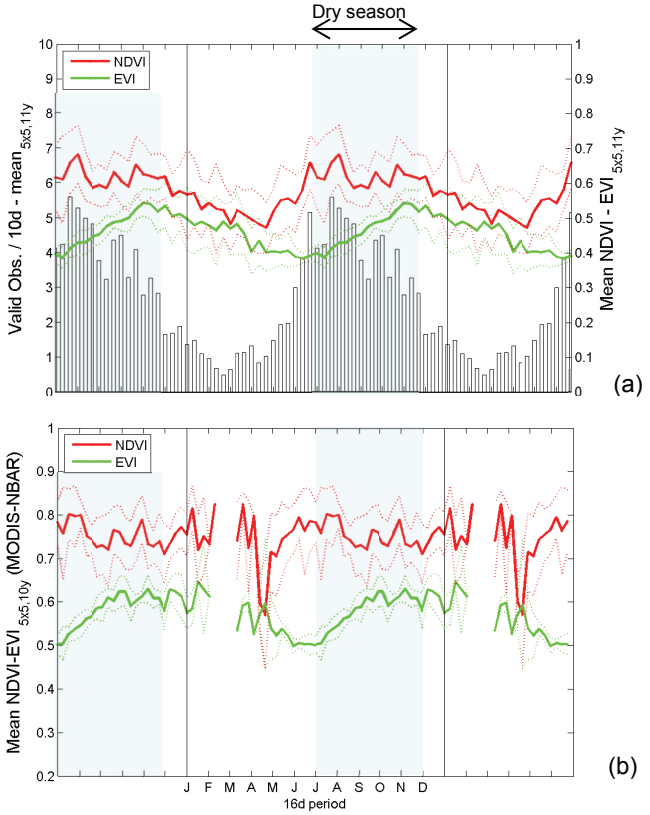


Figure 34 : Annual mean profiles of NDVI (red line) and EVI (green line) for a 5x5 pixels window centered at K67 fluxtower from (a) SPOT-VEGETATION time series 10-d composites (2000-2010) and (b) NBAR-MODIS time series (2000-2009). Bars in (a) are number of valid observations per decade averaged over the 11 years. Inter-annual variability corresponding to one standard deviation is represented by dotted lines. Half-year periods are repeated at the beginning and the end of the year (delimited by vertical lines). Shaded areas indicate the dry season.

## *4.2. EVI and NDVI seasonal dynamics*

### 4.2.1. EVI and NDVI comparison

Climatologies of EVI and NDVI were computed from the respective spectral bands averaging decade by decade the 11-year SPOT-VEGETATION time series and the 10-year MODIS-NBAR time series (Figure 34 (a) and (b)). The seasonal pattern of both indices with VEGETATION data differ significantly (Figure 34 (a)). Indeed, the NDVI profile increases two to three months earlier than for EVI profile. In addition, the EVI profile is less noisy

than the NDVI profile which presents a large inter-annual variability. The NDVI derived from the NBAR product clearly shows the saturation problem associated with the mathematic formulation of NDVI (Figure 34 (b)). Very low reflectance values in the red band, which are explained by dense vegetation, high chlorophyll activity and thus high absorption in the visible spectrum, have minor impacts on the calculation of NDVI. Consequently, NDVI remains at a plateau level. This problem is less present for the VEGETATION sensor that has higher reflectance values in general. Comparing VEGETATION and NBAR data, a clear phenological profile appears on the two 11-year annual mean profiles of EVI with a distinct trend of increasing values during the dry season from July to November and a peak in late dry season to early wet season.

The scatterplots in Figure 35 represent the relationship between vegetation indices and the reflectances (VEGETATION sensor). The NDVI is strongly negatively correlated with the red bands ($r^2 = 0.67$), but not with the NIR band ($r^2 = 0.01$). The EVI shows the opposite, with a strong positive correlation with the NIR ($r^2 = 0.63$). Results are similar for the NBAR product. In dense canopies such as Amazonian forests, the formulation of NDVI makes it relatively insensitive to NIR reflectance change as these are an order of magnitude higher than the red reflectance (Samanta et al., 2012). The relationship between NDVI and the red band confirms that seasonal NDVI variation over tropical forests in the Amazon region are primarily driven by variation of atmospheric conditions affecting the red band with the presence of persistent burning biomass aerosols during the late dry season and then cloud cover during the wet season. Indeed, NDVI tends to increase with the ratio of clear-sky as it can be observed by comparison of NDVI pattern with the number of valid observations by composite (Figure 34 (a), bars). Contrarily, the EVI is very sensitive to change in NIR as the red band is corrected with the blue band for aerosol influences. By relying on NIR canopy reflectance, the EVI is thus a better alternative to NDVI to study the seasonal variation of vegetation in the Amazon region. It remains effective to canopy variation even for areas of high biomass and chlorophyll content, as shown by Huete et al., 2002. Actually the most significant disagreement between EVI and NDVI anomalies occurred in areas with extensive fires (Xiao et al., 2003). Note that if an increase of NIR values is observed during the dry season, aerosols also absorb sunlight in higher wavelength and thus decrease the reflectance values in the NIR band, although to a lower level than the increased blue and red bands (Karnieli et al., 2001). Thus, this

profile should probably be a little higher during these months with a large amount of aerosols indicating that the green-up might then be underestimated.

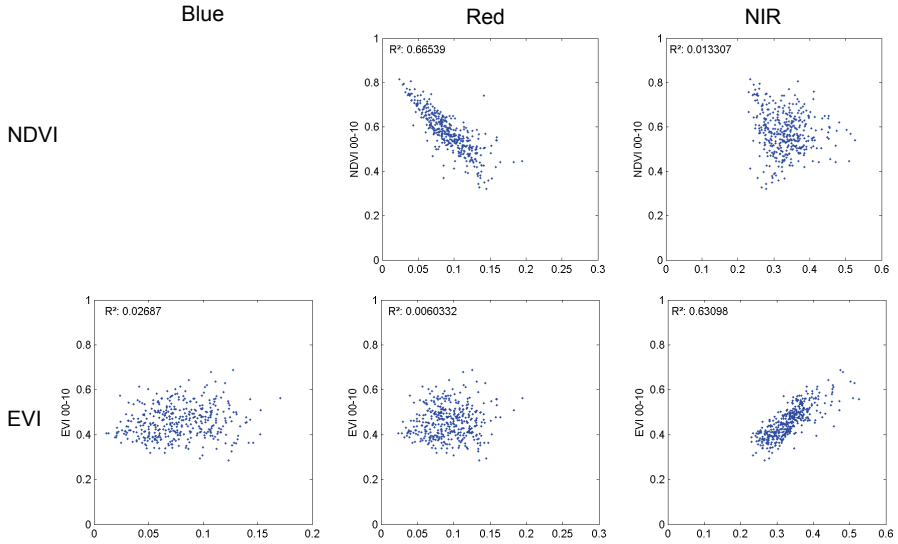


Figure 35 : Scatterplots between the NDVI/EVI and reflectances used to generate them, from SPOT- VEGETATION time series 10-d composites (2000-2010), at the location of the K67 flux tower, 5x5 km² window (spatial average values).

### 4.2.2. EVI and sun-sensor geometry

The Figure 36 (a) and (b) below shows EVI and SZA intra-annual dynamics based on the 11-y SPOT-VEGETATION time series for the K67 site and the Yangambi site in the Congo basin. While Galvão et al. (2011, 2013) and Moura et al. (2012) based their analysis from May to September to claim evidence of solar illumination effects on the EVI, increasing along the dry season with decreasing SZA, a look at the entire year dynamics show however that a few months is not enough to conclude such a correlation. Indeed, taking into account the entire year, there is no evident link between EVI and SZA ($R^2 = 0.01$ for K67, $R^2 = 0.08$ for Yangambi, using daily data). A study based on six high resolution (20m) images with varying sun-sensor geometry further supports this hypothesis, as they found no correlation between the NIR reflectance and the SZA in the Ngotto forest, Congo basin (de Wasseige et al., 2002).

Moreover, a correlation between SZA and EVI showing inverse pattern, even over an entire year, is not sufficient to conclude to a direct causal relationship. Indeed, for a forest site in temperate region with a well-known phenology, the strong negative correlation between EVI and SZA ($R^2$ = 0.68) cannot be interpreted as a solar illumination effects on the EVI, increasing with smaller SZA (Figure 36 (c)). Although EVI and SZA show clear opposite patterns for this temperate site, EVI variations are not a consequence of more or less shadow but only a reflect of phenological cycle as a response to climate variation. Indeed, in temperate zones, the seasonality of ecosystem metabolism is well marked. The NIR reflectance variation is not driven by BRDF effects but clearly dominated by leaves grow up in April-May and fall in October-November. Then, why couldn't it be the case also in the Amazon forest during the dry season months, to a lesser extent? Another striking result is the very different patterns between the EVI profiles from the K67 fluxtower site (Figure 36 (a)) and the Yangambi site in the Congo basin (Figure 36 (b)), while φ and SZA yearly variations are very similar. How could those two EVI profiles, extracted from two mature moist tropical forests, be so different according to the sun-sensor geometry driver hypothesis asserted in Morton et al. (2014)?

We suggest that correlations between NIR/EVI and angles patterns are not evidence of direct cause and effect, and that the EVI increase during the dry season is not an artefact due to seasonal changes in view-illumination geometry. It coincides with a recent study using EVI MAIAC MODIS data expressed in the fixed geometry of nadir-view direction and 45° sun zenith angle (Bi et al., 2015). They still found a distinct wet season decrease and dry season increase, showing evidence for seasonality after sun-sensor geometry correction. They also claim for a misinterpretation in Morton et al. (2014) coming from a reliance on prognostications of an untested radiative transfer model. To them, the model simulations on variation in sunlit and shaded proportions of the canopy, central to arguments about geometric artefacts, underestimates measurements by ~45%. In addition, the model is also unrealistically sensitive to litter reflectance in dense vegetation, an indication of incorrect physics and/or modeling of foliage spatial distribution.

It concludes that the EVI dynamics could be related to actual vegetation phenology following the green-up hypothesis. This is discussed in the next section in the light of ground and meteorological measurements.

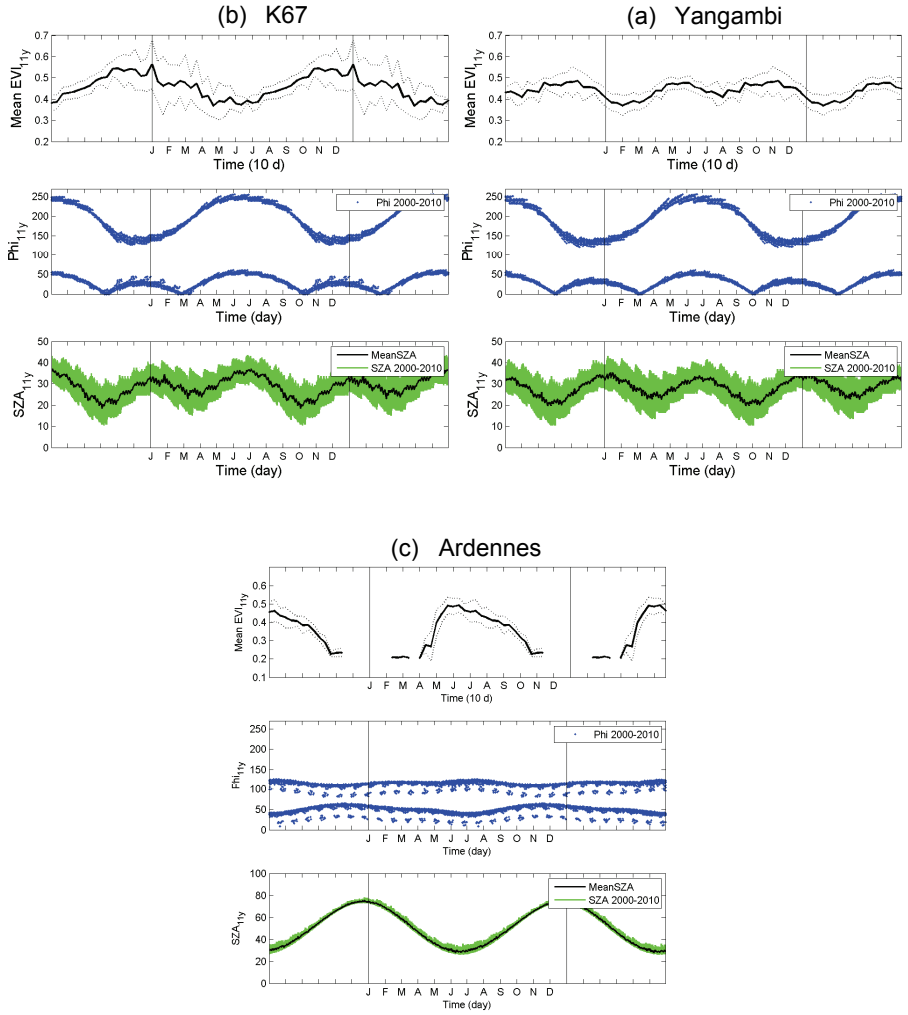


Figure 36 : Annual mean profiles of EVI 10-d composites (black line) and inter-annual variability (dotted line), relative azimuth angle (blue dots) and solar zenith angle (green dots, mean = black line) from SPOT- VEGETATION time series (2000-2010), 1x1 km² window, in (a) K67 fluxtower site, (b) Yangambi (Democratic Republic of Congo) and (c) the Ardennes (Belgium). Inter-annual variability corresponding to one standard deviation is represented by dotted lines. Half-year periods are repeated at the beginning and the end of the year (delimited by vertical lines). The EVI pattern for K67 is not exactly the same than in Figure 34 (a) because it is computed on a 1x1 pixel window basis, instead of 5x5, for the sake of SZA extraction.

## *4.3. In situ data*

### 4.3.1. Leaves studies

As for the NIR reflectance values, the EVI increase of Amazon forests during the light-rich dry season can be associated with the shedding of old leaves and the emergence of new leaves inducing a higher photosynthetic capacity as a result of change in both leaf area and leaf optical properties (Samanta et al., 2012), while the decrease of EVI in the wet season could be attributed to the aging processes of leaves. The mechanism of this dry season green-up is supported by many field studies on leaf phenology, from spectral measurements over the life cycle of leaves to litterfall collection and tower mounted cameras, showing that wet and dry seasons induce variation in vegetation phenology. The main outcomes of these field studies are summarized in Table 7.

The canopies of evergreen broadleaf trees in the Amazon tropical rainforests are composed of green leaves of various ages (Xiao et al., 2005), with some living over 4 years (Reich et al., 2004). Over the lifespan of a leaf, natural morphological and physiological changes or mechanical damages occur with leaf aging inducing spectral response evolution in terms of light transmitted, reflected and absorbed by leaves (Roberts et al., 1998). The onset of senescence of the mature leaves and envelopment by epiphylls, that inhibit light interception by host plant, begins in the late wet season and leads to changes in leaves spectral reflectance properties and photosynthesis (Roberts et al., 1998; Goulden et al., 2004). In Amazonian *caatinga* (woodland/forest on nutrient-deficient sandy soils) canopies, leaf-level spectral measurements showed indeed that NIR absorptance significantly increases as leaf aged from near 0 for young leaves to 10% for old leaves associated with leaf necrosis and epiphylls growth on leaf surfaces (Roberts et al., 1998). NIR reflectance decreases from 5.8 - 10.6 % for *terra firme* forest canopies for moderate to heavy infestations of epiphylls respectively (Toomey et al., 2009). The more the leaf ages, more the epiphyll loads is heavy. Their findings indicate that epiphylls can have a substantive effect on the remote sensing of tropical forest canopies. Conversely, new leaves display higher reflectance and increased transmittance relative to older leaves (Roberts et al., 1998). Thus, removal of old leaves from the canopy (leaf litterfall) and new leaves production is likely to result in an increase of NIR reflectance at the canopy level (Xiao et al., 2005).

Precisely, ground-based studies in many places of the Amazon basin have reported a distinct seasonality of leaf litterfall, one of the major pathways of nutrient cycling (Barlow et al., 2007), showing greater rates at the beginning of the dry season to reaches a peak in the middle of this season (Dantas and Phillipson, 1999; Goulden et al., 2004; Rice et al., 2004; Barlow et al., 2007; Malhado et al., 2009; Brando et al., 2010; Pennec et al., 2011; Wagner et al., 2013). This peak would be followed by a rapid leaf turnover for deep-rooting species midway through the dry season leading to significant increases in leaf area, NIR reflectance and photosynthesis. Fewer field studies reported measurements of leaf gain, indicating that the emergence of young leaves occurred mainly during the dry season (Roberts et al., 1998, Haugaasen and Peres, 2005). This turnover between leaf fall and leaf renewal, part of the green-up hypothesis, is recently further supported by tower mounted RGB cameras. They show that crown-scale leaf-flushing events are concentrated in dry seasons. From a 54m tall eddy-flux tower in Central Amazon (Manaus), Nelson et al. (2014) observed two easily recognized phenophases. The first one is a massive flushing of new leaves completed within 30 days and exhibited on average by 44% of live crowns each year in the five driest months (June-October) to reach peak abundance in late dry to early wet season. The second one is a complete or nearly complete leaf loss prior to adding new leaves observed on 40-50% of flushing crowns. This brief deciduous stage lasted 36+/- 25 days and is directly followed by dry season leaf flush. The exactly same phenomenon is observed for an evergreen tropical forest in Malaysia, with the help of daily canopy photographs taken by a digital camera (Nakaji et al., 2014). The emergence was observed together with defoliation, but defoliation was complete before the full expansion of new leaves which continued over 3 months. Following the green-up phenomenon, this new leaf production during the dry season is possible thanks to deep rooting allowing trees to maintain access to soil water year round. However, if it allows high transpiration and photosynthesis in the dry season, the wood production declines during this period reflecting a distinct seasonality in carbon allocation in tropical trees from long-lived pools (wood) to short-lived pools (leaves) (Wagner et al., 2013; Restrepo-Coupe et al., 2013).

Table 7: Field measurements of leaves dynamics in the Amazon basin.

| **Type of measurement** | **Wet Season**  | **Transition: late wet season to early dry season** | **Dry season**  | **Transition: late dry season to early wet season** | **Studies** |
|---|---|---|---|---|---|
| **Spectral measurements** | Mature leaves: NIR absorptance ↑ from 0 to 10%, NIR reflectance ↓ from 5.8 to 10.6% | Young leaves: NIR reflectance ↑ | NIR reflectance is maximum | - | Roberts et al., 1998; Goulden et al., 2004; Toomey et al., 2009 |
| **Litterfall colletions** | - | Start of litterfall at the beginning of the dry season | Peak of litterfall reached in the middle of this season | - | Dantas and Phillipson, 1999; Goulden et al., 2004; Rice et al., 2004; Barlow et al., 2007; Malhado et al., 2009; Brando et al., 2010; Pennec et al., 2011; Wagner et al., 2013 |
| **Leaf gain observations** | - | - | Leaf flushing | - | Roberts et al., 1998; Haugaasen and Peres; 2005 |
| **Tower-mounted cameras** | - | Complete or nearly complete leaf loss (36± 25 days ) directly followed by leaf emergence (40-50% of flushing crowns) | Massive flushing of new leaves completed within 30 days (44% of live crowns) | Peak of leaf flushing | Nelson et al., 2014; Nakaji et al., 2014 |
| ***Summary*** | ***Senescence of the mature leaves and envelopment by epiphylls*** | ***Removal of old leaves from the canopy (leaf litterfall) and leaf flushing of new young leaves*** | ***Peak of litterfall and leaf flushing*** | ***Peak of leaf flushing*** | |

### 4.3.2. Impact of leaves dynamics on EVI cycle

Together, these ground information about leaf spectral properties and phenological cycle fit the satellite-based EVI pattern. The EVI dynamic could be driven by the seasonal timing of leaf senescence, leaf shedding and leaf flush. First, the senescence of old leaves and covering by epiphylls reduces progressively the NIR reflectance and the EVI declines throughout the wet season. Then, at the start of the dry season, the shedding of old-leaves removes highly absorbing NIR leaves from the canopy, leading to a slight increase in EVI. Finally, the litterfall is rapidly followed by appearance and expansion of new leaves that replace aging or epiphyll-covered foliage and have high NIR reflectance, continuing the EVI augmentation until the end of the dry season.

Galvão et al. (2011, 2013) and Moura et al. (2012) did not examine the influence of leaf flush on NIR reflectance and even admit that other potential factors such as leaf flush can act in conjunction with view-illumination geometry to explain the dry season EVI increase. In addition, Morton et al. (2014) found with a 3D radiative transfer model that increasing leaf reflectance (+10%) led to a 35% increase in EVI with unchanging canopy properties while the impact of seasonal changes in sun-sensor geometry increases EVI by only 7.5% throughout the dry season.

### 4.3.3. EVI and GPP derived from fluxtower

Some studies demonstrated a consistent relationship between the seasonality of EVI and flux tower measurements of carbon uptake (GPP) in the Amazon basin (Xiao et al., 2005; Huete et al., 2006; Ichii et al., 2007), even after having removed the contamination of cloud and aerosol and corrected BRDF effects on EVI (Maeda et al., 2014), but also in tropical forests of Southeast Asia (Huete et al., 2008), across African and Australian savanna ecosystems (Sjöström et al., 2011; Ma et al., 2014) or temperate biomes in North America (Rahman et al., 2005; Sims et al., 2006). Integration of EVI and Normalized Difference Water Index (NDWI) in GPP simulation for the K67 site in Santarém showed a consistent agreement between GPP predicted and GPP estimated from Saleska et al. (2003) (Xiao et al., 2005). Light-use-efficiency (LUE) models even use EVI to parameterize successfully the LUE, one of the most essential parameters in production estimation models for terrestrial ecosystems, for GPP simulations (Ma et al., 2014).

The EVI computed from VEGETATION time series for the K67 site is compared with decadal average GPP values derived from fluxtower data from 2002 to 2004 (Figure 37). Both profiles show at first sight a very similar pattern, with seasonal variations in good agreement with the green-up phenomenon. Indeed, they start to increase at the beginning of the dry season, reach their maximum at the end of the dry season until early wet season, and then decline. The GPP increase in the dry season indicates canopy carbon uptake as well as no drought stress for photosynthesis which is consistent with a deep root system allowing to access water even during few-months dry periods. Respiration is reduced during the dry season, likely a consequence of moisture limitations on heterotrophic respiration. The forest ecosystem turns thus into a carbon sink given that GPP dominates. Contrarily, the evapotranspiration consistently increases at the start of the dry season and remains elevated throughout the entire dry season (Hutyra et al., 2007).

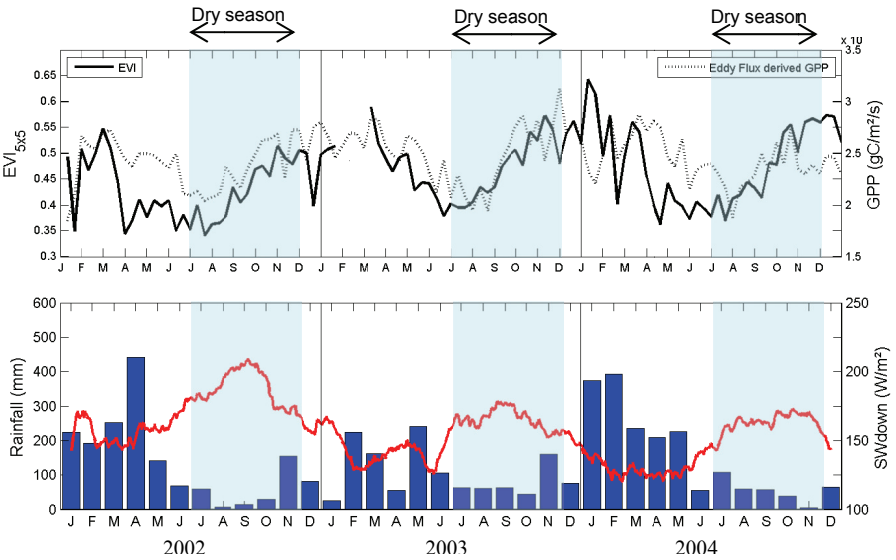


Figure 37 : Seasonal dynamics of 10-d composites of EVI for a 5x5 km² window from SPOT-VEGETATION time series (solid black line), decadal fluxtower derived GPP (gC/m²/s, dotted line), monthly precipitation (mm/month, bars) and daily running mean shortwave income radiation (SWdown, W/m², red line), at the location of the fluxtower K67 (2002-2004). GPP values are averaged by decade only for daytime (8h-16h). Years are separated by vertical lines. Shaded areas indicate the typical dry season.

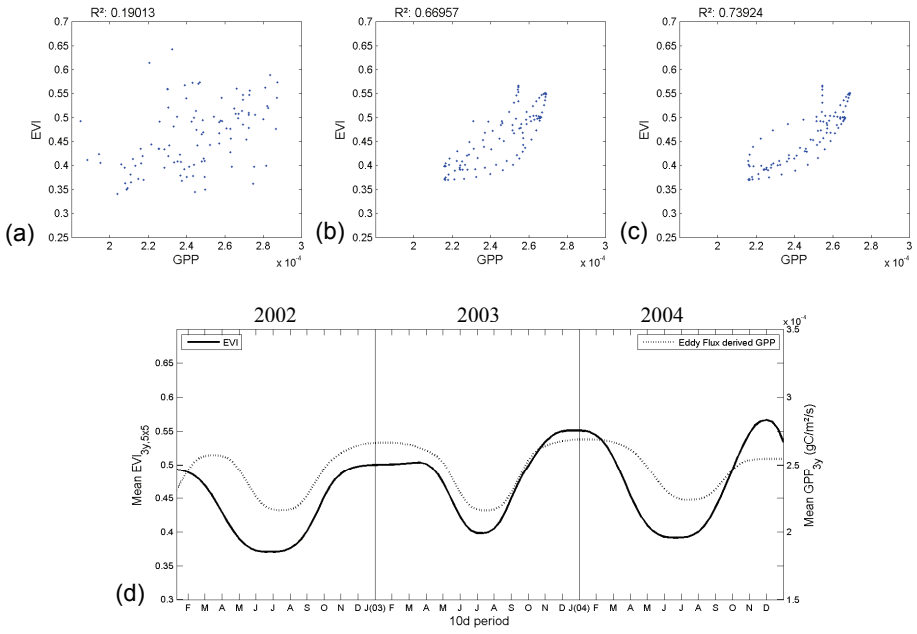


Figure 38: Relationship between EVI 10-d composites derived from SPOT- VEGETATION time series 10-d composites and decadal fluxtower derived GPP (gC/m²/s), at the location of the K67 flux tower (2002-2004) (a), with smoothed data (b) and with smoothed data shifted of one month. Smoothed seasonal dynamics of 10-d composites of EVI for a 5x5 km² window from SPOT-VEGETATION time series (2002-2004) (solid line), and decadal GPP data (g/m²/s) (dotted line), at the location of the K67 fluxtower (d). Years are separated by vertical lines.

The EVI and GPP profiles show however a weak correlation ($r^2$ = 0.19) (Figure 38 (a)). Unlike the rest of the study, these EVI data are not average profiles over 11-y but 10-d composites values. Even if the MC reduces significantly the cloud impact, the 10-d composites can still suffer from a lack of valid images, especially during the wet season where cloud cover is almost permanent. To further remove this noise, the EVI and GPP profiles are temporally smoothed with a Gaussian filter, thanks to the TIMESAT software (Figure 38 (d)). The smoothing or filtering suppresses short frequency variation while the signal retains its original temporal variability and remains a representative index for the vegetation conditions. Removing the random noise reveals an increased relationship between EVI and GPP ($r^2$ = 0.67) (Figure 38 (b)). In addition, the EVI decreases earlier during the wet season than GPP (April to March). By shifting smoothed GPP

values of one month, EVI and GPP show an even stronger correlation ($r^2$ = 0.74). This shift could be due to the covering of epiphylls during the wet season that reduces rapidly NIR reflectance (Roberts et al., 1998), and thus the EVI values, while the decrease of carbon uptake responds slower to this phenomenon.

The rates of leaf gas exchange decline as leaves age, young leaves at least one month old having a greater photosynthetic capacity than older leaves less efficient because of epiphylls and poor stomatal control (Myneni et al., 2007; Doughty and Goulden, 2008). Albert et al. (2014) assessed this photosynthesis variation with leaf age and shifts in leaf demography through fieldwork campaigns in the K67 site. Their results show indeed that photosynthetic capacity is higher for leaves that matured during the most recent dry season than for older leaves from previous periods of growth. Highly efficient leaves with high maximum carboxylation rate are 2-6 months age. They also have maximum effective leaf area, undiminished by accumulating herbivory, epiphylls or pathological damage. The massive flushing of new leaves observed in the dry season with tower mounted cameras (Nelson et al., 2014), coinciding with the increase of GPP, suggests that leaf turnover together with the effects of leaf age on leaf physiology can increase carbon assimilation observed during the dry season at the K67 site (Albert et al., 2014). Thus, it confirms that leaf phenology may be the dominant driver of seasonal variation of forest carbon exchange and EVI in moist tropical forests of the equatorial Amazon (Restrepo-Coupe et al., 2013, Nelson et al., 2014).

Even if there is strong evidence that environmental factors play a major role in the intra-annual variation of GPP (Maeda et al., 2014), the causality between GPP and EVI should be interpreted with caution as uncertainties remain in the mechanisms defining GPP seasonality (Hutyra et al., 2007; Hutyra et al., 2008; Restrepo-Coupe et al., 2013). Errors or uncertainties in characterizing the mean seasonality of photosynthetic patterns arise from at least three sources that should be taken into account: systematic measurement bias (e.g. from failing to correctly adjust for biases arising during periods of low turbulence), random sampling error, and variation in seasonality due to inter-annual variability in climate or other driver variables.

### 4.3.4. Sun radiation as driver

According to numerous studies reviewed in the introduction, the leaf flushing that causes the EVI and GPP increase during the dry season could be a consequence of solar radiation augmentation to optimize access to light, reflecting the green-up phenomenon. For instance, compiling 53 phenological studies conducted in tropical forests, van Schaik et al. (1993) showed that peaks of leaf flushing and flowering closely track the solar maxima. As young leaves present a higher photosynthetic capacity, canopies of drought-tolerant trees invest logically in new efficient leaves during months coinciding with seasonal peaks in solar irradiance. Applying artificially supplemented light levels only when cloud cover reduced incoming solar radiation, Graham et al. (2003) found that light was the primary factor limiting $CO_2$ uptake during the rainy season rather than water, temperature or leaf nitrogen. Supplemental illumination increased daily net carbon gain by an average of 18,4 % for exposed canopy leaves during the rainy season of a La Niña event. Also, over the long-term from the early 1980s to late 1990s, the Amazon had experienced a large increase in productivity in response to a reduced cloud cover and increased tropical radiation (Nemani et al., 2003) and GPP peaks in this period were caused by radiation anomalies exclusively (Ichii et al., 2005). It illustrates the large impact of variation in tropical cloud cover on $CO_2$ uptake.

Our results support this hypothesis, showing a similar pattern between the seasonal dynamics of the 3-y VEGETATION EVI profile and shortwave incoming radiation (SWdown), measured at the K67 tower site (Figure 37). EVI reaches its maximum value with a few months delay as compared to the SWdown radiation peak. This can be attributed to a lag time for emergence and expansion of all the new leaves and for them to develop their pigmentation and reach their maximum capacity of photosynthesis.

In addition to a reduced cloud cover, the presence of aerosol loadings during the dry season induces higher diffuse light levels especially in the wavelengths of the photosynthetically active radiation (PAR). This light scattering observed by the satellite is already demonstrated in Figure 29 (a). Actually, this scattering is beneficial for the trees as it enhances the photosynthetic rates and NEE over large areas in Amazonia (Hutyra et al., 2007; Oliveira et al., 2007). Indeed, diffuse irradiance penetrates canopies more efficiently than direct beam irradiance (Graham et al., 2003). However,

over a threshold of AOT larger than 2.7, strong reduction on the NEE was observed due to the reduction in the total downward radiation.

## *4.4. Spatial extent of EVI dynamics of Amazonian vegetation*

Even if Amazonia harbors roughly 16000 tree species, only 227 (1,4%) account for half of all trees (ter Steege et al., 2013). It implies that most biogeochemical cycling in this forest is performed by a tiny sliver of its diversity. A spatial distribution of EVI seasonal dynamics for the whole Amazon basin is shown in Figure 39. It illustrates that the EVI seasonal cycle observed at the K67 site is visible at the biome scale. A clear decrease of EVI is observed since the middle of the wet season (March to June) while precipitation and cloud cover dominates since December (Figure 40). Then, the green-up is pronounced throughout the basin from July-August, first in the Southeast region and then in the entire basin in November-December. Tropical rainforest is particularly well delineated using this vegetation index, especially during the dry season where savannas run dry strongly whereas the rain forest remains green. Deforested areas, such as the Mato Grosso region in the South of the basin, are clearly distinct from the forest and correspond to low EVI values during the dry season.

Even if a general trend in increase and decrease of greening is observed throughout the year, the entire Amazon shows a heterogeneous behavior. The spatial EVI variability questions the combination and the interactions with others mechanisms or environmental variables, in addition to solar radiation driver, that could influence vegetation productivity. First, the dry season across the Amazon's forests is variable in both duration and intensity (Xiao et al., 2006). The start of the dry season follows a gradient from the Southeast of the basin in June-July to the North in December-January (Figure 40). The gradient in EVI increase during the dry season can be explained by the fact that the North region presents still a high cloud cover and precipitations in June-July while a clear sky exempt of precipitation, favorable for an increase in photosynthesis activity, is already observed in this period in the South. This region is characterized by a longer dry season (5-6 months), less precipitation and more solar radiation. Contrarily, the Northwest region has a weaker radiation and precipitation seasonality with a shorter dry season that could be the cause of lower maximal EVI values.

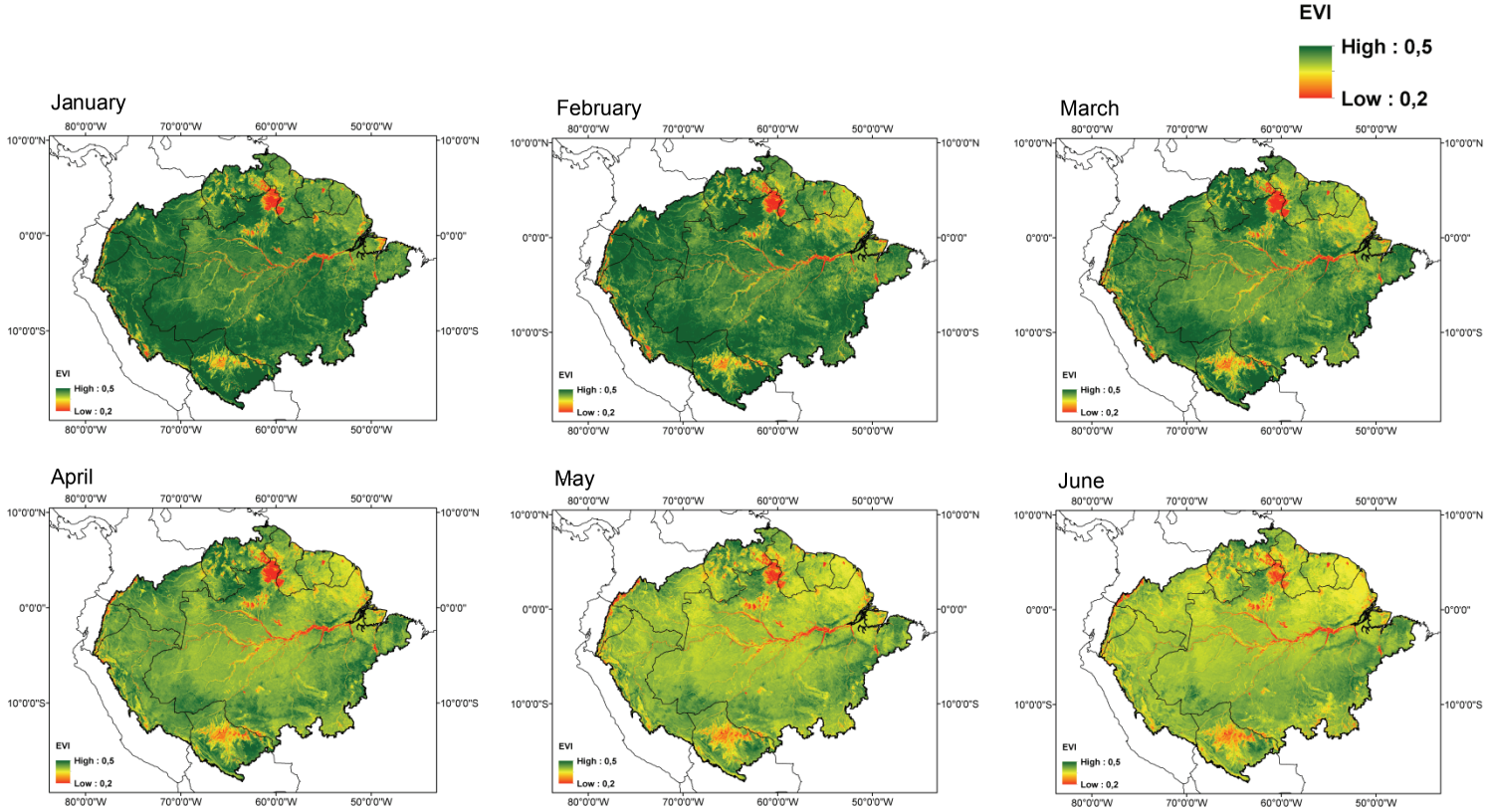
EVI
High : 0,5
Low : 0,2
January
February
March
April
May
June
80°0'0"W
70°0'0"W
60°0'0"W
50°0'0"W
10°0'0"N
0°0'0"
10°0'0"S

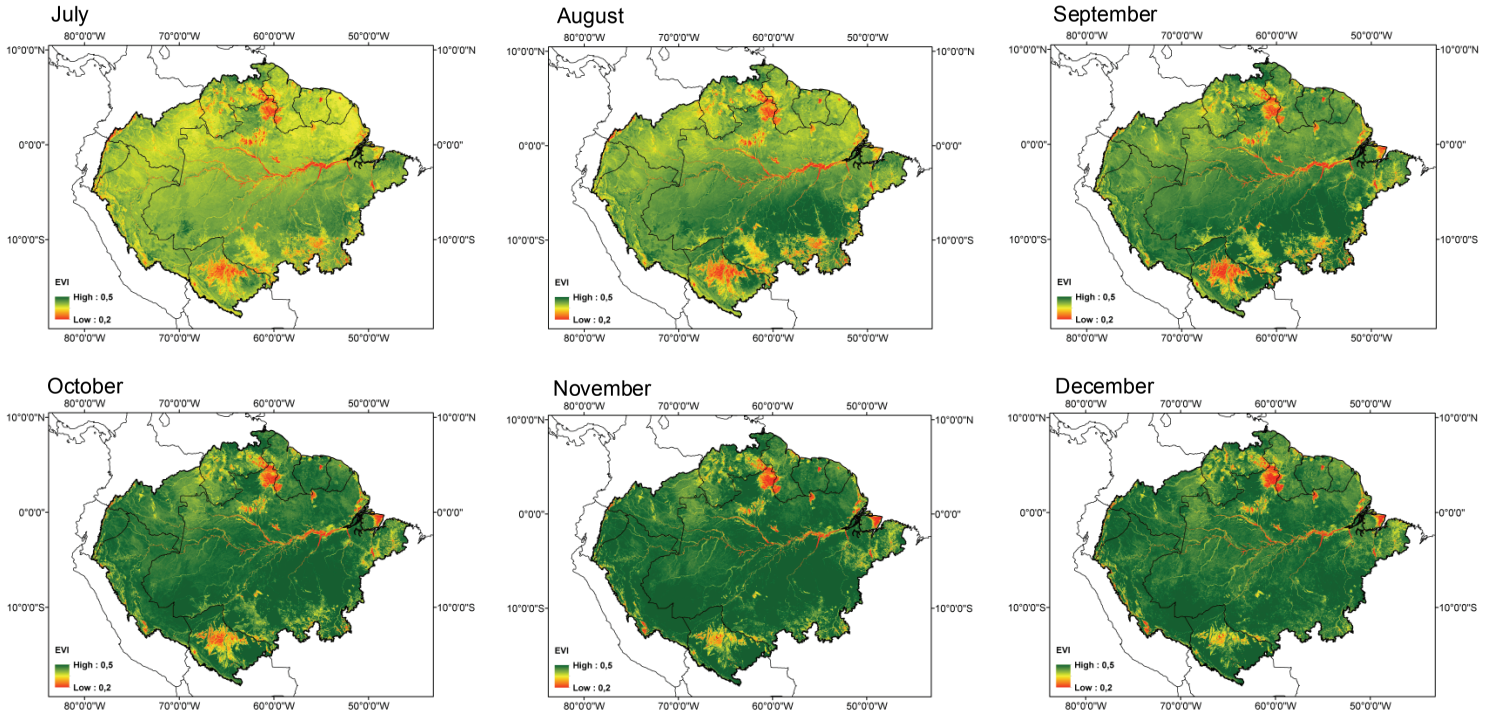


Figure 39 : Spatial distribution of EVI seasonal dynamics for the Amazon basin. Each months average is a mean of corresponding 30-d composites from the 11 years of data from SPOT- VEGETATION time series (2000-2010).

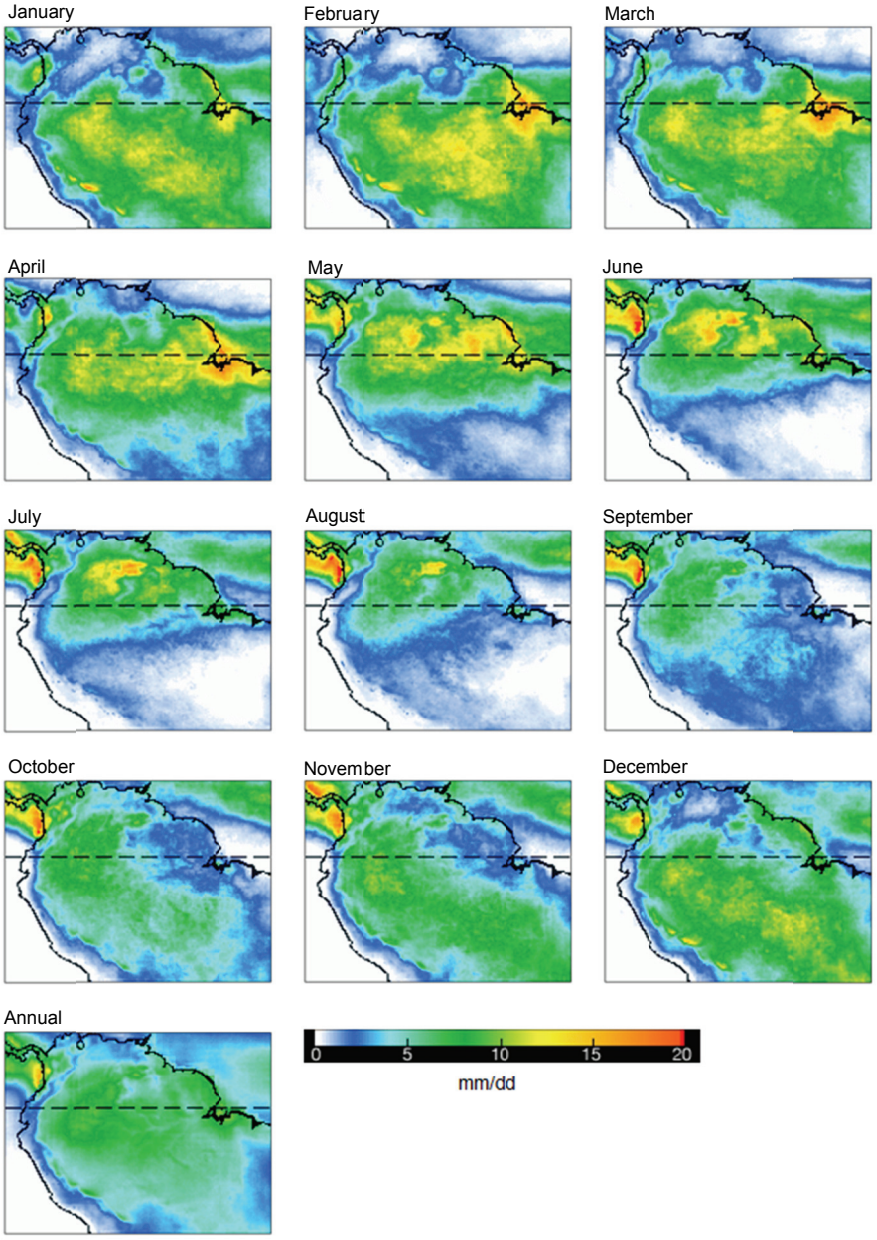


Figure 40: Rainfall climatologies from the Tropical Rainfall Measuring Mission (TRMM) using 1998 to 2011 data, mm/dd, 0.25° by 0.25° spatial resolution.

Second, the tropical forests of the Amazon basin occur on a wide variety of different soil types reflecting a rich diversity of geologic origins and geomorphic processes (Quesada et al., 2011, Figure 41). As moisture availability is dependent not only on incoming precipitation but also on depth and texture of the soil, depth of the water table, soil capillarity and site hydrology (Hutyra et al., 2007), different types of soil could provide more or less opportunity for trees to reach water during the dry season. For instance, the patch of low EVI observed in central Amazonia from January to March matches the delineations of Plinthosols showed in the basin wide distribution of soils in Quesada et al. (2011). Also, the spatial differences in the length of the roots could induce more or less access to water during the dry season.

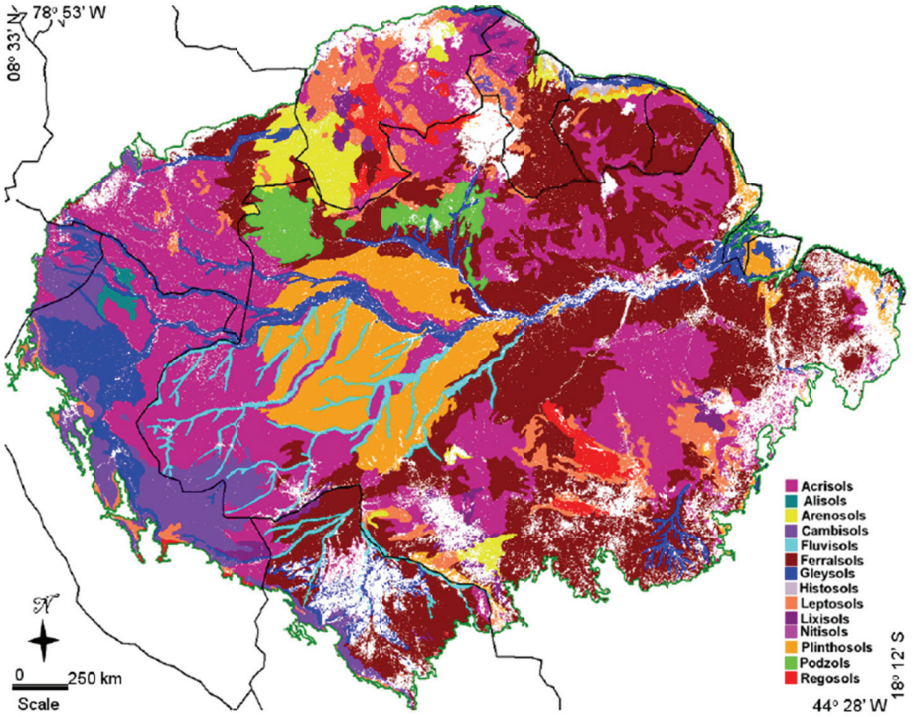


Figure 41: Basin wide distributions of soils under forest vegetation, based on the SOTERLAC–ISRIC soil database (version 2.0, 1:5 million scale) and the vegetation database of Saatchi et al. (2008) for South America (Quesada et al., 2011).

Third, soil phosphorus is currently considered as the dominant limiting nutrient in tropical ecosystems, more limiting than nitrogen, and net primary production (NPP) tends to increase with the availability of soil phosphorus (Aragão et al., 2009). However, its spatial distribution remains poorly understood and very few considered in carbon-climate models in part because of the complexity of its cycle at geological timescales (Yang et al. 2014). Spatial variability in length of the dry season, soil type, root length, phosphorus availability or even surface temperature may be secondary factors limiting the intensity of dry season greening and could play jointly to drive the spatial variation of gross primary production.

# 5. Conclusion

This study explored the potential of vegetation indices derived from Earth observation time series to detect seasonal signal and to map spatial characterization of leaf phenology in tropical rainforests.

The deep analysis on possible sources of signal noise allowed selecting the EVI as appropriate for studying vegetation phenology. First, the analysis of atmospheric contamination showed that the seasonality of reflectance in the red band is not driven by the degree of chlorophyll absorption but instead strongly contaminated by cloud cover and aerosols from biomass burning. The NIR band is less affected by these atmospheric contaminations and more related to the vegetation dynamic. As the NDVI has a strong relationship with the red band and the EVI follows the NIR dynamic, the EVI is better suited than NDVI to study the vegetation dynamic in the Amazon region. Second, if viewing directional effects are clearly present in the data, they do not affect significantly the shape of the NIR and EVI profile. In addition, the relationship between EVI and SZA/φ variations claimed by some studies is not verified here. It is concluded that the EVI increase during the dry season in the Amazon basin is not a consequence of view-illumination geometry.

Instead, the EVI seasonal cycle at site level and at basin scale corresponds closely to ground vegetation phenology following the green-up hypothesis. Together, the field information about leaf age spectral properties

and phenological events, such as ground-measurements and cameras images of leaf flushing and litterfall, fit the satellite-based EVI pattern. The EVI dynamic is driven by the seasonal timing of leaf senescence, leaf shedding and leaf flush. First, the senescence of old leaves and covering by epiphylls reduce progressively the NIR reflectance and the EVI declines throughout the wet season. Then, at the start of the dry season, the shedding of old-leaves removes highly absorbing NIR leaves from the canopy, leading to a slight increase in EVI. Finally, the litterfall is rapidly followed by appearance and expansion of new leaves that replace aging or epiphyll-covered foliage and have high NIR reflectance, continuing the EVI augmentation until the end of the dry season. The EVI presents also a very similar pattern than GPP derived from the fluxtower. The GPP increase in the light-rich dry season indicates canopy carbon uptake as well as no drought stress for photosynthesis, coherent with the massive flushing of new leaves observed during this period. Thus, it confirms that leaf phenology, itself driven by light availability, is the dominant driver of seasonal variations of forest carbon exchange and EVI in tropical rainforests of the equatorial Amazon.

This study suggests that EVI provides useful information about changes of vegetation behavior over time. This index could be useful to help characterizing tropical vegetation phenology in ecosystem models and used as a proxy to vegetation properties.

Nevertheless, at the basin scale, spatial variations in both length of the dry season, soil type, root length, phosphorus availability or even surface temperature may be secondary limiting factors in the intensity of dry season greening. They could act jointly in the spatial variations of gross primary production and warrant dedicated studies. In addition, four other flux towers in the Amazon basin offer the possibility to further explore the GPP-EVI relationship.

# Chapter 3 – Vegetation phenology of tropical rainforests in the Congo basin from 11-y SPOT-VEGETATION time series

## Abstract

Understanding vegetation phenology of tropical rainforests and its controlling mechanisms are crucial for anticipating how rainforests will respond to climate change. Very few studies on vegetation phenology have been carried out in the Congo basin although these vast forests are a significant component of the Earth's carbon budget. This study explores for the first time the potential of vegetation indices derived from the 11-y SPOT-VEGETATION time series (2000-2010) to characterize leaf phenology of central African tropical rainforests. The research investigates at site level and at the basin scale the causes of the intra-annual dynamic of reflectance and vegetation indices, from artefacts such as atmospheric contamination and directional effects to phenological events and environmental mechanisms. Leaf phenology and productivity in this tropical rainforest seems driven by solar radiation availability, as often concluded in the literature for the Amazon basin. Sun and rainfall seasonality presents however a double periodicity in the major part of the basin which complicates the phenological vegetation response to climate. Leaf phenology can be assessed by EVI dynamic in some part of the basin where low aerosol optical thickness values and high valid observation number are prevalent. It corresponds to the seasonal timing of leaf shedding and leaf flush and peak during the wet season, period with higher solar radiation. This study suggests that EVI provides useful information about vegetation behavior over time in

tropical region exempt of permanent cloud cover and of very high aerosol load.

# 1. Introduction

Central African rainforests constitutes the second largest continuous area of tropical rainforest in the world, next to the Amazon basin, and play significant roles from local to global scale in terms of biodiversity, carbon and water cycling and ecosystem services in a subsistence economy context. Indeed, the total mass of carbon stored above ground in live woody vegetation of tropical Africa is estimated to 64.5 Pg C, representing about 25% of the total stock held in woody vegetation of pan-tropical ecosystems (Baccini et al., 2012; Saatchi et al., 2011). In addition, the increase in carbon storage in intact African tropical forest of 0.34-0.61 Pg C $y^{-1}$ for the last decades (Lewis et al., 2009; Valentini et al., 2014) and of 0.04 Pg C $y^{-1}$ for the past century (Fisher et al., 2013) makes it a net carbon sink that reduces the rate of increase of atmospheric $CO_2$.

Although covering 30% of the global rainforest area, the African tropical forests have been relatively neglected compared to the other tropical forests, for a number of reasons including challenging and fragmented politics, civil conflicts and logistical as well as infrastructure challenges (Malhi et al., 2013). However, recent studies contribute to improve the state of knowledge about this region by providing information on deforestation and forest degradation estimates (Duveiller et al., 2008; Mane et al., 2010; Ernst et al., 2013; Mayaux et al., 2013), above-ground biomass estimates (Baccini et al., 2008; Gourlet-Fleury et al., 2011; Baccini et al., 2012; Mitchard et al., 2012; Lewis et al., 2013; Kearsley et al., 2013), carbon balance (Lewis et al., 2009; Friedlingstein et al., 2010; Ciais et al., 2011; Fisher et al., 2013; Valentini et al., 2014), forest management and conservation (Gourlet-Fleury et al., 2013), functional leaf trait diversity (Verbeeck et al., 2014), and maps of vegetation types based on commercial forest inventories (Fayolle et al., 2014) or on satellite images (Mayaux et al., 1999; Mayaux et al., 2004; Vancutsem et al., 2009; Verhegghen et al., 2012; Mayaux et al., 2013; Gond et al., 2013; Viennois et al., 2013).

Among these researches, very few long-term studies on the dynamics of leaf phenology (development and shedding of leaves) have been carried out in the region although seasonal patterns of phenological activity are common in African tropical rainforests and play a role in gas exchange. Most of the field studies on phenology in the Congo basin, mainly on fruit phenology, were completed till the 1990s but are then rather scarce maybe because of political instabilities preventing long-term field measurements. In addition, the infrastructure to support scientific research is much more limited than countries of the Amazon basin or Southeast Asia (Baccini et al., 2008). Given this scarcity of observation sites and the absence of fluxtower for land-atmosphere $CO_2$ exchange, the uncertainties of the African carbon cycle remain high, especially for the Democratic Republic of Congo (DRC) (Baccini et al., 2008; Weber et al., 2009; Lewis et al., 2009; Verbeeck et al., 2011a; Ciais et al., 2011). Investment in better understanding carbon cycling in the region should be a high priority (Pan et al., 2011).

The leaf phenology characterization for rainforest trees is notoriously difficult, but is however of major importance for forest typology as well as to improve the understanding of Earth–atmosphere–climate interactions and biogeochemical cycles (Viennois et al., 2013). Indeed, a better understanding of the annual dynamic of photosynthetic activity, its spatial variability and its link with climatic conditions would help in anticipating the response of vegetation formations to future environmental changes (Couralet et al., 2013; Gond et al., 2013). For example, a change in phenology could modify the biosphere-atmosphere exchange of $CO_2$, water vapour and energy. As a feed back, altered functionalities of tropical forests could, in turn, affect a range of biogeochemical processes in the region with cascading effects on the climate system (Koltunov et al., 2009). Atmospheric $CO_2$ fertilization may also stimulate the gross primary production (GPP, photosynthesis) across the tropical forest biome (Friedlingstein et al., 2010; Ciais et al., 2011; Valentini et al., 2014), causing a change in the trees phenology.

In response to the very scarce phenological field data in Central Africa, optical satellite remotely sensed imagery offers capabilities of observing foliage phenology over large areas with high temporal resolution. Linking this satellite information with leaf cycle is essential to assess tropical forest ecosystem functioning but remains a challenge due to frequent cloud cover reducing the data availability and periodic high aerosols concentration related to biomass burning. In the Amazon region, satellite

optical data has shown unexpected seasonal cycles with an increase of the Enhanced Vegetation Index (EVI) during the dry season, interpreted as a higher photosynthetic activity when rainfall is minimal and solar radiation is maximal (Xiao et al., 2005; Huete et al., 2006; Xiao et al., 2006; Poulter and Cramer, 2009; Pennec et al., 2011; Samanta et al., 2012; Wagner et al., 2013; Biudes et al., 2015). It suggests that light could be the most important driving factor of rainforests phenology, despite a large debate on the impact of Bidirectional Reflectance Distribution Function (BRDF) effects on the signal received by the sensor (Galvão et al., 2011, 2013; Moura et al., 2012; Morton et al., 2014, Maeda et al., 2014). The EVI increase could correspond to drought-tolerant species, with adaptive deep root system to reach water far below the surface (Nepstad et al., 1994; da Rocha et al., 2004; Ichii et al., 2007; Poulter et al., 2009; Verbeeck et al., 2011b). These tend to produce new leaves in response to increasing solar radiation to optimize access to light or as an effective widespread strategy to avoid insect herbivores which have lower abundance during the dry season (van Schaik et al., 1993; Coley and Barone, 1996; Huete et al., 2006; Caldararu et al., 2012; Restrepo-Coupe et al., 2013; Albert et al., 2014; Nelson et al., 2014).

Comparatively to other parts of the world, very few studies explored the phenological characterization of tropical forests in the Congo basin using remote sensing data. Combining high spatial resolution images to estimate the proportion of leaved trees in the canopy with continuous moderate resolution time series (MODIS), Viennois et al. (2013) provide a quantitative interpretation of the EVI variations in terms of canopy deciduousness at the regional level during the dry season. They showed that in West-Central African forests, a large share of the variability in canopy reflectance, as captured by the EVI, is due to variations in the proportion of leaved trees in the upper canopy. They distinguished and mapped several dense-forest types based on this quantitative phenological proxy. Also using MODIS EVI, Gond et al. (2013) describe a very detailed map of vegetation types according to their phenological pattern. The EVI profiles of all forest classes showed two peaks corresponding to the two rainy seasons. Indeed, compared to the Amazon basin presenting a rather homogeneous rainfall regime, seasons are more complex in the Congo basin as the movement of the Intertropical Convergence Zone (ITCZ) and the Inter-Oceanic Confluence (IOC) generates two wet and two dry seasons annually over a large part of Central Africa (Lewis et al., 2013). This double periodicity of wet and dry seasons is a particularity of the Congo basin that complicates the

phenological vegetation response to climate. Both studies provide very interesting information but cover only the Northwest part of the basin overlapping borders between Cameroon, Gabon, Republic of Congo and Central African Republic (CAR).

In this study, the vegetation phenology over the whole central African rainforest is explored thanks to 11 years of SPOT-VEGETATION images in the perspective of documentary on the intra-annual dynamics of the carbon sequestering capacity in this region. Two main research questions are: how much vary the vegetation dynamics over the basin, and what are the main drivers of this seasonality and its spatial diversity? The objectives of this study involve the following: (i) investigating at site level the potential perturbation on the intra-annual variability of individual reflectances and vegetation indices by seasonality of aerosols, clouds and directional effects; (ii) linking the EVI variations with ground observations of phenology and light availability to question a phenological mechanism for the seasonal greening of Earth observations; and (iii) mapping and exploring the spatial extent of EVI dynamics for the whole Congo basin.

## 2. Data description

The main dataset selected here to track the tropical forest phenology is a long time series of daily multispectral SPOT-VEGETATION surface reflectance measurements (S1). These S1 images, recorded from January 2000 to December 2010 at a spatial resolution of 1 km, are daily synthesis of land surface reflectance well calibrated and atmospherically corrected. Thanks to the instrument swath of 2250 km, almost a global coverage is acquired every day in four spectral bands (Table 8). These were selected to characterize the main features of plant canopy. Moreover, the VEGETATION instrument presents the advantage of a data acquisition system equipped with a linear charge-coupled device array technology (push-broom sensor) which produces high-quality images with a greatly reduced distortion, unlike other medium resolution scanner sensors such as MODIS. The reflectance measurements from one date to another are indeed more comparable, at the pixel level, over many years. The exposition length is higher for the same satellite velocity, implying an improved signal to noise

ratio and a more consistent pixel footprint. Daily images include the blue, red, near-infrared (NIR), and shortwave infrared (SWIR) spectral bands and information about the pixel quality. They also contain the view and solar zenith angles (VZA and SZA respectively) and view and solar azimuth angles (VAA and SAA respectively) which will be useful to investigate BRDF effects on reflectance values. Last but not least, a specific VEGETATION cloud screening strategy significantly improves the cloud and cloud shadow mask, in particular in equatorial regions.

In order to document the potential atmospheric contamination of reflectance values caused by biomass burning in the Amazon, the Aerosol Optical Thickness (AOT) at 550 nm from the Level 3 MODIS Gridded Atmospheric Product (MOD08_E3 Collection 5) is used in this study. AOT is a dimensionless measure of how aerosol particles (dust, cloud droplet, biomass smoke, desert dust etc.) distributed from the Earth's surface to the top of the atmosphere prevent the light transmission, primarily due to scattering and absorption. The data are collected globally from January 2000 to December 2010 at 1°x1° spatial resolution and on 8-day temporal interval.

Table 8 : Spectral channel characteristics of the VEGETATION sensor.

| **Channel** | **Wavelength Interval (µm)** | **Potential Applications** |
|---|---|---|
| B0 (Blue) | 0.43-0.47 | Atmospheric state |
| B2 (Red) | 0.61-0.68 | Absorption peak of chlorophyll |
| B3 (Near-Infrared, NIR) | 0.78-0.89 | Maximum vegetation spectral reflectance |
| SWIR (Shortwave-infrared) | 1.58-1.75 | Reflectance related to the water content of canopy components |

# 3. Methodology

First, two local studies explore the seasonal behaviour of reflectance patterns and assess the potential atmospheric contamination due to aerosols. Then, time series of vegetation indices are computed and analysed, notably concerning directional effects. For the Amazon basin, the EVI showed an increase, or green-up, during the dry season suggested to be caused by leaf

flushing itself driven by availability of solar radiation to maximize photosynthetic carbon uptake when cloudiness is at minimum. This phenomenon is analysed by comparing the EVI patterns, in terms of photosynthetic behaviour, with meteorological information and phenological field studies. Then, four other sites are taken into account to illustrate the spatial variation of phenological patterns over the basin. Finally, the seasonal study of central African rainforest is extended at the basin scale.

## 3.1. Climate patterns of the Congo basin

As already mentioned, the Congo basin presents a more complex cycle of seasons compared to the Amazon basin. In this region, seasons are determined by the displacement of two discontinuity surfaces which separate hot and dry continental air masses from cooler and more humid maritime ones: the ITCZ, formed by the convergence of sahelian and equatorial oceanic air masses, and the IOC which separates air coming from the Southern Atlantic from that of the Indian Ocean (Koffi et al., 1995). Southern and Northern extreme positions of these frontiers occur in January and July months, which correspond respectively to the peak of the dry season in Northern and Southern hemispheres. The duration of the dry season varies with the distance to the equator in both hemispheres and also along an east-to-west gradient (Asefi-Najafabady and Saatchi, 2013).

Areas close to the equator have bimodal rainfall regimes while Southern and Northern regions tend to a unimodal regime (See rainfall climatologies from the Tropical Rainfall Measuring Mission (TRMM), Figure 52). Unlike Amazonia, the rainforests of Central Africa exist under significant drier conditions, with an average precipitation of 1500-2000 mm $y^{-1}$ in the central Congo basin (Asefi-Najafabady and Saatchi, 2013). There are large variations in annual average precipitations, ranging from up to 10000 mm for coastal region of Cameroun to about 1000 mm in the Southwest of the basin (Mpounza and Samba-Kimbata, 1990).

## 3.2. Sites description

A first analysis focuses on two sites geographically opposed located in DRC, Yangambi and Luki. Both sites are widely studied and very well documented. According to the vegetation types map of Verhegghen et al.

(2012), they belong to the "Dense moist forest" (Figure 42), even if they are both closed to rural complex and young secondary forests. The dense moist forest class is the most represented vegetation type in Central Africa, mainly situated in central region (Verhegghen et al., 2012). These forests are known as the Lower Guineo-Congolian forests as defined by White (1983).

The first site is located in Yangambi, in North of the Congo River near Kisangani. Straddling the equator, the Yangambi region has a tropical rainforest climate (Af type from the revised Köppen classification (Peel et al., 2007)). This zone is characterized by an annual average temperature of 25°C and high precipitation throughout the year from 1500 mm to 2000 mm with a bimodal rainfall regime (Tshibangu, 2010). Two rainfall maxima occur in April-May and in September-October (Mpounza and Samba-Kimbata, 1990). Similarly, there are two dry seasons. The first one in December-February is drier than the second one in June-August (Mpounza and Samba-Kimbata, 1990). Several vegetation types are observed in the region, from primary (*Gilbertiodendron dewevrei sp.*), secondary and edaphic forests to fallow land and cropland (Tshibangu, 2010; Verbeeck et al., 2014). The average aboveground carbon stock is estimated to 162 +- 20 Mg C $ha^{-1}$ for intact old-growth forest in Yangambi (Kearsley et al., 2013).

The second site is located in the Luki Forest Reserve, in South-West of the country near Matadi. It is the southernmost remnant of the highly diverse Mayombe forest (Couralet et al., 2013). This region has a tropical savannah climate (Aw type from the revised Köppen classification (Peel et al., 2007)). While the average annual temperature of 24.6 °C is similar to in Yangambi, the mean annual rainfall is much lower with 1180 mm $y^{-1}$. This site located in Southwest region is chosen because rainfall and radiation don't present a double periodicity as in most of the Congo basin. It is thus interesting to analyze the seasonal variation of the reflectance observed in this region compared to other sites. Indeed, precipitations last 8 months from October to May (Schwartz and Tondo, 1988) and the major dry period lasts from June till September (Couralet et al., 2010). Solar radiation is very low, especially during the dry season (Schwartz and Tondo, 1988). The semi-evergreen forest of Luki is surrounded by a mosaic landscape with patches of rural complex and young secondary forest (Verhegghen et al., 2012). It consists of a mixture of deciduous and evergreen tree species in the upper-stratum and mostly evergreen species in the understory (Couralet et al., 2010).

Table 9 : Coordinates of sites selected to study the seasonality of tropical rainforests in Congo basin.

| **Site – Land cover** | **Coordinates** |
|---|---|
| Yangambi – Dense moist forest | 0°46'55.52"N, 24°27'48.46"E |
| Luki – Dense moist forest | 5°35'13.12"S, 13°08'38.76"E |
| Minkebe – Dense moist forest | 1°35’9.6"N, 12°26’49.2"E |
| Bonkondo – Dense moist forest | 0°2’39.71"S, 21°8’34.07"E |
| Imbo – Dense moist forest | 2°21’6.55"S, 21°30’54.92"E |
| Lusamba – Dense moist forest | 4°30’05.35"S, 23°21’41.64"E |

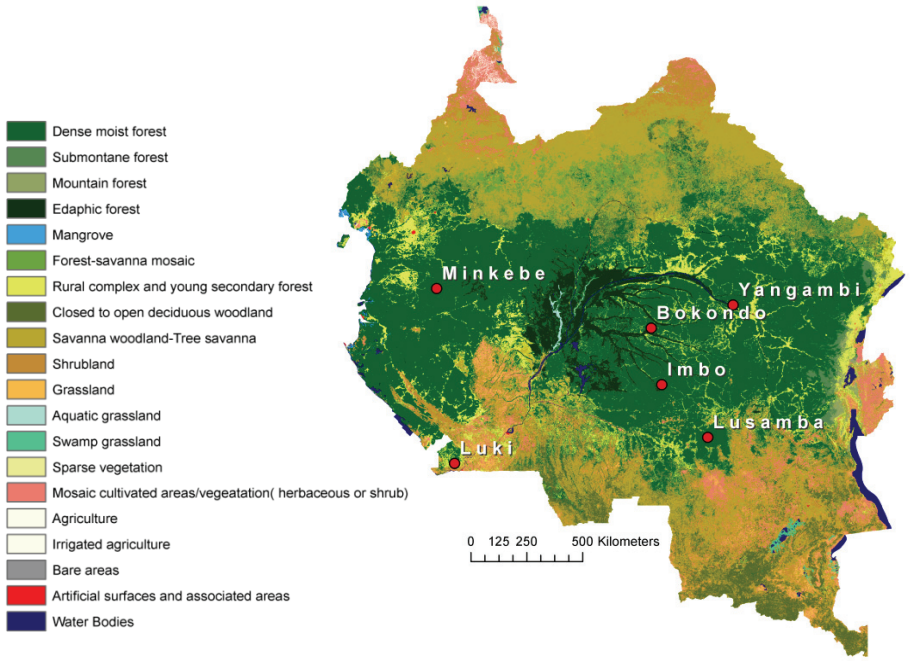


Figure 42 : Location of the six sites superimposed on the Congo basin Vegetation Types Map (Verhegghen et al., 2012).

Emphasis is given on Yangambi and Luki sites, but four other sites are also considered to document the spatial variability of phenological patterns over the basin (Figure 42). Two sites has a tropical rainforest climate (Af) (Bonkondo and Imbo), and two sites has a tropical savannah climate (Aw) (Minkebe and Lusamba). No site is selected in the most

Western part of the basin due to almost permanent cloud cover, neither in the most Eastern part to avoid altitudinal and topographic effects related to mountains.

## 3.3. Spectral bands analysis

SPOT-VEGETATION time series is compiled and multi-spectral reflectance dynamics are inspected for the Yangambi and Luki sites with regards to perturbing factors such as clouds and aerosols.

The frequent cloud cover in a moist tropical region and its strong variability between the wet and dry seasons may introduce seasonal perturbations in optical remote sensing. Compositing the VEGETATION-S1 reflectance products on a 10-day interval using the Mean Compositing (MC) method (Vancutsem et al., 2007) reduces significantly the cloud impact. This method averages valid atmospherically-corrected and cloud-free reflectance values based on enhanced cloud screening. All the quality-controlled reflectance values are averaged over each pixel and within each band. In order to document the quality of the composite, the number of valid observation available and used in the mean estimation is associated to each pixel of a composite. In order to further reduce the noise in the time series, outliers were removed using fixed thresholds selecting observations with low red and blue reflectance (< 0.25) and NIR reflectance typical of vegetated surfaces (0.15 – 0.7).

The VEGETATION 10-day composites are compiled in temporal profiles of reflectance in the blue, red and NIR bands from 2000 to 2010. The reflectance values extracted, centered on the Yangambi and Luki coordinates, are averaged within a 5x5 km² window by calculating the mean value at each time point. To characterize the average seasonal behaviour, a mean annual profile, also named a "climatological year", is compiled by averaging for each decade over the 11-year time series the reflectance value for each band. The standard deviation of each spectral reflectance is also calculated over the whole time series for each decade of the year.

These "climatological" multispectral profiles are compared with external factors which could corrupt the signal received by the sensor. Intra-annual variability is analyzed with regards to AOT seasonal cycle in order to depict the impact of dry season fire-induced aerosols on the reflectance values.

## 3.4. Vegetation indices analysis

Two vegetation indices are computed from individual spectral bands to characterize the vegetation phenology for the Luki and Yangambi sites. These are the Normalized Difference Vegetation Index (NDVI) (Tucker, 1979) and the Enhanced Vegetation Index (EVI) (Huete et al., 2002) defined as:

$$NDVI = \frac{\rho_{NIR} - \rho_R}{\rho_{NIR} + \rho_R} \quad (1)$$

$$EVI = 2.5 \frac{\rho_{NIR} - \rho_R}{\rho_{NIR} + C_1 \rho_R - C_2 \rho_B + L} \quad (2)$$

where $\rho_{NIR,R,B}$ are surface reflectances in near-infrared (NIR), red (R) and blue (B) bands, respectively; $C_1$ and $C_2$ are the aerosol resistance weights designed to correct for aerosol scattering and absorption; L is the canopy background adjustment factor for correcting nonlinear, differential NIR and red radiative transfer through a canopy. The coefficients of the EVI equation are $C_1 = 6$; $C_2 = 7.5$ and $L = 1$ (Huete et al., 2002).

NDVI remains very popular and widely used in spite of its limitations especially in tropical rainforest regions. Indeed, the dense vegetation with leaf area index (LAI) of 3-4 induces saturation due to high chlorophyll content, and atmospheric aerosols cause artefacts in NDVI variation throughout the year (Huete et al., 2002; Xiao et al., 2003, Kobayashi et al., 2005). The EVI was developed to minimize these effects. First, it enhances the vegetation signal with improved sensitivity to high green biomass level. Second, it improves vegetation monitoring through a reduction in atmosphere influences by using the additional blue band available on advanced optical sensors (VEGETATION, MODIS). The EVI directly adjusts the reflectance in the red band as a function of the reflectance in the more atmospheric-sensitive blue band to correct the red band for aerosol influences (Huete et al., 2002). This is an important feature for the study in the Congo basin strongly prone to fire that releases aerosols from biomass burning. Precisely, Huete et al. (2002) showed that EVI performs well in the heavy aerosol, biomass burning conditions in Brazil. Both indices are matched to individual spectral bands to track the source of

their variation. Given the comparison results, only the EVI is further used in the analysis.

Seasonal change in greenness is assessed by the EVI at three different scales. First, the annual mean profile of EVI is computed the same way than the reflectance profile. Its intra-annual variation is compared to SZA and φ distribution over the entire year in order to explore how illumination effects (SZA variation) and the relative position of the sun and the sensor (φ) influence the seasonal pattern of EVI. Even if BRDF effects are difficult to separate from temporal effects like plant phenology (de Wasseige et al., 2002), it is of crucial importance to try to assess the potential impact of observation geometry cycle on intra-annual variability of vegetation indices. Second, the four additional sites are studied to provide some insight into the diversity of phenological patterns from North to South and from West to East. Third, the time series analysis is extended to the whole rainforest in order to map the spatial variability and consistency of EVI seasonal dynamics. As for the sites, a "climatological" year is computed on a monthly basis. First, EVI 30-day composites are computed from the individual spectral bands. Then, each month composite is averaged pixel by pixel from the 11 corresponding EVI 30-day composites from 2000 to 2010.

### *3.5. In situ measurements analysis*

Based on the time series analysis, relationships between remotely sensed EVI dynamics and *in situ* measurements are discussed. To date, no estimate of gross primary productivity (GPP) has been reported for African tropical forests (Valentini et al., 2014). Comparisons of *in situ* measurements with EVI dynamics are thus realized from literature data about the climate, leaf and litterfall phenology observations.

## 4. Results

### *4.1. Reflectance time series analysis*

Exploring the respective contribution of atmosphere and land radiance, both being inherently coupled along the year throughout the different seasons, is a

prerequisite for a reliable interpretation of the phenological information contained in multi-year time-series.

Annual mean profiles in the blue, red, and NIR bands compiled from the SPOT- VEGETATION 10-day composites for the Yangambi and Luki sites are shown along with the number of valid observation for each decade composite in Figure 43. In order to better visualize the seasonal cycle over these yearly profiles, half-year periods are repeated at the beginning and at the end of the year (delimited by vertical lines). The typical dry season periods are indicated by the shaded areas.

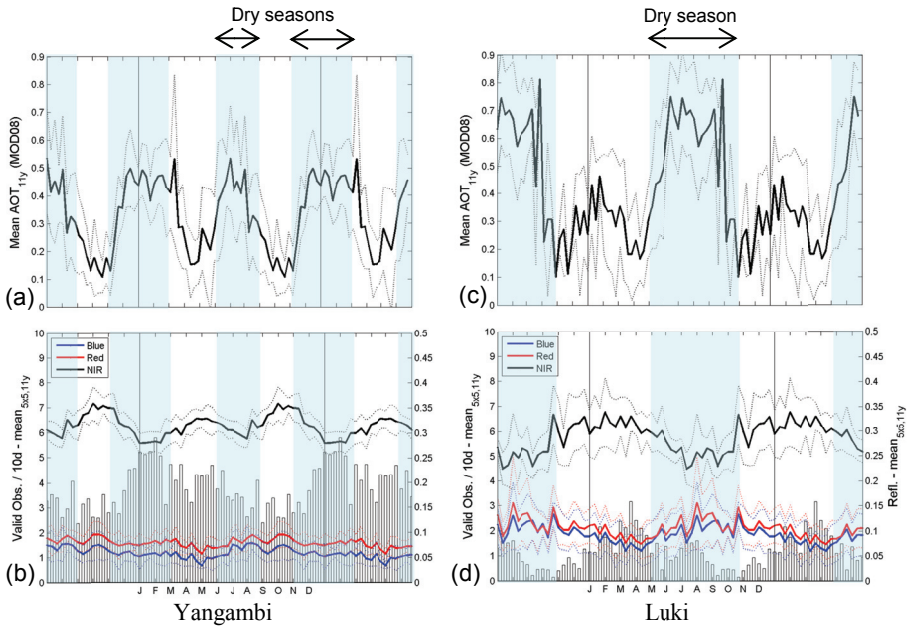


Figure 43 : Annual mean profiles of AOT (1°x1° window, 8-day period) (a,c), of reflectances in blue (dark blue line), red (red line), NIR (black line) bands, and number of valid observation by decade (bars) from SPOT-VGT time series 10-d composites (2000-2010) for a 5x5 pixels window centered at Yangambi and Luki site (b,d). Inter-annual variability corresponding to one standard deviation is represented by dotted lines. Half-year periods are repeated at the beginning and the end of the year (delimited by vertical lines). Shaded areas indicate the dry season.

A cycle is observed in the NIR band for Yangambi (Figure 43 (b)), presenting two distinct seasons per year, even if the amplitude does not exceed 0.1. The NIR reflectance increases from March until May and from

August until October, during the wet seasons, and decreases during the peaks of the dry seasons (November-January and June-July), contrasting with the dry season green-up in Amazon. AOT dynamics show also two distinct peaks, in July-August and in December-March. These periods of dense aerosols clearly correspond to the dry seasons. The blue and red bands do not seem to be strongly affected by this aerosols seasonal pattern in Yangambi. Indeed, reflectance in blue and red bands (Figure 43 (b)) only shows a very slight increase from May to August (little dry season).

In Luki, the inter-annual variability is higher, and profiles present more noise throughout the year (Figure 43 (d)). It is known that the cloud cover is more pronounced and persistent in the West of the basin as illustrated by the very low number of valid observation per decade (Figure 43 (d), bars). A seasonal cycle is nevertheless observed in the NIR band pattern, presenting only one large season per year. The NIR increase starts in November and reaches a peak in February. It occurs again during the wet season, contrarily to the dry season green-up in Amazon, and when the amount of AOT is at minimum (Figure 43 (c)). Reflectance in blue and red bands shows here a pronounced increase corresponding to the AOT dynamics. Indeed, these reflectance values increase from May to September, precisely the period presenting the higher amount of aerosols. In fact, aerosols scatter sunlight directly to the optical sensor and thus increase the apparent reflectance in the red and blue bands (Karnieli et al., 2001; Xiao et al., 2003). The seasonal cycle of AOT appears to be the cause of the red and blue bands variations, because of an atmospheric contamination due to aerosols from biomass burning. However, it is not obvious to separate the contribution of atmospheric contamination and the one related to photosynthetic activity. Indeed, the NIR reflectance strongly decreases as the red values increase which is typical of a reduction in photosynthesis activity, unlike the phenomenon in the Amazon basin where an increase in both NIR and red bands was surprising at first sight.

The monthly aerosols dynamics over the whole Congo basin are presented in Figure 44, extracted from the MODIS Gridded Atmospheric Product, to document the seasonality of the atmospheric contamination on reflectance values caused by seasonal burning and associated smoke. In Africa, 75% of the savannahs burn annually (Koffi et al., 1995). Fires represent a significant component of the African carbon cycle, in consuming $1.03 \pm 0.22$ Pg C $y^{-1}$ that has been sequestered by photosynthesis, which

contributes to 40% of global fire emissions, mostly from savannahs and dry woodland burning (Ciais et al., 2011; Valentini et al., 2014). Nevertheless, a large portion of the wild fire emissions are compensated by $CO_2$ uptake during the growing season (Valentini et al., 2014). In dense humid forests, the presence of fire is usually associated with forest clearing, while savannah vegetation is resilient to fires, thanks to well-adapted species. Fire activity is indeed strongly attenuated by the very wet and densely vegetated Guineo-Congolian zone (Koffi et al., 1995).

The aerosol loading comes directly from this dry vegetation burning which starts with the onset of the typical dry seasons, on average from November to March in the Northern Hemisphere and from June to October in the Southern Hemisphere (Figure 44). This inversion is typical of Central Africa which experiences an inversion of seasonality between the Northern and Southern part of the equator (White, 1983). The overwhelming regional influence of savanna fires on the troposphere has been assessed thanks to airborne aerosol samples by Ruellan et al. (1999). The flights started from Bangui and took place between 1030 and 1300 local time (UT + 1), south of the ITCZ. Their analysis of the chemical composition of the tropical atmosphere over Central Africa shows that biomass burning aerosols emitted at northern latitudes are transported in Harmattan flux, whereas those found in the boundary layer originated mostly from more local burns. Pyrogenic particles were abundant in all atmospheric layers, and high levels of black carbon concentrations were found from the forest boundary layer ($3.8 \pm 2.3$ $\mu g\ m^{-3}$) to the Harmattan layer ($8.7 \pm 1.6$ $\mu g\ m^{-3}$ from 3000m of altitude).

The fires lead the atmosphere of Central Africa to be contaminated throughout the year by fire emissions (Koffi et al., 1995). Indeed, contrarily to the Amazon basin, showing a very low amount of aerosols during eight months of the year and a sudden increase in the South of the basin from August to November coinciding with the dry season, the Congo basin as a whole presents a low amount of aerosol during only 4 months. Even if the timing of rainfall and rates of vegetation senescence define the predisposing conditions for fires, the proportion of early fires decreases and late fires become more prevalent when no human settlements are present (Bucini and Lambin, 2002).

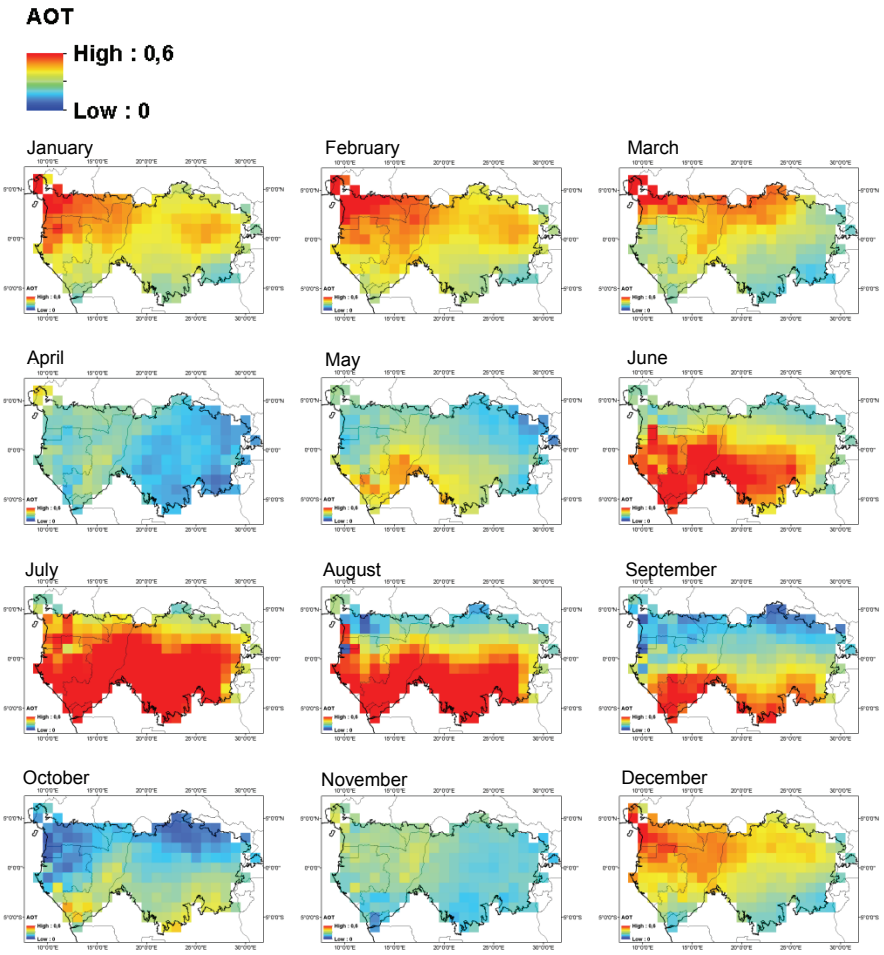


Figure 44 : Aerosols Optical Thickness 550 nm dynamics from the L-3 MODIS Gridded Atmospheric Product (MOD08_E3) at 1°x1° spatial resolution for the Congo basin, using data from January 2000 to December 2009. The average is computed on a monthly basis from the corresponding 8-day values.

## *4.2. EVI and NDVI seasonal dynamics*

Climatologies of EVI and NDVI were computed from the respective spectral bands averaging decade by decade the 11-year SPOT-VEGETATION time series (Figure 45). Contrarily to the Amazon basin, the seasonal patterns of both indices are rather similar. However, the EVI profile is less noisy than the NDVI profile which also presents a large inter-annual variability.

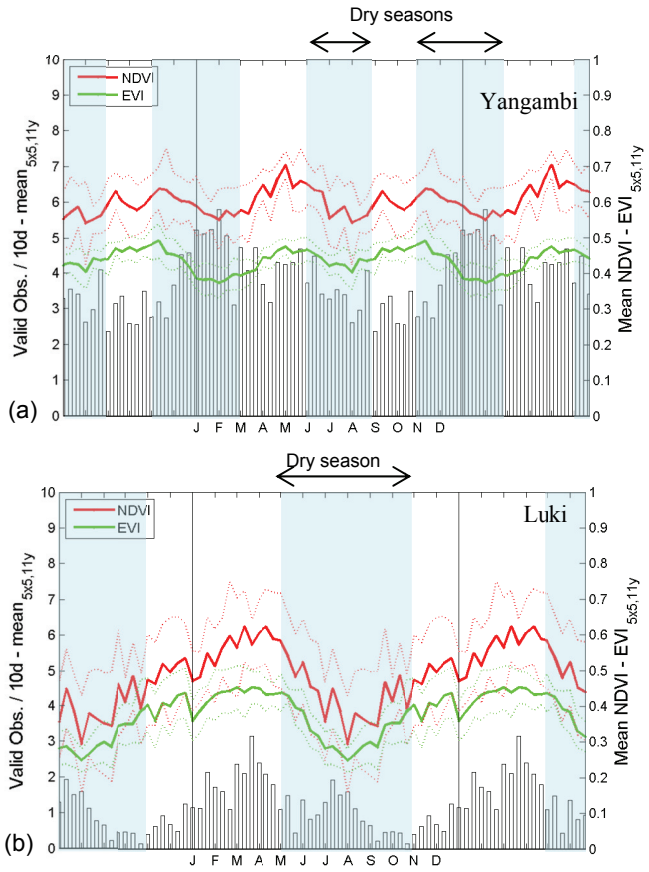


Figure 45 : Annual mean profiles of NDVI (red line) and EVI (green line), and number of valid observations by decade (bars) for a 5x5 pixels window centered at Yangambi (a) and Luki (b) sites from SPOT-VGT time series 10-d composites (2000-2010). Inter-annual variability corresponding to one standard deviation is represented by dotted lines. Half-year periods are repeated at the beginning and the end of the year (delimited by vertical lines).

The scatterplots in Figure 46 and Figure 47 show the correlation between vegetation indices and the reflectances. The NDVI (Figure 46) is strongly negatively correlated with the red band ($r^2$ = 0.69 and 0.65 for Yangambi and Luki sites respectively), but not with the NIR band ($r^2$ = 0.02 and 0.01 for Yangambi and Luki respectively). The EVI shows the opposite, with a strong positive correlation with the NIR ($r^2$ = 0.57 and 0.49 for Yangambi and Luki respectively). In dense canopies such as tropical forests, the NDVI is relatively insensitive to NIR reflectance change as these are an order of magnitude higher than the red reflectance (Samanta et al., 2012). By

relying on NIR canopy reflectance, the EVI is a good alternative to NDVI to study the seasonal variations of vegetation in this region as it remains effective to canopy variations even for areas of high biomass and chlorophyll content and it is less sensitive to atmospheric contaminations (Huete et al., 2002).

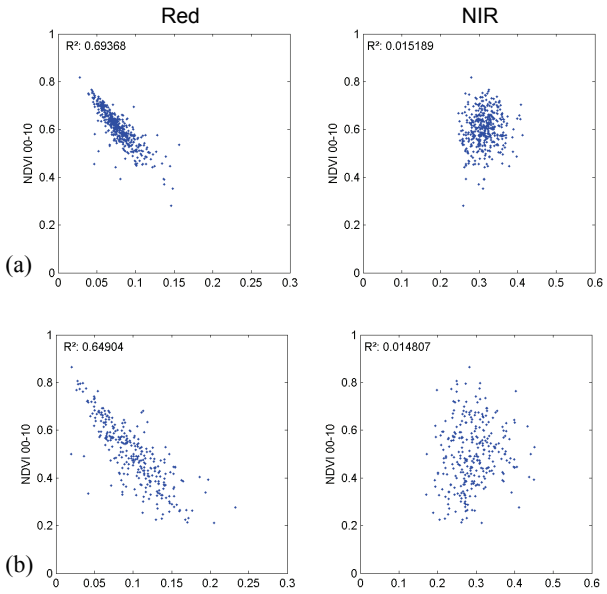


Figure 46 : Scatter plots between the NDVI and reflectances, from SPOT-VGT time series 10-d composites (2000-2009), at the location of Yangambi (a) and Luki (b) sites, 5x5 km² window (spatial average values).

Seasonal cycles clearly appear on the 11-year annual mean EVI profiles for both sites, but with very distinct timing. Indeed, EVI patterns of Yangambi (Figure 45 (a)) and of Luki (Figure 45 (b)) present totally different vegetation dynamics with regards to the number of season, the period of the year with highest values and the amplitude of the cycle. The EVI pattern of the Yangambi site, located in the center of the basin, shows two distinct seasons per year, with increases from March until May and from August until November corresponding to the two wet seasons. Inversely, the index values decrease during both drier seasons, especially during the long dry season from November to February. Minimum EVI values are found in January, concurring with the minimum of rainfall. In the South at Luki site, the profile of EVI reveals only one and large season but the highest values of

EVI correspond also to the wet season. Values increase from September until December, corresponding with the early wet season, and remain at a plateau from December until the end of April (late wet season). The lowest values of EVI are found in July, peak of the dry season. The amplitude is closed to 0.3 which is more than the double compared to Yangambi.

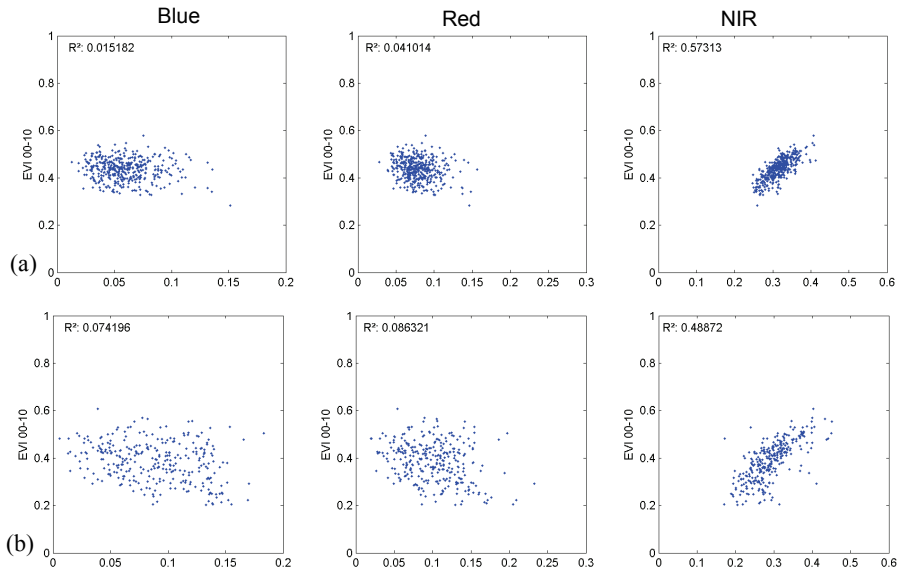


Figure 47 : Scatter plots between the EVI and reflectances, from SPOT-VGT time series 10-d composites (2000-2009), at the location of Yangambi (a) and Luki (b) sites, 5x5 km² window (spatial average values).

These important differences between both sites indicate the need to extend the analysis to the entire basin which probably presents a strong gradient of EVI seasonal cycle. However, the similar behaviour of the EVI cycle compared to the wet and dry seasons for both sites seems to document the phenological adaptation of vegetation to climate. Our results coincide with those of Viennois et al. (2013) and Gond et al. (2013) who found that mean dry-season EVI values were always lower than mean wet-season values for all forest types in Northwest of the Congo basin, at the borders between the Republic of Congo, Gabon and Cameroon. In addition, Viennois et al. (2013) highlighted a good correlation between the proportion of leaved trees in the canopy estimated from SPOT-5 dry-season images and mean EVI values averaged over a single dry season (MODIS). According to them, it provides strong evidence that a large share of the variability in canopy

reflectance summarized in the EVI at stand level (250-m) in the mixed forests of West-Central Africa is due to variation in the proportion of leaved trees in the upper canopy. This is discussed in the next section in the light of ground and meteorological measurements.

Figure 48 (a) and (b) below shows EVI, solar zenith angle (SZA) and relative azimuth angle (φ, difference between the solar azimuth angle (SAA) and the view azimuth angle (VAA)) intra-annual evolution based on the 11-y SPOT-VEGETATION time series for Luki and Yangambi sites in the Congo basin. In the Amazon basin, the EVI variation is interpreted in several studies as the consequence of bidirectional effects. Some are arguing for solar illuminations effects, suggesting that the decrease of the SZA during the dry season causes a reduction in shade fraction, a predominance of sunlit canopy components visible for the sensor, and thus the increase of EVI (Galvão et al., 2011; Moura et al., 2012; Galvão et al., 2013). Others claim that EVI variation observed in Amazon forests with optical remote sensing data is an artefact related to variations in sun-sensor geometry, arguing that the decrease of φ during the dry season until the sensor reaches the principal plane in October (φ = 0° - 180°, sensor and sun are aligned) is the reason of an apparent green-up, as reflectance values acquired in the hot spot of the principal plane are higher (Morton et al., 2014). In summary, they all claim that EVI seasonal change is not caused by biophysical change in leaf reflectance, leaf area or vegetation productivity driven by radiation, but instead by a combination of shadowing effect within the canopy and the sun-sensor geometry observing the forest during the dry season. To them, the Amazon forests maintain a constant greenness throughout the dry season. However, Maeda et al. (2014) showed more recently that, even if the annual EVI seasonality is partly explained by sun-sensor geometry variation, it remains an evident MODIS EVI seasonal pattern over the Amazon after removing atmospheric contamination and accounting for sun-sensor geometry effects.

Concerning the relation between φ and EVI values extracted from SPOT-VEGETATION time series, it is clearly observed in Figure 48 (a) and (b) that the moment when the sensor reaches the principal plane in October (φ = 0° - 180°, sensor and sun are aligned) does not correspond to the highest values of EVI. Also, there is no evident negative correlation between EVI and SZA throughout the year ($r^2 = 0.08$ for Yangambi and $r^2 = 0.01$ for Luki, using daily data). For example, SZA values in Luki increase from

October until January while EVI values also increase. A study based on six SPOT–HRVIR images (20m resolution) with varying sun-sensor geometry further supports this hypothesis, as they found no correlation between the NIR reflectance and the SZA in the Ngotto forest, located in North of the Congo basin (de Wasseige et al., 2002).

We suggest that correlations between EVI and angles patterns are not evidence of direct cause-effect. Instead, the EVI dynamics could be related to actual vegetation phenology following the green-up hypothesis. This is discussed in the next section in the light of ground and meteorological measurements.

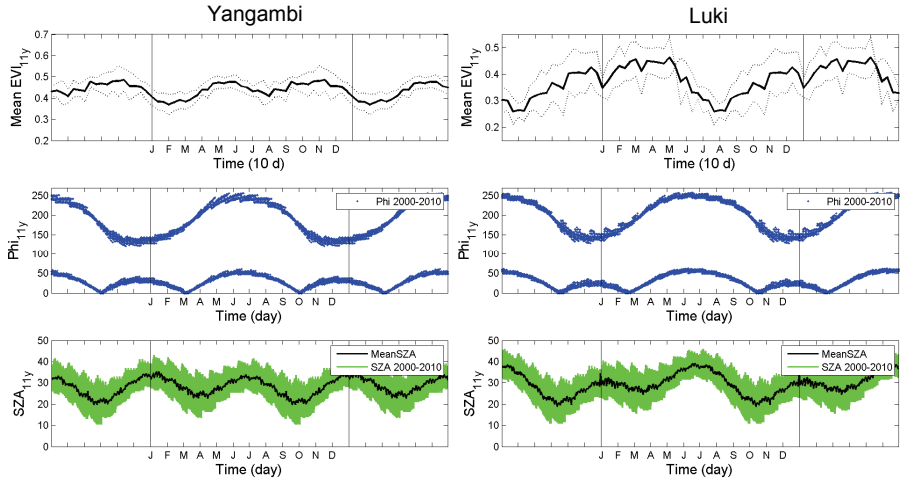


Figure 48 : Annual mean profiles of EVI 10-d composites (black line) and inter-annual variability (dotted line), relative azimuth angle (blue dots) and solar zenith angle (green dots, mean = black line) from SPOT- VEGETATION time series (2000-2010), 1x1 km² window, for Yangambi and Luki sites. Inter-annual variability corresponding to one standard deviation is represented by dotted lines. Half-year periods are repeated at the beginning and the end of the year (delimited by vertical lines). The EVI patterns are not exactly the same than in Figure 45 because it is computed on a 1x1 pixel window basis, instead of 5x5, for the sake of SZA extraction.

## *4.3. In situ data*

### 4.3.1. Sun radiation as driver

In the Congo basin, the EVI dynamics and rainfall seasonality shows unexpected results compared to the Amazon basin. In this more documented region, the EVI increase is observed during the dry season in phase with higher incoming light periods, interpreted as a leaf flush to maximize photosynthetic assimilation when rainfall is minimal and solar radiation is maximal (Xiao et al., 2005; Huete et al., 2006; Xiao et al., 2006; Poulter and Cramer, 2009; Pennec et al., 2011; Samanta et al., 2012; Wagner et al., 2013; Biudes et al., 2015). However, in the Congo basin, EVI peaks inversely during the wet seasons and lowest values are found during the dry seasons (Figure 45 (a) and (b)), which contrasts with findings from the Amazon basin.

Actually, air temperature and solar irradiance are positively correlated with rainfall over West-Central Africa (Couralet et al., 2013) unlike to what is usually observed in monsoonal climates (Malhi et al. 2002). During the driest months in Luki, from May to October, the cold Benguela stream in the Gulf of Guinea creates a thick, low-level but non-precipitating cloud layer dominates, blocking solar irradiance and causing temperature drop (Couralet, 2011; Couralet et al., 2013). Inversely, in the wet season, heavy rainfall is often preceded by several hours of very intense sunlight (Anderson et al., 2005) which leads to higher incoming light level than in the dry season. In Yangambi, higher radiation also coincides with the wet season and occurs in this site with a double periodicity, in March and in October (Tshibangu, 2010).

To summarize, EVI peaks in both basins during periods of higher solar radiation. In the Amazon region, the incoming radiation is maximal during the dry season. In the Congo basin, higher radiation coincides with the wet seasons while the most nebulous months occur during the dry seasons. This corresponds to findings of Gond et al. (2013) who showed in Southeast Cameroon, Southern CAR, Northeast Gabon and Northern Republic of Congo that the EVI profiles of all vegetation types were nearly the mirror image of the seasonal patterns of rainfall and light availability, including for swamp forests that are not limited by water availability but react such as terra-firme forest. This suggests their strong dependence to

light intensity. Light could be the main climatic driver or limiting factor of tropical rainforest phenology and productivity in the Congo basin, exactly as in the Amazon basin (Xiao et al., 2006; Huete et al., 2006; Myneni et al., 2007; Hutyra et al., 2007; Bradley et al., 2011; Caldararu et al., 2012; Wagner et al., 2013; Biudes et al., 2013). Equatorial forests seem adapted to maximize photosynthetic activity when the cloudiness is minimal.

This explanation is also supported by a multi-model analysis on Africa's ecosystem productivity, showing that radiation limits GPP in some regions, especially in the inner tropics (Weber et al., 2009). According this study, it makes sense since frequent cloud cover is present in the tropics, which controls incoming radiation with otherwise favorable climatic conditions for productivity. As Central Africa has lower annual rainfall than Amazonia (see Figure 40 and Figure 52), it may be an adaptive mechanism to combine high EVI (high photosynthesis activity) with both high light intensity and high rainfall during wet seasons to avoid soil moisture stress (Gond et al., 2013).

### 4.3.2. Leaves studies

In the Amazon basin, field studies about spectral properties according to leaf age (Roberts et al., 1998) and phenological cycle, such as ground-measurements of leaf litterfall (Dantas and Phillipson, 1999; Goulden et al., 2004; Rice et al., 2004; Barlow et al., 2007; Malhado et al., 2009; Brando et al., 2010; Pennec et al., 2011; Wagner et al., 2013) and cameras tower-mounted RGB cameras (Nelson et al., 2014) showed that crown-scale leaf-flushing events are well concentrated in the dry period and fit the satellite-based EVI pattern.

In the Congo basin, phenological field studies are much scarcer than in the Amazon basin or Southeast Asia. However, a systematic review of the literature allows pointing out some interesting field-based studies notably about leaf litterfall. These studies are summaries in Table 10.Although it rarely has been quantified for African tropical forests (Cizungu et al., 2014), litterfall is a central component of the biogeochemical cycle, as it is the main path for the return of dead organic matter and nutrients from the above parts of the plant to the soil and humus formation in tropical forest systems. It also affects the availability of resources for herbivory and decomposers (van

Schaik et al., 1993). In humid tropical region, annual litterfall weight is generally from 10 to 12 t/ha (Dommergues, 1965).

According to Hladik (1978), three main types of phenological sequences with respect to leaf-fall occur in a rainforest. For trees that are called deciduous, the leaves fall during a fairly short period once each year and trees remain bare for a few days or more. For trees that are called evergreen, two types exist: for one leaf-fall comes in peaks with concomitant flushes of new leaves, and for the other leaf-fall is more or less continuous throughout the year. Studying functional leaf trait diversity in Congolese secondary tropical forest, Verbeeck et al. (2014) show that species with diverse strategies coexist in this ecosystem. For evergreen trees, leafing periods often correspond to rainy periods (Hladik, 1978). Beside the most common evergreen trees, the deciduous trees of a rain forest play a particular role in the food availability for folivores. At the forest stand level, different mixture of these phenological tree behaviors correspond to the range from semi-deciduous forest to evergreen forest.

Some studies reported a distinct seasonality of leaves shedding in the Congo basin, most of them showing greater rates during the dry season. In Yangambi, Laudelout and Meyer (1954) have collected litterfall reaching 12.4 to 15.3 t/ha with two maxima corresponding to the end of the two dry seasons. In a recent research, Couralet et al. (2013) took advantage of an old large-scale and long-term phenological survey conducted at the rainforest reserve of Luki. During 10 year, 3750 trees of more than 150 species were monitored on a 10-day basis for leaf fall, flowering, fruiting and dispersal of fruits. The time series of phenological events revealed annual periodicity of all these phenophases for all groups of species, although most clearly for the heliophilous species. In the three functional groups studied, leaf shedding started during the dry period (July–August) and was maximum at the transition between the dry and rainy seasons (September–October). However, in Dimonika reserve (Mayombe) in South of Congo, Schwartz and Tondo (1988) report an important litterfall during the wet season, probably because of the wind being weak in the dry season but strong in the wet season. In rainforests of Ivory Coast, the two wet seasons and the intermediate short dry season show a low rate of litterfall while a massive litter fall occurs mainly during the main dry season (November-May with a peak in December) (Bernhard, 1970) with 75-85% of leaves fall (Devineau, 1982). In Ipassa (Gabon), Hladik (1978) collected leaf-fall which reaches a

low point in June and July, during the major dry season, and was higher during the minor rainy season in March and April likely because of storms. However, with direct observations of leaf fall, they revealed a major leaf fall during the dry season for the emergent trees. For example, the *Ficus sp.* shed leaves from February until the beginning of March, at the end of the dry season until the early wet season. For another species, *Piptadeniastrum africanum* which is deciduous, leaves fall during a very short period followed immediately by several days of leaf flush, in January (dry season). Nevertheless, some other emergent trees were not deciduous and had regular leafing and leaf-fall periods all the year round. More recently, litterfall was also measured by Cizungu et al. (2014) in the Nyungwe pristine forest in Southwest Rwanda, which peaks in the major (July–August) and minor (December–January) dry seasons and at the onset of the rainy season (September– October).

In addition of litterfall collects, another source of phenological field data is LAI (total leaf area per unit of ground area) measurement. Using LAI-2000 instrument, de Wasseige and Defourny (2003) measured LAI at a scale matching a 1-km spatial resolution of satellite during 7 months in Ngotto in a semi-deciduous forest located in the Southwest part of the CAR. They found a seasonal change of LAI of 0.34 with forest foliage gradual decrease during the dry season. From March to May, the LAI increased when the measured rainfall was always above 100mm per month.

Some studies reported also leaf flushing observations. Flushes of numerous new leaves are obvious in the tropics because these leaves are very often bright or dark red or at least light green (Hladik, 1978). Comparing 53 phenology studies, van Schaik et al. (1993) found that in wet tropical forests, both community-wide leaf flushing and flowering peaks occur during the time of year with the most hours of sunshine. This is clearly confirmed in Yangambi. Indeed, while the litterfall occurs in February at the end of the dry season (Laudelout and Meyer, 1954), flowering and leaf flushing was observed in March when radiation reaches its maximum, precisely at the beginning of the wet season (Tshibangu et al., 2010). In Ipassa (Gabon), Hladik (1978) reported that for the more common medium-size tree species (*Panda oleosa*) new leaves appear before old leaves fall, in November-December during the dry season, and keep growing for some weeks during the rainy season. In West Africa, in the Taï National Park in the Ivory Coast, Anderson et al. (2005) examined during 47 months the flowering, fruiting, and new leaf phenology for 797 rain forest trees from 38

species to determine the phenology cycles in relation to seasonal rainfall, temperature and solar radiation. They found that leaf flushing peaked in the long dry season but continued into the wet season, occurring between February and June.

In the long-term phenological survey in Luki, although peaks were distinct, the proportion of trees being simultaneously in the same phenological stage rarely exceeded 50% (Couralet et al., 2013). The apparent complexity of individual behaviors and the lack of synchrony within and among species make it difficult to identify patterns of leaf phenology exclusively on the basis of environmental predictors (Viennois et al., 2013).

However, a general trend of phenological patterns is brought out thanks to the field surveys on leaf fall and flush. To summarize, trees of the rainforest in Central Africa tend to shed their leaves during the dry season, followed by a more or less rapid turnover of leaf flushing lasting during the entire wet season. These findings coincide with the EVI patterns of Yangambi and Luki sites, having very different cycles but showing both decrease of EVI values during their driest months, corresponding to leaf fall, and increase during the wet seasons suggesting the leaf flushing. As for the Amazon region, the EVI dynamic could be driven by the seasonal timing of leaf shedding and leaf flush, suggesting that EVI provides useful information about changes of vegetation behavior over time in tropical region.

From an adaptive evolution perspective, the turnover of leaves would be regulated to maximize the carbon gain through canopy photosynthesis and resource-use efficiency of the plant (Nyirambangutse et al., 2014). Indeed, trees seem to produce new leaves in the wet season with higher insolation to optimize access to light and to take advantage of high photosynthetic activity, while the shedding of leaves during the dry season would be a strategy helping the plant to avoid transpiration water loss and enhance drought survival (Maharjan et al., 2011). Also, the leaf flushing in the dry season, when water stress is still high, before the seasonal increase in insect biomass, may be a plant adaptation to minimize herbivory on young vulnerable leaves (Coley and Barone, 1996). Indeed, many folivores feed primarily on young leaves which contain a maximum of protein and a minimum of lignocellulose and toxic secondary compounds (Hladik, 1978).

Table 10: Field measurements of leaves dynamics in the Congo basin. The bimodal rainfall regimes of areas close to the equator is not represented in this table but the characteristics of the two wet and two dry seasons are similar.

| **Type of measurement** | **Wet Season** | **Transition: late wet season to early dry season** | **Dry season** | **Transition: Late dry season to early wet season** | **Studies** |
|---|---|---|---|---|---|
| **Litterfall colletions** | Litterfall due to wind *vs* low rate of litterfall | - | Start/peak of litterfall | Peak of litterfall | Laudelout and Meyer, 1954; Couralet et al., 2013; Schwartz and Tondo, 1988; Bernhard, 1970; Devineau, 1982; Hladik, 1978; Cizungu et al. 2014 |
| **Leaf gain observations** | Leaf flushing, growing of new leaves | - | - | Leaf flushing | Tshibangu et al., 2010; Hladik, 1978; Anderson et al., 2005 |
| **LAI** | LAI increase | - | Gradual decrease of LAI | - | De Wasseige and Defourny, 2003 |
| ***Summary*** | ***Leaf flushing and growing, some litterfall because of storms*** | **-** | ***Litterfall*** | ***Peak of litterfall, leaf flushing*** | |

## 4.4. Scaling up to 6 sites

The vegetation indices dynamics for the six sites is presented in Figure 49. The mean of number of valid observations by decade over 11 years of satellite data (bars) indicates clearly the lack of valid data in the Western part of the basin due to a permanent cloud cover (Minkebe and Luki sites).

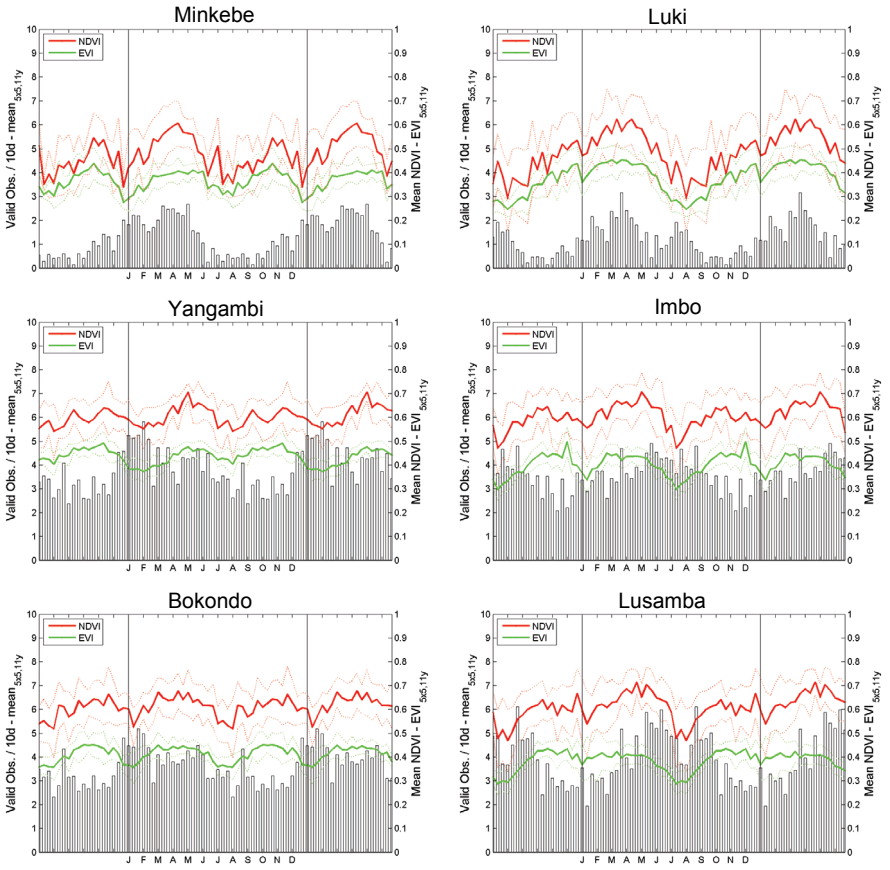


Figure 49 : Annual mean profiles of NDVI (red line) and EVI (green line) at the six sites, from SPOT-VGT time series 10-d composites (2000-2010), 5x5 km² window (spatial average values). Bars are number of valid observation by decade averaged over the 11 years. Inter-annual variability corresponding to one standard deviation is represented by dotted lines. Halves of the year are repeated at the beginning and the end of the year (delimited by vertical lines).

While in the Amazon basin EVI profiles are very similar from North to South and from West to East, although with different amplitude, the Congo basin presents a gradient of seasonality with one or two seasons. The gradient from areas close to the equator to the South of the basin is clearly visible. Yangambi, Minkebe and Bonkondo, located close to the equator, show two wet and dry seasons per year while Luki and Lusamba, in the Southern region, have one long season per year. Imbo, located between the equator and the South, presents an intermediate state. A site in the North of the basin could be taken into account to confirm the presence of an unimodal rainfall regime far from the equator.

## *4.5. Scaling up to basin scale*

A spatial distribution of EVI seasonal dynamics for the whole Congo basin is represented in Figure 50. Compared with the rainfall climatologies in Figure 52, it is observed that highest values of EVI correspond with wet seasons, as for the Luki and Yangambi sites. It confirms that the EVI peaks during periods of higher solar radiation that coincides with the wet seasons.

However, despite the similarity of EVI patterns and phenological field data of leaf fall and leaf flushing and climate conditions, the dynamics of EVI at the basin scale highlight an obvious atmospheric contamination of satellite data, from December to February in the Northwest of the basin and from June to October in the Southwest and central parts of the basin. Central and Eastern parts of the basin are relatively spared from aerosols and cloud cover. For example, Yangambi is particularly well situated and present EVI values around 0.4 without dropping. In these regions, the EVI dynamics is much more likely due to leaf phenology, itself controlled by light availability. Very low values of EVI observed in the West of the basin coincide in time and area with very high AOT values (Figure 44), suggesting that the EVI decrease in the Western part of the basin during the dry season is most probably much more driven by the aerosols than by the vegetation phenology, even if leaf shedding is precisely observed during the dry period between July and October (Couralet et al., 2013).

As already mentioned, aerosols scatter sunlight directly to the optical sensor and thus increase the apparent reflectance in the red and blue bands. However, aerosols also absorb sunlight in higher wavelength and thus decrease, although to a lesser degree, the near infrared band (Karnieli et al.,

2001; Xiao et al., 2003). This explanation is however very surprising as the EVI increase in the Amazon basin up to 0.5 is observed during the period of the year with the higher amount of aerosol in the atmosphere. It was concluded that NIR wavelength is less affected by atmospheric conditions and more related to the leaf internal structure. The composition of aerosols might be different in the two regions and interfere differently with light. If it is the case, the relationship between optical remotely-sensed data and different types of aerosols should be investigated. The days without aerosols might be more frequent in the dry period in the Amazon basin, but inexistent in the Congo basin. Also, coastal parts of the Western basin present an almost permanent cloud cover (Figure 51) due to the warming and rising of moisture-laden air as it moves from the Gulf of Guinea onto the central African land mass (Camberlin et al., 2001). It induces a very low number of valid observations from May to December which decreases strongly the possibility to have a clear day without aerosols. The only three months with both low aerosols amount and decent number of valid observation per month in the West region are March, April and May, showing the highest values of EVI throughout the year.

The site analysis highlights the effects of aerosols and cloud frequency. The aerosols spatio-temporal distribution and the number of valid observations define the regions where the EVI dynamics is mainly driven by the vegetation cycle. Only the areas never “red” on the aerosols map and never “blue” on number of valid observation should be considered for vegetation phenology analysis.

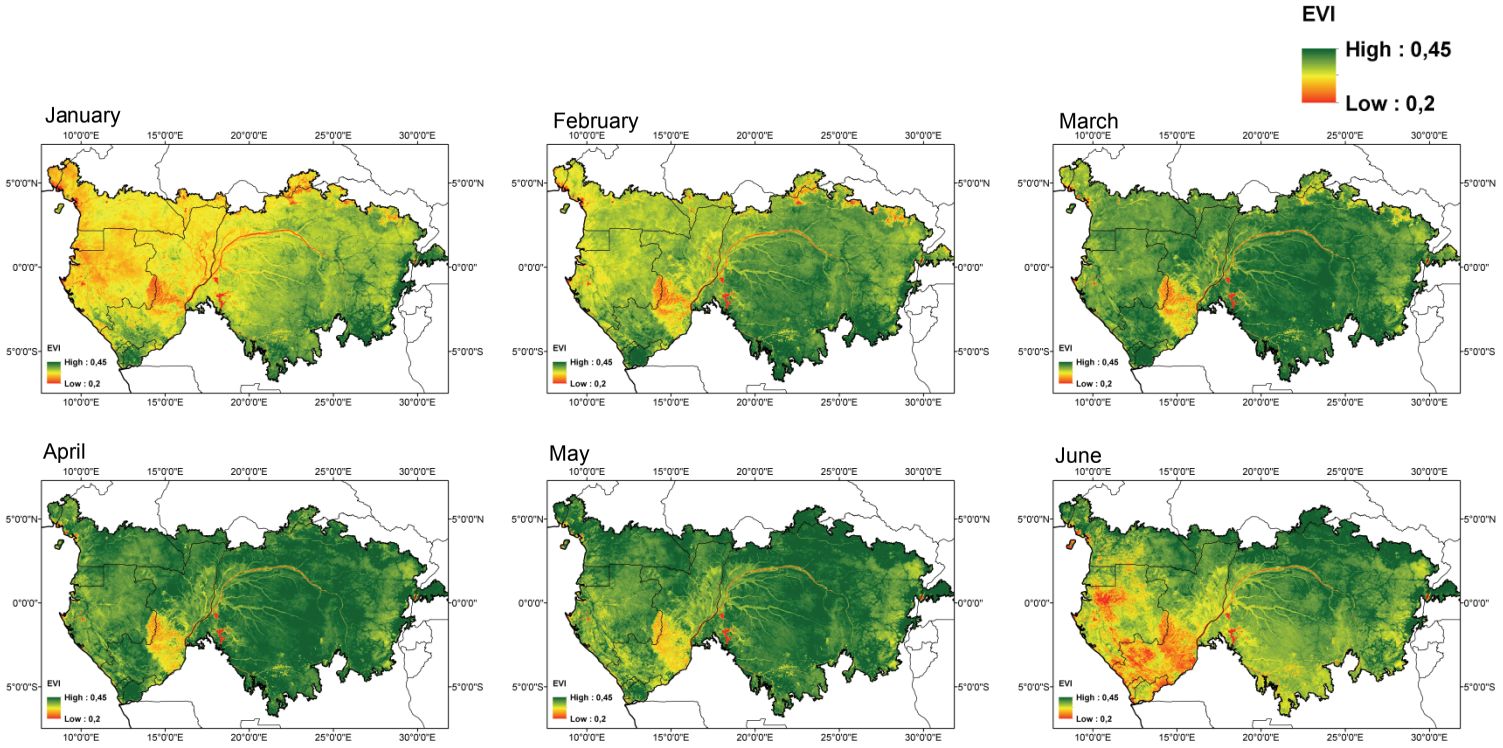
EVI
High : 0,45
Low : 0,2
January
February
March
April
May
June
10°0'0"E
15°0'0"E
20°0'0"E
25°0'0"E
30°0'0"E
5°0'0"N
0°0'0"
5°0'0"S

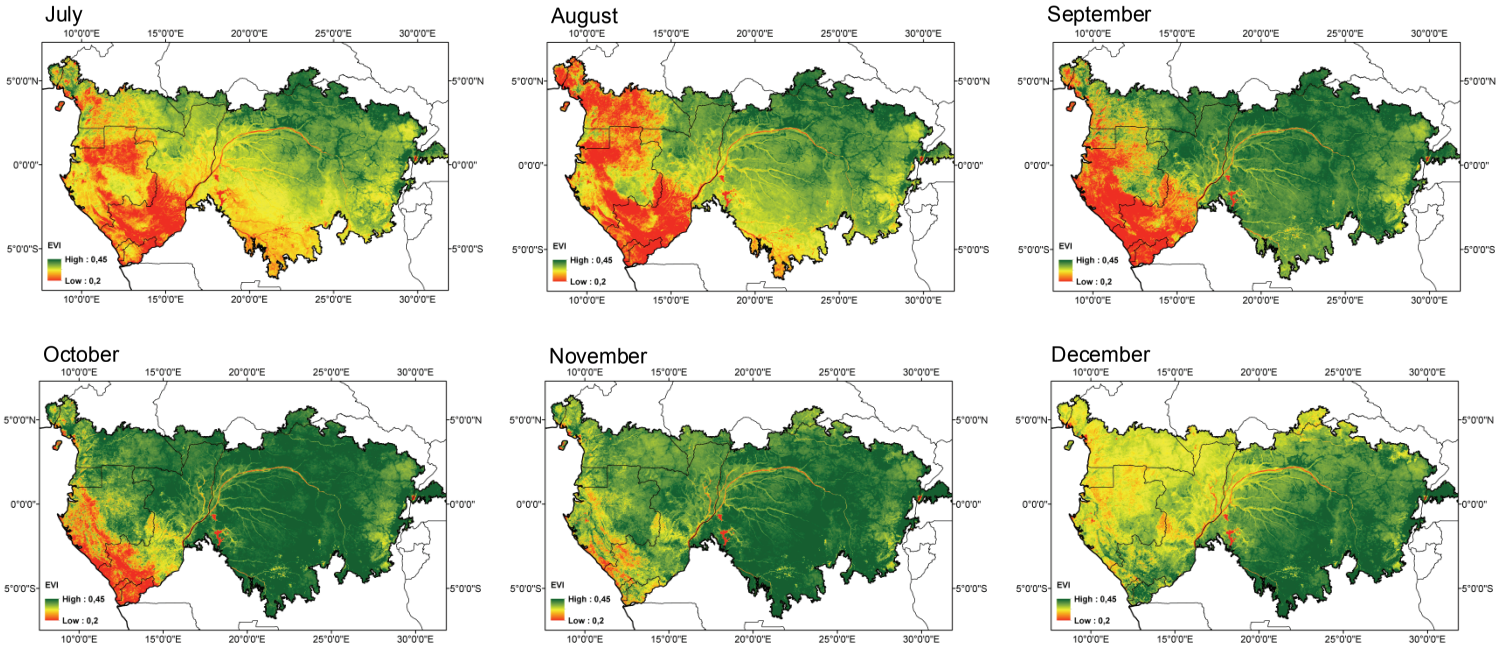


Figure 50 : Spatial distribution of EVI seasonal dynamics for the Congo basin. Each months average is a mean of corresponding 30-d composites from the 11 years of data from SPOT- VEGETATION time series (2000-2010).

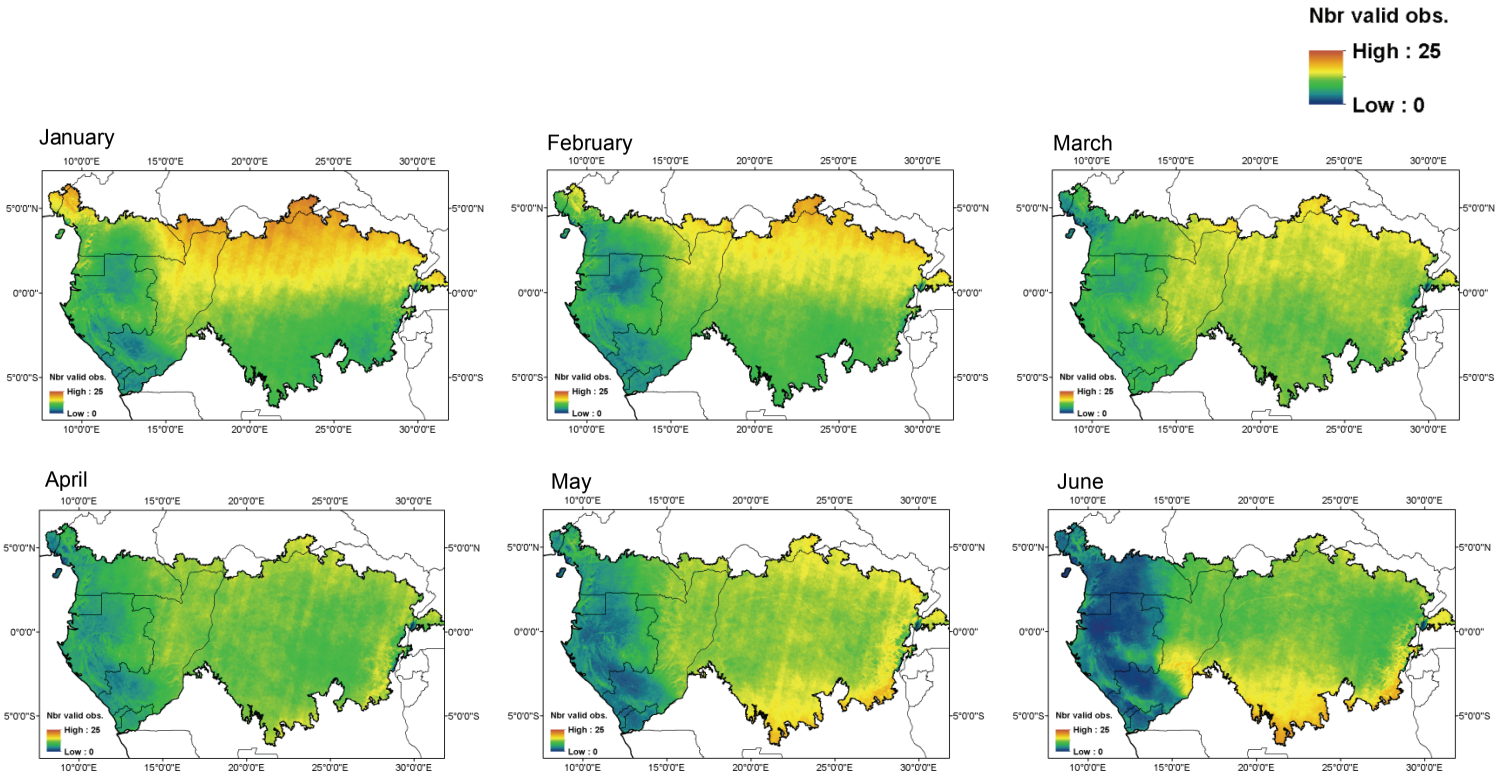
Nbr valid obs.
High : 25
Low : 0
January
February
March
April
May
June
10°0'0"E
15°0'0"E
20°0'0"E
25°0'0"E
30°0'0"E
5°0'0"N
0°0'0"
5°0'0"S

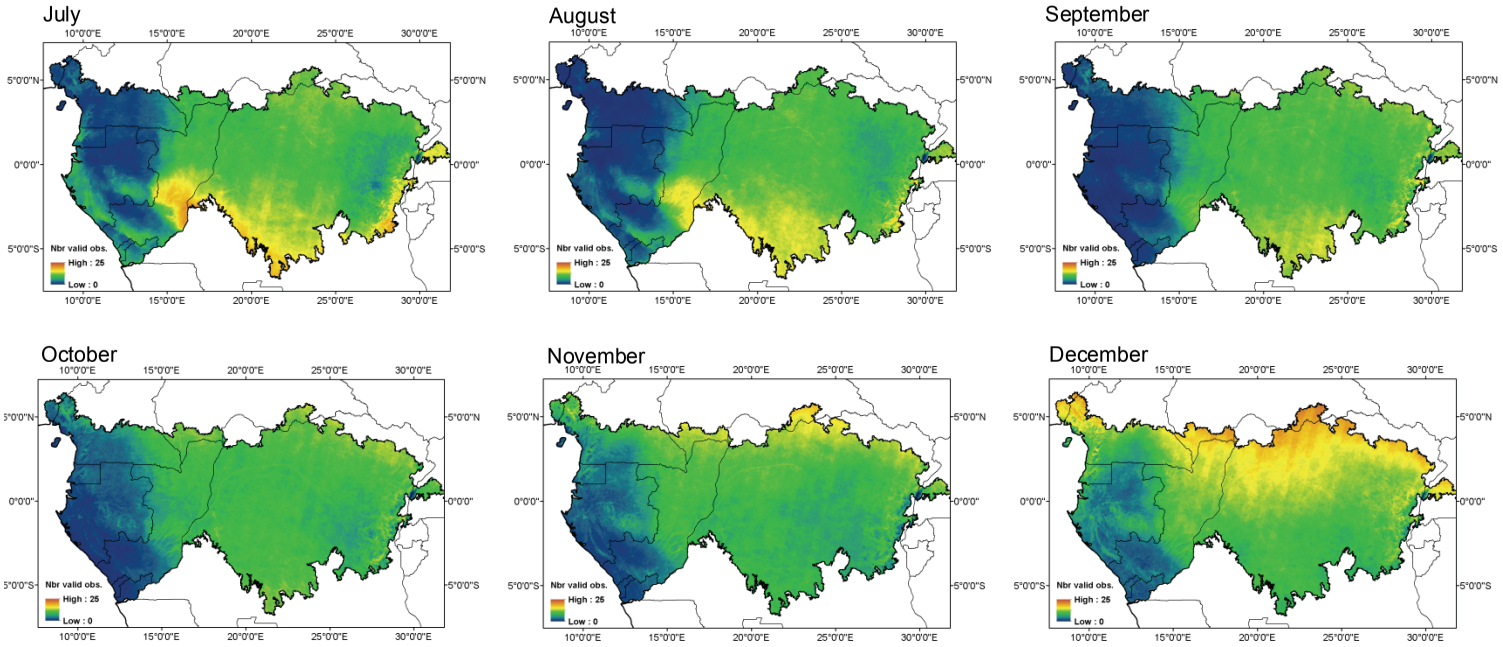


Figure 51: Spatial distribution of the number of valid observations per decade for the Congo basin. Each months average is a mean of corresponding 30-d composites from the 11 years of data from SPOT- VEGETATION time series (2000-2010).

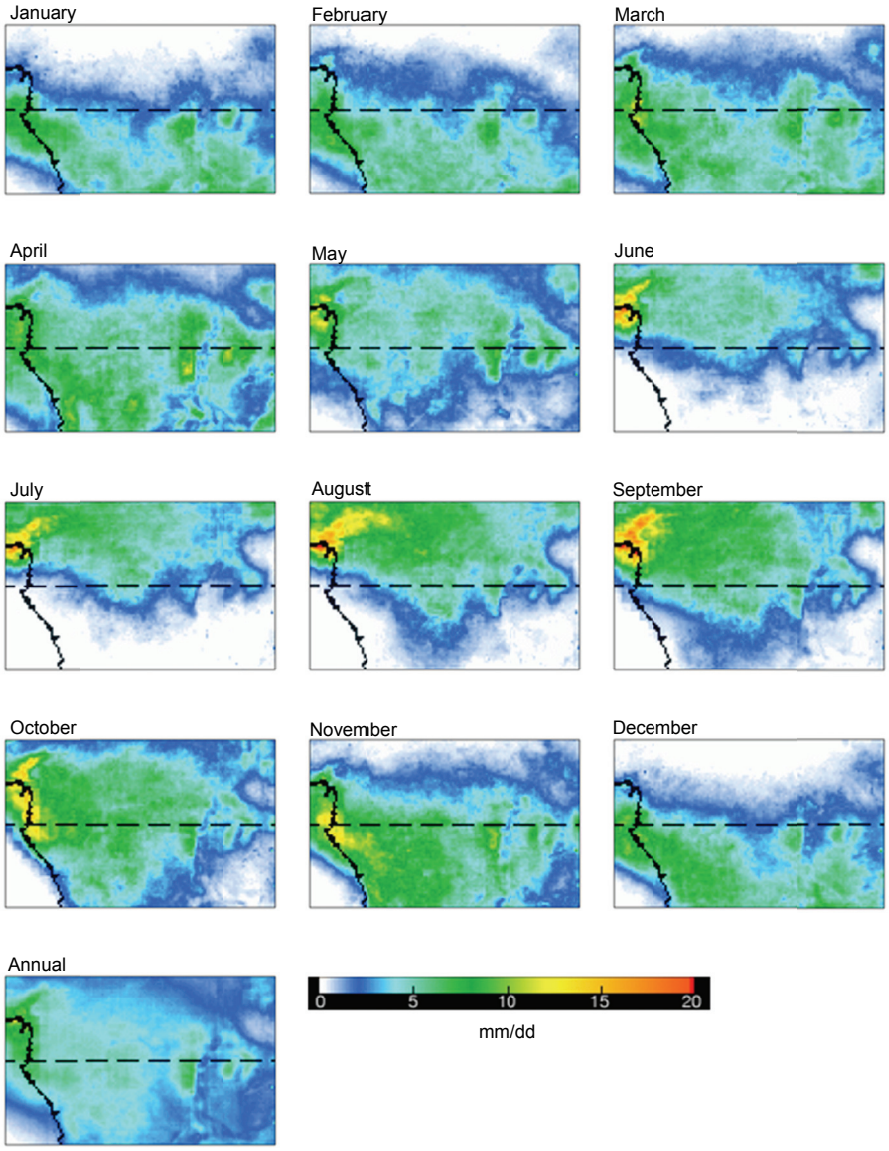


Figure 52: Rainfall climatologies from the Tropical Rainfall Measuring Mission (TRMM) using 1998 to 2011 data, mm/dd, 0.25° by 0.25° spatial resolution.

# 5. Discussion

***The need of field measurements to support remote sensing data***

Despite the scarcity of phenological field studies in rainforests of Central Africa, the information available on timing of leaf shedding and leaf flushing matches the seasonal variations of EVI throughout the year for the sites with usable time series. Species with deciduous or evergreen strategies coexist in this ecosystem. The EVI decrease during the driest months can come from a proportion of deciduous trees, that remain bare for few days or more, and evergreen trees showing nevertheless leaf-fall peaks with rapid turnover in leaf flushing.

The link between field sampling and remote sensing data remains a feasible challenge thanks to very high resolution datasets. For Central and East regions, optical satellite data with high to very-high spatial resolution can help to bridge the scale gap between field and medium resolution images, by providing snapshots of the canopy that allow separating the leaf-phenological stage of trees and the proportions of leaved crowns within the canopy (Viennois et al., 2013). In other areas, large noise still exists because of the aerosol contamination of the optical data, especially for the Western part of the basin. For this region, it is obvious that other instrument than optical remote sensing should be used to study tree phenology. A future integrated carbon-observing system would encompass notably a pan-African network of eddy covariance flux tower, allowing the characterization of spatial gradients and temporal variations of $CO_2$ fluxes (Ciais et al., 2011). Large scientific, logistic and training efforts are needed to establish permanent monitoring sites in the Congo basin's tropical forests, and to connect those sites to global networks (Verbeeck et al., 2011a). Also, tower-mounted cameras have proved efficient to follow the timing and amplitude of deciduousness in the Amazon basin (Nelson et al., 2014). Similar cameras could be easily installed in Central Africa and bring crucial information on phenology.

Another source of phenological measurement could be the dendrochronology (tree-ring analysis) that has the advantage to provide long-term records, although this kind of studies remains rare for tropical rainforests. Tree-rings are physiological responses of trees on seasonal variations of atmospheric parameters that can be used to evaluate tree growth

and therefore to estimate the production of individual trees in the forest (Djomo et al., 2011). Babst et al. (2014) propose to integrate tree-ring records with eddy-covariance measurements and remotely sensed observations to distinguish the timing of cambial growth and leaf phenology. Rainforest trees have long been thought not to form annual rings because of persistent high levels of rainfall, weak seasonality and low variability in temperature and day length in the tropics (Couralet et al., 2010; Groenendijk et al., 2014). Nevertheless, in West and Central Africa, the existence of annual tree-ring formation was proven by radiocarbon dating and tree-ring analysis (Worbes et al., 2003; Groenendijk et al., 2014). Indeed, across various tropical biomes, alternating environmental conditions induce periods of reduced or suspended cambial activity leading to the formation of identifiable growth layers (Couralet et al., 2010). For example, studying the formation of tree-rings in the tropics with the teak in Ivory Coast, Dié et al. (2012) found that the long dry season results in semi-deciduousness, cambial dormancy. In deciduous trees, leaf shedding is precisely an obvious sign of cambial dormancy (Couralet et al., 2010). The cambial reactivation and initiation of xylem and phloem formation occurs in February, at the end of the dry season. Also, in all sampled trees, xylem growth zones were formed during the seasonal development of new foliage, which might be a physiological response to the new foliage growth and to an increased demand for xylem water transport in order to supply sufficient water for increased transpiration and photosynthesis (Dié et al., 2012). The formation of new phloem was more intensive in May and June when trees were in full leaf at the peak of the rainy season. It shows that tree-rings analysis could be used as proxies of the tree productivity and climate at intra-annual resolution in tropical forests. The dendrochronological approach seems thus to be promising to link remote sensing information with the intern phenological functioning of trees and refine remotely-sensed estimates of forest productivity, as the timing of cambial activity follows the EVI pattern extracted in North part of the Congo basin and both increases in EVI and xylem growth zones occur during the rainy season.

***Forest disturbances and phenology***

In Amazonia, Koltunov et al. (2009) found strong evidence that selective logging changes the phenological pattern of tropical rainforests by inducing relative drying. They found that relatively low level of canopy

damage (5-10 %) causes significant and long-lasting (more than 3 years) changes in forest phenology inducing seasonal deficits in canopy moisture and greenness. Contrarily to the industrial plantation sector that is not well developed, industrial logging has been a major activity in the Congo basin countries for over four decades (Ruiz Pérez et al., 2005). It is generally highly selective and only a small number of trees are extracted per hectare, but a higher pressure is nevertheless found in small concessions (Ruiz Pérez et al., 2005). Even if Central African logged forests quickly recover their above-ground biomass after the disturbance (Gourlet-Fleury et al., 2013), the large extent of selective logging in Central Africa and the potential phenological disturbance associated could impact carbon and water fluxes, nutrient dynamics, and other functional processes in these forests (Koltunov et al., 2009). In particular, forests on nutrient poor soils, dominated by evergreen tree species (Gourlet-Fleury et al., 2011) and exhibiting low deciduousness, might be less resilient to recover after disturbance like logging (Fayolle et al., 2014).

Another type of disturbance is a drying trend, identified by Malhi and Wright (2004) in Africa since the mid-1970s. Fisher et al. (2013) show also a significant decrease in precipitation post-1968 in the African humid tropics using monthly climatic data covering the period 1901–2009. Thanks to MODIS EVI data, Zhou et al. (2014) observed a widespread decline in forest greenness over the past decade in the Congo basin that may be attributable to this long-term drying trend. However, Asefi-Najafabady and Saatchi (2013) found no significant impacts of extreme water deficit events on forest of Central Africa, suggesting potential adaptability of these forests. They hypothesize that the gradual drying trends since the 1970s have increased the adaptability of humid tropical forests in Africa to drought, unlike the Amazon forests that experienced two short-term, intense droughts in the past decade with high tree mortality and biomass loss (Phillips et al., 2009; Lewis et al., 2011). The effects of long-term drought are more complex than the short-term droughts as forest composition and structure change over time in order to adapt and respond to long-term reduction in rainfall (Asefi-Najafabady and Saatchi, 2013). The existence of a trend on the SPOT-VEGETATION time series and its impact on the averaged EVI profiles derived in this study should be investigated, for instance thanks to the trend analysis methodology develop by Verhegghen (2013).

Until now, despite relatively low annual rainfall and three to four months with less than 60 mm of precipitation per year, plants may not suffer extreme water stress during the dry season in the Congo basin (Couralet et al., 2013). Indeed, a thick cloud layer blocks solar irradiance and causes temperature drop, compensating partially the rainfall shortage, limiting the evapotranspiration and maintaining the relative air humidity constantly high, so soil moisture remains at non-stress levels (Couralet et al., 2013; Fisher et al., 2013). However, in West equatorial Africa, many climate models project an increase in dry season water deficits in response to global warming, amplified as global temperature increases, with potentially dangerous implications for African rainforests (James et al., 2013). Given this predicted increase of the current drying trend, the phenological response of trees to drier conditions has to be investigated. Indeed, changes in climate, especially declining rainfall, could have strong effects on species composition and abundance in these tropical forests (Maharjan et al., 2011). Species restricted to high-rainfall areas, namely the evergreen trees, are likely to be more vulnerable, whereas deciduous species occurring in low-rainfall areas are likely to become more abundant. Indeed, shedding of leaves during the dry season is a strategy helping the plant to avoid transpiration water loss and enhance drought survival (Maharjan et al., 2011). Deciduous species could then be more adapted to an increasing drying trend than evergreen species. The continued gradual decline could then alter the composition and structure of the Congolese forest to favour the spread of drought-tolerant species and thus affect biodiversity and carbon storage (Zhou et al., 2014). A better knowledge about the current phenological patterns and distribution of evergreen and deciduous species is thus essential to anticipate the effect of future climate changes on the resilience of Central African rainforest and on its ecology.

# 6. Conclusion

The potential of vegetation indices derived from Earth observation time series to detect seasonal signal and map spatial characterization of leaf phenology in the Congo basin have been explored at site level and, for the first time, over the whole central African rainforest.

Even if the Congo basin presents a lot of differences compared to the Amazon basin in terms of number of dry and wet seasons, cloud cover seasonality and rainfall dynamic, the key similarity is that leaf phenology and productivity in both tropical rainforests seems driven by solar radiation availability. A general trend of phenological patterns is brought out thanks to field surveys on leaf fall and flush found in literature. The vegetation in Central Africa seems to capitalize from the increases incoming radiation during the wet seasons by flushing new leaves to maximize carbon uptake.

This can be assessed by the satellite observation time series through the EVI dynamic, confirmed to be better suited than NDVI to study vegetation phenology in the tropical region. They correspond to the seasonal timing of leaf shedding and leaf flush and peak during periods of higher solar radiation, suggesting that EVI provides useful information about changes of vegetation behavior over time in tropical region.

However, this relationship dominates only in some part of the basin where low AOT values and high valid observation number are prevalent. In other parts, the atmospheric contamination due to permanent cloud cover and high aerosol loading strongly corrupt the signal received by the sensor and the use of EVI to study vegetation behavior is contraindicated. In those areas where optical satellite measurements fail to bring consistent information, future challenges remains to study tree phenology. There, flux towers and cameras network could bring decisive information to confirm tropical vegetation dynamic observed in clear regions. It is a crucial need in a context of climate change, especially given the increase of the current drying trend, for anticipating the phenological response of tropical trees to changes in climate and the potential feedback to the climate system.

# Conclusions and perspectives

Land cover and vegetation phenology, and their changes, are recognized to play important role in the global carbon budget. Land cover mapping and vegetation phenology detection are therefore two essential domains to address environmental concerns in a climate change context. The two main output of this research are (i) a global multi-year land cover mapping approach, taking into account the change occurring during the period of observations, and (ii) a better understanding of the characterization of tropical forest phenology using remote sensing time series. These two goals were addressed thanks to the long SPOT-VEGETATION time series, offering daily images at global scale over the last decade.

The thesis contributed to carefully exploit satellite time series in order to improve the consistency of global land cover mapping, to advance global land cover change detection, to reduce the uncertainty related to tropical vegetation phenology as observed from space and to better understand the mechanisms which control phenology and productivity of tropical rainforests. The main findings are summarized in this section, structured by the four specific objectives. Then, some perspectives concerning the improvement of the methods or the exploitation of the products are presented.

## 1. Findings

***1. Building a multi-year global land cover map can reduce the sensitivity to the inter-annual variability and to the year of observation as reported in current annual land cover maps***

Current global land cover mapping suffers from its single year strategy, consisting in using one year of satellite observation to characterize the land surface. As a result, land cover maps are highly sensitive to temporary events and to year-to-year variation related to meteorological and phenology

change. Taking advantage of the 13-y SPOT-VEGETATION time series, processed thanks to an automated classification chain, an innovative land cover mapping approach was developed to derive a multi-year global land cover product. This was found very efficient to reduce the sensitivity to the observation period found in all global annual land cover maps.

As a preliminary step to the multi-year map development, the inter-annual comparison of the 13 annual SPOT-VEGETATION classifications permitted to confirm the high sensitivity of annual land cover mapping to the year of observation. Furthermore, it was interestingly found that most of the year-to-year variation occurs between semantically close classes. This finding justified and gave confidence in the multi-year mapping concept consisting in using several years of observation to determine the most likely land cover type.

The use of multi-year time series has proved efficient to deal with the sensitivity to the period of observation compared to annual classifications for both methods tested: a multi-year classification based on 13-y summarized composites (MYC) and a synthesis of 13 annual classifications (SYC). The length of the dataset seems relevant to reduce the noise found in annual maps and to better delineate the landscape structure. This is a first step for meeting global observation closer to the needs of climate science, namely to provide stable component of the land cover characterization (Bontemps et al., 2012a). However, even if both products reach a satisfactory global accuracy around 72 %, a deeper understanding of the strengths and weaknesses of each method according to different regions of the world could be interesting, in order to eventually perform one or the other in specific areas and merge the results for an improved map.

Whether a selection has to be done at this stage, the SYC method offers some undisputable advantages. A first benefit is the flexibility of the conceived algorithm. The decision rules were adjusted and refined as a trade-off to take into account the most common cases of land cover time series at the pixel level but to be applicable on the global scale. Even if the selected thresholds are currently to some level empirical and rather subjective, the method permits already a better control of the recurrent classification discrepancies. Decision rules allow for instance reducing the proportion of mosaic pixels and favoring classes difficult to discriminate such as irrigated cropland or flooded vegetation. Compared to the MYC, a clearly reduced proportion of mosaic classes appears at the advantage of

pure classes, which increases the usefulness of the map. Second, also in the concern of a use-oriented product, the SYC is accompanied by several pixel-based confidence layers which allow documenting spatially the product quality. The maximum occurrence layer provide a per-pixel information on the number of time the most present land cover class appears in the time series, documenting clearly unstable regions. Another complementary layer could be the number of different classes present in each pixel time series. Indeed, if a pixel has a maximum of occurrence of 9 over the 13 years, it could be indeed interesting to know if the number of different classes is 2 or 5. Variability between 2 classes could reveal a region showing difficulties to discriminate two close classes, while variability between 5 land cover classes could indicate a region prone to climate variation or poor quality time series.

This innovative land cover mapping approach using a multi-year dataset is a start in the next generation of global land cover maps but certainly need tunings and refinements, exposed in the Perspective section.

### *2. Detecting land cover change globally is possible from medium resolution time series by disentangling the surface change from the inter-annual variability of the signal*

Land cover change occurred in many regions of the world over 13 years. Therefore, a change detection method had to be developed in parallel in order to determine at global scale the new land cover class for a change area and to integrate it to the multi-year land cover map. This was achieved by capitalizing on pixel temporal trajectories over the whole classification time series and distinguishing actual land cover change from inter-annual variability.

This trajectory-based change detection method provides a complete portrait of the Earth's land surface transformations by highlighting not only forest change but also croplands, grasslands, bare areas, urban areas and water bodies' losses and gains. To our knowledge, this is the first attempt to address the remaining gap of knowledge about the global change of these latter land cover types, by deriving the spatio-temporal dynamics of the land surface for all these classes in a same product. Individual layers are delivered for each type of change, as well as a common change layer regrouping all types of change. Each flagged pixel is labelled with the new land cover classes detected after the disturbance. Another important contribution of the

methodology conceived in this study is the capacity to provide the year of change. This information indicates the first year when a land cover type is no longer classified. A surface transformation can nevertheless take several years before reaching a new stable state, for instance a deforested area for agricultural purpose being classified first by shrublands, then by mosaic classes, and finally by croplands. Additional interesting information could be the number of years needed for the land cover to be stabilized.

A main strength of this post-classification method is the ability to determine the fate of the land cover over a changed area. In addition to the location and extent of the change, knowing the new land cover class after a disturbance is crucial information as land cover has considerable control on the biogeochemistry of the Earth system, through its physical characteristics such as albedo, emissivity, roughness, photosynthetic capacity or transpiration. A land cover change can impact climate by modifying for instance the amount of solar energy reflected. This highlights the importance to integrate the new land cover class detected after a change into the multi-year land cover map. Several examples illustrate this integration in Chapter 1. These examples demonstrate the requirement to take into account natural and anthropogenic land cover changes in a multi-year land cover mapping exercise. In addition, the different fates of land cover per change type offer interesting information about the proportion of vegetation loss or gains. This could help in deriving global net flux of carbon from land cover change which is by far the most uncertain term in the global carbon budget (Lewis, 2006; Ramankutty, 2007; Houghton et al., 2012).

The proposed trajectory-based method requires necessarily the use of Earth observations time series having highly consistent spatial and temporal coverage to provide successive yearly information for any place on Earth. This requirement leads to the main weakness of the method, namely the medium spatial resolution currently provided by these time series. At a 1-km spatial resolution, the results highlight the hot spots of land cover change, but change smaller than the pixel is undetectable. Absolute quantification of change at this scale is not recommended. However, this could be an interesting trade-off between a cost and time effective monitoring of land cover change at global scale and the possibility to catch the hot spots of change to be studied latter with higher resolution data. Indeed, high resolution (~30 m) data face a number of challenges to overcome in the global characterization and monitoring of the land cover

including unavailability of consistent global coverage, sheer volume of data, difficulties in preparing image mosaics and high performance computing requirements (Giri et al., 2013). The method could be applied on higher resolution time series such as PROBA-V which delivers images at the same temporal scale than SPOT-VEGETATION but at with an important upgrade in the spatial resolution from 1-km to 300 m and 100 m for the centre camera. It could allow extracting more detailed information and bring significant improvements by reducing the amount of mixed pixels. However, the time series is nowadays no longer enough to be implemented in a consistent way as the method relies on the analysis of a decade trajectory.

The use of a long time series, at least a decade, is indeed needed to distinguish actual surface conversion from spurious change. As the inter-annual variability between global annual land cover maps ranges in general from 25 to 30 % (Friedl et al., 2010; Bontemps et al., 2012a), and 31 % between annual SPOT-VEGETATION time series, the challenge was to establish decision rules capable to separate pixel trajectories representing inter-annual variability from trajectories describing an actual land cover change. This challenge was however facilitated by the length of the time series allowing using several years at the beginning and at the end of the sequence to confirm the trajectory. Also, strict conditions were applied when close classes and mosaic classes where present in the pixel time series. As a result, very few commission errors were found in the visual analysis showing that the method is able to complete this task.

The difficulty but also the advantage of the method was the tuning of the decision rules for areas representing specific issues and particularities. The aim was to work on the global scale with a general algorithm refined according to the 22 GlobCover strata. Unlike the multi-year SYC, it was a necessity in the change detection to adapt the decision rules for different cases as it copes with a large diversity of land surface trajectories. For instance, the “natural vegetation/cropland” mosaic class can often be confounded with an open forest class in temperate zones or in savannahs, while a transition from a closed forest to this “natural vegetation/cropland” mosaic in moist tropical regions represent likely a deforested area. As all forests classes are regrouped for the land cover change detection, the distinction of these the specificities is made by tuning the decision rules according to regions.

Visual analysis was performed to demonstrate the ability of the method developed to detect land cover changes and their spatial evolution over time. However, a validation is crucial to determine the reliability of this product. For instance, the level of omission and commission errors has to be known. A specific effort in that purpose is needed and discussed in the Perspectives section.

***3. Understanding the various perturbing factors of surface reflectance over tropical forests is a prerequisite to the vegetation indices use for studying vegetation phenology***

Confronting the seasonal cycles of atmospheric conditions and sun-sensor geometry with the intra-annual variability of individual spectral bands and vegetation indices revealed that appropriate vegetation index (EVI) is not significantly affected by these potential sources of signal noise and is consistent to monitor phenology in tropical regions, except where cloud coverage is nearly permanent. An 11-y time series provides sufficient data to carry out this essential investigation.

The analysis of atmospheric contamination firstly confirmed that the EVI is better suited than NDVI to study the vegetation seasonality in both Amazon and Congo basins. The seasonality of reflectance in the red band, strongly influencing NDVI values, is indeed not driven by the degree of chlorophyll absorption but instead strongly contaminated by cloud cover and by aerosols from biomass burning. The EVI follows the NIR dynamic, less affected by these atmospheric contaminations and more related to the vegetation dynamics. Secondly, the scaling up of EVI seasonal dynamics at biome scale allowed observing an inability to study leaf phenology in some parts of the Congo basin. In these areas, permanent cloud cover and high aerosol loading strongly corrupt the signal received by the sensor, even in the NIR band. For these areas, the days without aerosols might be more frequent in the Amazon basin even during the dry period, but inexistent in the Congo basin. Also, coastal parts of the Western Congo basin present an almost permanent cloud cover. It induces a very low number of valid observations which decreases strongly the possibility to have a clear day without aerosols. The number of valid observation over the 11 years provides a strong quality indicator, at regional scale but also at site level. It is concluded that optical remote sensing fails to describe vegetation behavior

when cloud coverage is nearly permanent, even with an 11-y time series, highlighting the limit of this remotely-sensed approach.

Concerning BRDF effects, the EVI seasonality is interpreted in several studies as driven by illuminations (SZA) and relative positions of the sun and the sensor (φ) variations. These researches studied these relationships particularly in the Amazon basin and interpreted the EVI increase during the dry season as a combination of shadowing effect within the canopy and the sun-sensor geometry. The analysis of these relationships with angles values extracted from daily SPOT-VEGETATION time series revealed however no correlation between EVI and SZA when looking at the entire year, for both basins. In addition, the decrease of φ until the sensor reaches the principal plane causing an increase of EVI and an apparent green-up is not verified in the Congo basin. In this region, it is clearly observed that the moment when the sensor reaches the principal plane does not correspond to the highest values of EVI. Another striking result is the very different patterns between the EVI profiles from the K67 fluxtower site and the Yangambi site in the Congo basin, while φ and SZA yearly variations are very similar. It is concluded that the view-illumination geometry is not the main driver of the EVI seasonality. The BRDF impacts could nevertheless be further analyzed thanks to radiative transfer simulations. Efforts have already been done in this way, thanks to the expertise of Dr. Yves Govaerts, using the 3D Raytran model (Govaerts, 1997) over the Ngotto forest (CAR). Refinements of the tropical scene were successfully realized, but the reactivation of the model showed strong inconsistencies and the results were unusable for any conclusion.

***4. In situ phenological and meteorological observations are crucial to validate the remotely-sensed vegetation seasonality and to question the mechanisms driving the tropical forest foliage phenology***

The objective was to make the link between the satellite-based variation with ground observation of phenology, flux tower $CO_2$ seasonal patterns and climate conditions to question the phenological mechanisms for the seasonal greening of Earth observation data. This was achieved by confronting EVI seasonality with ground information collected in literature and GPP and sun radiation measurements available in the Amazon basin, and comparing the results of the Amazon and the Congo regions.

This study provided a deeper understanding of the meaning of satellite-based greening compared to ground reality. It has demonstrated the ability of medium resolution time series to describe leaf phenology of a tropical rainforest. The timing of phenology was confirmed for both basins thanks to the support of several ground-based measurements on foliage phenology. It was found that the EVI seasonal changes correspond to phenological events such as leaf shedding and leaf flush, at site level and at basin scale. It is therefore suggested that leaf phenology is the dominant driver of seasonal variations of EVI in tropical rainforests, and that EVI provides useful information about changes of vegetation behavior over time. However, this relationship dominates only in some part of the basin where low AOT values and high valid observation number are prevalent. It is already observed that satellite images with finer resolution than VEGETATION can help bridge the gap between the 1km scale and the ground observation (Viennois et al., 2013). This should be realized at the basin scale to support the analysis realized here as leaf flushing observations and litterfall collects only provide local measurements. The EVI presents also a very similar pattern than GPP derived from the fluxtower, suggesting that the EVI could be related to carbon fluxes. However, this relationship should be tested for other fluxtower sites in the Amazon basin.

The analysis in the Congo basin allowed confirming the green-up theory developed in many studies led in the Amazon basin, arguing that vegetation in tropical forests capitalizes from the increasing incoming radiation by flushing new leaves to maximize carbon uptake. Indeed, even if the Congo basin presents a lot of differences compared to the Amazon basin in terms of number of dry and wet seasons, cloud cover seasonality and rainfall dynamics, the key similarity between both regions is that EVI peaks during periods of higher solar radiation (dry season for the Amazon basin, wet season for the Congo basin) suggesting an increase of vegetation photosynthesis activity. In addition, a similar pattern is found between the EVI seasonal dynamics shortwave incoming radiation measured at the K67 tower site. It is concluded that leaf phenology and productivity in both tropical rainforests are driven by solar radiation availability. This is an important finding that could be helpful to reduce the uncertainty concerning the tropical forest resilience or dieback to climate evolution.

# 2. Perspectives

Exploiting 13-y of daily Earth observation data brought out the power of long time series to describe the land surface. It also opens interesting perspectives concerning improvements of the current achievements or their concrete application. Several lines of investigations are identified in this section.

## *2.1. Potential improvements to the approaches developed and future research directions*

With regards to the characterization of the land cover at global scale, the issue of the sensitivity to the observation period was addressed by developing an innovative concept which considered for the first time a multi-year dataset. However, the exploratory strategy implemented lacks robustness with regards to the underlying decision rules to derive the most appropriate land cover for each square kilometre over the whole world. Further research is needed to examine in details the possibility offered by the confusion matrices and semantic distances between classes to analyse each pixel time series with its singularity and to determine the probability of the actual land cover type. Should this proposed strategy reveals insufficient, specific efforts should focus on a more complete validation dataset in order to build confident confusion matrices, lacking currently validation points for several classes. In addition, a deeper understanding of the links between inter-annual variabilities and particular meteorological events could reveal very helpful to tune decision rules according to specific regions. Potential causes of strong inter-annual variabilities in some areas of annual classifications, such as fires, droughts, El Niño events or climatic variability in general, deserve to be explored and to be taken into account in the multi-year process.

Interesting perspective could also come from the use of higher spatial resolution data that will probably provide significant gains in accuracy and reduce mixed pixels. The next generation of global land cover maps at finer spatial and thematic resolutions, if it copes with the challenges of data volume, cloud-free images acquisition, revisiting cycle or validation,

will probably describe the Earth's surface at a level of detail never reached. However, high resolution data sets acquired in terms of decades, such as Landsat (30-m), have currently low temporal repeat visits and thus a limited ability to provide annual global updates of land cover because of cloud-cover and phenological variability (Houghton et al., 2012; Hansen and Loveland, 2012). Improving the temporal revisit rate at high spatial resolution is the most pressing need regarding large areas of land cover and change monitoring (Hansen and Loveland, 2012). New sensors from the small Belgian satellite PROBA-V (300-m and 100 m for the central camera) launched on May 2013 and the Sentinel-3 (300-m) satellites to be launched in the framework of the European Copernicus programme, with a short revisit time of less than two days, will ensure the continuity of the SPOT-VEGETATION time series to characterize the land cover and its change.

In order to apply yearly updates to enrich continuously the multi-year land cover maps and the land cover change detection, for instance using PROBA-V data to complete the SPOT-VEGETATION time series, essential improvements are needed to make the complete process automatic. Currently, the difficulties encountered to easily update the product are due to manual tuning of the algorithms. For instance, as the trajectory-based method relies on the whole time series, adding one year of data to this time series in the land cover change process induces to modify each threshold previously defined. To deal with this design issue, threshold algorithms could be updated automatically based on the length of the time series, or a moving window could be applied with fixed thresholds as long as the time series increases. In this last case, challenges would remain concerning the merging of successive moving window results. The same remark can be done concerning the computation of “climatological years” for both Chapters on tropical vegetation phenology. However, the need to integrate a new year is less crucial in this case as these two studies are realized in the idea of an investigation and not dedicated to monitor the phenology change over years.

The importance of land surface change is now recognized in land change science, and there is consequently considerable need for accurate information on land cover dynamics. A future challenge needed to finalize the land cover change product concerns the validation of the change detected. While satisfactory results showed that the method succeeds in many areas, certain shortcomings have also been pointed thanks to visual analysis. An independent validation process should be an integral part of the

change detection approach. The difference between the strategy for validating land cover and land cover change products is detailed in Strahler et al. (2006). For instance, there is no possibility of deriving a static global set of validations sites as land cover change is dynamic over time. Changes represent relatively rare cases at global scale. Thus, any simple or stratified random sample would be inadequate for assessing change classes. Also, information must be gathered at each validation site for both time 1 and time 2 states, which increases costs and complicates sampling consideration. Furthermore, several information have to be verified, namely the location of change but also the timing of change and the fate of land cover determined over a changed area. Therefore, this validation is a huge task that should be a priority in future research. While in situ ground measurements may be a preferred source of validation data, their use at the global scale in assessing the accuracy of land cover change maps is limited due to high costs (Strahler et al., 2006). The easiest way to assess the product quality would be to capitalize on existing land cover change maps. These ones should nevertheless correspond to the time period of observations. An important source for the forest change is obviously the Global Forest Change map realized in 2013 by Hansen et al., recently updated to highlight forest losses and gains until 2014. This high resolution product (30 m) available at global scale is an opportunity to test the consistency of the product and to provide information on both commission and omission errors. However, this map does not provide any information on the state of land cover after change. For the other types of changes, to our knowledge, no such product exists at global scale. Regional maps should then be used to perform the assessment. High resolution imagery could also be used with more intensively sampling in hot spots of change.

An interesting outcome of our land cover change results is that some specific types of disturbance observed differ considerably among the countries and their policies (e.g. dams, deforestation for agriculture, irrigation). Understanding the role human plays in modifying ecosystems through changing land cover is central to address environmental challenges and to implement better resource managements (Hutyra et al., 2011). However, the ability to distinguish natural and anthropogenic source of disturbance at this spatial resolution is currently only possible visually in cases where high resolution imagery is available. In the future, sorting out the proportion of natural and anthropogenic drivers for the detected change would constitute a considerable source of information to drive sustainable

development policies and to assist decision-making. Ideally, with a much longer time series, the persistence of change for both sources of change should also be investigated.

Resolving the current debate surrounding the nature of seasonal variations of remotely-sensed data over tropical areas is critical to move forward and to study deeper the response of these forests to climate change. In order to validate the satellite-based cycles, the tower-mounted cameras could be an easy and very rich option to bring ground information about the trees behaviour over a year. They could help confirming rapidly the phenophases observed from satellite-based vegetation indices, their timing and amplitude of deciduousness, in a cost effective way. In addition, this kind of measurement would be much more realistic than litterfall collects asking for a biggest amount of work and logistic. Ideally, as EVI shows spatial variability, these ground data should be distributed over the whole basin and not focused on the few flux-tower sites already well-studied. Another alternative should be to compare results of the SPOT-VEGETATION time series with the new MODIS product generated with the MAIAC algorithm (Lyapustin et al., 2012). These data are standardized to a fixed sun and sensor geometry, compared to the NBAR product used in this study fixed only for sensor geometry. Being free of sun-sensor geometry effects, they could support the effort of sorting out actual vegetation phenology from artefacts in the signal sensor.

Future challenges remain also to study tree phenology in tropical zones where optical satellite measurements fail to bring consistent information because of strong atmospheric contamination. First of all, especially for the Western part of the Congo basin, an analysis comparing aerosols, fires and meteorological datasets with the MAIAC data should be realized to confirm or disprove that remotely-sensed data are unusable in this region. Indeed, the MAIAC data are significantly improved concerning atmospheric and cloud masking. Other instruments should also be used, such as eddy covariance flux towers and cameras networks to provide annual variations of $CO_2$ fluxes and foliage behavior. Another source of phenological measurement could be the dendrochronology (tree-ring analysis).

In areas exempt of a nearly permanent cloud cover, the analysis of EVI dynamics at regional scale brought significant information on how optical remote sensing time series can help detecting spatial and seasonal

variations of tropical rainforest phenology. The spatial distribution of EVI seasonal dynamics shows coherent results for the Amazon basin compared to analysis at site level, but a heterogeneous behavior can nevertheless be observed throughout the basin. In the future, questioning the combination and the interaction of the EVI spatial variability with mechanisms or environmental variables others than solar radiation (i.e. spatial variability in length of the dry season, soil type, root length, phosphorus availability, surface temperature, etc.) could be helpful to determine the secondary factors influencing or limiting vegetation productivity. In addition, the magnitude of phenology is still uncertain and requires further research. Indeed, species with deciduous or evergreen strategies can coexist in these tropical ecosystems meaning that the EVI seasonality can come from a proportion of deciduous trees, that remain bare for few days or more, and evergreen trees showing nevertheless leaf-fall peaks with rapid turnover in leaf flushing.

Finally, given the predicted increase of the current drying trend in the Congo basin and the two recent major droughts in the Amazon basin, the phenological response of trees and the impact on their carbon storage to drier conditions should be investigated. Indeed, climate change, especially declining rainfall, could have strong effects on species composition and structure in these tropical forests (Maharjan et al., 2011). Deciduous species could be more adapted to an increasing drying trend than evergreen species. A better knowledge about the current phenological patterns and distribution of evergreen and deciduous species is thus essential to anticipate the effect of future climate changes on the resilience of tropical rainforests. The work of Gond et al. (2013) provides significant results in this way and should be extended to the whole Amazon and Congo basins.

## *2.2. Applications of the methods developed*

***Toward operational implementation in the framework of ESA Climate Change Initiative (CCI) Land Cover***

The trajectory-based method developed in the thesis is currently implemented in the framework of the CCI Land Cover project (Phase 2). This application offered the opportunity to enhance the method. Firstly,

improvements include notably to extent the analysis on a 1999-2015 time series thanks to PROBA-V data. The addition of several years permits not surprisingly to detect much more changes. Secondly, modifications and refinements of the thresholds and conditions permit to correct some omission and commission mistakes and to spread the spatial structure of the changes already detected. Less strict number of years is used to determine the first state of the land cover. Thus the change is detected since 2003 for each time of change, although this was done previously only for well discriminated classes such as forests and bare areas. Thirdly, 13 types of land cover change are now processed instead of 7 in the thesis. For instance, croplands and grasslands are separated in individual land cover types, which provide interesting results. Shrublands and wetlands are also taken into account separately.

The information about the year of change will also be useful in the framework of this project. A need expressed by the climate modeling community in terms of land cover characterization is to obtain a suite of global land cover products over time. The year of land cover change can be used as a bridge to derive a suite of annual land cover maps from the multi-year CCI baseline and the land cover change detected with SPOT-VEGETATION and PROBA-V time series.

***Use in models***

Land cover change results are integrated to the SYC multi-year map in order to provide a coherent product. The effort to conceive a stable characterization of the land cover taking into account long term data and surface transformation makes it a relevant product for the land surface parameterization of global vegetation or climate models. The spatial distribution of uncertainty of the SYC on a pixel-basis could be also useful in that purpose. The land cover change results are currently used by the International Institute for Applied Systems Analysis (IIASA) team in the GLOBIOM model in the framework of the SIGMA project. They use an econometric model to estimate global land-use change projection from 2010 until 2050 taking into account the transitions between forest, cropland, grassland. The projection of land use change are realized along three Shared Socio-Economic Pathways (SSP): the first one represents sustainable development, the second one is a middle of the road scenario, while the third

one is characterized by continued divergence in economic growth. A paper is in preparation.

The characterization of phenology in the Amazon basin thanks to the spatial distribution of EVI dynamics could be used to help in the description of phenology in Earth system models. The use of EVI at regional scale is however not recommended for the Congo basin. A better representation of the cycle of carbon in important biomes like tropical rainforests is indeed essential, e.g. to anticipate impacts of climate change, but currently need improvements.

# Publications

## Peer-reviewed publications

Bontemps, S., Herold, M., Kooistra, L., van Groenestijn, A., Hartley, A., Arino, O., **Moreau, I.**, and Defourny, P. (2012). Revisiting land cover observations to address the needs of the climate modeling community. *Biogeosciences*, 9, 2145-2157.

**Moreau, I.** et al. Vegetation phenology of Amazonian tropical rainforests from 11-y SPOT-VEGETATION time series. *In preparation*.

**Moreau, I.** et al. Vegetation phenology of tropical rainforests in the Congo basin from 11-y SPOT-VEGETATION time series. *In preparation*.

Krisztin, T., Havlik, P., Leclere, D. and **Moreau, I**. Global high-resolution land-use change projections: A Bayesian multinomial logit downscaling approach incorporating model uncertainty and spatial effects. *In preparation*.

## Conference proceedings

Krisztin, T., Havlik, P., Leclere, D. and **Moreau, I**. Global high-resolution land-use change projections: A Bayesian multinomial logit downscaling approach incorporating model uncertainty and spatial effects. Poster presented at the International Institute for Applied Systems Analysis (IIASA) Systems Analysis Conference, Austria, 11-13 November 2015.

Bontemps, S., Boettcher, M., Brockmann, C., Kirches, G., Lamarche, C. Radoux, J., **Moreau, I.**, Santoro, M., Van Bogaert, E., Wegmüller, U., Herold, M., Achard, F., Ramoino, F., Arino, O. and Defourny, P. Multi-year

global land cover mapping at 300 m and characterization for climate modelling: achievements of the land cover component of the ESA climate change initiative. Proceedings of the 36th International Symposium on Remote Sensing of Environment, Berlin, Germany, 11-15 May 2015.

**Moreau, I.,** De Weirdt, M., Verbeeck, H., Maignan, F., Poulter, B., Najdovski, N. and Defourny P. The enhanced vegetation index (EVI) as a proxy of Gross Primary Production – The VEGECLIM project. Poster presented at the European Geosciences Union (EGU) General Assembly, Vienne, Austria, 27 April - 02 May 2014.

Defourny, P., Verbeeck, H., **Moreau, I.**, De Weirdt, M., Najdovski, N., MacBean, N., Verhegghen, A., Kibambe-Lubumba, J.-P., Jungers, Q., Maignan, F., Poulter, B. and Peylin, P. Integrating SPOT-VEGETATION 13-yr time series and land-surface modelling to forecast the terrestrial carbon dynamics in a changing climate - The VEGECLIM project: achievements and lessons learned. Pierre Defourny's oral presentation at the European Geosciences Union (EGU) General Assembly, Vienne, Austria, 27 April - 02 May 2014.

Defourny, P., Verbeeck, H., **Moreau, I.**, De Weirdt, M., Najdovski, N., MacBean, N., Verhegghen, A., Kibambe-Lubumba, J.-P., Jungers, Q., Maignan, F., Poulter, B. and Peylin, P. Integrating 13-y time series of daily SPOT-VEGETATION observation and land-surface modelling to forecast the terrestrial carbon dynamics of Congo Basin forests in a changing climate. Pierre Defourny's oral presetentation at the Belgian Earth Observations Day, Lier, 20 November 2014.

**Moreau I.** and Defourny P. The vegetation phenology detection in amazon tropical evergreen forests using SPOT-VEGETATION 11-y time series. Proceeding and oral presentation at the International Geoscience and Remote Sensing Symposium (IGARSS), Munich, Germany, 22-27 July 2012.

**Moreau, I.,** Defourny P., Hanert, E., De Weirdt, M., Verbeeck, H., and Steppe, K. Integrating SPOT-VGT 10-y time series to forecast terrestrial carbon dynamics: The vegetation phenology detection in tropical evergreen forests. Proceedings of the ESA-iLEAPS-EGU Earth Observation for Land-

Atmosphere Interaction Science Conference, Frascati, Italy, 3-5 November 2010.

Defourny, P., Verbeeck, H., **Moreau, I.**, De Weirdt, M., Hanert, E. and Peylin, P. and. 10-y SPOT-VEGETATION Time Series for Land-Surface Modelling - The VEGECLIM Project. Oral presentation at the the ESA-iLEAPS-EGU Earth Observation for Land-Atmosphere Interaction Science Conference, Frascati, Italy, 3-5 November 2010.

De Weirdt, M., Verbeeck, H., Maignan, F., **Moreau, I.**, Defourny, P., and Steppe, K. Modelling the foliage seasonal carbon cycle in tropical forests. Proceedings of the ESA-iLEAPS-EGU Earth Observation for Land-Atmosphere Interaction Science Conference, Frascati, Italy, 3-5 November 2010.

Defourny, P., Verbeeck, H., Steppe, K., De Weirdt, M., Peylin, P., **Moreau, I.**, Verghegghen, A. and Hanert, E. Tropical forests carbon dynamics using 10-d SPOT-VEGETATION time series and land-surface modelling – The VEGECLIM project. Pierre Defourny's oral presetentation at the Belgian Earth Observations Day, Chaudfontaine, 6 May 2010.

# Bibliography


Albert, L., Wu, J., Prohaska, N., Camargo, P., Cosme, R., Huxman, T. and Saleska, S. (2014). Leaf demography and physiology of the Tapajós National Forest: could phenology cause a forest-level increase in gross primary productivity during the dry season? *AGU Fall 2014*, Abstract B11G-0108.

Anderson, D. P., Nordheim, E. V., Moermond, T. C., Bi, Z. B. G. and Boesch, C. (2005). Factors influencing tree phenology in Taï National Park, Côte d'Ivoire. *Biotropica*, 37 (4), 631-640.

Anderson, L. O., Malhi, Y., Aragão. L, Ladle, R., Arai, E, Barbier, N. and Phillips, O. (2010). Remote sensing detection of droughts in Amazonian forest canopies. *New Phytologist*, 187, 733-750.

Anderson, L. O., Aragão, L. E. O. C., Shimabukuro, Y. E., Almeida, S. and Huete, A. (2011). Fraction images for monitoring intra-annual phenology of different vegetation physiognomies in Amazonia. *International Journal of Remote Sensing*, 32:2, 387-408.

Aragão, L. E. O. C., Malhi, Y., Roman-Cuesta, R. M., Saatchi, S., Anderson, L. O. and Shimabukuro, Y. (2007). Spatial patterns and fire response of recent Amazonian droughts. *Geophysical Research Letters*, 34, L07701.

Aragão, L. E. O. C., Malhi, Y., Metcalfe, D. B., Silva-Espejo, J. E., Jiménez, E., Navarrete, D., Almeida, S., Costa, A. C. L., Salinas, N., Phillips, O. L., Anderson, L. O., Alvarez, E., Baker, T. R., Goncalvez, P. H., Huamán-Ovalle, J., Mamani-Solórzano, M., Meir, P., Monteagudo, A., Patino, S., Penuela, M. C., Prieto, A., Quesada, C. A., Rozas-Dávila, A., Rudas, A., Silva Jr., J. A., and Vásquez, R. (2009) Above- and below-ground net primary productivity across ten Amazonian forests on contrasting soils. *Biogeosciences*, 6, 2759–2778.

Aragão, L. E. O. C., Poulter, B., Barlow, J. B., Anderson, L. O., Malhi, Y., Saatchi, S., Phillips, O. L. and Gloor, E. (2014). Environmental change and the carbon balance of Amazonian forests. *Biological Reviews*, 89, 913–931.

Arino, O., Bicheron, P., Achard, F., Latham, J., Witt, R. and Weber, J. L. (2008). Globcover: the most detailed portrait of Earth. *ESA Bulletin*, 136, 24-31, European Space Agency.

Arino, O., Ramos, J., Kalogirou, V., Defourny, P. and Achard, F. (2010). GlobCover 2009. *ESA Living Planet Symposium*, 27 June-2 July 2010, Bergen, Norway.

Asefi-Najafabady, S. and Saatchi, S. (2013). Response of African humid tropical forests to recent rainfall anomalies. *Philosophical Transactions of the Royal Society B*, 368, 20120306.

Asner, G., Nepstad, D., Cardinot, G., and Ray, D. (2004). Drought stress and carbon uptake in an Amazon forest measured with spaceborne imaging spectroscopy, *Proceedings of the National Academy of Sciences,* vo. 101, n° 16*,* 6039 – 6044.

Asner, P., and Alencar, A. (2010). Drought impacts on the Amazon forest: the remote sensing perspective, *New Phytologist,* 187, 569-578.

Babst, F., Alexander, M. R., Szejner, P., Bouriaud, O., Klesse, S., Roden, J., Ciais, P., Poulter, B., Frank, D., Moore, D. J. P. and Trouet, V. (2014). A tree-ring perspective on the terrestrial carbon cycle. *Oecologia*, 176, 307-322.

Baccini, A., Laporte, N., Goetz, S. J., Sun, M. and Dong, H. (2008). A first map of tropical Africa's above-ground biomass derived from satellite imagery. *Environmental Research Letters*, 3, 045011.

Baccini, A., Goetz, S. J., Walker, W. S., Laporte, N. T., Sun, M., Sulla-Menashe D., Hackler, J., Beck, P. S. A., Dubayah, R., Friedl, M. A., Samanta, S., and Houghton, R. A. (2012). Estimated carbon dioxide emissions from tropical deforestation improved by carbon-density maps. *Nature Climate Change*, 2, 182-185.

Bacour, C. and Bréon, F.-M. (2005). Variability of biome reflectance directional signatures as seen by POLDER. *Remote Sensing of Environment*, 98, 80-95.

Badeck, F.W., Bondeau, A., Bottcher, K., Doktor, D., Lucht, W., Schaber, J. and Sitch, S. (2004). Responses of spring phenology to climate change. *New Phytologist*, 162 (2), 295–309.

Barlow, J., Gardner, T. A., Ferreira, L. V. and Peres, C. A. (2007). Litter fall and decomposition in primary, secondary and plantation forests in the Brazilian Amazon. *Forest Ecology and Management*, 247, 91-97.

Bartholomé, E., and Belward, A. S. (2005). GLC2000: a new approach to global land cover mapping from Earth observation data. *International Journal of Remote Sensing*, 26 (9), 1959-1977.

Beer, C., Reichstein, M., Tomelleri, E., Ciais, P., Jung, M., Carvalhais, N., Roedenbeck, C., Arain, M. A., Baldocchi, D., Bonan, G. B., Bondeau, A., Cescatti, A., Lasslop, G., Lindroth, A., Lomas, M., Luyssaert, S., Margolis, H., Oleson, K. W., Roupsard, O., Veenendaal, E., Viovy, N., Williams, C., Woodward, F. I., and Papale, D. (2010). Terrestrial gross carbon dioxide uptake: Global distribution and covariation with climate. *Science*, 329, 834–838.

Bellassen, V. and Luyssaert, S. (2014). Managing forests in uncertain times. *Nature*, 506, 153-155.

Bernhard, F. (1970). Etude de la litière et de sa contribution au cycle des éléments minéraux en forêt ombrophile de Cote d'Ivoire. *Oecologia Plantarum*, 5 (3), 247-266.

Bicheron, P., Defourny, P., Brockmann, C., Schouten, L., Vancutsem, C., Huc, M., Bontemps, S., Leroy, M. (2008). GlobCover: Products description and validation report. ESA GlobCover project, 47 pp.

Biudes, M. S., Vourlitis, G. L., Machado, N. G., Zanella de Arruda, P. H., Neves, G. A. R., de Almeida, F., Neale, C. M. U. and de Souza Nogueira, J. (2015). Patterns of energy exchange for tropical ecosystems across a climate gradient in Mato Grosso, Brazil. *Agricultural and Forest Meteorology*, 202, 112-124.

Bonan, G. B. (2008). Forests and climate change: forcings, feedbacks, and the climate benefits of forests. *Science*, 320, 1444-1449.

Bontemps, S., Bogaert, P., Titeux, N., and Defourny, P. (2008). An object-based change detection method for dealing with temporal dependences in time series with medium to coarse spatial resolution. *Remote Sensing of Environment*, 112, 3181–3191.

Bontemps, S. (2010). Towards an automated satellite-based alarm system for global forest monitoring. Thesis at Faculté d'ingénierie biologique, agronomique et environnementale, Université catholique de Louvain.

Bontemps, S., Defourny, P., van Bogaert, E., Kalogirou, V., Ramos Perez, J. and Arino, O. (2011). GlobCover 2009: Products description and validation report. ESA GlobCover project, 53 pp.

Bontemps, S., Herold, M., Kooistra, L., van Groenestijn, A., Hartley, A., Arino, O., Moreau, I., and Defourny, P. (2012a). Revisiting land cover observations to address the needs of the climate modeling community. *Biogeosciences*, 9, 2145-2157.

Bontemps, S., Langner, A. and Defourny, P. (2012b). Monitoring forest changes in Borneo on a yearly basis by an object-based change detection algorithm using SPOT-VEGETATION time series, *International Journal of Remote Sensing*, 33, 4673–4699.

Bradley, A., V., Gerard, F. F., Barbier, N., Weedon, G. P., Anderson, L. O., Huntingford, C., Aragão, L. E. O. C., Zelazowski, P. and Arai, E. (2011). Relationships between phenology, radiation and precipitation in the Amazon region. *Global Change Biology*, 17, 2245-2260.

Brando, P., Goetz, S., Baccini, A., Nepstad, D., Beck, P. And Christman, M. (2010). Seasonal and interannual variability of climate and vegetation indices across the Amazon. *Proceedings of the National Academy of Sciences,* USA, 107, No. 33, 14685-14690.

Bright, C., Hicke, J. and Hudak, A. (2012). Estimating aboveground carbon stocks of a forest affected by mountain pine beetle in Idaho using lidar and multispectral imagery. *Remote Sensing of Environment*, 124, 270-281.

Brink, A. B., Bodart, C., Brodsky, L., Defourny, P., Ernst, C., Donney, F., Lupi, A. and Tuckova, K. (2014). Anthropogenic pressure in East Africa – Monitoring 20 years of land cover changes by means of medium resolution satellite data. *International Journal of Applied Earth Observation and Geoinformation*, 28, 60-69.

Brown, G. (2013). The relationship between social values for ecosystem services and global land cover: An empirical analysis. *Ecosystem Services*, In press.

Brown de Colstoun, E. and Walthall, C. (2006). Improving global scale land cover classifications with multi-directional POLDER data and a decision tree classifier. *Remote Sensing of Environment*, 100, 474-485.

Bucini, G. and Lambin, E. (2002). Fire impacts on vegetation in Central Africa: a remote-sensing-based statistical analysis. *Applied Geography*, 22, 27-48.

Caldararu, S., Palmer, P. I. and Purves, D.W. (2012). Inferring Amazon leaf demography from satellite observations of leaf area index. *Biogeosciences*, 9, 1389-1405.

Caldararu, S., Purves, D. W. and Palmer, P. I. (2014). Phenology as a strategy for carbon optimality: a global model. *Biogeosciences*, 11, 763-778.

Camberlin, P., Janicot, S. and Poccard, I. (2001). Seasonality and atmospheric dynamics of the teleconnection between African rainfall and tropical sea-surface temperature: Atlantic vs ENSO. *International Journal of Climatology*, 21 (8), 973-1005.

Carvalho, A., Monteiro, A., Flannigan, M., Solman, S., Miranda, A. I. and Borrego, C. (2011). Forest fires in a changing climate and their impacts on air quality. *Atmospheric Environment*, 45, 5545-5553.

Chen, X., Chen, J., Shi, Y. and Yamaguchi, Y. (2012). An automated approach for updating land cover maps based on integrated change detection and classification methods. *ISPRS Journal of Photogrammetry and Remote Sensing*, 71, 86-95.

Chipman, J. W. and Lillesand, T. M. (2007). Satellite-based assessment of the dynamics of new lakes in southern Egypt. *International Journal of Remote Sensing*, 28, 4365-4379.

Ciais, P., Bombelli, A., Williams, M., Piao, S. L., Chave, J., Ryan, C. M., Henry, M., Brender, P. and Valentini, R. (2011). The carbon balance of Africa: synthesis of recent research studies. *Philosophical Transactions of the Royal Society A*, 369, 2038-2057.

Cizungu, L., Staelens, J., Huygens, D., Walangululu, J., Muhindo, D., Van Cleemput, O. and Boeckx, P. (2014). Litterfall and leaf litter decomposition in a central African tropical mountain forest and *Eucalyptus* plantation. *Forest Ecology and Management*, 326, 109-116.

Colditz, R.R, Schmidt, M., Conrad, C., Hansen, M.C. and Dech, S. (2011). Land cover classification with coarse spatial resolution data do derive continuous and discrete maps for complex regions. *Remote Sensing of Environment*, 115, 3264-3275.

Coley, P. D., and Barone, J. A. (1996). Herbivory and plant defenses in tropical forests. *Annual Review of Ecology and Systematics*, 27, 305–335.

Coops, H., Beklioglu, M. and Crisman, T. L. (2003). The role of water-level fluctuations in shallow lake ecosystems - Work-shop conclusions. *Hydrobiologia*, 506-509, 23-27.

Couralet, C. (2010). Community dynamics, phenology and growth of tropical trees in the rain forest Reserve of Luki, Democratic Republic of Congo, Thesis at Faculteit Bio-Ingenieurswetenschappen, Ghent University.

Couralet, C. Sterck, F. J., Saas-Klaassen, U., Van Acker, J. and Beeckman, H. (2010). Species-specific growth responses to climate variations in understory trees of a Central African rainforest. *Biotropica*, 42, 503-511.

Couralet, C. (2011). Community dynamics, phenology and growth of tropical trees in the rain forest Reserve of Luki, Democratic Republic of Congo. Thesis at Faculteit Bio-Ingenieurswetenschappen, Ghent University.

Couralet, C., Van den Bulcke, J., Ngoma, L. M., Van Acker, J. and Beeckman, H. (2013). Phenology in functional groups of central African rainforest trees. *Journal of Tropical Forest Science*, 25 (3), 361-374.

Cox, P. M., Betts, R. A., Jones, C. D., Spall, S. A. and Totterdell, I. J. (2000). Acceleration of global warming due to carbon-cycle feedbacks in a coupled climate model. *Nature*, 408, 184-187.

da Rocha, H. R., Goulden, M. L., Miller, S. D., Menton, M. C., Pinto, L. D. V. O., de Freitas, H. C. and Figueira, A. M. S. (2004). Seasonality of water and heat fluxes over a tropical forest in eastern Amazonia. *Ecological Applications*, 14, S22–S32.

De Beurs, K. M. and Henebry, G. M. (2004). Land surface phenology, climatic variation, and institutional change: Analyzing agricultural land cover change in Kazakhstan. *Remote Sensing of Environment*, 89, 497-509.

de Gonçalves, L. G. G., Borak, J. S., Costa, M. H., Saleska, S. R., Baker, I., Restrepo-Coupe, N., Muza, M. N., et al. (2013). Overview of the large-scale biosphere–atmosphere experiment in Amazonia data model intercomparison project (LBA-DMIP). *Agricultural and Forest Meteorology*, 182–183, 111–127.

de Wasseige, C. and Defourny, P. (2002). Retrieval of tropical forest structure characteristics from bi-directional reflectance of SPOT images. *Remote Sensing of Environment*, 83, 362-375.

de Wasseige, C. and Defourny, P. (2003). Seasonal variation of tropical forest LAI based on field measurements in Central African Republic. *Agricultural and Forest Meteorology*, 119, 181-194.

De Weirdt, M., Verbeeck, H., Maignan, F., Peylin, P., Poulter, B., Bonal, D., Ciais, P. and Steppe, K. (2012). Seasonal leaf dynamics for tropical evergreen forests in a process-based global ecosystem model. *Geoscientific Model Development*, 5, 1091-1108.

Dantas, M. and Phillipson, J. (1999). Litterfall and litter nutrient content in primary and secondary Amazonian 'terra firme' rain forest. *Journal of Tropical Ecology*, 5, 27-36.

Defourny, P., Bicheron, P., Brockman, C., Bontemps, S., van Bogaert, E., Vancutsem, C., Pekel, J.F., Huc, M., Henry, C., Ranera, F., Achard, F., Di Gregorio, A., Herold, M., Leroy, M. and Arino, O. (2009a). The first 300 m global land cover map for 2005 using Envisat MERIS time series: a product of the GlobCover system. *Proceedings of the 33rd International Symposium on Remote Sensing of Environment*, Stresa, Italy, 4-8 May 2009, TS-5-1 (Ref 791).

Defourny, P., Schouten, L., Bartalev, S., Bontemps, S., Caccetta, P., de Wit, A.J.W., Di Bella, C.M., Gérard, B., Giri, C., Gond, V., Hazeu, G.W., Heiniman, A., Herold, M., Knoops, J., Jaffrain, G., Latifovic, R., Lin, H., Mayaux, P., Mucher, C.A., Nonguierma, A., Stibig, H.J., van Bogaert, E., Vancutsem, C., Bicheron, P., Leroy, M. and Arino O. (2009b). Accuracy assessment of a 300-m global land cover map: the GlobCover experience. *Proceedings of the 33rd International Symposium on Remote Sensing of Environment*, Stresa, Italy, 4-8 May 2009, PS-B1-3 (Ref 863).

DeFries, R. S. and Townshend, J. R. G. (1994). NDVI-derived land cover classification at a global scale. *International Journal of Remote Sensing*, 15, 3567-3586.

DeFries, R. S., Hansen, M., Townshend, J. R. G. and Sohlberg, R. (1998). Global land cover classifications at 8 km spatial resolution: the use of training data derived from Landsat imagery in decision tree classifiers. *International Journal of Remote Sensing*, vol. 19, n° 16, 3141-3168.

Demarée, G. R. (2009). Origins of the Word "Phenology". *Eos*, 34, 291.

Desclée, B., Bogaert, P., Defourny, P. (2006). Forest change detection by statistical object-based method. *Remote Sensing of Environment*, 102, 1−11.

Devineau, J. L. (1982). Etude pondérale des litères d'arbres dans deux types de forêts tropophiles en Côte d'Ivoire. In *Annales de l'Université d'Abidjan série E (écologie)*, 15, 27-62.

Di Gregorio, A. (2005). Land cover classification system: Classification concepts and user manual for software – version 2. *Food and Agriculture Organization of the United Nations,* Rome, Italy.

Dié, A., Kitin, P., N'Guessan Kouamé, F., Van den Bulcke, J., Van Acker, J. and Beeckman, H. (2012). Fluctuations of cambial activity in relation to precipitation result in annual rings and intra-annual growth zones of

xylem and phloem in teak (Tectona grandis) in Ivory Coast. *Annals of Botany*, 110(4), 861-873.

Djomo, A. N., Knohl, A. and Gravenhorst, G. (2011). Estimations of total ecosystem carbon pools distribution and carbon biomass current annual increment of a moist tropical forest. *Forest Ecology and Management,* 261, 1448-1459.

Dommergues, Y. (1965). Les cycles biogéochimiques des éléments minéraux dans les formations tropicales. *Bois et Forêts des Tropiques*, 87, 9-25.

Doughty, E., and Goulden, M. (2008). Seasonal patterns of tropical forest leaf area index and $CO_2$ exchange, *Journal of Geophysical Research, Vol. 113*, GB00B06.

Duveiller, G., Defourny, P., Desclée, B., Mayaux, P. (2008). Deforestation in Central Africa: Estimates at regional, national and landscape levels by advanced processing of systematically-distributed Landsat extracts. *Remote Sensing of Environment*, 112, 1969–1981.

Erlewein, A. (2013). Disappearing rivers - The limits of environmental assessment for hydropower in India. *Environmental Impact Assessment Review*, 43, 135-143.

Ernst, C., Mayaux, P., Verhegghen, A., Bodart, C., Musampa, C., and Defourny, P. (2013). National forest cover change in Congo Basin: deforestation, reforestation, degradation and regeneration for the years 1990, 2000 and 2005. *Global Change Biology*, 19, 1173–1187.

FAO (2010). Global Forest Resources Assessment 2010 – main report. In FAO (Ed.), Forestry Paper No. 163. Rome, Italy: Food and Agriculture Organization of the United Nations.

FAO (2012). Coping with water scarcity. FAO Water Reports, 38. Rome, Italy: Food and Agriculture Organization of the United Nations.

Fayolle, A., Picard, N., Doucet, J.-L., Swaine, M., Bayol, N., Bénédet, F. and Gourlet-Fleury, S. (2014). A new insight in the structure, composition and functioning of central African moist forests. *Forest Ecology and Management*, 329, 195-205.

Fisher, J. B., Sikka, M., Sitch, S., Ciais, P., Poulter, B., Galbraith, D., Lee, J., Huntingford, C., Viovy, N., Zeng, N., Ahlström, A., Lomas, M. R., Levy, P. E., Frankenberg, C., Saatchi, S. and Malhi, Y. (2013). African tropical rainforest net carbon dioxide fluxes in the twentieth century. *Philosophical Transactions of the Royal Society B*, 368, 20120376.

Foley, J., DeFries, R., Asner, G., Barford, C., Bonan, G., Carpenter, S., Chapin, S., Coe, M., Daily, G. Gibbs, H., Helkowski, J., Holloway, T.,

Howard, E., Kucharik, C., Monfreda, C., Patz, J., Prentice, I., Ramankutty, N., Snyder, P. (2005). Global consequences of land use. *Science*, 309, 570– 574.

Friedl, M.A., McIver, D.K., Hodges, J.C.F., Zhang, X.Y., Muchoney, D., Strahler, A.H., Woodcock, C.E., Gopal, S., Schneider, A., and Cooper, A. (2002). Global land cover mapping from MODIS: algorithms and early results. *Remote Sensing of Environment*, Vol. 83, Nos. 1 2, 287–302.

Friedl, M., Henebry, G.M., Reed, B.C., Huete, A., White, M.A., Morisette, J.T., Nemani, R., Zhang, X. and Myneni, R. (2006). Land Surface Phenology, A Community White Paper requested by NASA, ftp,//zeus.geog.umd.edu/Land_ESDR/Phenology_Friedl_white-paper.pdf, Apr 2006.

Friedl, M. A., Sulla-Menashe, D., Tan, B., Schneider A., Ramankutty, N., Sibley, A. and Huang, X. (2010). MODIS Collection 5 global land cover: Algorithm refinements and characterization of new datasets. *Remote Sensing of Environment*, 114, 168-182.

Friedlingstein, P., Cadule, P., Piao, S. L., Ciais, P. and Sitch, S. (2010). The African contribution to the global climate-carbon cycle feedback of the 21st century. *Biogeosciences*, 7, 513-519.

Fritz, H. M., Blount, C., Sokoloski, R., Singleton, J., Fuggle, A., McAdoo, B. G., Moore, A., Grass, C. and Tate, B. (2007). Hurricane Katrina storm surge distribution and field observations on the Mississippi Barrier Islands. *Estuarine, Coastal and Shelf Science*, 74, 12-20.

Fritz, S., Bartholome, E., Belward, A., Hartley, A., Stibig, H. -J., Eva, H., et al. (2003). Harmonization, mosaicking, and production of the Global Land Cover 2000 database. Ispra, Italy7 Joint Research Center (JRC).

Fritz, S., Bartholomé, E., Belward, A., Hartley, A., Stibig, H. -J., Eva, H., Mayaux, P., Bartalev, S. Latifovic, R., Kolmert, S., Roy, P. S., Agrawal, S., Bingfang, W., Wenting, X., Ledwith, M., Pekel, J.-F., Giri, C., Mucher, S., de Badts, E., Tateishi, R., Champeau, J.-L., and Defourny, P. (2003). Harmonisation, mosaicing and production of the Global Land Cover 2000 database (Beta Version). Ispra: European Commission, Joint Research Centre (JRC).

Fritz, S. and See, L. (2008). Identifying and quantifying uncertainty and spatial disagreement in the comparison of Global Land Cover for different applications. *Global Change Biology*, 14, 1057–1075.

Galvão, L., dos Santos, J., Roberts, D., Breunig, F., Toomey, M., Mendes de Moura, Y. (2011). On intra-annual EVI variability in the dry season of

tropical forest: A case study with MODIS and hyperspectral data, *Remote Sensing of Environment, 115, 2350-2359*.

Galvão, L. S., Breunig, F. M., dos Santos, J. R. and de Moura, Y. M. (2013). View-illumination effects on hyperspectral vegetation indices in the Amazonian tropical forest. *International Journal of Applied Earth Observation and Geoinformation*, 21, 291-300.

Gardiner, B., Blennow, K., Carnus, J.-M., Fleischer, P., Ingemarson, F., Landmann, G., Lindner, M., Marzano, M., Nicoll, B., Orazio, C., Peyron, J.-L., Reviron, M.-P., Schelhaas, M.-J., Schuck, A., Spielmann, M., and Usbeck, T. (2010). Destructive Storms in European Forests: Past and Forthcoming Impacts. European Forest Institute, Final report to European Commission - DG Environment, 138 pp.

GCOS – Global Climate Observing System: Implementation plan for the Global Observing System for Climate in Support of the UNFCCC, World Meteorological Organisation, GCOS report 138 (August 2010 – update), 186 pp., 2010.

Giri, C., Zhu, Z. and Reed, B. (2005). A comparative analysis of the Global Land Cover 2000 and MODIS land cover data sets. *Remote Sensing of Environment*, 94, 123-132.

Giri, C., Pengra, B., Long, J., Loveland, T.R. (2013). Next generation of global land cover characterization, mapping, and monitoring. *International Journal of Applied Earth Observation and Geoinformation*, 25, 30-37.

Gond, V., Fayolle, A., Pennec, A., Cornu, G., Mayaux, P., Camberlin, P., Doumenge, C., Fauvet, N. and Gourlet-Fleury, S. (2013). Vegetation structure and greenness in Central Africa from MODIS multi-temporal data. *Philosophical Transactions of the Royal Society B*, 368, 20120309.

Goulden, M. L., Miller, S. D., da Rocha, H. R., Menton, M. C., de Freitas, H. C., e Silva Figueira, A. M. and de Sousa, C. A. D. (2004). Diel and seasonal patterns of tropical forest $CO_2$ exchange. *Ecological Applications*, 14, 42–54.

Gourlet-Fleury, S., Rossi, V., Rejou-Mechain, M., Freycon, V., Fayolle, A., Saint André, L., Cornu, G., Gérard, J., Sarrailh, J.M., Flores, O., Baya, F., Billand, A., Fauvet, N., Gally, M., Henry, M., Hubert, D., Pasquier, A. and Picard N. (2011). Environmental filtering of dense-wooded species controls above-ground biomass stored in African moist forests. *Journal of Ecology*, 99, 981-990.

Gourlet-Fleury, S., Mortier, F., Fayolle, A., Baya, F., Ouédraogo, D., Bénédet, F. and Picard, N. (2013). Tropical forest recovery from

logging: a 24 year silvicultural experiment from Central Africa. *Philosophical Transactions of the Royal Society B*, 368, 20120302.

Govaerts, Y. (1997). Characterization of the impact of forest architecture on AVHRR bands 1 and 2 observations. Technical report, Space Applications Institute.

Graham, E., Mylkey, S., Kitajima, K., Phillips, N. and Wrights, S. (2003). Cloud cover limits net $CO_2$ uptake and growth of a rainforest tree during tropical rainy season, *Proceedings of the Natural Academy of Sciences,* 100, 572-576.

Griffiths, P., Kuemmerle, T., Baumann, M., Radeloff, V. C., Abrudan, I. V., Lieskovsky, J., Munteanu, C., Ostapowicz, K. and Hostert, P. (2014). Forest disturbances, forest recovery, and changes in forest types across the Carpathian ecoregion from 1985 to 2010 based on Landsat image composites. *Remote Sensing of Environment*, 151, 72-88.

Groenendijk, P., Sass-Klaassen, U., Bongers, F. and Zuidema, P. A. (2014). Potential of tree-ring analysis in a wet tropical forest: A case study on 22 commercial tree species in Central Africa. *Forest Ecology and Management*, 323, 65-78.

Han, D. Song, X., Currell, M. J., Cao, G., Zhang, Y. and Kang, Y. (2011). A survey of groundwater levels and hydrogeochemistry in irrigated fields in the Karamay Agricultural Development Area, northwest China: Implications for soil and groundwater salinity resulting from surface water transfer for irrigation. *Journal of Hydrology*, 405, 217-234.

Hansen, M. C., DeFries, R. S., Townshend, J. R. G. and Sohlberg, R. (2000). Global land cover classification at 1 km spatial resolution using a classification tree approach. *International Journal of Remote Sensing*, vol. 21, n° 6-7, 1331-1364.

Hansen, M.C., Roy, D.P., Lindquist, E., Adusei, B., Justice, C.O., and Altstatt, A. (2008). A method for integrating MODIS and Landsat data for systematic monitoring of forest cover and change in the Congo Basin. *Remote Sensing Of Environment*, 112 (5), 2495–2513.

Hansen, M. C. and Reed, B. (2000). A comparison of the IGBP DISCover and University of Maryland 1 km global land cover products. *International Journal of Remote Sensing*, vol. 21, n° 6-7, 1365-1373.

Hansen, M. C. and Loveland, T. R. (2012). A review of large area monitoring of land cover change using Landsat data. *Remote Sensing of Environment*, 122, 66-74.

Hansen, M. C., Potapov, P. V., Moore, R., Hancher, M., Turubanova, S. A., Tyukavina, A., Thau, D., Stehman, S. V., Goetz, S. J., Loveland, T. R.,

Kommareddy, A., Egorov, A., Chini, L., Justice, C. O. and Townshend, J. R. G. (2013). High-Resolution Global Maps of 21st-Century Forest Cover Change. *Sciences*, vol. 342, 850-853.

Haugaasen, T. and Peres, C. A. (2005). Tree phenology in adjacent Amazonian flooded and unflooded forests. *Biotropica*, 37 (4), 620-630.

Herold, M., Mayaux, P., Woodcock, C. E., Baccini, A. and Schmullius C. (2008). Some challenges in global land cover mapping: An assessment of agreement and accuracy in existing 1 km datasets. *Remote Sensing of Environment*, 112, 2538-2556.

Hladik, A. (1978). Phenology of leaf production in rain forest of Gabon: Distribution and composition of food for folivores. *The Ecology of arboreal Folivores*, Smithsonian Institution Press, Washington, 51-71.

Hope, B. (2012). Egypt's new Nile Valley: Grand plan gone bad. *The National*, 12 April.

Houghton, R. A. (2010). How well do we know the flux of $CO_2$ from land-use change? *Tellus B*, 62, 337-351.

Houghton, R. A., House, J. I., Pongratz, J., van der Werf, G. R., DeFries, R. S., Hansen, M. C., Le Quéré, C. and Ramankutty, N. (2012). Carbon emissions from land use and land-cover change. *Biogeosciences*, 9, 5125-5142.

Huang, C., Kim, S., Altstatt, A., Townshend, J., Davis, P., Song, K., Tucker, C., Rodas, O., Yanosky, A., Clay, R., Musinsky, J. (2007). Rapid loss of Paraguay's Atlantic forest and the status of protected areas — A Landsat assessment. *Remote Sensing of Environment*, 106, 460-466.

Huang, X. and Friedl, M. A. (2014). Distance metric-based forest cover change detection using MODIS time series. *International Journal of Applied Earth Observation and Geoinformation*, 29, 78-92.

Huete, A. R., Liu, H. Q., Batchily, K. and van Leeuwen, W. (1997). A comparison of Vegetation Indices over a global set of TM images for EOS-MODIS. *Remote Sensing of Environment*, 59, 440-451.

Huete, A., Didan, K., Miura, T., Rodriguez, E. P., Gao, X. and Ferreira, L. G. (2002). Overview of the radiometric and biophysical performance of the MODIS vegetation indices. *Remote Sensing of Environment*, 83, 195-213.

Huete, A., Didan, K., Shimabukuro., Y., Ratana, P., Saleska, S., Hutyra, L., Yang, W., Nemani, R., and Myneni, R. (2006). Amazon rainforests green-up with sunlight in dry season. *Geophysical Research Letters,* 33, L06405.

Huete, A., Restrepo-Coupe, N., Didan, K., Saleska, S. R., Ichi, K., Panuthai, S. and Gamo, M. (2008). Multiple site tower flux and remote sensing comparisons of tropical forest dynamics in Monsoon Asia. *Agricultural and Forest Meteoroloy,* 148, 748-760.

Huntingford, C., Zelazowski, P., Galbraith, D., Mercado, L. M., S.itch, S, Fisher, R., Lomas, M., Walker, A. P., Jones, C. D., Booth, B. B. B., Malhi, Y., Hemming, D., Kay, G., Good, P., Lewis, S. L., Phillips, O. L., Atkin, O. K., Lloyd, J., Gloor, E., Zaragoza-Castells, J., Meir, P., Betts, R., Harris, P. P., Nobre, C., Marengo, J. and Cox, P. M. (2013). Simulated resilience of tropical rainforests to $CO_2$-induced climate change. *Nature Geoscience*, 6 (4), 268-273.

Hussain, M., Chen, D., Cheng, A., Wei, H. and Stanley, D. (2013). Change detection from remotely sensed images: From pixel-based to object-based approaches. *ISPR Journal of Photogrammetry and Remote Sensing*, 80, 91-106.

Hutyra, L., R., Munger, J. W., Nobre, C. A., Saleska, S. R., Vieira, S. A. and Wofsy, S. C. (2005). Climatic variability and vegetation vulnerability in Amazonia. *Geophysical Research Letters*, 32, L24712.

Hutyra, L., Munger, J., Nobre, C., Saleska, S., Vieira, S., and Wofsy, S. (2007). Seasonal controls on the exchange of carbon and water in Amazonian rain forest. *Journal of Geophysical Research*, 112, G03008.

Hutyra, L.R., Munger, J. W., Hammond-Pyle, E., Saleska, S. R., Restrepo-Coupe, N., Daub, B. C., de Camargo, P. B. and Wasfy, S. C. (2008). Resolving systematic errors in estimates of net ecosystem exchange of $CO_2$ and ecosystem respiration in a tropical forest biome. *Agricultural and Forest Meteorology*, 48, 1266-1279.

Hutyra, L., Yoon, B., Hepinstall-Cymerman, J., Alberti, M. (2011). Carbon consequences of land cover change and expansion of urban lands: A case study in the Seattle metropolitan region. *Landscape and urban planning*, 103, 83-93.

Ichii, K., Hashimoto, H., Nemani, R. and White, M. (2005). Modeling the interannual variability and trends in gross and net primary productivity of tropical forests from 1982 to 1999. *Global and Planetary Change*, 48, 274-286.

Ichii, K., Hashimoto, H., White, M., Potter, C., Hutyra, L., Huete, A., Myneni, R., and Nemani, R. (2007). Constraining rooting depths in tropical rainforests using satellite data and ecosystem modeling for accurate simulation of gross primary production seasonality. *Global Change Biology,* 13, 67-77.

IPCC (2014). Climate Change 2014: Synthesis Report. Contribution of Working Groups I, II and III to the Fifth Assessment Report of the Intergovernmental Panel on Climate Change [Core Writing Team, R.K. Pachauri and L.A. Meyer (eds.)]. IPCC, Geneva, Switzerland, 151 pp.

James, R., Washington, R. and Rowell, D. P. (2013). Implications of global warming for the climate of African rainforests. *Philosophical Transactions of the Royal Society B*, 368, 20120298.

Jansen, L. J. M. and Di Gregorio, A. (2002). Parametric land cover and land-use classifications as tools for environmental change detection. *Agriculture Ecosystems and Environment*, 91, 89-100.

Jeong, S.-J., Ho, C.-H., Gim, H.-J. and Brown, M. E. (2011). Phenology shifts at start vs. end of growing season in temperate vegetation over the northern hemisphere for the period 1982–2008. *Global Change Biology*, 17, 2385–2399.

Jin, S., Yang, L., Danielson, P., Homer, C., Fry, J. and Xian, G. (2013). A comprehensive change detection method for updating the National Land Cover Database to circa 2011. *Remote Sensing of Environment*. 132, 159-175

Jung, M., Henkel, K., Herold, M. and Churkina, G. (2006). Exploiting synergies of global land cover products for carbon cycle modeling. *Remote Sensing of Environment*, 101, 534-553.

Kaptué Tchuenté, A. T., Roujean, J.-L. and De Jong, S. (2011). Comparison and relative quality assessment of the GLC2000, GLOBCOVER, MODIS and ECOCLIMAP land cover data sets at the African continental scale. *International Journal of Applied Earth Observation and Geoinformation*, 13, 207-219.

Karnieli, A., Kaufman, Y., Remer, L., and Wald, A. (2001). AFRI – aerosol free vegetation index. *Remote Sensing of Environment,* 77, 10-21.

Karnieli, A., Gilad, U., Ponzet, M., Svoray, T., Mirzadinov, R. and Fedorina, O. (2008). Assessing land-cover change and degradation in the Central Asian deserts using satellite image processing and geostatistical methods. *Journal of Arid Environments*, 72, 2093-2105.

Kearsley, E., de Haulleville, T., Hufkens, K., Kidimbus, A., Toirambe, B., Baert, G., Huygens, D., Kebede, Y., Defourny, P., Bogaert, J., Beeckman, H., Steppe, K., Boeckx, P. and Verbeeck, H. (2013). Conventional tree height–diameter relationships significantly overestimate aboveground carbon stocks in the Central Congo Basin. *Nature Communications*, 4, 2269.

Klein, I., Dietz, A. J.,, Gessner, U., Galayeva, A., Myrzakhmetov, A. and Kuenzer, C. (2014). Evaluation of seasonal water body extents in Central Asia over the past 27 years derived from medium-resolution remote sensing data. *International Journal of Applied Earth Observation and Geoinformation*, 26, 335-349.

Kobayashi, H. and Dye, D. (2005). Atmospheric conditions for monitoring the long-term vegetation dynamics in the Amazon using normalized difference vegetation index. *Remote Sensing of Environment,* 97, 519-525.

Koffi, B., Grégoire, J.-M., Mahé, G. and Lacaux, J.-P. (1995). Remote sensing of bush fire dynamics in Central Africa from 1984 to 1988 : analysis in relation to regional vegetation and pluviometric patterns. *Atmospheric Research*, 39, 179-200.

Koltunov, A., Ustin, S. L., Asner, G. P., and Fung, I. (2009). Selective logging changes forest phenology in the Brazilian Amazon: Evidence from MODIS image time series analysis. *Remote Sensing of Environment*, 113, 2431-2440.

Kumar, D. and Katoch, S. S. (2014). Sustainability in indicators for run of the river (RoR) hydropower projects in hydro rich regions of India. *Renewable and Sustainable Energy Reviews*, 35, 101-108.

Lambin, E. F., Turner, B. L., Geist, H. J., Agbola, S. B., angelsen, A., Bruce, J. W., Coomes, O. T., Dirzo, R., Fisher, G., Folke, C., George, P. S., Homewood, K. et al. (2001). The causes of land-use and land-cover change: moving beyond the myths. *Global Environmental Change*, 11, 261-269.

Langner, A., Miettinen, J. and Siegert, F. (2007). Land cover change 2002–2005 in Borneo and the role of fire derived from MODIS imagery. *Global Change Biology*, 13, 2329–2340.

Latifovic, R. and Olthof, I. (2004). Accuracy assessment using sub-pixel fractional error matrices of global land cover products derived from satellite data. *Remote Sensing of Environment*, 90, 153-165.

Latifovic, R., Fytas, K., Chen, J., Paraszczak, J. (2005). Assessing land cover change resulting from large surface mining development. *International Journal of Applied Earth Observation and Geoinformation*, 7, 29–48.

Laudelout, H. and Meyer, J. (1954). Les cycles d'éléments minéraux et de matière organique en forêt équatoriale congolaise. *5ème Congrès international scientifique du sol*, Léopoldville, 2, 312-321.

Lepers, E., Lambin, E., Janetos, A., DeFries, R., Achard, F., Ramankutty, N. and Scholes, R. (2005). A synthesis of information on rapid land-cover change for the period 1981-2000. *BioScience*, 55, 115-124.

Lewis, S. L. (2006). Tropical forests and the changing earth system. *Philosophical Transactions of the Royal Society B*, 361, 195-210.

Lewis, S. L., Lopez-Gonzalez, G., Sonke, B., Affum-Baffoe, K., Baker, T. R., Ojo, L. O., Phillips, O. L., Reitsma, J. M., White, L., Comiskey, J. A., Djuikouo K, M.-N., Ewango, C. E. N., Feldpausch, T. R., Hamilton, A. C., Gloor, M., Hart, T., Hladik, A., Lloyd, J., Lovett, J. C., Makana, J.-R., Malhi, Y., Mbago, F. M., Ndangalasi, H. J., Peacock, J., Peh, K. S. H., Sheil, D., Sunderland, T., Swaine, M. D., Taplin, J., Taylor, D., Thomas, S. C., Votere, R. and Woell, H. (2009). Increasing carbon storage in intact African tropical forests. *Nature*, 457, 1003-U1003.

Lewis, S. L., Brando, P. M., Phillips, O. L., van der Heijden, G. M. F. and Nepstad, D. (2011). The 2010 Amazon drought. *Sciences*, 331, 554.

Lewis, S. L., Sonké, B., Sunderland, T., Begne, S. K., Lopez-Gonzalez, G., van der Heijden, G. M. F., Phillips, O. L., Affum-Baffoe, K., Baker, T. R., Banin, L., Bastin, J. F., Beeckman, H., Boeckx, P., Bogaert, J., De Cannière, C., Chezeaux, E., Clark, C. J., Collins, M., Djagbletey, G., Djuikouo, M. N. K., Droissart, V., Doucet, J. L., Ewango, C. E. N., Fauset, S., Feldpausch, T. R., Foli, E. G., Gillet, J. F., Hamilton, A. C., Harris, D. J., Hart, T. B., de Haulleville, T., Hladik, A., Hufkens, K., Huygens, D., Jeanmart, P., Jeffery, K. J., Kearsley, E., Leal, M. E., Lloyd, J., Lovett, J. C., Makana, J. R., Malhi, Y., Marshall, A. R., Ojo, L., Peh, K.S.-H., Pickavance, G., Poulsen, J. R., Reitsma, J. M., Sheil, D., Simo, M., Steppe, K., Taedoumg, H. E., Talbot, J., Taplin, J. R. D., Taylor, D., Thomas, S. C., Toirambe, B., Verbeeck, H., Vleminckx, J., White, L. J. T., Willcock, S., Woell, H. and Zemagho, L. (2013). Above-ground biomass and structure of 260 African tropical forests. *Philosophical Transactions of the Royal Society B,* 368, 20120295.

Li, W., Fu, R. and Dickinson, R. E. (2006). Rainfall and its seasonality over the Amazon in the 21st century as assessed by the coupled models for the IPCC AR4. *Journal of Geophysical Research*, 111, D02111.

Li, W., Fu, R., Juárez, R. I. N. and Fernandes, K. (2008). Observed change of the standardized precipitation index, its potential cause and implications to future climate change in the Amazon region. *Philosophical Transactions of the Royal Society B: Biological Sciences*, *363*(1498), 1767–1772.

Link, L. E. (2010). The anatomy of a disaster, an overview of Hurricane Katrina and New Orleans. *Ocean Engineering*, 37, 4-12.

Loveland, T. R., Reed, B. C., Brown, J. F., Ohlen, D. O., Zhu, Z., Yang, L. and Merchant, J. W. (2000). Development of a global land cover characteristics database and IGBP DISCover from 1 km AVHRR data. *International Journal of Remote Sensing*, vol. 21, n° 6-7, 1303-1330.

Lubini, C. A. (1997). La végétation de la Réserve de Biosphère de Luki au Mayombe (Zaïre). *Jardin Botanique National de Belgique,* Meise, Belgium.

Lyapustin, A. I., Wang, Y., Laszlo, I., Hilker, T., Hall, F. G., Sellers, P. J., Tucker, C. J. and Korkin, S. V. (2012). Multiangle implementation of atmospheric correction (MAIAC): 3. Atmospheric correction. *Remote Sensing of Environment*, 127, 385-393.

Lunetta, R. S., Knight, J. F., Ediriwickrema, J., Lyon, J. G. and Worthy, L. D. (2006). Land-cover change detection using multi-temporal MODIS NDVI data. *Remote Sensing of Environment*, 105, 142-154.

Ma, X., Huete, A., Yu, Q., Restrepo-Coupe, N., Beringer, J., Hutley, L. B., Kanniah, K. D., Cleverly, J. and Eamus, D. (2014). Parameterization of an ecosystem light-use-efficiency model for predicting savanna GPP using MODIS EVI. *Remote Sensing of Environment*, 154, 253-271.

Maeda, E. E., Heiskanen, J., Aragão, L. E. O. C. and Rinne, J. (2014). Can MODIS EVI monitor ecosystem productivity in the Amazon rainforest? *Geophysical Research Letters*, 41, doi:10.1002/2014GL061535.

Maharjan, S. K., Poorter, L., Holmgren, M., Bongers, F., Wieringa, J. J. and Hawthorne, W. D. (2011). Plant functional traits and the distribution of west African rain forest trees along the rainfall gradient. *Biotropica*, 43 (5), 552-561.

Maignan, F., Bréon, F.-M. and Lacaze, R. (2004). Bidirectional reflectance of Earth targets: Evaluation of analytical models using a large set of spaceborne measurements with emphasis on the Hot Spot. *Remote Sensing of Environment*, 90, 210-220.

Maignan, F. (2011). Télédétection des surfaces continentales: corrections des signatures directionnelles et suivi phénologique, Doctorat de l'Université de Versailles Saint-Quentin en Yvelines, Ecole Doctorale des Sciences de l'Environnement d'Ile de France.

Malhado, A. C. M., Costa, M. H., de Lima, F. Z., Portilho, K. C. and Figueiredo, D. N. (2009), Seasonal leaf dynamics in an Amazonian tropical forest. *Forest Ecology and Management*, 258(7), 1161-1165.

Malhi, Y., Pegoraro, E., Nobre, A.D., Pereira, M. G. P., Grace, J., Culf, A. D. and Clement, R. (2002). Energy and water dynamics of a central Amazonian rain forest. *Journal Geophysical Research*, 107.

Malhi, Y. and Wright, J. (2004). Spatial patterns and recent trends in the climate of tropical rainforest regions. *Philosophical Transactions of the Royal Society of London Series B: Biological Sciences,* 359, 311–329.

Malhi, Y., Wood, D., Baker, Wright, J., Phillips, O., Cochrane, T., Meir, P., Chave, J., Almeida, S., Arroyo, L., Higuchi, N., Killen, T., Laurance, S., Laurance, W., Lewis, S., Monteagudo, A., Neill, D., Vargas, P., Pitman, N., Quesada, C., Salomao, R., Silva, J., Lezama, A., Terborgh, J., Martinez, R., Vinceti, B. (2006). The regional variation of aboveground live biomass in old-growth Amazonian forests. *Global Change Biology*, 12, 1-32.

Malhi, Y., Roberts, J., Betts, R., Killen, T., Li, W., Nobre, C. (2008). Climate change, deforestation, and the fate of the Amazon. *Science, Vol. 319,* 169-172.

Malhi, Y., Adu-Bredu, S., Asare, R. A., Lewis, S. L. and Mayaux, P. (2013). African rainforests : past, present and future. *Philosophical transactions of the Royal Society B, 368*, 20120312.

Mane, L., Adusei, B., Altstatt, A., Amani, P., Bankanza, B., Bong- wele, E., Broich, M., Devers, D., Hansen, M., Justice, C., Mun- zimi, Y., Potapov, P., and Turubanova, S. (2010). Monitoring the forests of Central Africa using remotely sensed data sets (FACET). Forest cover and forest cover loss in the Democratic Republic of Congo from 2000 to 2010, South Dakota State University, Brookings, South Dakota, USA, 2010.

Matthews, E. (1983). Global vegetation and land-use: New-high resolution data bases for climate studies. *Journal of Climate and Applied Meteorology*, 22, 474–487.

Mayaux, P., Richards, T. and Janodet, E. (1999). A vegetation map of Central Africa derived from satellite imagery. *Journal of Biogeography*, 25, 353-366.

Mayaux, P., Bartholome, E., Fritz, S. and Belward, A. (2004). A new land-cover map of Africa for the year 2000. *Journal of Biogeography*, 31 (6), 861-877.

Mayaux, P., Eva, H., Gallego, J., Strahler, A. H., Herold, M., Agrawal, S., Naumov, S., De Miranda, E. E., Di Bella, C. M., Ordoyne, C. and Kopin, Y. (2006). Validation of the Global Land Cover 2000 Map. *IEEE Transactions on Geoscience and Remote Sensing*, 44, 1728-1739.

Mayaux, P., Pekel, J.-F., Desclée, B., Donnay, F., Lupi, A., Achard, F., Clerici, M., Bodart, C., Brink, A., Nasi, R. and Belward, A. (2013). State and evolution of the African rainforests between 1990 and 2010. *Philosophical Transactions of the Royal Society B*, 368, 20120300.

McCallum, I., Obersteiner, M., Nilsson, S. and Shvidenko, A. (2006). A spatial comparison of four satellite derived 1 km global land cover datasets. *International Journal of Applied Earth Observation and Geoinformation*, 8, 246-255.

McGuire, B. (2009). Event Report: Disasters bulletin 31 October 2008 to 30 July 2009. *Catastrophe risk management (Global Reinsurance Special Report)*, Sept. 2009, 62-63.

McRoberts, R. E. (2013). Post-classification approaches to estimating change in forest area using remotely sensed auxiliary data. *Remote Sensing of Environment*, 151, 149-156.

Menzel, A. (2002). Phenology: Its Importance to the Global Change Community. *Climatic Change*, 54 (4), 379–385.

Menzel, A., Sparks, T.H., Estrella, N., Koch, E., Aasa, A., Ahas, R., Alm-Kübler, K., Bissolli, P., Braslavská, O., Briede, A., Chmielewski, F.M., Crepinsek, Z., Curnel, Y., Dahl, Å., Defila, C., Donnelly, A., Filella, Y., Jatczak, K., Måge, F., Mestre, A., Nordli, Ø., Peñuelas, J., Pirinen, P., Remišová, V., Scheifinger, H., Striz, M., Susnik, A., Van Vliet, A.J.H., Wielgolaski, F.-E., Zach, S., Zust, A., Alm-Kuebler, K., Braslavska, O., Dahl, A., Jatcza, K., Mage, F., Nordli, O., Penuelas, J. and Remisova, V. (2006). European phenological response to climate change matches the warming pattern. *Global Change Biology*, 12 (10), 1969–1976.

Migliavacca, M., Sonnetag, O., Keenan, T. F., Cescatti, A., O'Keefe, J. and Richardson, A. D. (2012). On the uncertainty of phenological responses to climate change, and implications for a terrestrial biosphere model. *Biogeosciences*, 9, 2063-2083.

Mitchard, E. T. A., Saatchi, S. S., White, L. J. T., Abernethy, K. A., Jeffery, K. J., Lewis, S. L., Collins, M., Lefsky, M. A., Leal, M. E., Woodhouse, I. H. and Meir, P. (2012).Mapping tropical forest biomass with radar and spaceborne LiDAR in Lopé National Park, Gabon: overcoming problems of high biomass and persistent cloud. *Biogeosciences*, 9, 179-191.

Morisette, J.T., Richardson, A.D., Knapp, A.K., Fisher, J.I., Graham, E. a, Abatzoglou, J., Wilson, B.E., Breshears, D.D., Henebry, G.M., Hanes, J.M. and Liang, L. (2009). Tracking the rhythm of the seasons in the face of global change: phenological research in the 21st century. *Frontiers in Ecology and the Environment*, 7 (5), 253–260.

Morton, D. C., Nagol, J., Carabajal, C. C., Rosette, J., Palace, M., Cook, B. D., Vermote, E. F., Harding, D. J. and North, P. R. J. (2014). Amazon forests maintain consistent canopy structure and greenness during the dry season. *Nature*, 506, 221-224.

Moura, Y. M., Galvão, L. S., dos Santos, J. R., Roberts, D. A. and Breunig, F. M. (2012). Use of MISR/Terra data to study intra- and inter-annual EVI variations in the dry season of tropical forest. *Remote Sensing of Environment*, 127, 260-270.

Mpounza, M and Samba-Kimbata, M. J. (1990). Aperçu sur le climat de l'Afrique centrale occidentale. *Paysages quaternaires de l'Afrique Centrale*, R. Lanfranchi and D. Schwartz, eds. ORSTOM, Paris, 31-41.

Myneni, R. B., Yang, W. Z., Nemani, R. R., Huete, A. R., Dickinson, R. E., Knyazikhin, Y., Didan, K., Fu, R., Juarez, R. I. N., Saatchi, S. S., Hashimoto, H., Ichii, K., Shabanov, N. V., Tan, B., Ratana, P., Privette, J. L., Morisette, J. T., Vermote, E. F., Roy, D. P., Wolfe, R. E., Friedl, M. A., Running, S. W., Votava, P., El-Saleous, N., Devadiga, S., Su, Y., and Salomonson, V. (2007). Large seasonal swings in leaf area of Amazon rainforests. *Proceedings of the National Academy of Sciences* USA, 104, 4820-4823.

Nakaji, T., Kosugi, Y., Takanashi, S., Niiyama, K., Noguchi, S., Tani, M., Oguma, H.,Nik, A. R. and Kassim, A. R. (2014). Estimation of light-use efficiency through a combinational use of the photochemical reflectance index and vapor pressure deficit in an evergreen tropical rainforest at Pasoh, Peninsular Malaysia. *Remote Sensing of Environment*, 150, 82-92.

Nelson, B. W., Tavares, J. V., Wu, J., Valeriano, D. M., Lopes, A. P., Marostica, S. F., Martins, G., Prohaska, N., Albert, L., De Araujo, A. C., Manzi, A. O., Saleska, S. R. and Huete, A. R. (2014). Seasonality of central Amazon forest leaf flush using tower-mounted RGB camera. *AGU Fall* 2014, Abstract B11G-107.

Nemani, R. R., Keeling, C. D., Hashimoto, H., Jolly, W. M., Piper, S. C., Tucker, C. J., Myneni, R. B. and Running, S. W. (2003). Climate-driven increases in global terrestrial net primary production from 1982 to 1999. *Science*, 300, 1560– 1563.

Nepstad, D., de Carvalho, C., Davidson, E., Jipp, P., Lefebvre, P., Negreiros, G., da Silva, E., Stone, T., Trumbore, S., and Vieira, S. (1994). The role of deep roots in the hydrological and carbon cycles of amazonian forests and pastures. *Nature,* 372, 666– 669.

Nunes, E. L., Costa, M. H., Malhado, A. C. M., Dias, L. C. P., Vieira, S. A., Piton, L. B. and Ladle, R. J. (2012). Monitoring carbon assimilation in South America's tropical forests: Model specification and application to the Amazonian droughts of 2005 and 2010. *Remote Sensing of the Environment*, 117, 449-463.

Nyirambangutse, B., Dusenge, E. M., Nsabimana, D., Bizuru, E., Pleijel, H., Fredin, J. U. and Wallin, G. (2014). Variation in leaf litter production and resorption of nutrients in abundant tree species in Nyungwe Afromontane tropical rainforest in Rwanda. *Geophysical Research Abstracts*, 16, EGU2014-14278.

Oliveira, P. H. F., Artaxo, P., Pires, C., De Lucca, S., Procopio, A., Holben, B., Schafer, J., Cardoso, L. F., Wofsy, S. C. and Rocha, H. R. (2007). The effects of biomass burning aerosols and clouds on the $CO_2$ flux in Amazonia. *Tellus*, 59B, 338-349.

Olson, J. S., and Watts, J. (1982). Major world ecosystem complexes. In Earth's Vegetation And Atmospheric Carbon Dioxide, In Carbon Dioxide Review, D. B. Jones (ed.), Oxford University Press, Oxford, pp. 388–399.

Olson, J., Watts, J. A. and Allison, L. J. (1983). Carbon in Live Vegetation of Major World Ecosystems. ORNL-5862, Oak Ridge National Laboratory, Oak Ridge, Tennessee, 164 pp.

OSFAC (2010). Forêts d'Afrique centrale évaluées par télédétection (FACET). Etendue et perte du couvert forestier en République Démocratique du Congo de 2000 à 2010, South Dakota State University, Brookings, South Dakota, USA.

Othman, A. A., Al-Saady, Y. I., Al-Khafaji, A. K. and Gloaguen, R. (2014). Environmental change detection in the central part of Iraq using remote sensing data and GIS. *Arab Journal Geoscience*, 7, 1017-1028.

Pan, Y., Birdsey, R., Fang, J., Houghton, R., Kauppi, P., Kurz, W., Phillips, O., Shvidenko, A., Lewis, S., Canadell, J., Ciais, P., Jackson, R., Pacala, S., McGuire, D., Piao, S., Rautiainen, A., Sitch, S. and Hayes, D. (2011). A Large and Persistent Carbon Sink in the World's Forests. *Sciences*, 333, 988-993.

Peel, M. C., Finlayson, B. L., and McMahon, T. A. (2007). Updated world map of the Köppen-Geiger climate classification. *Hydrology and Earth System Sciences*, 11, 1633–1644.

Pennec, A., Gond, V., and Sabatier, D. (2011), Tropical forest phenology in French Guiana from MODIS time-series. *Remote Sensing Letters*, 2:4, 337-345.

Pflugmacher, D., Krankina, O., Cohen, W., Friedl, M. A., Sulla-Menashe, D., Kennedy, R., Neslon, P., Loboda, T., Kuemmerle, T., Dyukarev, E., Elsakov, V. and Kharuk, V. (2011). Comparison and assessmenf of coarse resolution land cover maps for Northern Eurasia. *Remote Sensing of Environment*, 115, 3539-3553.

Phillips, O. L., Aragão, L. E. O. C., Lewis, S. L., Fisher, J. B., Lloyd, J., Lopez-Gonzalez, G., Malhi, Y., Monteagudo, A., Peacock, J., Quesada, C. A., van der Heijden, G., Almeida, S., Amaral, I., Arroyo, L., Aymard, G., Baker, T. R., Banki, O., Blanc, L., Bonal, D., Brando, P., Chave, J., Alves de Oliveira, A. C., Cardozo, N. D., Czimczik, C. I., Feldpausch, T. R., Freitas, M. A., Gloor, E., Higuchi, N., Jimenez, E., Lloyd, G., Meir, P., Mendoza, C., Morel, A., Neill, D. A., Nepstad, D., Patino, S., Cristina Penuela, M., Prieto, A., Ramirez, F., Schwarz, M., Silva, J., Silveira, M., Thomas, A. S., ter Steege, H., Stropp, J., Vasquez, R., Zelazowski, P., Alvarez Davila, E., Andelman, S., Andrade, A., Chao, K. J., Erwin, T., Di Fiore, A., Honorio C, E., Keeling, H., Killeen, T. J., Laurance, W. F., Pena Cruz, A., Pitman, N. C. A., Nunez Vargas, P., Ramirez-Angulo, H., Rudas, A., Salamao, R., Silva, N., Terborgh, J., and Torres-Lezama, A. (2009). Drought sensitivity of the amazon rainforest. *Science*, 323, 1344–1347.

Pouliot, D., Litifovic, R., Zabcic, N., Guindon, L. and Olthof, I. (2014). Development and assessment of a 250 m spatial resolution MODIS annual land cover time series (2000-2011) for the forest region of Canada derived from change-based updating. *Remote Sensing of Environment*, 140, 731-743.

Poulter, B., Heyder, U. and Cramer, W. (2009). Modeling the sensitivity of the seasonal cycle of GPP to dynamic LAI and soil depths in tropical rainforests. *Ecosystems*, 12, 517-533.

Poulter, B. and Cramer, W. (2009). Satellite remote sensing of tropical forest canopies and their seasonal dynamics. *International Journal of Remote Sensing,* Vol. 30, No. 24*,* 6575-6590.

Poulter, B., Hattermann, F., Hawkins, E., Zaehles, S., Sitch, S., Restrepo-Coupe, N., Heyder, U. and Cramer, W. (2010). Robust dynamics of Amazon dieback to climate change with perturbed ecosystem model parameters. *Global Change Biology*, 16, 2476-2495.

Poulter, B., Ciais, P., Hodson, E., Lischke, H., Maignan, F., Plummer, S., and Zimmermann, N.E. (2011). Plant functional type mapping for earth system models. *Geoscientific Model Development*, 4, 993–1010.

Quaife, T., Quegan, S., Disney, M., Lewis, P., Lomas, M., and Woodward, F. I. (2008). Impact of land cover uncertainties on estimates of biospheric carbon fluxes. *Global Biogeochemical Cycles*, 22, GB4016.

Quesada, C. A., Lloyd, J. Anderson, L. O., Fyllas, N. M., Schwarz, M. and Czimczik, C. I. (2011). Soils of Amazonia with particular reference to the RAINFOR sites. *Biogeosciences*, 8, 1415-1440.

Rahman, A. F., D. A., Sims, V. D., Cordova and El-Masri, B. Z. (2005). Potential of MODIS EVI and surface temperature for directly estimating per-pixel ecosystem C fluxes. *Geophysical Research Letters,* 32, L19404.

Ramankutty, N., Graumlich, L., Achard, F., Alves, D., Chhabra, A., DeFries, R. S., Foley, J. A., Geist, H., Houghton, R. A., Goldewijk, K. K., Lambin, E. F., Millington, A., Rasmussen, K., Reid, R. S. and Turner, B. L. (2006). Global land cover change: Recent progress, remaining challenges. In E. F. Lambin, & H. Geist (Eds.), In land-use and land cover change local processes and global impacts (pp. 9–40). Berlin Heidelberg: Springer-Verlag.

Ramankutty, N., Gibbs, H. K., Achard, F., Defries, R., Foley, J. A. and Houghton, R. A. (2007). Challenges to estimating carbon emissions from tropical deforestation. *Global Change Biology*, 13, 51-66.

Reed, B. C., Brown, J. F., Vanderzee, D., Loveland, T. R., Merchant, J. W., and Ohlen, D. O. (1994). Measuring Phenological Variability From Satellite Imagery. *Journal Of Vegetation Science*, 5 (5), 703–714.

Reed, B. C., Schwartz, M. D. and Xiao, X. (2009). Remote Sensing Phenology, Status and the Way Forward. In Phenology of Ecosystem Processes, A. Noormets (ed.), pp. 231-246.

Reich, P. B., Uhl, C., Walters, M. B., Prugh, L. and Ellsworth, D. S. (2004). Leaf demography and phenology in Amazonian rain forest: a census of 40000 leaves of 23 tree species. *Ecological Monographs*, 74, 3-23.

Reichstein, M., Bahn, M., Ciais, P., Frank, D., Mahecha, M. D., Seneviratne, S. I., Zscheischler, J., Beer, C., Buchmann, N., Frank, D. C., Papale, D., Rammig, A., Smith, P., Thonicke, K., van der Velde, M., Vicca, S., Walz, A. and Wattenbach, M. (2013). Climate extremes and the carbon cycle. *Nature*, 500, 287-295.

Restrepo-Coupe, N., da Rocha, H. R., Hutyra, L. R., da Araujo, A. C., Borma, L. S., Christoffersen, B., Cabral, O. M. R., de Camargo, P. B., Cardoso, F. L., da Costa, A. L. C., Fitzjarrald, D. R., Goulden, M. L., Kruijt, B., Maia, J. M. F., Malhi, Y. S., Manzi, A. O., Miller, S. D., Nobre, A. D., von Randow, C., Sá, L. A. D., Sakai, R. K., Tota, J., Wofsy, S. C., Zanchi, F. B. and Saleska S. R. (2013). What drives the seasonality of photosynthesis across the Amazon basin? A cross-site analysis of eddy flux tower measurements from the Brasil flux network. *Agricultural and Forest Meteorology*, 182-183, 128 - 144.

Rice, A., Pyle, E., Saleska, S., Hutyra, L., Palace, M., Keller, M., Camargo, P., Portilho, K., Marques, D., and Wofsy, S. (2004). Carbon balance

and vegetation dynamics in an old-growth Amazonian forest. *Ecological Applications*, 14(4), 55-71.

Richardson, A. D., Keenan, T. F., Migliavacca, M., Ryu, Y., Sonnentag, O. and Toomey, M. (2013). Climate change, phenology, and phenological control of vegetation feedbacks to the climate system. *Agricultural and Forest Meteorology*, 169, 156-173.

Roberts, D., Nelson, B., Adams, J., and Palmer, F. (1998). Spectral change with leaf aging in Amazon caatinga. *Tree-Structure and Function*, 12, 315-325.

Rosenzweig, C., Casassa, G., Karoly, D. J., Imeson, A., Liu, C., Menzel, A., Rawlins, S., Root, T. L., Seguin, B. and Tryjanowski, P. (2007). Assessment of observed changes and responses in natural and managed systems. Climate Change 2007: Impacts, Adaptation and Vulnerability, Contribution of Working Group II to the Fourth Assessment Report of the Intergovernmental Panel on Climate Change, edited by: Parry, M. L., Canziani, O. F., Palutikof, J. P., van der Linden, P. J., and Hanson, C. E., Cambridge University Press, Cambridge, UK, 79–131.

Rudel, T., K., Coomes, O. T., Moran, E., Achard, F., Angelsen, A., Xu, J. and Lambin, E. (2005). Forest transitions: towards a global understanding of land use change. *Global Environmental Change*, 15, 23-31.

Ruellan, S., Cachier, H., Gaudichet, A., Masclet, P. and Lacaux, J.-P. (1999). Airborne aerosols over central Africa during the Experiment for Regional Sources and Sinks of Oxidants (EXPRESSO). *Journal of Geophysical Research*, 104, 30673-30690.

Ruiz Pérez, M., Ezzine de Blas D., Nasi, R., Sayer, J. A., Sassen, M., Angoué, C., Gami, N., Ndoye, O., Ngono, G., Nguinguiri, J. C., Nzala, D., Toirambe, B. and Yalibanda Y. (2005). Logging in the Congo Basin: A multi-country characterization of timber companies. *Forest Ecology and Management*, 214, 221-236.

Saatchi, S. S., Harris, N. L., Brown, S., Lefsky, M., Mitchard, E. T. A., Salas, W., Zutta, B. R., Buermann, W., Lewis, S. L., Hagen, S., Petrova, S., et al. (2011). Benchmark map of forest carbon stocks in tropical regions across three continents. *Proceedings of the National Academy of Sciences* USA, 108, 9899–9904.

Saatchi, S., Asefi-Najafabady, S., Malhi, Y., Aragão, L. E. O. C., Anderson, L. O., Myneni, R. B. and Nemani, R. (2013). Persistent effects of a severe drought on Amazonian forest canopy. *Proceedings of the National Academy of Sciences,* 110, 565-570.

Saleska, S., Miller, S., Mtross, D., Goulden, M., Wofsy, S., da Rocha, H., de Camargo, P., Crill, P., Daube, B., Freitas, H., Hutyra, L., Keller, M., Kirchhoff, V., Menton, M., Munger, J., Pyle, E., Rice, A., and Silva, H. (2003). Carbon in amazon forests: Unexpected seasonal fluxes and disturbance-induced losses. *Science*, 302(5650), 1554-1557.

Saleska, S., Didan, K., Huete, A., and da Rocha, H. (2007). Amazon forests green-up during 2005 drought, *Science*, *318,* 612.

Samanta, A., Ganguly, S., Hashimoto, H., Devadiga, S., Vermote, E., Knyazikhin, Y., Nemani, R., Myneni, R. (2010a). Amazon rainforests did not green-up during the 2005 drought. *Geophysical Research Letters, Vol. 37,* L05401.

Samanta, A., Ganguly, S. and Myneni, R. B. (2010b). MODIS Enhanced Vegetation Index data do not show greening of Amazon forests during the 2005 drought. *New Phytologist*, 189, 11-15.

Samanta, A., Knyazikhin, Y., Xu, L., Dickinson, R. E., Fu, R., Costa, M. H., Saatchi, S. S., Nemani, R. R. and Myneni, R. B. (2012). Seasonal changes in leaf area of Amazon forests from leaf flushing and abscission. *Journal of Geophysical Research*, 117, G01015.

Schaaf, C., Gao, F., Strahler, A., Lucht, W., Li, X., Tsang, T., Strugnell, N., Zhang, X., Jin, Y., Muller, J-P., Lewis, P., Barnsley, M., Hobson, P., Disney, M., Roberts, G., Dunerdale, M., Doll, C., d'Entremont, R., Hu, B., Liang, S., Privette, J., and Roy, D. (2002). First operational BRDF, albedo nadir reflectance products from MODIS. *Remote Sensing of Environment,* 85, 135-148.

Schafer, J. S., Eck, T. F., Holben, B. N., Artaxo, P., Yamasoe, M. A. and Procopio, A. S. (2002). Observed reductions of total irradiance by biomass-burning aerosols in the Brazilian Amazon and Zambian Savanna. *Geophysical Research Letters*, 29(17), 1823–1826.

Schwartz, D. and Tondo, F (1988). La production de litière en forêt dense équatoriale. Bilan d'un an de collecte à Dimonika (Mayombe, Congo) : février 1987-février 1988. *Pointe Noire : ORSTOM*, 14 p.

Sexton, J., Urban, D. L., Donohue, M., J. and Song, C. (2013). Long-term land cover dynamics by multi-temporal classification across the Landsat-5 record. *Remote Sensing of Environment*, 128, 246-258.

Sharma, N. K., Tiwari, P. K. and Sood, Y., R. (2013). A comprehensive analysis of strategies, policies and development of hydropower in India: Special emphasis on small hydro power. *Renewable and Sustainable Energy Reviews*, 18, 460-470.

Sheikh, P.A. (2005). The Impact of Hurricane Katrina on Biological Resources. Congressional Research Service Report to Congress. Order Code RL33117. Washington, DC.

Sims, D. A., Rahman, A. F., Cordova, V. D., El-Masri, B. Z., Baldocchi, D.D., Flanagan, L. B., et al. (2006b). On the use of MODIS EVI to assess gross primary productivity of North American ecosystems. *Journal of Geophysical Research*, 111(G4), G04015.

Singh, A. (1989). Review article digital change detection techniques using remotely-sensed data. *International Journal of Remote Sensing*, 10, 989-1003.

Sitch, S., Brovkin, V. and Bloh, W. (2005). Impacts of future land cover changes on atmospheric $CO_2$ and climate. *Global Biogeochemical Cycles*, 19, GB2013.

Sjöström, M., Ardö, J., Arneth, A., Boulain, N., Cappelaere, B., Eklundh, L., de Grandcourt, A., Kutsch, W. L., Merbold, L., Nouvellon, Y., Scholes, R. J., Schubert, P., Seaquist, J. and Veenendaal, E. M. (2011). Exploring the potential of MODIS EVI for modelling gross primary production across African ecosystems. *Remote Sensing of Environment*, 115, 1081-1089.

Strahler, A. H., Boschetti, L., Foody, G. M., Friedl, M. A., Hansen, M. A., Mayaux, P., Morisette, J. T., Stehman, S. V., and Woodcock, C. E. (2006). Global Land Cover Validation: Recommendations for evaluation and accuracy assessment of global land cover maps, Office for Official Publications of the European Communities, Luxembourg, 48 pp.

ter Steege, H., Pitman, N., Sabatier, D., Baraloto, C. et al. (2013). Hyperdominance in the Amazonian Tree Flora. *Science*, 342, 1243092.

Tewkesbury, A. P., Comber, A. J., Tate, N. J., Lamb, A and Fisher, P. F. (2015). A critical synthesis of remotely sensed optical image change detection techniques. *Remote Sensing of Environment*, 160, 1-14.

Thevs, N., Peng, H., Rozi, A., Zerbe, S. and Abdusalih, N. (2014). Water allocation and water consumption of irrigated agriculture and natural vegetation in the Aksu-Tarim river basin, Xinjiang, China. *Journal of Arid Environment*, 112, 87-97.

Tollefson, J. (2013). A line in the sands. *Nature*, 500, 136-137.

Tollefson, F. (2015). Climate modellers take tropical approach. *Nature*, 519, 398-399.

Toomey, M., Roberts, D. and Nelson, B. (2009). The influence of epiphylls on remote sensing of humid forests. *Remote Sensing of Environment*, 113, 1787-1798.

Townsend, P., Helmers, D., Kingdon, C., McNeil, B., de Beurs, K., and Eshleman K. (2009). Changes in the extent of surface mining and reclamation in the Central Appalachians detected using a 1976–2006 Landsat time series. *Remote Sensing of Environment*, 113, 62-72.

Townshend, J. R. G., C. Justice, W. Li, C. Gurney, and J. McManus (1991). Global land cover classification by remote sensing: Present capabilities and future possibilities. *Remote Sensing of Environment,* 35, 243–255.

Tshibangu, K. T. (2010). Correlative study between the phenology of the Pericopsis elata HARMS and the ecoclimatical parameters in the area of Yangambi in Democratic Republic of Congo. *Geo-Eco-Trop.*, 34, 127-138.

Tucker, C. J. (1979). Red and photographic infrared combinations for monitoring vegetation. *Remote Sensing of Environment, 8*, 127-150.

Turner, B. L., Lambin, E. F. and Reenberg, A. (2007). The emergence of land change science for global environmental change and sustainability. *Proceedings of the National Academy of Sciences,* vo. 104, n° 52, 20666-20671.

UNFPA. (2007). United Nations: State of the World Population. New York, NY: United Nations Population Fund.

van Schaik, C. P., Terborgh, J. W., and Wright, S. J. (1993). The phenology of tropical forests — Adaptive significance and consequences for primary consumers. *Annual Review of Ecology and Systematics*, 24, 353–377.

Valentini, R., Arneth, A., Bombelli, A., Castaldi, S., Cazzolla Gatti, R., Chevallier, F., Ciais, P., Grieco, E., Hartmann, J., Henry, M., Houghton, R. A., Jung, M., Kutsch, W. L., Malhi, Y., Mayorga, E., Merbold, L., Murray-Tortarolo, G., Papale, D., Peylin, P., Poulter, B., Raymond, P. A., Santini, M., Sitch, S., Vaglio Laurin, G., van der Werf, G. R., Williams, C. A. and Scholes, R. J. (2014). A full greenhouse gases budget of Africa: synthesis, uncertainties, and vulnerabilities. *Biogeosciences*, 11, 381-407.

Vancutsem, C., Pekel, J.-F., Bogaert, P. and Defourny, P. (2007). Mean compositing, an alternative strategy for producing temporal syntheses. Concepts and performance assessment for SPOT-VEGETATION time series. *International Journal of Remote Sensing*, vol. 28, 5123 – 5141.

Vancutsem, C., Peckel, J.-F., Evrard, C., Malaisse, F. and Defourny, P. (2009). Mapping and characterizing the vegetation types of the Democratic Republic of Congo using SPOT-VEGETATION time series. *International Journal of Applied Earth Observation and Geoinformation*, 11 (1), 62-76.

Vargo, J., Habeeb, D. and Stone Jr., B. (2013). The importance of land cover change across urbanerural typologies for climate modelling. *Journal of Environmental Management*, 114, 243-252.

Verbeeck, H., Boeckx, P. and Steppe, K. (2011a). Tropical forests: include Congo Basin. *Nature*, 479, 179.

Verbeeck, H., Peylin, P., Bacour, C., Bonal, D., Steppe, K. and Ciais, P. (2011b). Seasonal patterns of $CO_2$ fluxes in Amazon forests: Fusion ofeddy covariance data and the ORCHIDEE model. *Journal of Geophysical Research*, 116, G02018.

Verbeeck, H., Betehndoh, E., Maes, W. H., Hubau, W., Kearsley, E., Buggenhout, L., Hufkens, K., Huygens, D., Acker, J. V., Beeckman, H., Mweru, J. P. M., Boeckx, P. and Steppe, K. (2014). Functional leaf trait diversity of 10 tree species in Congolese secondary tropical forest. *Journal of Tropical Forest Science*, 26 (3), 409-419.

Verhegghen, A., Mayaux, P., deWasseige, C. and Defourny, P. (2012). Mapping Congo Basin vegetation types from 300m and 1km multi-sensor time series for carbon stocks and forest areas estimation. *Biogeosciences*, 9, 5061-5079.

Verhegghen, A. (2013). Global land surface vegetation phenology using 13 years of SPOT-VEGETATION daily observations. Thesis at Faculté d'ingénierie biologique, agronomique et environnementale, Université catholique de Louvain.

Viennois, G. Barbier, N. Fabre, I. and Couteron, P. (2013). Multiresolution quantification of deciduousness in West-Central African forests. *Biogeosciences*, 10, 6957-6967.

Wagner, F., Rossi, V., Stahl, C., Bonal, D. and Hérault, B. (2013). Asynchronism in leaf and wood production in tropical forests: a study combining satellite and ground-based measurements. *Biogeosciences*, 10, 7307-7321.

Warner, J. (2013). The Toshka mirage in the Egyptian desert – River diversion as political diversion. *Environmental Science and Policy*, 30, 102-112.

Weber, U., Jung, M., Reichstein, M., Beer, C., Braakhekke, M. C., Lehsten, V., Ghent, D., Kaduk, J., Viovy, N., Ciais, P., Gobron, N., and

Rödenbeck, C. (2009). The interannual variability of Africa's ecosystem productivity: a multi-model analysis. *Biogeosciences*, 6, 285-295.

White, F. (1983). The vegetation of Africa. *A descriptive memoir to accompany the Unesco/AEFTFAT/UNSO vegetation map of Africa*, Unesco.

Wilson, M., and A. Henderson-Sellers, 1985, A global archive of land cover and soils data for use in general circulation climate models. *Journal of Climatology*, 5, 119 – 143.

Worbes, M. Staschel, R., Roloff, A. and Junk, W. J. (2003). Tree ring analysis reveals age structure, dynamics and wood production of a natural forest stand in Cameroon. *Forest Ecology and Management*, 173, 105-123.

Wright, S. J. and van Schaik, C. P. (1994). Light and the phenology of tropical trees. *The American Naturalist*, 143, 192-199.

Xiao, X., Braswell, B., Zhang, Q., Boles, S., Frolking, S., and Berrien, M. (2003). Sensitivity of vegetation indices to atmospheric aerosols: continental-scale observations in Northern Asia. *Remote Sensing of Environment,* 84, 385-392.

Xiao, X., Zhang, Q., Saleska, S., Hutyra, L., de Camargo, P., Wofsy, S., Frokling, S., Boles, S., Keller, M., Moore, B. (2005). Satellite-based modeling of gross primary production in a seasonally moist tropical evergreen forest. *Remote Sensing of Environment*, 94(1), 105-122.

Xiao, X., Hagen, S., Zhang, Q., Keller, M. And Moore, B. (2006). Detecting leaf phenology of seasonally moist tropical forests in South America with multi-temporal MODIS images. *Remote Sensing of Environment*, 103(1), 465-473.

Yang, X., Thornton, P. E., Ricciuto, D. M. and Post, W. M. (2014). The role of phosphorus dynamics in tropical forests – a modelling study using CLM-CNP. *Biogeosciences*, 11, 1667-1681.

Zhang, X., Friedl, M. And Schaaf, C. (2008). Sensitivity of vegetation phenology detection to the temporal resolution of satellite data, *International Journal of Remote Sensing,* Vol. 30, No. 20, 2061-2074.

Zhang, Y., Guindon, B., Lantz, N., Shipman, T., Chao, D. and Raymond, D. (2014). Quantification of anthropogenic and natural changes in oil sands mining infrastructure land based on RapidEye and SPOT5. *International Journal of Applied Earth Observation and Geoinformation*, 29, 31-43.

Zhou, L., Tian, Y., Myneni, R. B., Ciais, P., Saatchi, S., Liu, Y. Y., Piao, S., Chen, H., Vermote, E. F., Song, C. and Hwang, T. (2014). Widespread decline of Congo rainforest greenness in the past decade. *Nature*, 509, 86-90.